NASA
TT
F-504
c.1

Series: Mechanics of Space Flight

V. A. Egorov

# THREE-DIMENSIONAL LUNAR TRAJECTORIES

LOAN COPY: RETURN
AFWL (WLOL)
KIRTLAND AFB, N M
0068984
TECH LIBRARY KAFB, NM

TRANSLATED FROM RUSSIAN

Published for the National Aeronautics and Space Administration
and the National Science Foundation, Washington, D.C.
by the Israel Program for Scientific Translations

TECH LIBRARY KAFB, NM
0068984

Series: *Mechanics of Space Flight*

V. A. Egorov

# THREE-DIMENSIONAL LUNAR TRAJECTORIES

(Prostranstvennaya zadacha dostizheniya luny)

Izdatel'stvo "Nauka"
Glavnaya Redaktsiya Fiziko-Matematicheskoi Literatury
Moskva 1965

Translated from Russian

Israel Program for Scientific Translations
Jerusalem 1969

NASA TT F-504
TT 68-50306
Published Pursuant to an Agreement with
THE NATIONAL AERONAUTICS AND SPACE ADMINISTRATION, U.S.A.
and
THE NATIONAL SCIENCE FOUNDATION, WASHINGTON, D.C.

Copyright © 1969
Israel Program for Scientific Translations Ltd.
IPST Cat. No. 5074

U. D. C. 629.195.3

Translated and Edited by Ron Hardin

Printed in Jerusalem by IPST Press
Binding: Wiener Bindery Ltd., Jerusalem

Available from the
U.S. DEPARTMENT OF COMMERCE
Clearinghouse for Federal Scientific and Technical Information
Springfield, Va. 22151

VIII/16/3

## *PREFACE*

In recent years the science of space flight has undergone very intensive development. Unmanned spacecraft have been injected into earth orbits; the moon has been hit by spacecraft and flown around, and its averted side has been photographed; the first manned flights aboard earth satellites have been carried out; and space probes have been launched into outer space, even to the planets.

This book presents a rough study of three-dimensional lunar trajectories, with a view toward selecting trajectories having the required characteristics. Such subjects as circumlunar flights, moon landings, the creation of artificial lunar satellites, the processing of trajectory measurements, and the correction of lunar trajectories will not be discussed. The basic purpose of the book will be to make a detailed study of various questions related to determining appropriate trajectories for reaching the moon. In such a study, certain limiting factors must of course be taken into account (for example, geometrical or dynamic factors), as well as secondary factors like the ellipticity of the lunar orbit, the oblateness of the earth, etc. Our main attention will be devoted to finding energetically optimum trajectories which satisfy all the necessary conditions.

Systematic studies of three-dimensional spacecraft trajectories to the moon were made as early as 1957 or 1958. However, to the best of our knowledge, no books on moon-flight theory have as yet appeared, either in the USSR or outside of it, and relevant articles have only recently begun to be published in journals. The present book should partially fill this vacuum.

Some of the results of this study were presented at the annual meeting of the American Rocket Society in 1959 /17/ and also at the All-Union Conference on General and Applied Problems in Theoretical Astronomy in 1961.

The subject matter of the book is presented in considerable detail. Consequently, it should prove useful to undergraduates and graduate students in the corresponding fields, as well as to specialists. The reader is assumed to have a basic knowledge of higher mathematics and theoretical mechanics, and to have completed a general course in astronomy.

The supplement contains the results of a study made by the author: "Some Problems Related to the Dynamics of Moon Flight," published in 1957 /21/. These results are an addition to (but not a repetition of) the contents of Chapters I through V. The basic findings of /21/ were discussed quite thoroughly in V.I. Levantovskii's book: Raketoi k lune (By Rocket Ship to the Moon), Fizmatgiz, 1960; therefore, the author has taken the liberty of presenting these results in a summary manner.

The author is very grateful to D. E. Okhotsimskii for many stimulating discussions concerning the book, and for his useful criticism and valuable observations. T. M. Eneev and L. I. Sedov deserve thanks for their discussions of certain questions related to the results of the study and to the presentation of these results. Finally, the author would like to express his gratitude to R. K. Kazakova, G. P. Taratynova, N. S. Malinina, and V. K. Shelukhina for their great assistance in carrying out the calculations and formulating the results.

# CONTENTS

PREFACE ..... iii

NOMENCLATURE ..... vii

INTRODUCTION ..... 1

Chapter I. AN ANALYSIS OF LUNAR-FLIGHT CONDITIONS ..... 6
1.1. Equations of three-dimensional motion and general description of lunar-approach trajectories ..... 6
1.2. Lunar impacts from high latitudes ..... 13
1.3. Lunar-impact trajectories starting from a given latitude ..... 21
1.4. Length of active part of flight ..... 28

Chapter II. ENERGETICALLY OPTIMUM LUNAR TRAJECTORIES ..... 34
2.1. Required energy expenditures corresponding to given initial data .. 34
2.2. Lunar trajectories with specified inclinations of flight plane to plane of equator ..... 36
2.3. Optimum initial data for specified inclination of trajectory plane to equatorial plane ..... 39
2.4. Selection of energetically optimum inclinations for trajectories of first type ..... 42
2.5. Selection of energetically optimum inclinations for trajectories of second type ..... 46

Chapter III. NOMINAL IMPACT TRAJECTORIES AND EFFECT OF INITIAL-DATA SCATTER, TAKING INTO ACCOUNT LUNAR ATTRACTION ..... 50
3.1. Nominal lunar-impact trajectories ..... 50
3.2. Calculation of modified trajectories ..... 55
3.3. Effect of initial-data scatter on location of point of entry into moon's sphere of action ..... 59
3.4. Effect of initial-data scatter on location of impact point ..... 64

Chapter IV. DETERMINATION OF POINT OF LUNAR IMPACT AND CALCULATION OF PARAMETERS OF MOTION RELATIVE TO EARTH'S SURFACE . . . . . 71
4.1. Determination of point of lunar impact for specified inclination of trajectory plane to plane of equator . . . . . 71
4.2. Selection of unperturbed lunar trajectory, allowing for direct viewing of impact from specified point . . . . . 76
4.3. Characteristics of motion relative to earth and moon . . . . . 80
4.4. Results of a sample calculation . . . . . 84

Chapter V. EFFECTS OF SECONDARY FACTORS . . . . . 88
5.1. Effect of the moon as a material body . . . . . 88
5.2. Effect of ellipticity of moon's orbit . . . . . 91
5.3. Effect of the earth's oblateness . . . . . 93
5.4. Effect of the sun . . . . . 98
Concluding remarks . . . . . 101

Supplement. A GENERAL ANALYSIS OF LUNAR TRAJECTORIES WITH APPLICATION TO THE TWO-DIMENSIONAL CASE . . . 104
D.1. Theoretical determination of minimum initial velocities . . . . . 104
D.2. Numerical determination of two-dimensional trajectories . . . . . 107
D.3. Trajectories of minimum absolute initial velocity . . . . . 110
D.4. Impossibility of lunar capture of spacecraft launched from earth . . . . . 113
D.5. An approximate method for studying trajectories . . . . . 115
D.6. Analysis of approach trajectories . . . . . 117
D.7. Two-dimensional problem of lunar impact . . . . . 123
D.8. Two-dimensional problem of circumlunar flight . . . . . 129
D.9. Special problem of circumlunar flight . . . . . 134
D.10. Two-dimensional problem of periodic circumlunar flight . . . . . 136
D.11. Two-dimensional problem of acceleration or braking using perturbing action of moon . . . . . 141
Remarks . . . . . 143

REFERENCES . . . . . 145

INDEX . . . . . 147

## *NOMENCLATURE*

| Symbol | Units | Meaning |
|---|---|---|
| $hls$ | | Rectangular coordinate system with origin at beginning of passive part of trajectory |
| $m_1\xi_1\eta_1\zeta_1$ | | Nonrotating geocentric coordinate system |
| $m_2\xi_2\eta_2\zeta_2$ | | Nonrotating selenocentric coordinate system |
| $X_eY_eZ_e$ | | Equatorial coordinate system |
| $a$ | km | Mean distance between centers of earth and moon |
| $a_1$ | deg | Azimuth of vector of initial geocentric velocity (absolute velocity) at point of entry into passive part of trajectory |
| $d$ | km | Distance from moon's center to tangent to selenocentric trajectory at point of entry into moon's sphere of action |
| $H_1$ | km | Height of beginning of passive part of trajectory; initial height |
| $h_0$ | hr | Moment moon passes through point of minimum velocity |
| $i$ | deg | Inclination of lunar orbital plane to ecliptic plane |
| $i_e$ | deg | Inclination of trajectory plane to equatorial plane |
| $i_1$ | deg | Inclination of trajectory plane to lunar orbital plane |
| $m_1$ | | Earth's center |
| $m_2$ | | Moon's center |
| $R$ | km | Radius of upper layers of atmosphere |
| $r$ | km | Geocentric distance (distance from earth's center to spacecraft) |
| $r_0$ | km | Earth's radius |
| $r_1$ | km | Initial geocentric radius (geocentric radius of initial point of passive part of trajectory) |
| $r_2$ | km | Geocentric entry radius (radius of point of entry into moon's sphere of action); radius of point of spacecraft impact at moon's center |
| $r_3$ | km | Geocentric exit radius (geocentric radius of point of spacecraft exit from moon's sphere of action) |
| $T_0$ | hr | Optimum flight time in passive part of trajectory |
| $T_{1,2}$ | hr | Flight time from initial point to point where spacecraft encounters sphere of action or nonattracting moon |
| $U$ | km/sec | Magnitude of selenocentric spacecraft velocity at boundary of moon's sphere of action |
| $U_i$ | km/sec | Magnitude of spacecraft velocity at moment of lunar impact |
| $U_x$ | km/sec | Characteristic velocity |
| $u_i$ | | Latitude argument of terminal point of passive part |
| $u_0$ | | Latitude argument of launch point |
| $u_1$ | | Latitude argument of point corresponding to beginning of passive part of trajectory |
| $V_L$ | km/sec | Geocentric velocity of moon |
| $V_p$ | km/sec | Local geocentric parabolic velocity of spacecraft |
| $V_r$ | km/sec | Radial component of absolute geocentric velocity of spacecraft |
| $V_\tau$ | km/sec | Transverse component of absolute geocentric velocity of spacecraft |
| $V_\Omega$ | km/sec | Velocity increment (in addition to spacecraft velocity relative to earth's surface) due to earth's rotation |
| $V_1$ | km/sec | Initial geocentric velocity of spacecraft |
| $V_2$ | km/sec | Geocentric entry velocity of spacecraft |
| $V_3$ | km/sec | Geocentric exit velocity of spacecraft |
| $V_p'$ | km/sec | Selenocentric parabolic velocity at boundary of moon's sphere of action |
| $V_2'$ | km/sec | Selenocentric entry velocity of spacecraft |

| Symbol | Units | Meaning |
|---|---|---|
| $V_3'$ | km/sec | Selenocentric exit velocity of spacecraft |
| $\Delta V_1$ | km/sec | Amount by which initial geocentric velocity exceeds local parabolic |
| $v_i$ | | True anomaly of impact point |
| $\alpha$ | deg | Angle between selenocentric entry and exit velocities |
| $\alpha_1$ | deg | Angle between initial spacecraft velocity and initial geocentric radius |
| $\alpha_2$ | deg | Angle between geocentric entry velocity and geocentric entry radius |
| $\alpha_2$ | deg | Angle between selenocentric entry velocity and selenocentric radius of point of entry into moon's sphere of action |
| $\gamma_0$ | | Angular radius of circle on earth's surface from points of which spacecraft is visible on horizon |
| $\delta$ | deg | Declination of spacecraft |
| E | | Equatorial plane |
| $\varepsilon$ | deg | Angle of elevation of point-spacecraft above horizon of observation point |
| $\varepsilon_0$ | deg | Inclination of ecliptic to celestial equator |
| $\theta$ | deg | Angle between equatorial plane and lunar orbital plane |
| $\theta_1$ | deg | Angle of inclination of initial-velocity vector of spacecraft to local horizon |
| $\lambda$ | deg | Angle between initial geocentric radius and initial direction of earth-moon line in two-dimensional problem |
| $\lambda_g$ | deg | Geographical longitude of spacecraft |
| $\lambda_{g_0}$ | deg | Geographical longitude of launch point |
| $\lambda_H$ | deg | Geographical longitude of observation point |
| $\Delta\lambda_{11}$ | deg | Interlaunch interval |
| $\Delta\lambda_L$ | deg | Launch interval |
| $\mu_1$ | $km^3/sec^2$ | Gravitational potential of earth |
| $\mu_2$ | $km^3/sec^2$ | Gravitational potential of moon |
| $\Pi$ | | *Ecliptic plane* |
| $\Pi'$ | | Lunar orbital plane |
| $\rho$ | km | Selenocentric distance (distance from spacecraft to moon's center) |
| $\rho_L$ | km | Radius of moon |
| $\rho_{min}$ | km | Minimum distance of flight path from moon's center |
| $\rho_*$ | km | Radius of moon's sphere of action |
| $\sigma_g$ | $km^2/sec$ | Geocentric area constant after spacecraft leaves moon's sphere of action |
| $\sigma_1$ | $km^2/sec$ | Initial geocentric areal velocity |
| $\Phi$ | deg | Total angular range of trajectory (angle between geocentric radii of initial and final points) |
| $\Phi_a$ | deg | Angular range of active part of trajectory |
| $\Phi_1$ | deg | Angular range of passive part of trajectory |
| $\varphi_2$ | deg | Angle between geocentric radii of moon and entry point |
| $\varphi_3$ | deg | Angle between geocentric exit radius and earth-moon line |
| $\psi_g$ | deg | Geographical latitude of spacecraft |
| $\psi_H$ | deg | Geographical latitude of observation point |
| $\psi_0$ | deg | Geographical latitude of launch point |
| $\psi_1$ | deg | Geographical latitude of beginning of passive part of trajectory |
| $\Omega$ | $sec^{-1}$ | Angular velocity of earth's diurnal rotation |
| $\omega$ | $sec^{-1}$ | Angular velocity of revolution of moon |
| $\omega_g$ | $sec^{-1}$ | Geocentric angular velocity of spacecraft |
| $\omega_1$ | deg | Longitude of perigee of geocentric part of flight path |
| $\Upsilon$ | | Vernal equinox |
| $\Omega_L$ | deg | Longitude of ascending node of lunar orbit |
| $\Omega_1$ | deg | Longitude of ascending node of geocentric part of trajectory |
| $\Omega_a$ | deg | Longitude of advance point on lunar orbit |

## *INTRODUCTION*

Between 1953 and 1956 the author carried out an analysis of the passive [coasting] part of a two-dimensional spacecraft trajectory to the moon /21/. The trajectory was assumed to lie in the moon's orbital plane. This analysis indicated which initial data are required in order to plan such a trajectory, and also what effect errors in the initial data have on the trajectory calculation. For a flight taking place in the moon's orbital plane, the following subjects were considered: reaching the moon; returning to earth after approaching the moon; flying around the moon and making a slanting re-entry into the earth's atmosphere; making periodic circuits of the moon; and using the approach to the moon to accelerate or brake a spacecraft, without the aid of the engines. In particular, it was found that lunar trajectories with horizontal initial velocities were more advantageous energetically than other trajectories in the moon's orbital plane. This is because for these trajectories the energy needed to overcome gravity is a minimum, and the velocity of rotation of the launch point, together with the earth, can be utilized most effectively. The effect of the scatter of initial data for these trajectories may be summarized as follows: when the initial speed is somewhat higher than parabolic, velocity errors of the order of 30 m/sec and directional errors of the order of 0.5° do not cause the spacecraft to miss the moon; however, these errors are close to the critical values.

If the launch point is located in the middle or high latitudes, on the other hand, it turns out to be impossible to obtain trajectories lying in the moon's orbital plane. Moon flights in the lunar orbital plane are feasible only provided that the launch point has a latitude less than the inclination of the lunar orbit to the equatorial plane. This inclination varies from 18°18' to 28°36', with a period of 18.6 years.

For flight paths that are essentially three-dimensional, it is of interest to ascertain which initial data are optimum and what the effects of errors in the initial data will be. These problems will be considered in this book.

Quite a few papers have been published on moon flights, the majority of them outside of the Soviet Union. In 1956 trajectory problems related to the creation of an artificial lunar satellite were considered /1/. Earth-moon flights were also dealt with in /2/ and /3/, and in /2/ the effects which initial-data variations have on the trajectory were studied (in particular, the derivatives of the parameters of selenocentric motion with respect to the initial data were determined in this work). In 1958 two-dimensional and three-dimensional flight paths were compared /4/. At this same time the effect of initial-data scatter for certain types of three-dimensional trajectories was considered /5/.

More detailed studies of three-dimensional lunar flight paths were made in /6/ through /8/. It was demonstrated in /6/ that, in an analysis of orbits, the limitations determined by the orbit's destination are very important. An approximate analytical study of three-dimensional trajectories was made in /7/; this study made it possible to construct families of curves for the trajectory characteristics, to ascertain the interrelationships between the determining parameters and limiting conditions, and to evaluate the effect of the scatter of initial data. In this work the creation of an artificial lunar satellite was also considered, as well as the achievement of a soft landing on the lunar surface. In /8/ the results of the foregoing approximate analysis were compared with numerical results, and it was established that the accuracy of the approximate analysis was satisfactory.

Moon-flight trajectories were also studied in /9/ through /12/. Flight paths corresponding to elliptical and hyperbolic initial velocities were determined in /9/, and in addition the use of braking rockets to transfer to a lunar-satellite orbit and to return earthward was considered. In /10/ some trajectory problems associated with the creation of an artificial lunar satellite (for taking photographs of the lunar surface) were discussed. A perturbation method for carrying out numerical integrations in trajectory calculations was proposed in /11/. This method made it possible to take into account solar perturbations, the effect of the earth's atmosphere, the earth's oblateness, etc. In /33/ the problem of hitting the moon was considered, together with some other problems in space ballistics.

Approximate moon-flight trajectories are usually calculated without taking into account the influence of the moon outside its sphere of action or the influence of the earth outside the moon's sphere of action. In these calculations the sphere of action of the moon is defined as follows /21/. First, the following ratio is found: the force with which the earth perturbs the motion of a vehicle relative to the moon, divided by the force of attraction of the moon. Then, a second ratio is determined: the force with which the moon perturbs the motion of a vehicle relative to the earth, divided by the force of attraction of the earth. The region of space around the moon in which the first ratio is less than the second is designated as the sphere of action of the moon.

For the boundary of the moon's sphere of action, simple formulas can be used to determine the parameters of motion relative to the moon, in terms of the parameters of motion relative to the earth (and vice versa). Such calculations were used successfully in /12/, which dealt with computer methods for studying the effect of initial-data errors on the trajectory and the effectiveness of a different kind of trajectory correction. Calculations of the motion, without taking into account perturbations within the spheres of action, result in approximate formulas for determining the point of impact on the moon and the moment of launch, for various conditions /13/. Such calculations also make it possible to construct nomograms enabling rapid determination of the instantaneous position of a space rocket which is already on its way to the moon /14/. In addition, using this method, a series of approximate operations (using graphs and formulas) can be specified, in order to select lunar trajectories (or return trajectories), at the same time taking into account the various limiting conditions, geometrical (for instance, the allowable launch azimuths), dynamical (for instance, the allowable launch times), or other.

The approximate method is very widely used, as noted in /15/. In the latter work a system of diagrams was worked out, making it possible to calculate various maneuvers quite simply (flights to the moon and back, transfers from a hyperbolic orbit to a satellite orbit, etc.). Finally, to conclude this very brief survey of the pertinent literature, we should also mention /16/.

However, none of the publications known to the author present a detailed, systematic theory of three-dimensional moon-flight trajectories, at the same time taking into account all the limiting factors (such as the continuity of the powered part of the flight) and all the secondary factors. The secondary factors related to lunar trajectories include the accelerating effect of the moon and its dimensions, the ellipticity of the moon's orbit, the earth's oblateness, and solar perturbations.

The mass of the moon is equal to 1/81.37 of the earth's mass, and the radius of the moon is about 1740 km. If the initial geocentric velocity of a spacecraft exceeds the local parabolic velocity by only 0.1 to 0.2 km/sec, the reduction of the flight time to the moon, as a result of the accelerating action of the latter, amounts to about 2000 seconds. The eccentricity of the lunar orbit is about 0.055. Consequently, for an average orbital radius of 384,400 km, the maximum earth-moon distance will be more than 40,000 km greater than the minimum distance.

The oblateness of the earth is around 1/300. Because of this oblateness, the acceleration due to gravity varies with latitude, from a maximum at the equator to a minimum at the poles; the variation amounts to about 1/150 of the mean acceleration. Since a moon-flight trajectory must pass over different latitudes, the trajectory shape and the corresponding law of motion will both be somewhat different than they would be for a spherical earth. For example, the flight time to the moon (parabolic initial velocity) may be reduced by as much as 1600 seconds, due to the nonsphericity of the earth.

The earth is about 150 million km from the sun. When an object moves out from the earth's center to a distance equivalent to the radius of the lunar orbit, the perturbing force (the vector difference between the solar attraction exerted on the object and on the earth) may increase from zero to 1/100 of the terrestrial pull on the object. The trajectory characteristics will vary in accordance with the increased perturbation. In spite of the relatively small effect which the secondary factors have on the initial data, this effect should nevertheless be evaluated and, when necessary, taken into account.

In this book the study will be carried out by the simplest means possible. For example, when determining the energetically optimum three-dimensional trajectories and evaluating the effect of errors in the initial data, there is no need to take into account all the forces acting (this was pointed out in /21/). It is quite sufficient just to take into account the attraction of the earth and moon, with these bodies considered to be material points moving in circles about their common center of mass. The results of such a study are valid for any positions of the sun and planets.

The variation in a nominal trajectory (that is, a trajectory directed toward the moon's center) as a result of lunar perturbations is relatively small. Therefore, when determining the initial data for the passive [coasting] part of the trajectory, it is in general permissible to neglect the attraction of the moon. Thus it is possible to evaluate the characteristics

of a moon-flight trajectory from any given latitude, assuming continuity of the active [powered] part of the flight; this is discussed in Chapter I. It turns out that for northern launch latitudes these trajectories can be classified into two basic types: I) those passing over the earth's northern hemisphere, and II) those passing over the southern hemisphere.

In Chapter II a method is worked out for determining the optimum combinations of initial data, corresponding to the minimum energy expenditures. For trajectories of the first type a northeastern direction is optimum, and for the second type southeastern trajectories are best. It was established that northeastern trajectories require rockets with considerably higher energy capabilities, in comparison with trajectories of the two-dimensional problem. The required energy expenditures will be less, the lower the declination of the moon at the moment of impact. The trajectory plane, the initial-velocity vector, and other characteristics of the energetically optimum trajectories are determined in this chapter. For southeastern trajectories, the energy capabilities required for their implementation are approximately the same as in the two-dimensional problem.

In Chapter III more accurate calculations of the nominal trajectories (trajectories directed toward the center of the moon) are carried out: these calculations take into account the influence of the moon in its sphere of action. In addition, a more accurate method for calculating divergent trajectories (trajectories whose initial data are close to nominal) is presented in this chapter. Using this method, it was possible to find the maximum allowable errors for each of the initial parameters, as well as the shifts in trajectory points caused by a variation in the initial data. In particular, the shifts of the points where the flight path intersects the boundary of the moon's sphere of action and the lunar surface were considered. The shift of the boundary of the sphere of action was found to be very nearly linear; moreover, a region in the sphere of action was specified, incidence into which ensures impact on the moon. The latter region is nearly circular, with its center at the nominal point of intersection between the flight path and the lunar surface.

The shift in the point of impact, relative to the nominal point, is determined by the shift in the corresponding point on the moon's sphere of action. The shift corresponding to an error in any given initial parameter (or combination of parameters) will be along a great circle passing through the nominal point of impact.

For errors in any of the initial parameters (or combinations of these), the dependence of the shifts on the ratio between the error and the maximum allowable error will be one and the same. The second derivatives of the shifts along the sphere of action, with respect to the initial-data errors for the region corresponding to lunar impact, are quite small. Thus it is possible to study the effect of the scatter of initial data using some linear approximation which is sufficiently accurate. This means that it is not necessary to introduce an image plane during the calculations, as must be done when considering wider pencils of trajectories /17, 18/.

In Chapter IV the problem of determining the point of rocket impact on the moon is solved. The parameters of the corresponding trajectory, various requirements being satisfied, are found. For example, solutions are given which correspond to some desired flight time, or to some specified angle of elevation of the initial-velocity vector above the local

horizon, or to the minimum energy expenditures for optimum conditions of direct visibility when approaching the moon from a specified point on the earth's surface.

In addition, formulas are given for determining different characteristics of the motion of a vehicle relative to specified observation points. The results of trajectory calculations are also presented and analyzed in Chapter IV.

The effects of the secondary factors are analyzed and taken into account in Chapter V. These factors (the attraction of the moon, the ellipticity of the lunar orbit, the oblateness of the earth, and solar perturbations) vary the energy of motion and the shape of the trajectory only slightly. Consequently, in determinations of the point of impact on the moon, the effect of these factors on the nominal initial data and on the moment of entry into the passive part of the trajectory can be taken into account by introducing corrections.

Thus, an approximation technique is worked out, making it possible to determine the moment of entry into the passive part of the trajectory to within about 5 minutes, to determine the initial velocity to within 1 m/sec in magnitude and 0.1° in direction, and to determine the direction of the rocket's radius vector at the end of flight to within about 1°.

*Chapter I*

## *AN ANALYSIS OF LUNAR-FLIGHT CONDITIONS*

### 1.1. EQUATIONS OF THREE-DIMENSIONAL MOTION AND GENERAL DESCRIPTION OF LUNAR-APPROACH TRAJECTORIES

The following fact was established during the course of a general study of moon flights /21/: when evaluating and classifying the various possible shapes of the passive [coasting] part of the trajectory, and also when determining the effect of the scatter of initial data, it is not necessary to take into account all the forces acting. It is sufficient just to consider the principal forces, namely the attractions which the earth and moon, considered to be material points, exert on an object in space. This reduces to a **three-body problem** (earth, moon, and spacecraft). However, the attraction exerted on the earth and moon by the spacecraft has a negligible effect on terrestrial and lunar motion. Consequently, in this case we are dealing with a **restricted three-body problem.** The relative motion of the two attracting masses (earth and moon) thus obeys Kepler's laws. The orbit of the moon about the earth can be taken as circular in this problem.

Therefore, the equations of motion for the passive part of a spacecraft trajectory turn out to be equations of a restricted, circular three-body problem /25/. Let us introduce a **geocentric** coordinate system $xyz$, with its origin at the earth's center, its $xy$ plane coinciding with the moon's orbital plane, and its axes invariably fixed in space. The equations of motion of a spacecraft in this coordinate system will be:

$$\left.\begin{aligned}
&\ddot{x} = -\frac{\mu_1 x}{r^3} + \frac{\mu_2}{\rho^3}(x_1 - x) - \frac{\mu_2 x_1}{a^3},\\
&\ddot{y} = -\frac{\mu_1 y}{r^3} + \frac{\mu_2}{\rho^3}(y_1 - y) - \frac{\mu_2 y_1}{a^3},\\
&\ddot{z} = -\frac{\mu_1 z}{r^3} - \frac{\mu_2 z}{\rho^3},\\
&\frac{dr}{dt} = \frac{x\dot{x} + y\dot{y} + z\dot{z}}{r},\\
&\frac{d\rho}{dt} = \frac{1}{\rho}[(x_1 - x)(\dot{x}_1 - \dot{x}) +\\
&+ (y_1 - y)(\dot{y}_1 - \dot{y}) + (z_1 - z)(\dot{z}_1 - \dot{z})].
\end{aligned}\right\} \qquad (1.1)$$

Here $r$ and $\rho$ designate, respectively, the distances of the spacecraft from the centers of the earth and moon (the quantities which are differentiated with respect to time), $a = 384{,}400$ km is the mean distance between the centers of the earth and moon, $\mu_1$ and $\mu_2$ are the gravitational potentials of the earth and moon, and the letter "L" refers to the lunar coordinates and velocity components.

Using the above equations it is possible to determine (for example, by numerical integration) the flight path corresponding to any initial data. Trajectories which begin at the earth and then, on the first circuit around the earth, enter the moon's sphere of action are called **approach trajectories**. Such trajectories have certain characteristics enabling an evaluation of their basic properties without having to integrate equations (1.1). In /21/ it was pointed out that, when analyzing approach trajectories, the influence of the moon outside its sphere of action and the influence of the earth inside the moon's sphere of action can both be neglected. Consequently, motion along an approach trajectory outside the moon's sphere of action proceeds along a geocentric conic section, while motion inside this sphere of action proceeds along a selenocentric conic section. **A geocentric conic section** here refers to an ellipse, hyperbola, or parabola plotted in geocentric coordinates and having its focus at the earth's center. The **selenocentric coordinate system** and a **selenocentric conic section** are determined in exactly the same way as in the geocentric case.

Accordingly, the following approximate method was developed for calculating approach trajectories section-by-section. The part of the motion up to the moon's sphere of action is first calculated from the initial position of the radius vector $r_1$ of the spacecraft and the velocity $V_1$,* by taking the geocentric integrals of the energy and the areas.

At the point of entry into the moon's sphere of action, the geocentric radius $r_2$** and velocity $V_2$ (geocentric entry data) must be converted into selenocentric coordinates. Thus we obtain the selenocentric position and the selenocentric velocity $V_2 = V_2 - V_L(t_2)$, where $V_L(t_2)$ is the moon's velocity at the moment $t_2$ when the spacecraft enters the moon's sphere of action.

The part of the motion which takes place in the moon's sphere of action is determined by calculating the selenocentric integrals of the energy and areas, in the same way as in the geocentric case. At the point of exit from the moon's sphere of action, the geocentric exit coordinates and the exit velocity $V_3 = V_3' + V_L(t_3)$ are calculated, where $t_3$ is the moment of exit from the moon's sphere of action.† The part of the motion taking place outside the moon's sphere of action is then once again calculated by taking the geocentric integrals of the energy and the areas, with new values of the constants.

Certain results relating to approach trajectories, obtained in /21/, will be useful for the following analysis. Let us now review and supplement these results. First, we consider the scalar difference $\Delta V_1 = V_1 - V_p$, where $V_p = \sqrt{2\mu_1/r_1}$ is the geocentric parabolic velocity of a spacecraft at a distance

* Subscript 1 designates parameters corresponding to the beginning of the passive part of the flight path.

** Subscript 2 designates parameters corresponding to the point of entry into the moon's sphere of action or, in the case of a nonattracting moon, to the end of the passive part of the trajectory.

† Subscript 3 designates parameters corresponding to the point of exit from the moon's sphere of action.

$r_1$ from the earth's center. The amount $\Delta V_1$ by which the initial geocentric velocity exceeds the local parabolic velocity is a basic parameter determining the properties of the approach trajectories.

The initial height $H_1$ above the earth's surface, and the geocentric radius $r_2$ of the point of entry into the moon's sphere of action, on the other hand, are parameters of minor significance. Figure 1.1 shows the curves for a set of approach trajectories, plotted as a function of $\Delta V_1$ /21/. These trajectories correspond to a height $H_1 = 200$ km and a mean geocentric entry radius $r_2 = a$.

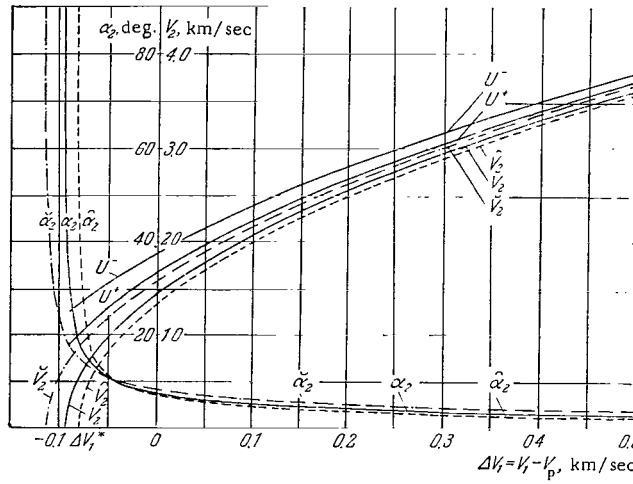


FIGURE 1.1. Trajectory parameters at point of entry into moon's sphere of action, as functions of amount $\Delta V_1$ by which initial velocity exceeds local parabolic velocity. $\check{V}_2$, $\hat{V}_2$ and $\check{\alpha}_2$, $\hat{\alpha}_2$ are end values of geocentric entry velocity $V_2$ and its angle $\alpha_2$ with respect to geocentric entry radius. $U^+$ and $U^-$ are selenocentric entry velocities corresponding to angles $\alpha_1 = \pm 90°$ between directions of initial velocity and initial geocentric radius.

The magnitude $V_2(\Delta V_1)$ of the geocentric entry velocity, according to the energy integral, does not depend on the angle $\alpha_1$ between the initial velocity and the initial radius. However, the angle $\alpha_2$ between vector $V_2$ and the geocentric entry radius $r_2$ does depend on $\alpha_1$. In Figure 1.1 the function $\alpha_2(\Delta V_1)$ is plotted for $\alpha_1 = 90°$, that is, for a horizontal initial velocity. For lower values of $\alpha_1$ the corresponding curves will once again begin at the 90° ordinate, but then will pass everywhere beneath the $\alpha_2(\Delta V_1)$ curve in Figure 1.1.

As $\alpha_1 \to 0$, the curve approaches the sides of the angle formed by the vertical line $\Delta V_1 = \Delta V_{1\,\min}$ and the abscissa axis. Here $\Delta V_{1\,\min}$ is the minimum value of the quantity $\Delta V_1$. For lower values of $\Delta V_1$ the apogee (maximum) radius of the trajectory turns out to be less than the radius of the lunar orbit, so that there is no point on the trajectory with a radius $r_2 = a$.

The curves for $\hat{V}_2(\Delta V_1)$ and $\hat{\alpha}_2(\Delta V_1)$, and for $\check{V}_2(\Delta V_1)$ and $\check{\alpha}_2(\Delta V_1)$, correspond respectively to the values $r_2 = a + \rho_*$ and $r_2 = a - \rho_*$ (where $\rho_*$ is the radius of the moon's sphere of action). These curves show that, for initial velocities not

close to the minimum, the variations in the vector of the geocentric entry velocity will be small in the region $|r_2 - a| < \rho_*$. Therefore, for these initial flight velocities and for fixed values of $r_1$, $V_1$ and $\alpha_1$, as well as of the inclination $i_1$ of the flight plane to the moon's orbital plane, the following approximate assumption may be made: the magnitude and direction of the geocentric entry velocity do not depend on the geocentric radius vector of the point of entry, and they have the average values

$$V_2(r_2) \equiv V_2(a) \text{ and } \alpha_2(r_2) \equiv \alpha_2(a).$$

The position of the entry point will naturally be determined completely by the node longitude $\Omega_1$ and the perigee longitude $\omega_1$ of the geocentric part of the trajectory.

It should be noted that the selenocentric entry velocity is found from the geocentric entry velocity by subtracting the lunar velocity $V_L(t_2)$, which makes an angle close to a right angle with the geocentric entry radius $r_2$. The difference between this angle and a right angle does not exceed the angle between vector $r_2$ and the earth-moon line. The latter angle is small (less than 10°), so that in this approximate analysis the angle between vector $V_L(t_2)$ and the geocentric entry radius may be considered to be a right angle. Moreover, the radius $r_2$ can be replaced in this case by its average value, a vector directed from the center of the earth to the center of the moon. Then, it is obvious that the magnitude and direction of the selenocentric entry velocity $V_2'$ will be the same for all the approach trajectories considered, irregardless of the values of $\Omega_1$ and $\omega_1$.

Consequently, for initial velocities which are not close to the minimum values, the first parts of the selenocentric trajectories will represent nearly parallel lines. The shapes of these trajectories in any selenocentric plane containing the direction $V_2'$ will thus be close to those shown in Figure 1.2. The entry points in this case will obviously be distributed around half the sphere of action of the moon. The selenocentric part of a trajectory in the sphere of action will always be a hyperbola, no matter what the initial data are /19, 22/.

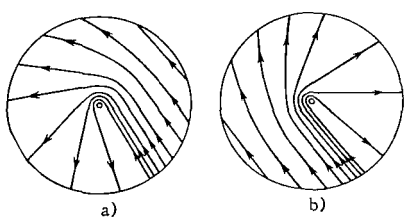


FIGURE 1.2. Selenocentric trajectories in moon's sphere of action, in one of the planes parallel to the vector of the selenocentric entry velocity and passing through the moon's center. Entry points distributed over approximately half the sphere of action.

The angle $\alpha$ between selenocentric entry and exit velocities with equal absolute magnitudes $U$ is a monotonically decreasing function of the distance $d$ from the moon's center to the tangent to the selenocentric trajectory at the point of entry into the moon's sphere of action. The function $\alpha(d)$ is plotted in Figure 1.3 for various values of $U$.

Figure 1.4 shows the curves for approach trajectories tangent to the moon's surface. Inspection of the figure shows that for these trajectories the angle $a$, the distance $d$, and the selenocentric angle $\Phi'$ (through which the selenocentric radius vector of the spacecraft turns during the time of motion inside the moon's sphere of action) are all decreasing functions of the velocity $U$.

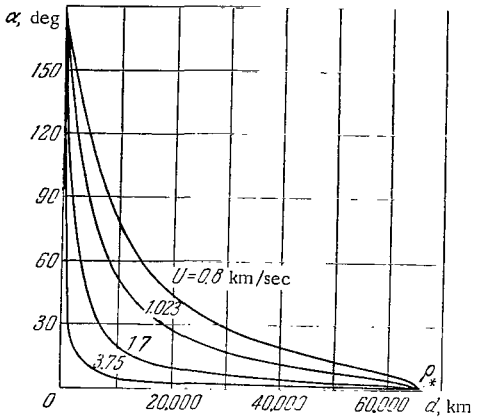


FIGURE 1.3. Angle between tangents to hyperbola at points of entry into and exit from moon's sphere of action, as function of distance $d$ from moon's center to tangent to selenocentric trajectory at entry point. $U$ is magnitude of selenocentric entry velocity.

Let us now express the quantity $U = |\boldsymbol{V}_2'|$ in terms of the initial data $r_1$, $V_1$, $i_1$, and $\alpha_1$. We first write the components of velocity $\boldsymbol{V}_2'$ along the selenocentric axes $\xi$, $\eta$, and $\zeta$. These axes are oriented, respectively, toward the earth's center, opposite to the direction of the moon's velocity, and along the normal to the lunar orbit (Figure 1.5). The components have the approximate values

$$-V_2 \cos \alpha_2, \quad V_L - V_2 \sin \alpha_2 \cos i_1, \quad -V_2 \sin \alpha_2 \sin i_1,$$

where $V_2$ is the magnitude of the geocentric entry velocity, and $\alpha_2$ is the angle between this velocity and the geocentric entry radius $r_2$. Using the geocentric integral of the areas

$$r_2 V_2 \sin \alpha_2 = r_1 V_1 \sin \alpha_1, \tag{1.2}$$

we obtain

$$U^2 = V_L^2 + V_2^2 - 2 \frac{r_1}{r_2} \cdot V_L V_1 \cos i_1 \sin \alpha_1, \tag{1.3}$$

where $V_2$, according to the energy integral, does not depend on $\alpha_1$.

This expression shows that the magnitudes $U^+$ and $U^-$ corresponding to $\alpha_1 = \pm 90°$ (and thus to $i_1$ values of 0° and 180°) are the limiting values of the range of all possible $U(i_1, \alpha_1)$. The functions $U^+(\Delta V_1)$ and $U^-(\Delta V_1)$ were plotted in Figure 1.1. This figure shows that the difference $U^- - U^+$ is small and diminishes rapidly with an increase in $\Delta V_1$.

For the approach trajectories, it follows from area integral (1.2) that the transversal component of the geocentric entry velocity is small:

$$V_{2\tau} \leqslant \frac{r_1}{r_2} V_1 \approx 0.2 \text{ km/sec}, \quad \text{for} \quad \Delta V_1 < 0.5 \text{ km/sec}$$

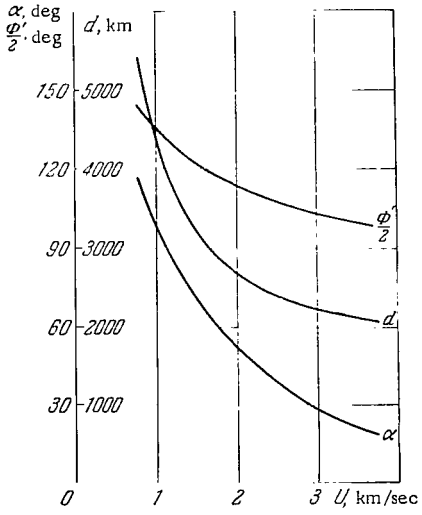


FIGURE 1.4. Characteristics of trajectories passing near lunar surface: $\Phi'$ is selenocentric angle traversed by spacecraft inside sphere of action, $\alpha$ is angle between directions of selenocentric entry and exit velocities, $U$ is magnitude of both these velocities, and $d$ is distance from moon's center to tangent to selenocentric trajectory at entry point.

(since the ratio $r_1/r_2$ is of the same order as the ratio of the earth's radius to the earth-moon distance, namely 1/60, while $V_1$ is of the order of 10 or 11 km/sec). This means that the pencil of selenocentric entry velocities (Figure 1.5) for any approach trajectories will lie within a quite narrow cone (the sine of angle $OA_1O_1$ in the figure does not exceed 0.2).

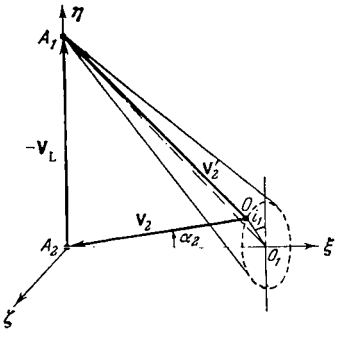


FIGURE 1.5. Relation between geocentric ($V_2$) and selenocentric ($V_2'$) entry velocities in three-dimensional space. A cone of entry velocities is obtained for different angles $i_1$.

The curves in Figure 1.6 show the flight times required to reach the lunar orbit, calculated assuming an initial height of 200 km. The duration of the flight is found to decrease rapidly as the initial velocity is raised above its minimum value. The curves corresponding to vertical ($\alpha_1 = 0$) and horizontal ($\alpha_1 = \frac{\pi}{2}$) initial velocities are practically identical. The flight time depends only slightly on the initial height $H_1$. For example, when $H_1$ is increased from 200 to 1000 km, the flight duration is reduced by only about 7 minutes (less than 0.5%).

The flight duration $T_{1,2}$ plotted in Figure 1.6 pertains to an approach along the ascending branch of the trajectory.

For $\Delta V_1 < 0$, that is, for elliptical initial velocities, an approach along the descending branch of the trajectory is still possible. The corresponding flight durations up to the moon's orbit can be calculated accurately enough by subtracting the flight time $T_{1,2}$ from the period

$$T_0 = 2\pi \frac{a^{3/2}}{\sqrt{\mu_1}}, \tag{1.4}$$

where $a = \left[-\frac{\Delta V_1}{V_p}\left(2 + \frac{\Delta V_1}{V_p}\right)\right]^{-1} \cdot \frac{r_1}{2}$ is the semimajor axis of the ellipse.

In the three-dimensional problem of achieving lunar impact, just as in the two-dimensional problem, the possibility of approaching the moon either via the ascending branch of the trajectory or via the descending branch results in the creation of two classes of solutions. In contrast to the classes of two-dimensional solutions, however (see Supplement), these classes will not be divided into subclasses according to the direction of motion around the earth.

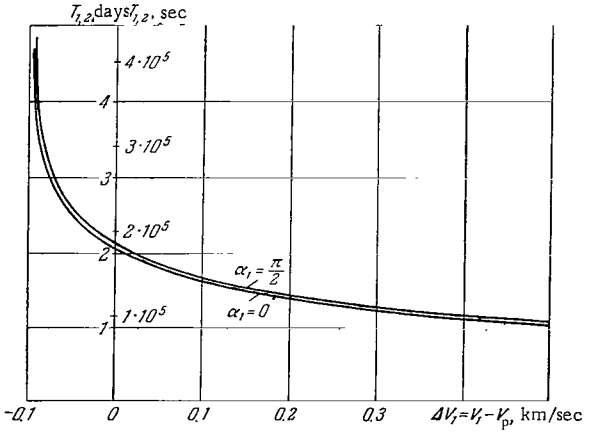


FIGURE 1.6. Flight time to lunar orbit (minimum for vertical initial velocity, and maximum for horizontal initial velocity).

Just as in the two-dimensional case, approach trajectories along the ascending branch will be of greater interest, since for these trajectories the effect of initial-data scatter will be less (especially on the velocity) and the flight time will be shorter. Consequently, in the following only this class of trajectories will be considered.

It is less important, by the way, to take into account the effect of the moon when determining the initial data for impact trajectories along the ascending branch. Numerical integration of equations (1.1) indicates the following: even for minimum initial flight velocities in the horizontal direction and for a zero slope of the trajectory with respect to the moon's orbital plane, in which case (according to expression (1.3)) the selenocentric velocities are a minimum and the moon's effect is especially great, trajectories directed toward the center of the moon (when the lunar

attraction is not taken into account) will deviate from the center by only about 100 km when this attraction is considered. Therefore, in the following, when analyzing all the various nominal impact trajectories (that is, trajectories passing through the moon's center), the lunar attraction will not be taken into account.

## 1.2. LUNAR IMPACTS FROM HIGH LATITUDES

Moon shots differ essentially from similar terrestrial missions. This is because the target does not participate in the diurnal motion of the earth, together with the launch point, so that the relative position of target and launch point varies continuously with time. In order to see how this variation takes place, let us find the angle $\Theta$ between the equatorial plane E and the plane $\Pi'$ of the lunar orbit.

Plane $\Pi'$ makes a constant angle $i \approx 5°9'$ with the ecliptic plane $\Pi$ (Figure 1.7). The line of intersection between these planes (the line of nodes) rotates in a clockwise direction through the ecliptic plane (as viewed from the north pole); one complete rotation takes 18.6 years.* Let us designate $\Omega$ as the longitude of the ascending node of the lunar orbit, reckoned from the vernal equinox $\gamma$. The spherical triangle $x\gamma\Omega$ in the figure will then have a side $\Omega$ and angles $\varepsilon_0$ and $i$, where $\varepsilon_0 \approx 23°27'$ is the inclination of the ecliptic to the equator. Thus we obtain the following formula for determining $\Theta$:

$$\cos\Theta = \cos\varepsilon_0 \cos i - \sin\varepsilon_0 \sin i \cos\Omega. \qquad (2.1)$$

It follows from this formula that the angle $\Theta(\Omega)$ fluctuates between a minimum $\Theta(180°) = \varepsilon_0 - i = 18°18'$ and a maximum $\Theta(0) = \varepsilon_0 + i = 28°36'$. Since on 1 January 1950 the longitude $\Omega$ was 12.1°, formula (2.1) shows that $\Theta$ passed through a minimum (18°18') late in December 1959, and then began to increase gradually, attaining a maximum after 9.3 years. Because of the gradual nature of the change in $\Theta$, we can neglect its variability during the course of a flight along the trajectories considered. In subsequent calculations, we assume that $\Theta = 18°20'$.

Consequently, the moon will be considered to move in a plane inclined to the equator by a constant angle $\Theta$, completing one circuit every 27.32 days. The initial point of the passive part of the trajectory moves parallel to the equator at a latitude $\psi_0$. The angle between the geocentric radius of the launch point and the moon's orbital plane will thus vary from $\alpha_0 = \psi_0 - \Theta$ to $\beta_0 = \psi_0 + \Theta$. In the following it will be assumed, for definiteness, that the latitude of the initial point $\psi_0 > 0$. At the same time, the flight path is taken to be outside the plane of the lunar orbit (so that $\alpha_0 > 0$). The latitude and longitude of Baikonur,** a well-known space port in the northern hemisphere, will be used as the coordinates of the launch point:

$$\psi_0 = 47°, \quad \lambda_0 = 65°.$$

* Kulikovskii, P. G., Spravochnik lyubitelya astronomii (Amateur Astronomer's Handbook). — Fizmatgiz. 1961.

** Pravda No. 128 (11068). 1 June 1961.

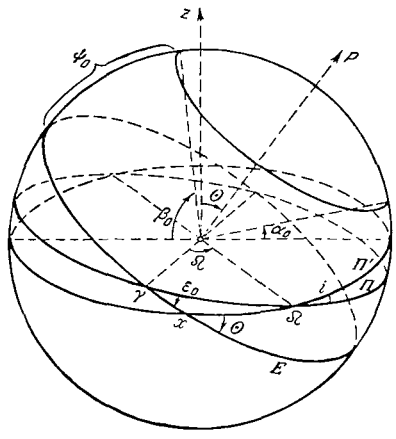


FIGURE 1.7. Position of lunar orbital plane Π' relative to equatorial plane E and ecliptic plane Π.

Let us now consider the passive part of the flight path, which begins at an angle $\theta_1$ to the horizon, with an initial velocity $V_1$ and a height $H_1$ (obviously, $\theta_1 = 90° - \alpha_1$). The length of the active part is here assumed to be zero (later this restriction will be lifted).

Let us consider trajectories having elliptical initial velocities, directed parallel to the plane of the horizon at the launch point (Figure 1.8). If $V_1 \to V_p$, the trajectories will be stretched out considerably along the geocentric radius of the impact point. For such trajectories, the angle between the major axis and the radius equal to the distance to the moon will be less than 15° (this is easily demonstrated).

The minimum angle between the direction of the initial geocentric radius and the moon's orbital plane cannot be less than $\alpha_0$ (see Figure 1.8). Moreover, the major axis of the conic section is oriented along this radius. Thus it is clear that, for elliptical initial velocities in the horizontal direction, a spacecraft will intersect the moon's orbital plane before it has covered the distance from the earth to the moon, making a lunar impact impossible. The reason for this is as follows: for low values of $\Delta V_1$ and low $\theta_1$ (the inclination of the initial-velocity vector to the local horizon), the trajectory of a spacecraft will be bent too much as a result of the earth's attraction.

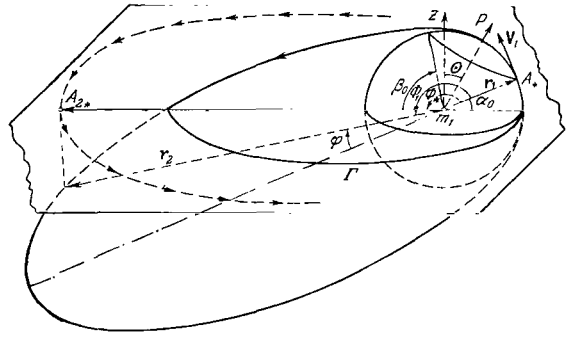


FIGURE 1.8. Position of set of elliptical trajectories with different azimuths relative to lunar orbit. Initial geocentric velocity $V_1$ has same amplitude in all cases and is horizontal.

The curvature of the trajectory (and thus also the angle $\Phi_1$ between the initial radius $r_1$ and the radius $|r_2| = a$, where $a$ is the mean distance between the earth and the moon) can be reduced in either of two ways: by increasing the initial velocity or by increasing the angle $\theta_1$ of inclination of the

initial-velocity vector to the local horizon. Obviously, both of these ways will be associated with additional energy expenditures, in comparison with the two-dimensional case. In the first case greater acceleration of the spacecraft will be necessary, and in the second case the gravity component in the direction of the tangent to the trajectory will have to be increased. For specified values of $H_1$, $V_1$, and $\theta_1$, and for an initial radius $|r_1| = m_1A_*$ (Figure 1.8) forming a minimum angle $\alpha_0$ with the moon's orbital plane, it is possible to construct a surface which will contain the trajectories corresponding to the given $V_1$ and $\theta_1$, and to different azimuths. This surface is symmetrical with respect to the line $m_1A_*$.

Let us consider the line of intersection $\Gamma$ of this surface with the moon's orbital plane. For quite low values of $V_1$ and $\theta_1$, all of line $\Gamma$ will be located inside the moon's orbit. For values of $V_1$ and $\theta_1$ corresponding to an angle $\Phi_1 = \Phi_* = \pi - \alpha_0$, this line will be tangent to the lunar orbit at a point $A_2$, where the orbit intersects the meridian plane of initial point $A_*$; in principle, lunar impact is possible for this case. However, in practice it turns out to be unfeasible, since at the moment when the **advance point** [see p. 19] passes through $A_2$, the launch point will not in general be at point $A_*$.

For larger values of $V_1$ and $\theta_1$ (that is, as $\Phi_1$ is reduced below $\Phi_*$), there is an ever-increasing interval on the lunar orbit (with its middle point at $A_2$) from which the moon can be reached. Let us call this region the **striking interval.** When the angular size of the striking interval becomes equal to the geocentric angle traversed by the moon in one day (about 13.2°), there will obviously be at least one day during each sidereal month on which it is possible to launch a rocket and achieve lunar impact. Thus, reaching the moon becomes feasible.

With a further increase in $V_1$ and $\theta_1$ (that is, as $\Phi_1$ is reduced to $\Phi^* = \pi - \beta_0$), the striking interval grows until it becomes a complete circle, and moon launches become possible on every day of the month.

The above-mentioned angle $\Phi$ between the initial and final geocentric radii of the passive part of the flight may be called the **passive angular range of the flight,** by analogy with similar terrestrial missions. However, whereas for a terrestrial mission larger angular ranges are more difficult to attain than smaller ranges, for a moon shot the opposite is true: it is more difficult to obtain smaller angular ranges than larger ones.

The passive angular range $\Phi_1$ of the flight depends on the height $H_1$ of the end of the active part, as well as on $V_1$ and $\theta_1$. However, the effect of the height is small, and the calculations will be carried out only for $H_1 = 300$ km and $H_1 = 1000$ km, assuming that $-0.1 \text{ km/sec} \leqslant \Delta V_1 \leqslant 0.5 \text{ km/sec}$, as was assumed in /21/. Here $\Delta V_1$ is the amount by which the initial velocity exceeds the local parabolic velocity $V_p$.

Calculations will be made only for the ascending branches of the trajectories. Therefore, the angle $\Phi_1$ will be single-valued for known values of $\Delta V_1$, $\theta_1$, $r_1$, and $r_2$, for both hyperbolic and elliptical initial velocities. Let us assume that

$$\Delta\beta_1 = \frac{\Delta V_1}{V_p}\left(2 + \frac{\Delta V_1}{V_p}\right), \quad \beta_1 = 1 + \Delta\beta_1 = \left(\frac{V_1}{V_p}\right)^2. \tag{2.1'}$$

From the theory of conic sections we have:

$$
\left.
\begin{aligned}
p &= 2r_1\beta_1\cos^2\theta_1,\\
a &= -\frac{r_1}{2\Delta\beta_1},\\
e^2 &= 1-\frac{p}{a},\\
\cos v_1 &= \frac{1}{e}\left(\frac{p}{r_1}-1\right),\\
\cos v_2 &= \frac{1}{e}\left(\frac{p}{r_2}-1\right),\\
\Phi_1 &= v_2 - v_1,\\
\beta_1 &= \left(\frac{V_1}{V_p}\right)^2,\\
\Delta\beta_1 &= \beta_1 - 1.
\end{aligned}
\right\} \qquad (2.2)
$$

Here, $V_1 = V_p + \Delta V_1$ is the initial velocity, $p_1$, $a_1$, and $e_1$ are the parameter, semimajor axis, and eccentricity of the conic section, and $v_1$ and $v_2$ are the true anomalies of the beginning and end of the trajectory.

The curves for $\Phi_1(\Delta V_1)$ have been plotted in Figure 1.9. The solid curves pertain to $H_1 = 300$ km and the dashed curves to $H_1 = 1000$ km, for $\theta_1 = 0°$, 5°, ... 40°. Clearly, the effect of a variation in the initial height $H_1$ is only slight, whereas each 5° change in $\theta_1$ causes an almost equidistant 10° shift in the curve for $\Phi_1(\Delta V_1)$. On the other hand, for a specified value of $\theta_1$, a 10° variation of the passive angular range $\Phi_1$ (for velocities not close to the minimum) corresponds to a 200 or 300 m/sec change in $\Delta V_1$.

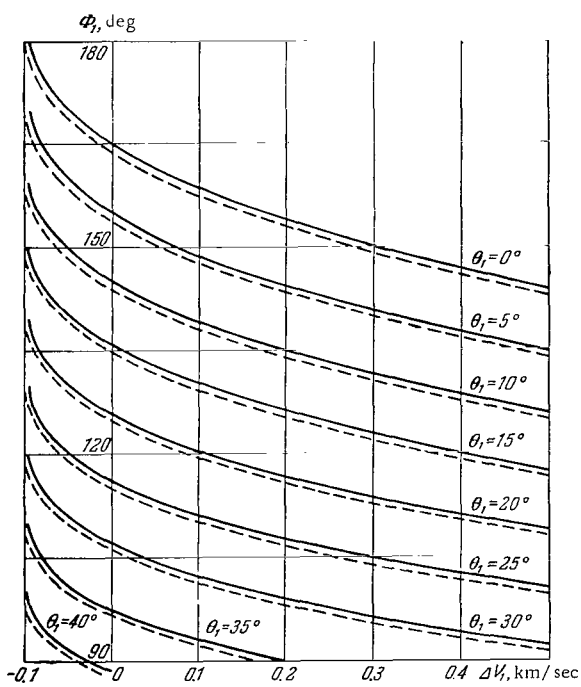


FIGURE 1.9. Passive angular range $\Phi_1$ of moon flight as function of $\Delta V_1$ (amount initial velocity exceeds local parabolic), for various angles of elevation $\theta_1$.

In the subsequent analysis it will be necessary to know how the quantity $\beta_1 = (V_1/V_p)^2$ varies with $\theta_1$, for various constant angular ranges $\Phi_1$. Although this relation can be found from calculations based on Figure 1.9, it will be more convenient here to use the analytical formula

$$\left.\begin{aligned} \Delta\beta_1 &= \frac{\cos^2\left(\frac{\Phi_1}{2}+\theta_1\right) - \nu\cos^2\theta_1}{\nu\cos^2\theta_1 - \cos(\Phi_1+\theta_1)\sqrt{\cos\theta_1}}, \\ \beta_1 &= 1 + \Delta\beta_1. \end{aligned}\right\} \qquad (2.3)$$

where $\nu = \frac{r_1}{r_2} \approx 0.018$ (a small quantity) is the ratio of the initial radius to the final radius.

Figure 1.10 shows the curves for $\bar{v}^2 = \frac{V_1^2}{V_p^2} = \beta_1(\theta_1, \Phi_1)$ for $H_1 = 1000$ km and for various $\Phi_1$. The values of the latter angle are shown next to the corresponding curves. For $H_1 = 300$ km the curves can be obtained from the 1000-km curves by shifting them slightly along the ordinate axis.

As the initial velocity approaches the minimum value, the tangents to the curves in Figure 1.10 become parallel to the abscissa axis, while the tangents in Figure 1.9 become parallel to the ordinate axis. This makes it more difficult to determine the points on the curves corresponding to the lowest velocities. Let us derive a formula making it possible to determine, for different angles $\theta_1$, the minimum initial velocities required to obtain apogee radii $r_2 = |F_0A_2|$ equal to the distance from the earth to the moon (Figure 1.11).

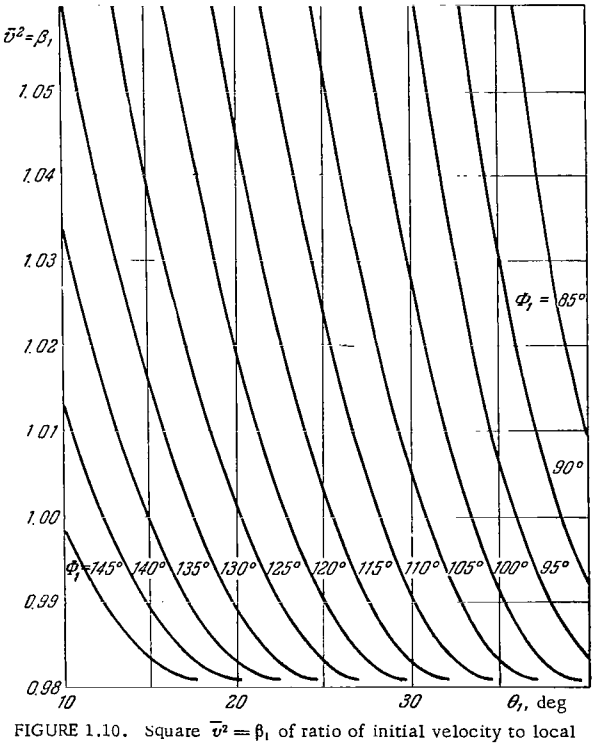


FIGURE 1.10. Square $\bar{v}^2 = \beta_1$ of ratio of initial velocity to local parabolic, as function of initial angle of elevation, for various angular ranges $\Phi_1$ of passive part of moon-flight trajectory.

Because of the properties of the tangent to an ellipse, the angle $F_0A_1F$ (where $F$ is the second focus of the ellipse) of triangle $A_1FF_0$ (Figure 1.11) will be equal to $\pi - 2\alpha_1$, if $\alpha_1 = \frac{\pi}{2} - \theta_1$. In addition, it is easy to see that

$$FA_1 = 2a - r_1, \quad FF_0 = 2ae,$$

where $a$ is the semimajor axis and $e$ is the eccentricity. Now let us express side $FF_0$ of triangle $A_1FF_0$ as

$$4a^2e^2 = (2a - r_1)^2 + r_1^2 + 2(2a - r_1) r_1 \cos 2\alpha_1.$$

Then, since $e = \frac{r_2 - a}{a}$ (see Figure 1.11), we can substitute this expression into the above formula to obtain:

$$a = \frac{1}{2} \frac{r_2^2 - r_1^2 \sin^2 \alpha_1}{r_2 - r_1 \sin^2 \alpha_1}. \tag{2.4}$$

Next, from formulas (2.2) through (2.4), we obtain:

$$\beta_{1min} = \frac{1 - \nu}{1 - \nu^2 \sin^2 \alpha_1}, \quad \cos \Phi_{max} = 1 - \frac{2(1 - \nu^2) \sin^2 \alpha_1}{1 - \nu(2 - \nu) \sin^2 \alpha_1},$$

where $\nu = \frac{r_1}{r_2}$. These expressions can also be put into the following form, which is more convenient for calculation:

$$\Delta\beta_{1\,min} = -\nu \frac{1 - \nu \sin^2 \alpha_1}{1 - \nu^2 \sin^2 \alpha_1}, \tag{2.5}$$

where $\Delta\beta_{1\,min} = \beta_{1\,min} - 1$, and

$$\sin \frac{\Phi_{max}}{2} = \frac{(1 - \nu) \sin \alpha_1}{\sqrt{1 - \nu(2 - \nu) \sin^2 \alpha_1}}. \tag{2.6}$$

These formulas make it possible to calculate, from $\theta_1 = \frac{\pi}{2} - \alpha_1$, the minimum initial velocity $V_{1\,min}$ and the maximum angle $\Phi_{max}$ attainable for a given $\theta_1$.

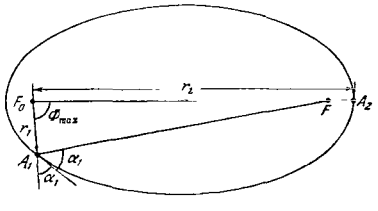


FIGURE 1.11. Minimum-energy trajectory required to attain specified radius $r_2$, for given $r_1$ and $\alpha_1$.

It follows from formulas (2.1') and (2.5) that $\Delta V_{1\,min}(\theta_1)$ is a small quantity which is of the same order as $\frac{V_p}{2}\nu$. Moreover, its relative variation will also be small, of the same order as $\nu\cos^2\theta_1$. This was to be expected from Figure 1.11, since the variations of the major axis of the minimum ellipse corresponding to changes in $\theta_1$ do not exceed $r_1$ (that is, they are relatively small).

In addition, if we set $\sin^2\alpha_1 = 1$ in the denominator of (2.6), it follows that

$$\sin \frac{\Phi_{max}}{2} \leqslant \sin \alpha_1 \text{ for } 0 \leqslant \alpha_1 \leqslant \frac{\pi}{2} \text{ (that is, for } \frac{\pi}{2} \geqslant \theta_1 \geqslant 0).$$

If we consider velocities other than minimum, it is easy to verify that the specified radius $r_2$ of the conic section will be reached for an angle $\Phi_1 < \Phi_{max}$ (since $\Phi_{max}$ corresponds to the minimum velocity). Hence, the following simple inequality will always be valid:

$$\sin \frac{\Phi_1}{2} \leqslant \sin \alpha_1. \tag{2.7}$$

For the minimum velocities the equality sign corresponds to $\alpha_1 = 0$ and $\alpha_1 = \frac{\pi}{2}$; for higher velocities it corresponds only to $\alpha_1 = 0$ $\left(\theta_1 = \frac{\pi}{2}\right)$. Inequality (2.7) can be used to evaluate the maximum attainable values of $\Phi_1$.

Let us now determine what the conic section having fixed values of $r_1$, $r_2$, $V_1$ and $\theta_1$ (that is, having a fixed angular range $\Phi_1$) will be, for which a lunar impact takes place. Clearly, a spacecraft will not impact on the moon at the point $A_2^0$ where the moon was when the rocket was launched (Figure 1.12). Rather, it will reach the moon at a point $A_2$ which is further ahead (the advance point,* to which the moon has moved during the time the spacecraft has covered the distance $A_1A_2$). The flight time $T_{1,2}$ corresponding to the given initial data $r_1$, $r_2$, $\Delta V_1$, and $\theta_1$ is determined unambiguously. Consequently, if these initial data are specified, the advance point where lunar impact will take place will move along ahead of the moon at a constant speed, its angular distance from the moon being $\omega T_{1,2}$, where $\omega$ is the moon's angular velocity of revolution.

Since $r_1$ and $\Phi_1$ are specified, the geometric locus of points from which a lunar impact is possible for the initial data $r_1$, $r_2$, $\Delta V_1$, $\theta_1$ should obviously lie along a circle of radius $r_1 \sin \Phi_1$. This circle will be the line of intersection between a geocentric sphere of radius $r_1$ and a right circular cone whose axis always joins the earth's center $m_1$ to the advance point $A_2$, while the generatrices make an angle $\Phi_1$ with this axis.

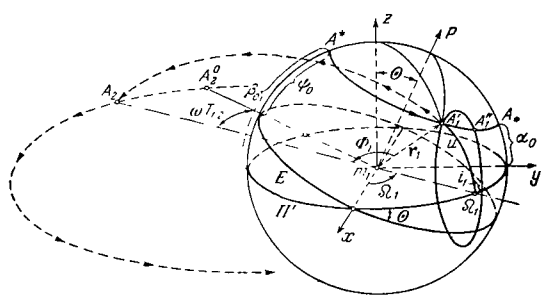


FIGURE 1.12. Geocentric trajectories of launch point, spacecraft, and moon.

The planes of all the trajectories with the given values of $r_1$, $r_2$, $\Delta V_1$, and $\theta_1$ pass through the initial point $A_1$, the advance point $A_2$, and the earth's center $m_1$. Therefore, all these planes will intersect the moon's orbital

* [Also known as the set-forward point or predicted point.]

plane along the line $m_1A_2$. Let us take the plane of the lunar orbit as a base plane for determining the Keplerian elements of the flight paths to the moon. Then, the line $m_1A_2$ will be the line of nodes for all the impact trajectories. Its position can be determined from the longitude $\Omega_1$ of the node opposite the advance point. This node longitude is reckoned from the line of intersection between the plane of the lunar orbit and the equator, where the moon passes from the southern to the northern hemisphere. In Figure 1.12 this line lies along the $x$ axis. In accordance with the definition of $\Omega_1$, the inclination $i_1$ of the trajectory plane to the base plane will be assumed to vary from $-180°$ to $+180°$.

Let us now define the following two quantities in the usual way: the longitude $\omega_1$ of the perigee of the geocentric part of the trajectory, and the true anomaly $v$ of the initial point $A_1$ of the passive part, relative to the perigee. We can then write $v+\omega_1=u$, where $u$ is the argument of the latitude of the initial point. From Figure 1.12 it is clear that $u=180°-\Phi_1$. The circle of initial points for trajectories with angular range $\Phi_1$ will be called the $u$-circle, for short.

Let us next take into account the condition that the launch point lies at some given latitude $\psi_0$ and that this point moves along the parallel with the earth's diurnal velocity of rotation. It is obvious that the initial points of the impact trajectories determined by parameters $r_1$, $\Delta V_1$, $\theta_1$, and $\psi_0$ must lie on both the $u$-circle and the $\psi_0$ parallel. There may be two (intersecting circles), one (tangent circles), or none (circles have no common points) such points.

Due to the monthly motion of the moon, the center of the $u$-circle moves uniformly on a sphere, along the great circle of the base plane. The parallel of the launch point, however, does not change its position in absolute space (Figure 1.12). Consequently, for $u<\alpha_0$, where $\alpha_0=\psi_0-\Theta$ (that is, for quite high values of $\Phi_1$), the $\psi_0$ parallel and the $u$-circle do not have any common points. When the latitude argument $u$ is in the interval $\alpha_0<u<\beta_0$, however, where $\beta_0=\psi_0+\Theta$, there will be a portion of the $\psi_0$ parallel along which, for different $\Omega_1$ close enough to 90°, intersection between the $\psi_0$ parallel and the $u$-circle is possible. Let us call this interval the **launch interval**. As $u\to\alpha_0$ this interval narrows down to point $A_*$ (corresponding to tangency of curve $\Gamma$ to the lunar orbit in Figure 1.8). As $u\to\beta_0$ it increases until it covers the entire $\psi_0$ parallel, so that its ends converge at point $A^*$, which is opposite to point $A_*$ in Figure 1.12.

When the latitude argument $u$ lies in the range $\beta_0<u<\pi-\beta_0$, the $u$-circle will obviously intersect the $\psi_0$ parallel twice. This will be the case, no matter what the position $\Omega_1$ of the line of nodes (that is, no matter what the position of the advance point). In this case the launch interval covers the entire parallel.

When the inequality

$$\pi-\beta_0<u<\pi-\alpha_0$$

is satisfied, a forbidden interval exists at the $\psi_0$ parallel on both sides of point $A^*$, within which there can be no initial points for angles $\Omega_1$ quite close to 90°. As $u\to\pi-\beta_0$, this interval narrows down to point $A^*$; as $u\to\pi-\alpha_0$, it increases to include the whole parallel, so that its ends converge at point $A_*$. Correspondingly, the launch interval is reduced from the entire parallel down to nothing.

Finally, for $u > \pi - \alpha_0$, there is no point of intersection between the parallel and the $u$-circle and no launch interval exists.

## 1.3. LUNAR-IMPACT TRAJECTORIES STARTING FROM A GIVEN LATITUDE

As mentioned in §1.2, for $u > \alpha$ a lunar impact is possible in practice only when the striking interval on the moon's orbit is so large that the advance point lies within it for at least one sidereal day. Obviously, in this case there will always be some day during the sidereal month on which the launch point, in the course of its diurnal motion, passes through one or two points common to the $\psi_0$ parallel and the $u$-circle. On this day a lunar impact will be practicable for the given initial data $r_1$, $V_1$, and $\theta_1$. If the advance point passes through the striking interval on the lunar orbit on two days, then on each of these days there will be a moment when the launch point passes through a point common to the $\psi_0$ parallel and the $u$-circle, so that impact is possible, etc. Finally, for $\Phi_1 \to \pi_1 - \beta_0$, the striking and launch intervals both reach 360° and impacts are possible every day.

Let us illustrate how, for the range $\alpha_0 < u < \beta_0$, points which are also on the $u$-circle can appear upon and move along a launch interval stationary in $xyz$ space and pertaining to the $\psi_0$ parallel. For $\Omega_1 = -90°$ and $\alpha_0 < u < \beta_0$, there will evidently be no such points. However, as $\Omega_1$ is increased to some value $\Omega_1 = \Omega_*'$, the $u$-circle in question touches the $\psi_0$ parallel at some point $A_*'$ (Figure 1.13). For values of $\Omega_1$ in the range $\Omega_*' < \Omega_1 < \Omega_*''$, there will be two points $A_1'$ and $A_1''$ at which this $u$-circle intersects the $\psi_0$ parallel. For low values of $(\Omega_1 - \Omega_*') > 0$, intersection points $A_1'$ and $A_1''$ will be located along the $u$-circle, on opposite sides of point $A_*'$. Then, as $\Omega_1$ is increased further, the movable point $A_1'$ reverses its direction of motion at position $A_\kappa'$. Therefore, this point begins to move toward the same side as point $A_1''$, so that at $\Omega_1 = 90°$ these two points will be on the same side of $A_*'$ (Figure 1.13).

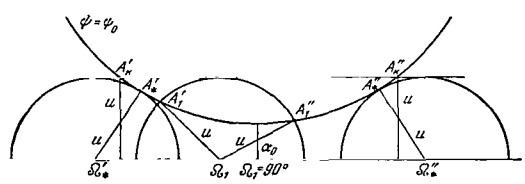


FIGURE 1.13. Terminal and intermediate positions of $u$-circle of equal angular ranges, relative to $\psi_0$ parallel.

As $\Omega_1$ increases above $\Omega_*'$, the distance between points $A_1'$ and $A_1''$ increases monotonically, reaching a maximum at $\Omega_1 = 90°$. Then, this distance decreases monotonically, until at $\Omega_1 = \Omega_*''$ it is reduced to zero at a point $A_*''$, symmetric to point $A_*'$ (relative to the meridian), for which $\Omega_1 = 90°$. Here, point $A_1''$, before merging with point $A_1'$, reverses its direction of motion at point $A_\kappa''$, analogously to the motion of point $A_1'$ near point $A_\kappa'$. The end points of the launch interval ($A_\kappa'$ and $A_\kappa''$) will obviously be the points of

intersection of the $\psi_0$ parallel with the small circle parallel to the base plane and constantly touching the $u$-circle.

The motion of points $A_1'$ and $A_1''$ with an increase in $\Omega_1$ is easy to calculate. Figure 1.14 shows the spherical right triangle $P\Omega_1 y$, in which the vertex $P$ is the pole and the sides are $= 90° - \Theta$ and $\Omega_1 y = 90° - \Omega_1$. From the figure we find that:

$$\left.\begin{aligned} \sin\lambda_{\Omega} &= -\frac{\cos\Omega_1}{\sin m}, \\ \cos\lambda_{\Omega} &= \frac{\sin\Omega_1 - \sin\Theta\cos m}{\cos\Theta\sin m}, \end{aligned}\right\} \tag{3.1}$$

where $\lambda_{\Omega}$ is the angular distance between the meridians of the $y$ axis and the line of node $\Omega_1$. Obviously, the directions $PA_1'$ and $PA_1''$ are symmetric about the great-circle arc $P\Omega_1$ and they form angles $\sigma$ and $-\sigma$ with it. In order to determine angles $\lambda$ and $\sigma$, let us consider the side $m = P\Omega_1$ of triangle $P\Omega_1 y$:

$$\cos m = \sin\Theta\sin\Omega_1. \tag{3.2}$$

Now, from triangle $A_1'P\Omega_1$, let us use the law of cosines to find the angle $\sigma$ (in the first or second quadrant) and angles $\lambda'$ and $\lambda''$:

$$\left.\begin{aligned} \cos\sigma &= \frac{\cos u - \cos m\sin\psi_0}{\sin m\cos\psi_0}, \\ \lambda' &= \lambda_{\Omega} - \sigma, \\ \lambda'' &= \lambda_{\Omega} + \sigma. \end{aligned}\right\} \tag{3.3}$$

The difference $\Delta\lambda_{11} = \lambda'' - \lambda' = 2\sigma$ is obviously the angular distance between the meridians of points $A_1'$ and $A_1''$.

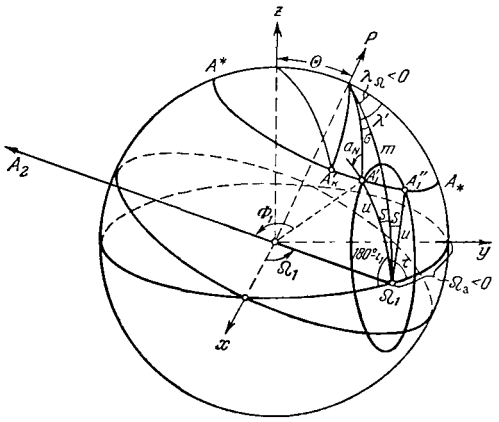


FIGURE 1.14. Spherical angles for calculating parameters of flight path to moon.

Figure 1.15 ($M_1N_1$ curves) shows $\lambda'$ and $\lambda''$ as functions of $\Omega_1$, for the case when $\Phi_1 = 150°$ (that is, for $u = 30°$). The quantity $\Delta\lambda_{II}$ ($\Omega_1$) gives us an idea of the **interlaunch time**, which is the time required for the launch point $A_1$ to traverse interval $A_1'A_1''$ in the course of its diurnal rotation.

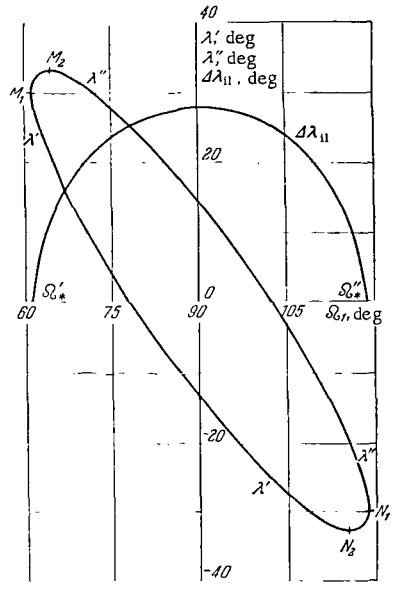


FIGURE 1.15. Variation of launch-interval limits $\lambda'$ and $\lambda''$ and angular size $\Delta\lambda_{II}$ of interlaunch interval, with variation in node longitude $\Omega_1$ of trajectory, for specified angular range of flight.

The interlaunch time can be obtained in hours simply by dividing $\Delta\lambda_{II}$ by 15° (without taking into account the time variation of $\Omega_1$). If the variation $\Omega_1(t)$ is allowed for, the interlaunch time will change by an amount of the order of the ratio of a day to a month (that is, by 4%), for values of $\Omega_1$ not close to $\Omega_*'$ and $\Omega_*''$ (near these values the changes may be greater).

The range ($\Omega_*'$, $\Omega_*''$) obviously corresponds to the striking interval, while the range ($\lambda_\kappa'$, $\lambda_\kappa''$) between the ordinates of points $M_2$ and $N_2$ (that is, between the extreme values of functions $\lambda'(\Omega_1)$ and $\lambda''(\Omega_1)$) corresponds to the launch interval. The region between the ordinates of points $M_1$ and $N_1$ constitutes the basic part of the launch interval. Within this region points $A_1'$ and $A_1''$ move in the same direction as $\Omega_1$ varies, while outside it they move in opposite directions.

Let us calculate the striking interval for different angular flight ranges $\Phi_1$. From the condition of tangency we have (Figure 1.14):

$$\sigma = 0, \quad m = 90° + u - \psi_0.$$

Accordingly, from (3.2) we obtain

$$\left.\begin{aligned} \sin \Omega_{1\,\text{lan}} &= \frac{\sin(\psi_0 - u)}{\sin \Theta}, \\ \Delta\Omega_1 &= 2\left(\frac{\pi}{2} - \Omega_{1\,\text{lan}}\right), \\ u &= \pi - \Phi_1. \end{aligned}\right\} \tag{3.4}$$

where $\Delta\Omega_1$ is the size of the striking interval.

In order to calculate the size $\Delta\lambda_L$ of the launch interval as a function of $\Phi_1$, let us first find the angle $\lambda'_K = \lambda(A'_K)$. When point $A'_1$ coincides with point $A'_K$, the sides of spherical triangle $A'_K zP$ will be equal (Figure 1.14):

$$zA'_K = 90° - u, \quad zP = \Theta, \quad PA'_K = 90° - \psi_0.$$

Therefore,

$$\lambda'_K = 180° - \triangle A'_K Pz$$

and according to the law of cosines we have

$$\cos \lambda'_K = \frac{\cos\Theta \sin\psi_0 - \sin u}{\sin\Theta \cos\psi_0} \tag{3.5}$$

and

$$\Delta\lambda_1 = 2\lambda'_K. \tag{3.6}$$

Let us next derive a formula giving the maximum size $(\Delta\lambda_{1l})_{max}$ of the interlaunch interval. This maximum is attained for $\Omega_1 = 90°$. Then,

$$\lambda = 0, \quad m = 90° - \Theta$$

and

$$\cos\sigma_{max} = \frac{\cos u - \sin\Theta \sin\psi_0}{\cos\Theta \cos\psi_0}, \tag{3.7}$$

$$(\Delta\lambda_{1l})_{max} = 2\sigma_{max}. \tag{3.8}$$

This angle, like the angle $\Delta\lambda_L$, can be measured in hours as well as in degrees. Thus, the striking interval can be expressed in hours (or days) as well. Figure 1.16 includes additional scales in these units; this figure shows $\Delta\Omega_1$, $\Delta\lambda_L$ and $(\Delta\lambda_{1l})_{max}$ as functions of $\Phi_1$, the angular range of the passive part of the flight, in the range $\pi - \beta_0 < \Phi_1 < \pi - \alpha_0$ (where $\Phi_1 = \pi - u$), corresponding to variations of $\Delta\Omega_1$ and $\Delta\lambda_L$ from zero to 360°. The functions for $\alpha_0 < \Phi_1 < \beta_0$ can be obtained from the curves in Figure 1.16, as the mirror images of the latter relative to the $\Phi_1 = 90°$ line. For the range $\beta_0 < \Phi_1 < \pi - \beta_0$, we have $\Delta\Omega_1 = \Delta\lambda_L = 360°$. As $\Phi_1$ is reduced, the two intervals (interlaunch and striking) become narrower. For $\Phi_1 = \alpha_0$ they degenerate to a point, and for $\Phi_1 < \alpha_0$ they disappear.

All the considered curves for $\Phi_1 = 180° - \alpha_0$ have vertical tangents. This means that the possibilities for reaching the moon, which first occur at $\Phi_1 = \Phi_{max} = 180° - \alpha_0$, rapidly multiply as $\Phi_1 = \pi - u$ is reduced. For example, for the middle latitudes we have $\Phi_{max} \approx 150°$, and when $\Phi_1$ is reduced to only

2° below $\Phi_{max}$ there are already several days in the month on which a lunar impact is feasible for given values of $r_1$, $V_1$, and $\theta_1$. Such a reduction of $\Phi_1$ can be attained (see Figure 1.10) by raising velocity $V_1$ by about 100 m/sec or else by increasing angle $\theta_1$ (the inclination of the initial-velocity vector to the local horizon) by about 1.5°. Such variations are small in comparison with the nominal values of $V_1$ and $\theta_1$, required to reach the moon starting from the middle latitudes.

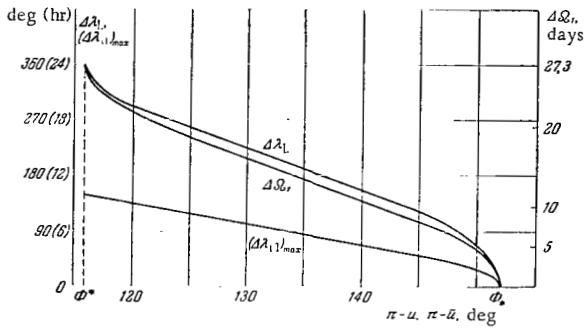


FIGURE 1.16. Launch interval $\Delta\lambda_1$, maximum interlaunch interval $(\Delta\lambda_{i1})_{max}$, and striking interval $\Delta\Omega_1$, as functions of angular range of flight (or of its complement with respect to 360°)

Finally, let us determine the azimuths and inclinations for points $A_1'$ and $A_1''$. If we reckon angle $a_N$ in Figure 1.14 counterclockwise from the northerly direction, then the azimuth will be $a_N'' = -a_N$. For spherical triangle $A_1'P\Omega_1$, the law of cosines and the law of sines give, respectively,

$$\cos|a_N| = -\frac{\cos m - \sin\psi_0 \cos u}{\cos\psi_0 \sin u} \tag{3.9}$$

and

$$\sin a_N = \frac{\sin m \sin\sigma}{\sin u}. \tag{3.10}$$

Let us find the maximum value of the angle $|a_N(\Omega_1)|$. If we differentiate (3.9), we can use (3.2) to obtain

$$\frac{d|a_N|}{d\Omega_1} = \frac{\sin\Theta\cos\Omega_1}{\sin a_N \cos\psi_0 \sin u},$$

from which it follows that the maximum azimuth $|a_N|$ corresponds to $\Omega_1 = 90°$. Now we can write:

$$\cos(a_N)_{max} = \frac{-\sin\Theta + \cos u \sin\psi_0}{\sin u \cos\psi_0}. \tag{3.11}$$

Figure 1.17 shows a graph of functions $a_N'(\Omega_1)$ and $a_N''(\Omega_1)$, for $\Phi_1 = 150°$. The variation of the maximum azimuth as a function of $\Phi_1 = \pi - u$ has been plotted in Figure 1.18. For the middle latitudes the azimuth $(a_N)_{max}(\Phi^*)$ is close to 90° ($\Phi^* = \pi - \beta_0$).

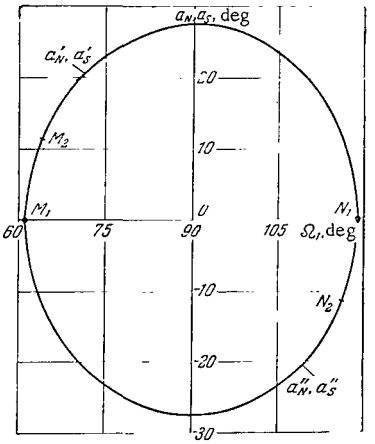


FIGURE 1.17. Launching azimuth as function of node longitude $\Omega_1$, for given angular range of flight.

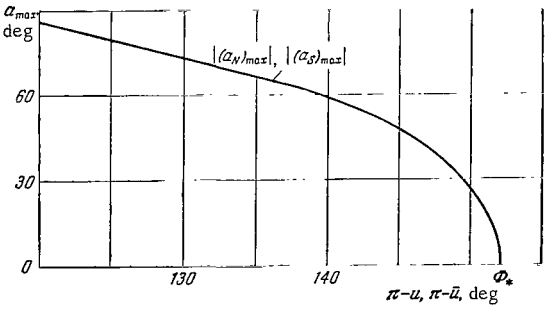


FIGURE 1.18. Maximum launching azimuth as function of angular range of flight.

Now let us determine the inclination $i_1$ of the flight-path plane to the plane of the lunar orbit. First, from spherical right triangle $yP\Omega_1$ we find the magnitude $\tau$ of angle $y\Omega_1 P$:

$$\left.\begin{aligned} \sin\tau &= \frac{\cos\Theta}{\sin m}, \\ \cos\tau &= \frac{\sin\Theta - \cos m \sin\Omega_1}{\sin m \cos\Omega_1}. \end{aligned}\right\} \qquad (3.12)$$

Then, from spherical triangle $A'_1 P\Omega_1$, we determine the magnitude $s$ of angle $P\Omega_1 A'_1$:

$$\left.\begin{aligned} \sin s &= \frac{\sin a_N \cos\psi_0}{\sin m}, \\ \cos s &= \frac{\sin\psi_0 - \cos u \cos m}{\sin u \sin m}. \end{aligned}\right\} \qquad (3.13)$$

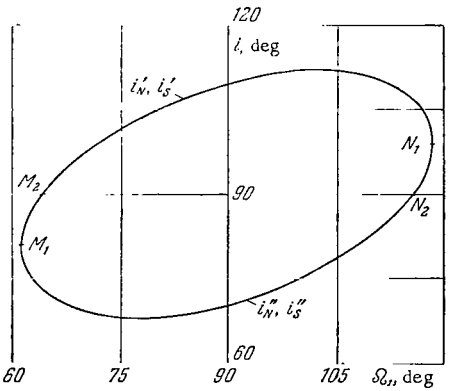


FIGURE 1.19. Inclination of flight-path plane to plane of lunar orbit, as function of node longitude $\Omega_1$.

For points $A'_1$ and $A''_1$ we have, respectively,

$$i'_N = \tau + s. \quad i''_N = \tau - s. \tag{3.14}$$

The extreme value of the inclination will obviously be reached for the values of $\Omega_1$ at which points $A'_1$ and $A''_1$ pass through point $A_*$ (Figure 1.14). Then, we have

$$\sin (i_N)_{\min} = \frac{\sin (\psi_0 - \Theta)}{\sin u} \tag{3.15}$$

Figure 1.19 shows the inclinations $i'_N$ and $i''_N$ as functions of the node longitude $\Omega_1$. Points $M_1$, $N_1$, $M_2$, and $N_2$ in Figures 1.17 and 1.19 have the same significance as in Figure 1.15.

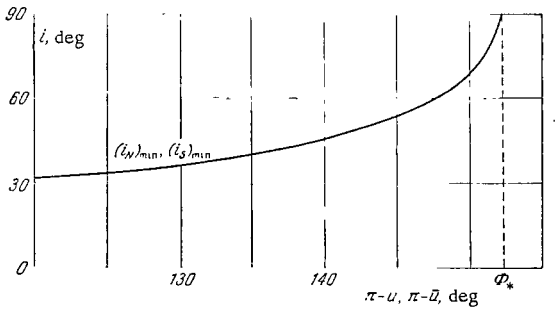


FIGURE 1.20. Extreme values of inclination of flight-path plane to lunar orbital plane, as functions of angular range of flight (or of its complement with respect to 360°).

The curve for the dependence of the minimum inclinations $(i_N)_{min}$ on the angular range $\Phi_1 = \pi - u$ of the passive part of the flight is shown in Figure 1.20.

## 1.4. LENGTH OF ACTIVE PART OF FLIGHT

For a moon shot the active part of the flight may have to be considerably longer than in the case of a terrestrial mission. This is because of the high initial velocity required for the passive part of the flight.

Let us call the geocentric angle between the radii of the initial and final points of the active part the **active angular range** $\Phi_a$. Let us assume that the launching azimuth and the vector $\boldsymbol{V}_1$ of the initial velocity in the passive part of the flight are specified, and that the magnitude $V_1$ and the angle of elevation $\theta_1$ above the local horizon are also given. Obviously, in this case the programed pitch of the spacecraft and also the course of the active part of the flight will be unambiguously determined by the condition for optimum injection (maximum payload injected into orbit). Accordingly, the height of the end of the active part, as well as the active angular range of the flight, will be uniquely determined as functions of the initial velocity and its angle of elevation.

The initial velocity of the active part will affect the absolute geocentric velocity at the end of this part of the flight somewhat. This initial velocity is the speed the spacecraft had at the launch point, as it rotated in diurnal motion together with the earth's surface. If the launching azimuth is not exactly to the east or exactly to the west, the existence of this initial velocity will cause the spacecraft to leave the plane passing through the initial and final geocentric radii of the active part. For constant thrust and pitch programs, the length and height of the active part of the injection, for specified values of $V_1$ and $\theta_1$, will obviously depend on the magnitude and direction of the projection of the initial-velocity vector onto the plane passing through the initial and final radii (that is, they depend on the latitude of the launch point and the launching azimuth).

However, in the present case the initial velocity will be small in comparison with the total characteristic velocity imparted to the spacecraft by its engines. Thus it can be assumed that, for a given magnitude $V_1$ of the initial velocity in the passive part and for a given angle of elevation $\theta_1$ above the horizon, the active part of the flight has the same length $\Phi_a$ for all azimuths. Moreover, the projection of the terminal-velocity vector onto the horizontal plane can be assumed to lie along an arc of the great circle connecting the launch point with the projection of the end of the active part onto the spherical surface of the earth. Then we can assume that the launch point, which rotates along the $\psi_0$ parallel together with the earth, is the center of a $\Phi_a$-circle on the earth. In other words, it is the center of a circle with a given angular radius $\Phi_a$, above any point of which (at the given height $H_1$ and for the given angle $\theta_1$ above the local horizon) the specified $V_1$ can be obtained at any moment. The passive angular range, that is, the geocentric angle between the initial and final points of the passive part of a trajectory with given $H_1$, $V_1$, and $\theta_1$, will once again be uniquely determined. Consequently, as previously, the lunar-impact trajectories corresponding to parameters $H_1$, $V_1$, and $\theta_1$ will lie along a circle of radius $u_1 = \pi - \Phi_1$, with its center at point $\Omega_1$.

In order to ensure a lunar impact, the end $A_1$ of the active part (Figure 1.21) will obviously have to lie on the $u_1$-circle and the radius of the $\Phi_a$-circle will have to be in the plane passing through the line of nodes and point $A_1$ (that is, it will be an extension of the radius of the $u_1$-circle). The latter condition means that the $u_1$-circle and the $\Phi_a$-circle must be (internally) tangent to one another at point $A_1$. Moreover, the total angular range $\Phi$, reckoned from the launch point, can be expressed as the sum $\Phi = \Phi_1 + \Phi_a$. Thus we have

$$u_1 = u + \Phi_a, \text{ where } u = 180° - \Phi.$$

Let us now consider the conditions for which tangency of a circle of radius $u_1$ (with its center moving uniformly along a great circle in the base plane $xy$) and a circle of radius $\Phi_a$ (with its center moving uniformly along a given $\psi_0$ parallel) is possible. The minimum distance between the centers of the circles $\alpha_0 = \psi_0 - \Theta \neq 0$. Consequently, it is easy to show that only two cases of internal tangency are possible: case I, when $u_1 - \Phi_a > \alpha_0$, and case II, when $\Phi_a - u_1 > \alpha_0$ (Figures 1.21 and 1.22).

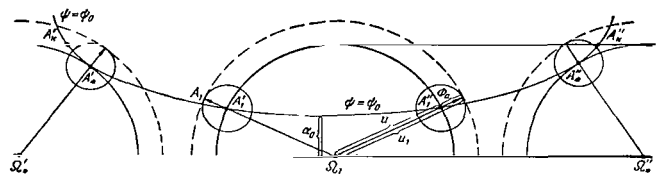


FIGURE 1.21. Internal tangency of $\Phi_a$-circle and $u_1$-circle, for $u_1 - \Phi_a > \alpha_0$ and for different successive positions of advance point.

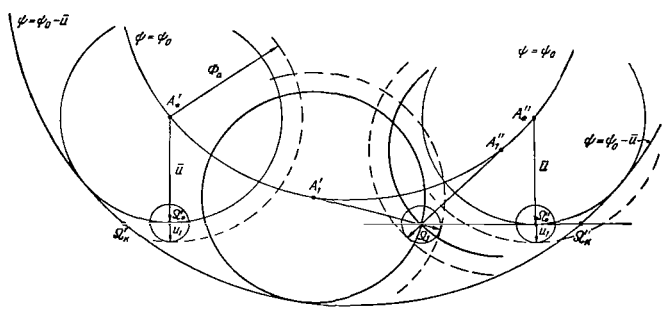


FIGURE 1.22. Internal tangency of $\Phi_a$-circle and $u_1$-circle, for $\Phi_a - u_1 > \alpha_0$ and for different successive positions of advance point.

For case I the difference $u_1 - \Phi_a$ must be quite large, since $u_1 - \Phi_a \geqslant \alpha_0$. If, in the absence of an active part of the flight, the condition $\Phi_1 \leqslant \pi - \alpha_0$ ensures arrival at the moon, then when the length $\Phi_a$ of the active part is taken into account the analogous condition will be $\Phi_1 \leqslant \pi - \alpha_0 - \Phi_a$. This means that the presence of an extended active part makes hitting the moon more complicated, since the original end value $\Phi_1$ must be replaced by the

small quantity $\Phi_1 - \Phi_a$. Moreover, in case I, in order to increase the probability of a lunar impact, it is desirable to reduce both the passive and active angular ranges of the flight.

The limitations as to launch time are determined, just as in the previous case, by the argument $u$ of the latitude of initial point $A_1$ (Figure 1.21). Consequently, they are characterized by the previously given relations for $\Delta\lambda_1$, $\Delta\Omega_1$, and $(\Delta\lambda_{11})_{max}$ as functions of $u$, or else of the total angular range $\Phi = \pi - u$ (Figure 1.16), in spite of the fact that the corresponding dependences of these quantities upon parameters $r_1$, $V_1$, and $\theta_1$ will obviously be different. Analogously, the dependences of the maximum values of the azimuth and inclination upon $\pi - u$ will remain valid in this case (Figures 1.18 and 1.20).

For case II it will be necessary that $\Phi_a - u_1 \geqslant \alpha_0$; thus, the active angular range must be sufficiently great and, at any rate, it must exceed $\alpha_0 = \psi_0 - \Theta$ (Figure 1.22). This means that for case II, in order to increase the probability of a lunar impact, it is advisable to increase the active and passive angular ranges. Accordingly, the initial velocity should be reduced to a minimum, rather than increased, while the angle $\theta_1$ of its inclination to the horizon should be reduced to zero (the angle $\Phi_1$ then increases to 180°, and $u_1$ drops to zero). The launch directions for case II are thus, on the whole, opposite to the directions for case I.

Let us now consider the limitations as to launch time for case II. Whereas for case I these were determined by the $u$-circle, for case II they are determined by a circle of radius $\bar{u} = \Phi_a - u_1$ (the $\bar{u}$-circle, for short). According to Figure 1.22, the total angular range is the sum of $\pi$ (the angle below the plane of the lunar orbit) plus $\bar{u}$ (the angle above the plane of the lunar orbit): $\bar{\Phi} = \pi + \bar{u} = \pi - u_1 + \Phi_a = \Phi_1 + \Phi_a$; thus, it is expressed by the previous formula in terms of $\Phi_a$ and $\Phi_1$. Here, as previously, the dependence of $\Phi_1 = \pi - u_1$ on $\theta_1$ and $\beta_1$ is shown by Figure 1.10.

In case II the limits of the launch interval (but not of the striking interval) will be determined by the condition of tangency between the $\bar{u}$-circle (Figure 1.22) and the base plane. The limits of the striking interval, on the other hand, will be determined by end points $\Omega_\kappa'$ and $\Omega_\kappa''$, which are the intersection points between the $(\psi_0 - \bar{u})$ parallel and the base plane. Consequently, to sum up, in case I (Figure 1.21) tangency points $A_*'$ and $A_*''$ determine the limits $\Omega_*'$ and $\Omega_*''$ of the striking interval, and end points $A_\kappa'$ and $A_\kappa''$ are the limits of the launch interval. In case II (Figure 1.22), analogously, tangency points $\Omega_*'$ and $\Omega_*''$ determine the limits $A'$ and $A''$ of the launch interval, and end points $\Omega_\kappa'$ and $\Omega_\kappa''$ are the limits of the striking interval.

Just as in case I, in case II the spacecraft must enter into the passive part at the moment when the $\Phi_a$-circle, in the course of its diurnal motion along the $\psi_0$ parallel, touches the $u_1$-circle with its center at $\Omega_{11}$, which moves at about 1/27 of the speed of the former (Figure 1.22). Here, similarly to case I, if point $A_1$ does not coincide with $A_*'$ or $A_*''$, there will be two moments at which tangency is possible: one corresponding to a southeast launch direction (point $A_1'$) and the other to a southwest launch (point $A_1''$). Let us call the interval $\Delta\lambda_{11}$ between these moments the **interlaunch interval**, by analogy with case I; the maximum interlaunch interval $(\Delta\lambda_{11})_{max}$ is attained at $\Omega_1 = 0$.

Let us now consider the characteristics of case II when $\bar{u}$ is constant, which are analogous to those of case I for constant $u$. The symbols $\Omega_1'$ and $\Omega_1''$ designate the advance positions of the line of nodes, for which a lunar

impact is possible from launch point $A_1$ (Figure 1.23), the latter point being determined by the polar angle $\lambda$, measured from the meridian of point $A_*$.

In order to determine angles $\Omega_1'$ and $\Omega_1''$, let us find side $zA_1 = \bar{m}$ and angle $A_1zP = \bar{\tau}$ of spherical triangle $zPA_1$:

$$\cos\bar{m} = \cos\Theta\sin\psi_0 - \sin\Theta\cos\psi_0\cos\lambda, \tag{4.1}$$

$$\sin\bar{\tau} = \cos\psi_0\frac{\sin\lambda}{\sin\bar{m}}. \tag{4.2}$$

Now, from triangle $zA_1\Omega_1''$, which has a side $z\Omega_1'' = 90°$, we obtain the angle $\Omega_1''zA_1 = \bar{s}$:

$$\cos\bar{s} = \frac{\cos\bar{u}}{\sin\bar{m}}. \tag{4.3}$$

By virtue of the symmetry of points $\Omega_1'$ and $\Omega_1''$ relative to arc $zA_1B$, and also taking into account that the longitudes of the nodes are reckoned counterclockwise from the $x$ axis (as seen from the north pole), we obtain:

$$\Omega_1'' = 90° - (\bar{\tau} + \bar{s}), \quad \Omega_1' = 90° - (\bar{\tau} - \bar{s}). \tag{4.4}$$

Next let us find the corresponding azimuths and inclinations. If angle $zA_1P$ in triangle $A_1zP$ is designated as $a_*$ (Figure 1.23), then we have

$$\sin a_* = \sin\Theta\frac{\sin\lambda}{\sin\bar{m}}. \tag{4.5}$$

Angle $\Omega_1''A_1B = \bar{\sigma}$ in right triangle $A_1\Omega_1''B$ can be determined, giving

$$\sin\bar{\sigma} = \frac{\sin\bar{s}}{\sin\bar{u}}. \tag{4.6}$$

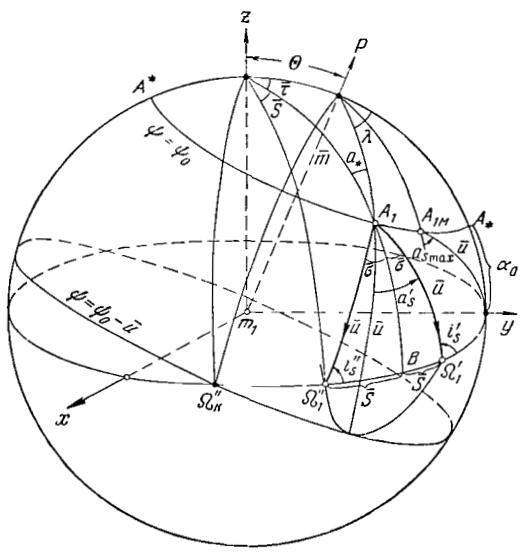


FIGURE 1.23. Spherical angles for calculating flight paths to moon, on condition that $\bar{u} = \Phi_a - u_1 > \alpha_0$.

The azimuths $a_S$, reckoned counterclockwise from the southerly direction, are then given by the relations

$$\left.\begin{aligned} a'_S &= a_* + \bar{\sigma}, \\ a''_S &= a_* - \bar{\sigma}. \end{aligned}\right\} \tag{4.7}$$

and the ordinary azimuths are

$$\left.\begin{aligned} a'_1 &= \pi - a'_S, \\ a''_1 &= \pi - a''_S. \end{aligned}\right\} \tag{4.8}$$

In order to determine the inclination $i_1$ from right triangle $\Omega''_1 A_1 B$, we obtain (Figure 1.23):

$$\sin i'_S = \sin i''_S = \frac{\cos \bar{m}}{\sin \bar{u}}, \quad i'_S = -i''_1, \quad i''_S = -i'_1, \tag{4.9}$$

angle $i''_S$ being taken in the first quadrant and angle $i'_S$ being taken in the second.

Figure 1.15 shows the results of the calculations of functions $\lambda'(\Omega_1)$ and $\lambda''(\Omega_1)$, inverse functions $\Omega'_1(\lambda)$ and $\Omega''_1(\lambda)$, and interlaunch interval $\Delta\lambda_{1l}$, for $\bar{u} = 30°$. It turns out that these curves are identical for cases I and II (case II differs from case I only in that the curves for $\lambda'(\Omega_1)$ and $\lambda''(\Omega_1)$ begin at points $M_2$ and $N_2$, where the tangents are horizontal, rather than at $M_1$ and $N_1$, where the tangents are vertical). This was to be expected, since, for $\bar{u} = u$, the circle around which the determining $u$-circle moves, and the circle on which the intersection point lies, exchange roles. Clearly, for $u = \bar{u}$, the corresponding values of $\lambda$ and $\Omega_1$ for the region between the tangency points in cases I and II should coincide. The shifting of the ends of the representative curves from $M_1$ and $N_1$ to $M_2$ and $N_2$ (Figures 1.15, 1.17, and 1.19) can be explained as follows. In case II lunar impacts from points such as $A'_1$ lying inside the launch interval (Figure 1.22) become possible prior to the entry of node $\Omega_1$ into the region $(\Omega'_*, \Omega''_*)$ determined by the tangency condition. On the other hand, impacts are still possible from points such as $A''_1$ even some time after the node leaves this region. In case II the interlaunch interval is determined only within the region $(\Omega'_*, \Omega''_*)$, that is, only between the abscissas of points $M_2$ and $N_2$. It begins and ends not at zero but at the positive constant value $\Delta\lambda(M_2) = \Delta\lambda(N_2)$.

Similarly to functions $\lambda'(\Omega_1)$ and $\lambda''(\Omega_1)$, the azimuths $a_S(\Omega_1)$ and the inclinations $i_S(\Omega_1)$ are represented by the same curves as for case I, except that here the curves are limited by points $M_2$ and $N_2$ rather than points $M_1$ and $N_1$.

Finally, let us consider the range of the basic parameters for case II, as functions of the latitude argument $\bar{u}$ of the initial point. From the foregoing analysis, it is to be expected that the parameters for case II will be described by the same curves as for case I, except that $u$ is replaced by $\bar{u}$. Actually, from the condition of tangency between the $\bar{u}$-circle and the base plane, we obtain the following value for the launch interval: $\bar{m} = 90° - \bar{u}$, so that (Figure 1.23, formula (4.1))

$$\left.\begin{aligned} \cos \lambda_* &= \frac{\cos\theta \sin\psi_0 - \sin \bar{u}}{\sin\theta \cos\psi_0}, \\ \Delta\lambda_{1l} &= 2\lambda_*. \end{aligned}\right\} \tag{4.10}$$

which is identical to (3.5) and (3.6) for $\bar{u} = u$.

As formerly, the largest interlaunch interval corresponds to $\Omega_1 = 90°$; it can be found from spherical triangle $A_{1M}Py$, which has sides $Py = 90°$, $PA_{1M} = 90° - \psi_0$ and $A_{1M}y = \bar{u}$ (Figure 1.23):

$$\cos\lambda''\Big|_{\Omega_1=90°} = \frac{\cos\bar{u} - \sin\psi_0 \sin\Theta}{\cos\psi_0\cos\Theta}, \quad (\Delta\lambda_{11})_{\max} = 2\lambda''\Big|_{\Omega_1=90°}, \tag{4.11}$$

which is identical to (3.7) and (3.8) for $\bar{u} = u$.

Now let us determine the limits of the striking interval, in terms of the points $\Omega_K'$ and $\Omega_K''$ of intersection between the $(\psi_0 - \bar{u})$ parallel and the base plane. From spherical triangle $\Omega_K'' zP$ (Figure 1.23), which has sides $z\Omega_K'' = 90°$, $zP = \Theta$, and $P\Omega_K'' = 90° - (\psi_0 - \bar{u})$, the law of cosines for side $P\Omega_K''$ gives:

$$\left.\begin{aligned} \sin\Omega_K'' &= \frac{\sin(\psi_0 - \bar{u})}{\sin\Theta}, \\ \Delta\Omega_1 &= 2\left(\frac{\pi}{2} - \Omega_K''\right), \end{aligned}\right\} \tag{4.12}$$

which is identical to (3.4) for $\bar{u} = u$.

Functions $\Delta\Omega_1(\bar{u})$, $\Delta\lambda_1(\bar{u})$, and $(\Delta\lambda_{11})_{\max}(\bar{u})$ were plotted in Figure 1.16.

Since, as in the previous case, the azimuth reaches its extreme value at $\Omega_1 = 90°$, from triangle $A_{1M}Py$ we obtain

$$\cos(a_S)_{\max} = \frac{-\sin\Theta + \sin\psi_0\cos\bar{u}}{\cos\psi_0\sin\bar{u}}, \tag{4.13}$$

and, by virtue of (3.11), we also obtain $(a_S)_{\max} = (a_N)_{\max}$ (Figure 1.18). This also follows from the equality of the vertical angles $a_N$ (Figure 1.14) and $a_S$ (Figure 1.23) for $\bar{u} = u$.

Lastly, to determine the extreme values of the inclination, we have, as in case I, the relation

$$\sin(i_S)_{\max} = \frac{\sin(\psi_0 - \Theta)}{\sin\bar{u}}, \tag{4.14}$$

which is identical to (3.15) for $\bar{u} = u$ (Figure 1.20).

Therefore, the dependences of the considered parameters on the latitude argument $u$ (or $\bar{u}$) are more universal than the dependences on the total angular range $\Phi$. That is, they are universal in the sense that they apply to any values of the active angular range $\Phi_a$, for both case I and case II. Trajectories corresponding to cases I and II will in the following be referred to simply as trajectories of types I and II.

*Chapter II*

# *ENERGETICALLY OPTIMUM LUNAR TRAJECTORIES*

## 2.1. REQUIRED ENERGY EXPENDITURES CORRESPONDING TO GIVEN INITIAL DATA

The given initial data will here be understood to refer to some definite combination of initial-velocity direction and ratio of initial velocity to local parabolic, for a specified trajectory azimuth. The energy expenditures will be measured in terms of the magnitude $U_x$ of the spacecraft's characteristic velocity (the speed imparted to the craft by the same propellant consumption for undisturbed rectilinear motion). In the following calculations, the square $\beta_1$ of the ratio of initial velocity to local parabolic will be used, instead of the ratio itself. The direction of the initial velocity during the passive part of the flight will once again be given as the angle of elevation $\theta_1$ of the velocity vector above the local horizon. The azimuth of the direction of the initial velocity is assumed to be fixed.

The program for injecting a spacecraft into a trajectory with given $\theta_1$ and $\beta_1$ can be considered fixed if it has only two free parameters; it may be different if it is a multiparameter program. The free parameters $q_i$ may be, for example, the points of division between the active part and the parts in which thrust and pitch-variation rate are constant. The latter two quantities may also be free parameters for the injection program.

In the case of a multiparameter program, the only alternative is to consider optimum combinations of parameters; these are parameter combinations (for the active parts) for which the terminal characteristic velocity $U_x$ will be a maximum for the given values of $\theta_1$ and $\beta_1$. The optimum combinations can be selected using some method such as the method of envelopes. Once some value of $\beta_1$ and all the free parameters have been specified, it is possible to plot the $U_x(\theta_1)$ curve in the $\theta_1 U_x$ plane.

By varying one of the parameters (say $q_1$), we obtain a family of these curves for $U_x|_{\beta_1=\text{const},\ q_1=\text{const}}$, which has an envelope $U_x(\theta_1)|_{\beta_1=\text{const}}$ (the existence of the envelope follows from energy considerations). Next we vary the other free parameter $q_2$. Then, using the method referred to above, we plot the envelopes $U_x(\theta_1)|_{\beta_1=\text{const}}$ on the same graph and draw the envelope of these envelopes. Thus parameter $q_2$ is eliminated, in the same way as $q_1$ was eliminated earlier. Similarly, it is possible to eliminate a large number of parameters (provided enough graphical work is done).

Energy considerations show that the value of $U_x$ corresponding to minimum expenditures will increase with a rise in $\beta_1$ for constant $\theta_1$ and also with a rise in $\theta_1 \left(0 \leqslant \theta_1 \leqslant \frac{\pi}{2}\right)$ for constant $\beta_1$. Let us connect points of equal minimum energy expenditures $U_x$ in the $\theta_1\beta_1$ plane (Figure 2.1). This

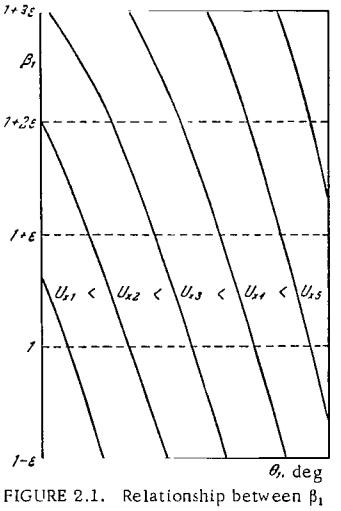


FIGURE 2.1. Relationship between $\beta_1$ and $\theta_1$, for different constant magnitudes $U_x$ of characteristic velocity.

gives the curves for optimum combinations of $\theta_1$ and $\beta_1$. The points on each curve for a given abscissa $\theta_1$ correspond to the minimum outlays $U_x$ required to attain the ordinate $\beta_1$.

When we plot the curves of $\beta_1(\theta_1)|_{U_x=\text{const}}$ for a series of values of $U_x$, we obtain a family of optimum curves $U_x = U_x(\theta_1, \beta_1)$. These optimum curves, which show the velocity as a function of two variables, have been plotted in Figure 2.1 for $1-\varepsilon < \beta_1 < 1+3\varepsilon$. The quantity $\varepsilon \approx 0.02$ is small, of the order of $1-\beta_{1\,\min}$, where $\beta_{1\,\min}$ corresponds to attainment of a lunar orbit with a minimum velocity. The function $U_x = U_x(\theta_1, \beta_1)$ is obtained by processing the results of the calculations for the active part of the flight.

The values of the radius $r_1 = r_0 + H_1$ (where $r_0$ is the earth's radius) and of the angular range $\Phi_a$ of the active part which correspond to the optimum combinations of $\theta_1$ and $\beta_1$ are by no means arbitrary. Rather, they form single-parameter families of functions of $\theta_1$. Figure 2.2 shows the limits of the single-parameter pencil of optimum curves of $r_1(\theta_1)|_{\beta_1=\text{const}}$. On the

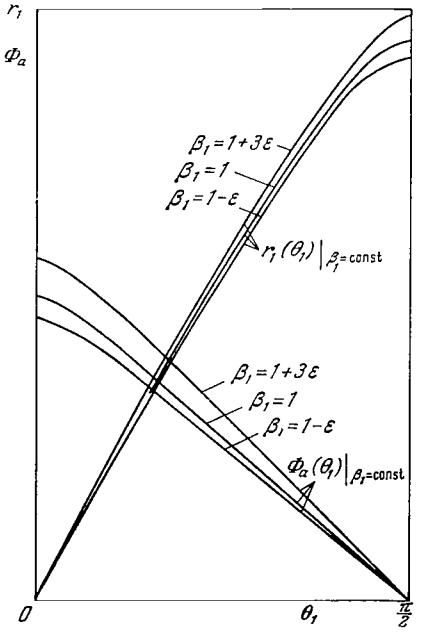


FIGURE 2.2. Geocentric radius $r_1$ and angular range $\Phi_a$ of active part, as functions of $\beta_1 = \bar{v}^2$ (square of ratio of initial velocity to local parabolic) and $\theta_1$ (angle of elevation of initial-velocity vector above local horizon).

same graph are plotted the limits of another single-parameter pencil of optimum curves of $\Phi_a(\theta_1)|_{\beta_1=\text{const}}$. The second pencil was obtained (analogously to the first) according to the trajectories which turned out to be the best with respect to the magnitude $U_x$ of the characteristic velocity. The observed variations of $r_1$ and $\Phi_a$ as $\theta_1$ increases are to be expected: the steeper the trajectory along which acceleration takes place, the smaller the ranges and the greater the heights at which the active part must terminate.

The pencil of curves for $r_1(\theta_1)|_{\beta_1=\text{const}}$ has its maximum width at $\theta_1=\frac{\pi}{2}$ and zero width at $\theta_1=0$. The pencil of curves for $\Phi_a(\theta_1)|_{\beta_1=\text{const}}$, on the other hand, narrows down to zero at $\theta_1=\frac{\pi}{2}$ and widens to a maximum at $\theta_1=0$. At the point of greatest pencil width, the curves of both pencils have horizontal tangents.

It should be noted that $\Phi_a$ and $r_1$ vary less with $\beta_1$ than with $\theta_1$, at any rate within the narrow range considered ($1-\varepsilon<\beta_1<1+3\varepsilon$). Therefore, for approximate calculations the variations of $r_1$ and $\Phi_a$ with $\beta_1$ can be neglected, and sometimes the variations with $\theta_1$ as well, provided the range of $\theta_1$ considered is narrow enough.

## 2.2. LUNAR TRAJECTORIES WITH SPECIFIED INCLINATIONS OF FLIGHT PLANE TO PLANE OF EQUATOR

In §2.1 the energy expenditures required to attain specified combinations of speed and velocity-vector elevation above the local horizon (at the beginning of the passive part) were determined, for a given trajectory azimuth.

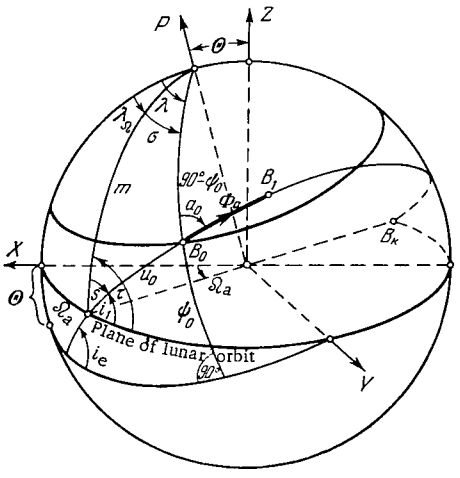


FIGURE 2.3. Spacecraft route (radial projection of flight path onto earth's surface) on nonrotating sphere, for northeastward launch.

In this section we consider the total angular range and some other characteristics of a lunar trajectory which has its beginning at a fixed point $B_0$ (Figure 2.3). The position of the trajectory plane will be characterized by its inclination $i_1$ to the plane of the lunar orbit. If the inclination $i_e$ of the trajectory plane to the equatorial plane is specified, a trajectory beginning at $B_0$ will obviously have a fixed azimuth $a_0^*$. For example, if the trajectory plane lies at an angle of about 65° to the equator (the first Soviet satellites and space probes had such trajectory inclinations), and if the coordinates of the initial point are those assumed in Chapter I, the azimuth will be close to 35°.

Let us designate the node longitude as the angle $\Omega_a$, reckoned counterclockwise from the midpoint of the striking interval (that is, from the $y$ axis in Figure 1.14); here it will be somewhat more advantageous to

use $\Omega_a$ instead of $\Omega_1$.* Accordingly, instead of the previously used $x$ and $y$ axes, let us introduce a geocentric $X$ axis directed toward a point lying opposite to the midpoint of the striking interval, and a $Y$ axis directed toward the descending node (relative to the equator) of the lunar orbit. As a comparison of Figures 1.12 and 2.3 shows, the conversion relations are:

$$\left.\begin{aligned} X &= y, \quad Y = -x, \quad Z = z, \\ \sin \Omega_a &= -\cos \Omega_1, \quad \cos \Omega_a = \sin \Omega_1. \end{aligned}\right\} \tag{2.1}$$

Formula (3.2) and the second formula of (3.12) of Chapter I thus become:

$$\cos m = \sin \Theta \cos \Omega_a. \tag{2.2}$$

$$\cos \tau = -\frac{\sin \Theta - \cos m \cos \delta_{\odot a}}{\sin m \sin \delta_{\odot a}}. \tag{2.3}$$

When these are used in formulas (3.12) and (3.13), we obtain the second formula of (3.14) in Chapter I:

$$i_1 = i_1'' = \tau - s.$$

From the relations expressing the law of cosines for side $u_0$ and angle $\sigma$, we obtain:

$$\cos u_0 = \frac{\cos m \sin \psi_0 + \cos s \cos a_0 \sin m \cos \psi_0}{1 - \sin s \sin a_0 \sin m \cos \psi_0}. \tag{2.4}$$

Figure 2.4 shows sample calculations of $u_0(\Omega_a)$ and $i_1(\Omega_a)$ for two azimuth values ( $a_0 = 35°$ and $a_0 = 60°$). It turns out that $u_0(\Omega_a)|_{a_0=60°} > u_0(\Omega_a)|_{a_0=35°}$, since as the azimuth increases, the total angular ranges differ more and more from their maximum values. In accordance with the results in Chapter I, the latitude argument $u_0$ is a minimum at $\Omega_a = 0$. The extreme values of the inclination $i_1$ are reached at $\Omega_a = 90°$; for an increase of 25° in the azimuth, the $i_1(\Omega_a)$ and $u_0(\Omega_a)$ curves will be shifted approximately equidistantly along the ordinate axis (10 to 15° upward and 14 to 16° downward, respectively). Since $u_0$ reaches a minimum at $\Omega_a = 0$, quite substantial variations of $\Omega_a$ do not increase $u_0$ much. For example, when $\Omega_a$ is increased from zero to 17.5°, $u_0$ is raised by only 1°. The value $\Omega_a = 17.5°$ corresponds to a striking interval $\Delta\Omega = 35°$ (that is, an interval of two or three days).

It is easy to see from Figure 2.3 that, if the trajectory azimuth $a_0$ is specified, for each advance-point position $\Omega_a$ the angle $\lambda$ between the meridians of the $X$ axis and the launch point will have some nonarbitrary value. The relation $\lambda(\Omega_a)$ can be determined without trouble from Figure 2.3 (or Figure 1.14), using formulas (3.1) through (3.3) of Chapter I. The results of a calculation of this relation have been plotted in Figure 2.5. The function $\lambda(\Omega_a)$ is seen to increase monotonically everywhere, in a nearly uniform manner. The existence of the $\lambda(\Omega_a)$ dependence means that, in order to achieve lunar impact at a given time for a specified azimuth (that is, for a given position $\Omega_a$ of the moon in its orbit), some specific position of the initial point in absolute space at the moment of launch is necessary. Obviously, due to the earth's diurnal motion, the initial

* Subscript "a" refers to parameters corresponding to the advance point of the flight path.

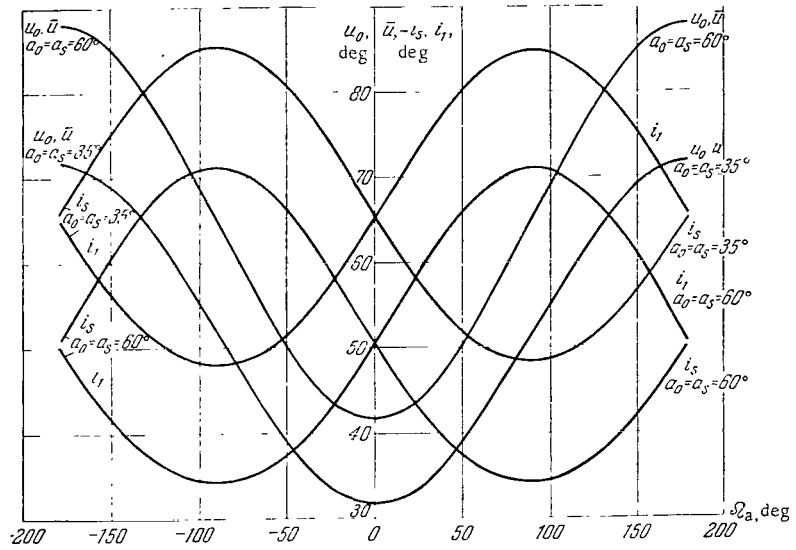


FIGURE 2.4. Latitude arguments $u_0$ and $\bar{u}$, and inclinations $i_S$ and $i_1$, as functions of longitude $\delta\Omega_a$ of advance point.

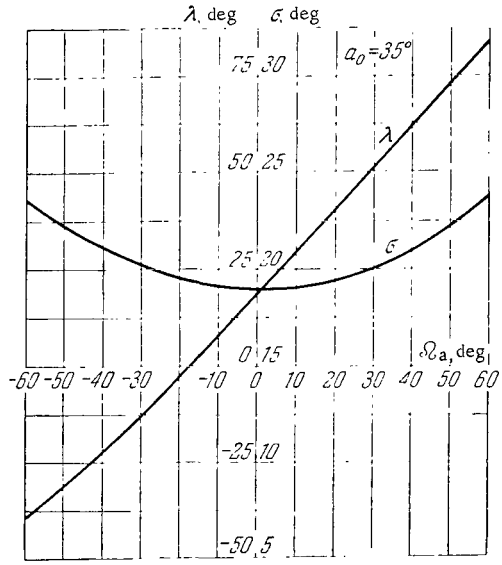


FIGURE 2.5. Angle $\lambda$ between meridians of $X$ axis and launch point, and angle $\sigma$ between meridians of node and launch point, as functions of longitude $\delta\Omega_a$ of advance point.

point will be in this position once each day, when the launch plane passes through the given advance point $\Omega_a$. The corresponding launch time will be determined unambiguously for each sidereal day, and thus it is obvious that the possible flight times for each sidereal day must be specified exactly as well. For example, for a launch on the following day, the flight time must be reduced by one sidereal day. The fact that, for a specified trajectory azimuth, lunar impacts cannot be achieved at any given moment of time constitutes an essential difference between moon shots and terrestrial missions.

## 2.3. OPTIMUM INITIAL DATA FOR SPECIFIED INCLINATION OF TRAJECTORY PLANE TO EQUATORIAL PLANE

Let us determine the initial data corresponding to a minimum characteristic velocity $U_x$, when the spacecraft is launched from a specified latitude $\psi_0$ and when the inclination $i_e$ of the trajectory plane to the equator is given. The inclination $i_e$ is related to the azimuth $a_0$ by the law of sines (Figure 2.3):

$$\sin a_0 = \frac{\cos i_e}{\cos \psi_0}. \tag{3.1}$$

One value of $i_e$ corresponds to two different azimuths $a_N$ and $a_S$. The first of these azimuths is reckoned clockwise from the northerly direction, and the second counterclockwise from the southerly direction, but each of them has a range of $-90°$ to $+90°$. In order to be definite, we assume that $a_0 = a_N$.

In the determination of the optimum initial data, it will be assumed that the spacecraft may be launched on any day during some specified interval of dates. We define $\Delta\Omega$ as the angular size of the striking interval corresponding to the given interval of dates. From $\Omega_a = \frac{\Delta\Omega}{2}$ we can find $u_0 = u_0(\Omega_a)$ using the graphs in Figure 2.4. The value of $u_0$ is found for the end of the striking interval, rather than for its midpoint $\Omega_a = 0$. Obviously, since $u_0$ decreases with a reduction of $|\Omega_a|$, the corresponding fuel supply will also be sufficient to hit the moon for points inside the striking interval. The required fuel supply determined for some point inside the striking interval, however, will not be sufficient to reach the moon at the end of the interval.

If the average value $\Phi_a^0$ of the active angular range is given, we can determine the average passive angular range $\Phi_1^0 = 180° - (u_0 + \Phi_a^0)$. Then, for any point $(\theta_1, \beta_1)$ on the $\Phi_1 = \Phi_1^0$ curve (Figure 1.10), we can find the corresponding value of $U_x$ from the family of $U_x(\theta_1, \beta_1)$ curves (Figure 2.1).

Obviously, along the $\Phi_1(\theta_1, \beta_1) = \Phi_1^0$ curve, the continuous function $U_x(\theta_1, \beta_1)$ will go through a minimum $(U_x)_{min}$ in the limited region corresponding to the $\theta_1, \beta_1$ values of practical interest. The point $(\theta_1^*, \beta_1^*)$ at which this minimum is reached also indicates the optimum combination of initial data. This point can be found using the usual rules for determining the relative extreme value. However, it is easier to find it graphically, by plotting the curves for constant $\Phi_1(\theta_1, \beta_1)$ (Figure 1.10) and constant $U_x(\theta_1, \beta_1)$ (Figure 2.1) on a single graph. Actually, on such a graph the points $(\theta_1^*, \beta_1^*)$ at which the extreme values of $U_x(\theta_1, \beta_1)|_{\Phi_1 = const}$ or $\Phi_1(\theta_1, \beta_1)|_{U_x = const}$ are reached will obviously be the points of tangency of the curves of the different families.

The curvatures of the curves in these families will have opposite signs. Consequently, there will be only one point of tangency $(\theta_1^*, \beta_1^*)$ on each curve. Thus, for the value $\Phi_1 = \Phi_1^0$, the minimum $(U_x)_{min}$ will be reached at the point $(\theta_1^*, \beta_1^*)$ where the $U_x = (U_x)_{min}$ curve of the $U_x = \text{const}$ family touches the curve for $\Phi_1 = \Phi_1^0 = \text{const}$.

The preceding analysis was carried out for some average value $\Phi_a^0$ of the active angular range and for the height $H_1$ assumed when plotting the curves in Figure 1.10. Now, however, when the approximate values of $\theta_1^*$ and $\beta_1^*$ are known, it is easy to make the analysis more accurate. From points $\theta_1^*$ and $\beta_1^*$ in Figure 2.2, it is possible to find the exact values of $H_1(\theta_1^*, \beta_1^*)$ and $\Phi_a(\theta_1^*, \beta_1^*)$. Then, the point of tangency for the new value of $\Phi_a$ is determined and the variation in $H_1$ due to the shift in the curves in Figure 1.10 along the ordinate axis is taken into account. In this way, after several iterations we obtain sufficiently accurate optimum values of $\theta_1^*$, $\beta_1^*$, and $(U_x)_{min}$.

It should be noted that the need to find the optimum trajectory characteristics in the plane of variables $\theta_1$ and $\beta_1$ is an essential feature of the problem. This is because parameters $\theta_1$ and $\beta_1$ are universal determining parameters for both the active and passive parts of the flight.

A study of the curves for constant $\Phi_1$ and constant $U_x$ in the $\theta_1$, $\beta_1$ plane, at the same time taking into account the relations $\Phi_a(\theta_1, \beta_1)$ and $r_1(\theta_1, \beta_1)$, makes it possible to obtain initial data for very different constraints. Thus the increase in the energy expenditures, in comparison with those corresponding to the optimum initial data, can be evaluated.

As an example, let us determine $U_x$ for initial data enabling lunar impact during a given striking interval $2\Omega_a$, for a given flight time $T$ and a specified trajectory azimuth. The flight times for the optimum combinations of $\theta_1$ and $\beta_1$ considered (Figure 2.1) are determined basically by the amount $\Delta V_1$ by which the initial velocity exceeds local parabolic. Here, the initial height and the flight direction, in the considered ranges of variation of these quantities, have only a minor effect on the flight time. The initial data are determined as follows. Given the flight time $T$, we find $\Delta V_1$. Then, since we know the average values $r_1^0$ and $\Phi_a^0$, we can find the parabolic velocity $V_p(r_1^0)$, the quantity $\beta_1^0 = \bar{v}^2 = \left(\frac{V_p + \Delta V_1}{V_p}\right)^2$, the latitude argument $u_0(\Omega_a)$ (from the graphs in Figure 2.4), and the passive angular range $\Phi_1^0 = 180° - (u_0 + \Phi_a^0)$. The abscissa of the point of intersection between the $\Phi_1(\theta_1, \beta_1) = \Phi_1^0$ curve and the $\beta_1 = \beta_1^0$ line (Figure 1.10) will obviously be the desired value $\theta_1^0$. Once $\theta_1^0$ is known, we can find the exact values of $r_1(\theta_1^0, \beta_1^0)$ and $\Phi_a(\theta_1^0, \beta_1^0)$ from Figure 2.2 and then repeat the calculations of $V_p(r_1)$, $\beta_1$, $\Phi_1$, and $\theta_1$, taking into account the shift of the curves in Figure 1.10 with a variation in $H_1$. The iterations are continued until the required accuracy is obtained. The final values of $\theta_1$ and $\beta_1$ are then used to find $U_x(\theta_1, \beta_1)$.

It is also of interest to determine the energy expenditures required to obtain lunar trajectories for which the velocity vector at the beginning of the passive part forms some specific angle $\theta_1$ with the local horizon. The solution in this case is obtained in approximately the same way as in the previous one. Given $\theta_1$ and an arbitrary value of $\Omega_a$, we find the latitude argument $u_0(\Omega_a)$ (Figure 2.4). Then we determine the corresponding value of $V_1$, for which we first find (by iterations) $\beta_1 = \left(\frac{V_1}{V_p}\right)^2 = \bar{v}^2$.

Once some zero approximation $\beta_1 = \beta_1^0$ has been specified, the known relations for $\Phi_a(\theta_1, \beta_1)$ and $r_1(\theta_1, \beta_1)$ (Figure 2.2) can be used to find the active

angular range $\Phi_a$ and the geocentric radius $r_1$. Next the latitude argument $u_1$ of the end of the active part is calculated, as well as the angular range $\Phi_1$ of the passive part of the trajectory:

$$u_1 = u_0 + \Phi_a, \quad \Phi_1 = 180^\circ - u_1. \tag{3.2}$$

Finally, the exact value of $\beta_1$ is found using the formulas

$$\left.\begin{aligned} \Delta\beta_1 &= \frac{1 - 2\nu\cos^2\theta_1 + \cos(\Phi_1 + 2\theta_1)}{2\nu\cos^2\theta_1 - \cos\Phi_1 - \cos(\Phi_1 + 2\theta_1)}, \\ \beta_1 &= 1 + \Delta\beta_1. \end{aligned}\right\} \tag{3.3}$$

Here, $\nu = \frac{r_1}{r_2}$ is a small quantity which varies slightly, since $r_1$ and the radius $r_2$ of the impact point vary slightly. Using the new values of $\beta_1$ and $\theta_1$, we once again find $r_1$ and $\Phi_a$ as functions of $u_1$, $\Phi_1$, $\Delta\beta_1$, etc. The iterations are repeated until the required accuracy is obtained. Due to the fact that $\Phi_a$, and especially $r_1$, depend only slightly on $\beta_1$, the iterations converge rapidly. In fact, in order to obtain three correct decimal places, only two iterations are necessary. Because of the slight dependence of $\Phi_a$ and $r_1$ on $\beta_1$, these two quantities will also vary slightly with $\Omega_a$. Therefore, it is convenient to represent the results of these calculations as curves of $\Phi_a(\theta_1)$ and $r_1(\theta_1)$ with the parameter $|\Omega_a|$. These curves will obviously vary monotonically with $\theta_1$ and will be identical for values of $\Omega_a$ differing only in sign.

When $\Phi_a$, $r_1$, $\theta_1$, and $\Delta\beta_1$ have been determined, we can find the local parabolic velocity $V_p$ and the initial geocentric velocity $V_1$:

$$V_p = \sqrt{\frac{2\mu_1}{r_1}}, \quad V_1 = V_p\sqrt{\beta_1}, \tag{3.4}$$

where $\mu_1$ is the gravitational potential of the earth. The amount $\Delta V_1 = V_1 - V_p$ by which the initial velocity exceeds parabolic can be found more accurately using the formula

$$\Delta V_1 = V_p \frac{\Delta\beta}{1 + \sqrt{1 + \Delta\beta}}, \tag{3.5}$$

since there is no loss in accuracy.

Parameters $U_x$, $r_1$, $\Phi_a$, $\Delta V_1$, $\theta_1$, and others can be determined as functions of $\Omega_a$ using the above method, for the entire range $-180^\circ < \Omega_a < 180^\circ$. However, it turns out to be sufficient just to find these quantities for the range $0^\circ < \Omega_a < 180^\circ$. The function $u_0(\Omega_a)$ is an even function. This means that the curves for $-180^\circ < \Omega_a < 0^\circ$ will be symmetrical about the ordinate axis, with respect to the corresponding curves for $0^\circ < \Omega_a < 180^\circ$. As $|\Omega_a|$ increases from 0 to 90°, the quantity $u_0$ becomes larger and reaches a maximum value. However, it varies as an odd function relative to the point ($\Omega_a = 90^\circ$ $u_0 = u_0(90^\circ)$). If the function $U_x(\theta_1, \beta_1) = \text{const}$ is close to linear, while the effect of a change in the height $H$ and range $\Phi_a$ of the active part is only slight, then we can make the following approximating assumption: the function $U_x(\Omega_a)$ determining the minimum energy expenditures also behaves as an odd function in the ranges from 0° to 180° and from −180° to 0°, relative to points with an abscissa $|\Omega_a| = 90^\circ$.

If we move away from the optimum point along a curve $\Phi_1 = \text{const}$ in the $(\theta_1, \beta_1)$ plane (Figures 1.10 and 2.1), the flight time may be changed substantially (for example, by 1 to 1.5 days) without entailing large energy losses. This is because the curves for constant $\Phi_1$ and constant $U_x$ are tangent to one another at the optimum point.

It should also be noted that the latitude of the initial point has a considerable effect on the energy expenditures required to reach the moon. For higher latitudes these expenditures will be greater. As the latitude is reduced to $\psi_0 = \Theta$, the required energy outlay drops, approaching that of the two-dimensional case. With a decrease in latitude, the derivative of function $u_0(\Omega_a)$ everywhere decreases in absolute value. Accordingly, the required energy expenditures and the other parameters change more gradually with a deviation of the launch date from optimum.

## 2.4. SELECTION OF ENERGETICALLY OPTIMUM INCLINATIONS FOR TRAJECTORIES OF FIRST TYPE

A method for determining the energetically optimum initial data for the passive part of a lunar trajectory was presented above. In that case the inclination $i_c$ or, which comes to the same thing, the azimuth $a_0^*$ of the trajectory was specified.

Clearly, if such calculations were carried out for a sufficient number of azimuths, a repeated use of the above method would make it possible to determine the dependence of the energy expenditures $U_{x\min}(a_0)$ and to find the optimum azimuth (that is, the azimuth corresponding to the highest characteristic velocity). However, this rather laborious means of determining the optimum azimuth can be avoided if we take into account the nature of the variation of the initial velocity with the azimuth. Then, the results of the calculations for the azimuth $a_0^*$ can be used, together with an appropriate conversion.

Actually, for different azimuths only the Coriolis force and the centrifugal force will be changed, and the additions to the relative velocity caused by the earth's rotation. For the active part of the flight, the centrifugal force is so small in comparison with the thrust that it can in general be neglected. The Coriolis force is also small compared to the thrust, and analysis shows that it only changes the direction of the velocity vector, without changing the magnitude appreciably. Consequently, the Coriolis force has an inconsiderable effect on the energy requirements of the spacecraft and it will also be neglected during this analysis.

Thus, if we go from one azimuth to another, the only thing that will change will be the difference between the vectors of the absolute velocity $V_1$ and the relative velocity $V_0$, caused by the rotation of the earth. Let us see how the differences $\Delta V_\Omega = V_1 - V_0$ and $\Delta\theta = \theta_0 - \theta_1$ (where $\theta_0$ is the angle of elevation of the relative-velocity vector $V_0$ above the horizon for the initial point of the passive part) vary with the azimuth $a_0$. The latter azimuth gives the direction of absolute motion at the launch point, taking into account the relations between initial data which were established in §2.1.

Since the differences $V_1 - V_0$ and $\theta_0 - \theta_1$ are quite small, an approximate calculation of these quantities is very simple. Let us consider the vector

triangle with sides $V_0$, $V_1$, and $V_\Omega$, where $V_\Omega$ is the velocity increment due to the earth's rotation. From this triangle we obtain

$$V_0^2 = V_1^2 - 2V_1 \Delta V_\Omega^0 + V_\Omega^2, \tag{4.1}$$

where $\Delta V_\Omega^0 = V_\Omega \cos \theta_1 \sin a_1$, $a_1$ being the azimuth of the absolute-velocity vector at the point of arrival at the passive part of the trajectory.

The peripheral velocity will be

$$V_\Omega = \Omega r_1 \cos \psi_1, \tag{4.2}$$

where $\Omega$ is the angular velocity of rotation of the earth, and $\psi_1$ is the latitude of the initial point of the passive part. From (4.1) we obtain

$$\Delta V_\Omega = V_1 - V_0 = \frac{2V_1 \Delta V_\Omega^0 - V_\Omega^2}{V_1 + V_0} = \frac{\Delta V_\Omega^0 - \frac{V_\Omega^2}{2V_1}}{1 - \frac{\Delta V_\Omega^0}{2V_1}}.$$

Now, taking into account the smallness of $V_\Omega$ and $\Delta V_\Omega^0$ in comparison with $V_1$ and the closeness of $V_1$ to the local parabolic velocity $V_p$, we can expand the latter expression as a Taylor series, retaining terms of second order only:

$$\Delta V_\Omega = \Delta V_\Omega^0 - \left( \frac{V_\Omega^2}{2V_p} - \frac{\Delta V_\Omega^{0^2}}{2V_p} \right).$$

Next, if we discard the second-order terms, we have: $\Delta V_\Omega = \Delta V_\Omega^0$. Since the law of sines gives

$$\sin a_1 = \cos \psi_0 \frac{\sin a_0}{\cos \psi_1}, \tag{4.3}$$

we obtain:

$$\Delta V_\Omega = \Delta V_\Omega^0 = \Omega r_1 \cos \psi_0 \sin a_0 \cos \theta_1, \tag{4.4}$$

where $\psi_0$ is the latitude of the launch point. From the obvious formula $V_1 \sin \theta_1 = V_0 \sin \theta_0$, it follows that the difference $\theta_0 - \theta_1$ only amounts to a fraction of a degree. Thus, with an accuracy up to terms of second order, we can assume that $0 = \Delta V_\Omega^0 \sin \theta_1 - V_p \Delta\theta \cos \theta_1$. In this case

$$\theta_0 - \theta_1 = \Delta\theta = \frac{\Delta V_\Omega^0}{V_p} \tan \theta_1. \tag{4.5}$$

Formula (4.4) shows that the velocity increment $\Delta V_\Omega$ caused by the rotation of the earth does not depend on the length $\Phi_a$ of the active part. Rather, it depends only on the azimuth of the velocity vector at the initial point and on its angle of elevation at the end of the active part.

The calculations using formulas (4.4) and (4.5) can be simplified if the slight variation of the radius $r_1$ with $\beta_1$ is neglected. Figure 2.6 shows a typical curve for $\Delta V_\Omega$ as a function of the azimuth $a_0$. It is to be expected that similar curves for $\Delta V_\Omega(a_0)$ will be obtained for different values of $\theta_1$,

since $r_1$ increases with $\theta_1$ (see § 2.1), and this more or less compensates for the drop in cos $\theta_1$. Thus the curve turns out to be the same.

The variation of $\Delta\theta$ with $\theta_1$, as is evident from formulas (4.4) and (4.5), is almost sinusoidal (the deviation from sinusoidality being due to the increase of $r_1$ with $\theta_1$). Figure 2.7 shows an example of this relation.

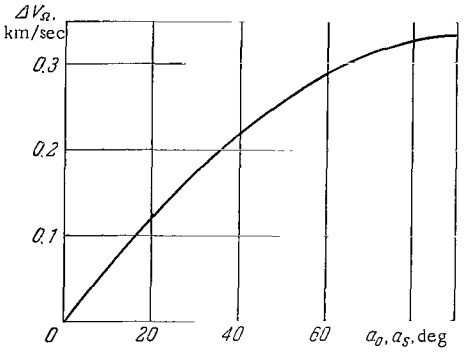


FIGURE 2.6. Velocity increment $\Delta V_\Omega$ caused by earth's rotation, as function of azimuth.

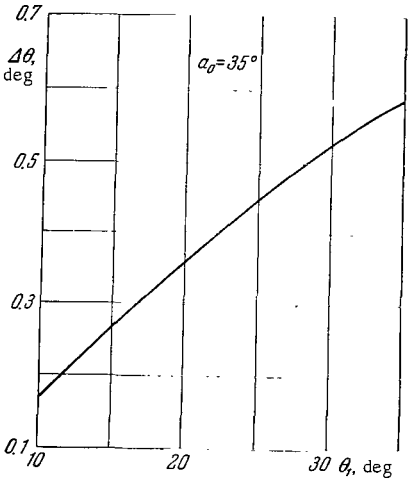


FIGURE 2.7. Difference of angles of elevation above horizon, for vectors of relative and absolute spacecraft velocities at beginning of passive part.

Now that we have made the calculations for the active part for some given azimuth $a_0^*$, it is easy to pass to some other azimuth $a_0$, simply by adding the following increment to the velocity:

$$\Delta V_\Omega(a_0) - \Delta V_\Omega(a_0^*).$$

In the range $0 \leqslant a_0 \leqslant 90°$ there is some azimuth for which the function $U_x(a_0)$ passes through a minimum $(U_x)_{min}$. Actually, if the earth's rotation is neglected, then (according to Chapter I) the optimum azimuth will be the one for which the total angular range of the flight is a maximum $\Phi_{max}$ (that is, the azimuth $a_0 = 0$).

However, when the earth's rotation is taken into account, this azimuth is no longer optimum. As $a_0$ is increased above zero, the required energy expenditures will increase by small amounts of second order due to the reduction of $\Phi$, while at the same time they decrease by small amounts of first order due to the rise in $\Delta V_\Omega(a_0)$. As $a_0$ increases to 90°, however, the function $\Delta V_\Omega(a_0)$ goes through a maximum, increasing by small amounts of second order, while $\Phi(a_0)$ diminishes by small amounts of first order. Consequently, the required energy expenditures will increase by small amounts of first order. This means that in the range $0° \leqslant a_0 \leqslant 90°$ the energy expenditures reach a minimum. This minimum may be the only one, since in the range considered the azimuth variations determining this parameter change monotonically.

According to Chapter I, for $\Omega_a = 0$ the azimuth goes through a maximum for each given angular range, and there is a corresponding maximum of the angular range for any given azimuth. Consequently, the position of the advance point which is energetically optimum when the velocity increment (due to the earth's rotation) is not taken into account will remain the optimum point even when the effect of the earth's rotation is considered. Figure 2.8 shows the curves for $a_0(u_0)$ obtained using formula (2.4), for $\Omega_a$ values of 0°, 26°30', and 40°. The value $\Omega_a = 26°30'$ corresponds to a two-day striking interval, and $\Omega_a = 40°$ corresponds to a three-day interval.

It is interesting to compare the energy expenditures $\bar{U}_x$ corresponding to the optimum advance point (that is, the point $\Omega_a = 0$), for different azimuths $a_0'$. The quantity $\bar{U}_x(a_0')$ can be found without using Figure 2.6. First, with the aid of the $\Omega_a = 0$ curve in Figure 2.8, we find the total angular range $\Phi_0 = \pi - u_0$ corresponding to the azimuth $a_0'$. Then, having designated the average values $\Phi_a^0$ and $H_1^0$ of the active angular range and the height of the end of the active part as a zero approximation, we go on to determine the passive angular range $\Phi_1^{(0)} = \Phi_0 - \Phi_a^{(0)}$ and the point $(\theta_1^{(0)}, \beta_1^{(0)})$ where the curve $\Phi_1(\theta_1, \beta_1, H_1^{(0)}) = \Phi_1^{(0)} = \text{const}$ is tangent to one of the curves for $U_x(\theta_1, \beta_1) = \text{const}$ (Figure 2.1).

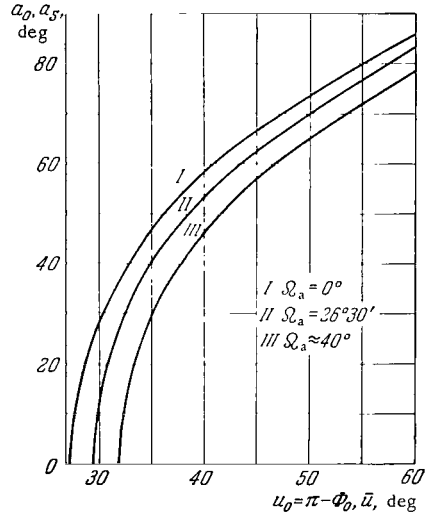


FIGURE 2.8. Azimuths $a_0$ and $a_S$ as functions of latitude arguments $u_0$ and $\bar{u}$ of launch point, for trajectories encountering moon at different angular distances $\Omega_a$ from energetically optimum point.

Using the values $\theta_1^{(0)}$ and $\beta_1^{(0)}$, we can find new, more exact values of $\Phi_a^{(1)}$ and $H_1^{(1)}$ from Figure 2.2. This gives a new point $(\theta_1^{(1)}, \beta_1^{(1)})$. Such iterations are then repeated until the required accuracy is obtained. The final values $\theta_1$ and $\beta_1$ give the point $U_x(\theta_1, \beta_1) = \bar{U}_x(a_0')$.

We obtain the values $\bar{U}_x(a_0)$, where $a_0 \neq a_0'$, using Figure 2.6. Once again designating the average values $\Phi_a^{(0)}$ and $H_1^{(0)}$ as a zero approximation, we determine $\Phi_1^{(0)} = \Phi_0(a_0) - \Phi_a^{(0)}$ and then calculate the corrections

$$\delta V_1 = \Delta V_\Omega^0(a_0) - \Delta V_\Omega^0(a_0') \text{ and } \delta\beta_1 = \frac{\delta V_1}{2V_p(H_1)^-}.$$

Next, we shift the curves for $U_x(\theta_1, \beta_1) = \text{const}$ by an amount $\delta\beta_1$, in the negative direction along the ordinate axis (Figure 2.1). Then we find the point $(\theta_1^0, \beta_1^0)$ at which one of these curves is tangent to the curve for $\Phi_1(\theta_1, \beta_1, H_1^{(0)}) = \Phi_1^{(0)} = \text{const}$.

The tangency point $(\theta_1^{(0)}, \beta_1^{(0)})$ is found more precisely using iterations, taking into account the shift of the $U_x(\theta_1, \beta_1) = \text{const}$ curves along the ordinate axis. These calculations are carried out in the same way as those for the case when $a_0 = a_0'$. However, whereas for $a_0 = a_0'$ the values of $\Phi_a$ and $H_1$ corresponded to $\beta_1$, in this case (for $a_0 \neq a_0'$) they correspond to $\beta_1 + \delta\beta_1$. Since $\Phi_a$ and $H_1$ vary only slightly with $\beta_1$, though, the correction $\delta\beta_1$ can sometimes be neglected when determining these quantities. Lastly, from the final values of $\theta_1$ and $\beta_1$, we find $U_x(\theta_1, \beta_1) = \bar{U}_x(a_0)$.

In the foregoing analysis the spacecraft is assumed to encounter the moon at the point where $\Omega_a = 0$ (that is, at the optimum point of its orbit). In any actual flight this condition will not be satisfied exactly. Therefore, it is interesting to know how much $U_x$ will increase with an increase in $\Omega_a$ (that is, with an increase in the striking interval on the moon's orbit). This question can obviously be answered if we determine the values of $U_x(a_0)$ corresponding to various $\Omega_a \neq 0$, using the method described above. The values of $u_0(a_0)\big|_{\Omega_a = \text{const}}$ required for this are calculated using formula (2.4), and for $\Omega_a = 0°$, 26°30', and 40° they have been plotted in Figure 2.8. By finding the optimum azimuths for each of the considered values of $\Omega_a$, it is also possible to determine the optimum inclinations $i_c$ of the trajectory plane to the plane of the equator, using formula (3.1).

## 2.5. SELECTION OF ENERGETICALLY OPTIMUM INCLINATIONS FOR TRAJECTORIES OF SECOND TYPE

In order to execute a lunar-impact trajectory of type II, the corresponding active part of the flight must extend to the plane of the lunar orbit. This means that the latitude $\psi_1$ of the point $B_1$ at the end of the active part cannot be greater than the inclination $\Theta$ of the lunar orbital plane to that of the equator. Accordingly, the active angular range $\Phi_a$ cannot be less than $\alpha = \psi_0 - \Theta$, where $\psi_0$ is the latitude of the launch point. Consequently, it will be advisable to consider only type-II trajectories for which the latitude argument of point $B_1$ is

$$u_1 = \Phi_a - \bar{u} \geqslant 0, \tag{5.1}$$

where the absolute value of the latitude argument of the launch point $|\bar{u}| > \alpha$.

It follows from Figures 1.10 and 2.1 that the energetically optimum initial data for type-II trajectories are: $\theta_1 = 0$ and $V_1 = V_{1\min}$. Since the value $\Phi_1 = 180°$ corresponds to these data, therefore $u_1 = 180° - \Phi_1 = 0$ and so (5.1) gives $\bar{u} = \Phi_a$.

Figure 2.2 shows that, for minimum initial velocities (that is, for $\beta_1 = \bar{v}^2_{min}$), the active angular range $\Phi_a$ is close to its minimum value $(\Phi_a)_{min}$. Therefore, the highest values of the parameter $\bar{u} = \Phi_a - u_1$, which are reached when $u_1 \approx 0$, are also close to $(\Phi_a)_{min}$. As demonstrated in Chapter I, the azimuth $a_S$ (reckoned counterclockwise from the southerly direction) corresponding to a constant value $\bar{u}$ reaches its highest value when $\Omega_a = 0$. The following relation will be approximately true:

$$(a_S)_{max} = a_S(\bar{u}_{max})\big|_{\Omega_a = 0}$$

in cases where

$$\bar{u}_{max} = \Phi_a = (\Phi_a)_{max}$$

(Figure 2.8).

The maximum azimuth will obviously correspond to the maximum velocity increment $\Delta V_\Omega$ due to the earth's rotation. This increment can be calculated using formulas (4.2) through (4.4) which are valid for type-II trajectories as well as type-I trajectories.

The results of this calculation of $\Delta V_\Omega(a_S)$ for $r_{1\,min}$ can be represented by a curve similar to the one in Figure 2.6, due to the smallness of the variation in the radius $r_1$. For $a_S = (a_S)_{max}$ we find:

$$\Delta V_\Omega = (\Delta V_\Omega)_{max}, \quad \delta V_\Omega = (\Delta V_\Omega)_{max} - \Delta V_\Omega(a_1).$$

$$\delta\beta_1 = \frac{2\,\delta V_\Omega}{V_p}.$$

It is now easy to find the maximum values of the required energy expenditures $U_x$. To do this, we shift the curves (Figure 2.1) upward by an amount $\delta\beta_1$ and find the value $U_x = (U_x)_{max}$ from the point with coordinates $\theta_1 = 0$ and $\beta_1 = \beta_{1\,min}$.

Let us now consider trajectories with a specified range $\Phi_a$ of the active part and a given azimuth $a_S$ which is less than the maximum aximuth $(a_S)_{max}$. For such trajectories the striking interval on the lunar orbit will narrow down to zero as $a_S \to (a_S)_{max}$. Let us determine the size of this interval as a function of $\Phi_a$, by finding the relation between the node longitude $\Omega_a$ of the advance point on the lunar orbit and the following two quantities: the inclination $i_1$ of the trajectory plane to the lunar orbital plane, and the quantity $\bar{u} = \Phi_a - u_1$, where $u_1$ is the latitude argument of the point corresponding to the end of the active part.

From the spherical right triangle $XP\Omega_a$ (Figure 2.9) we have

$$\cos\Omega_a = \frac{\cos m}{\sin\Theta}, \tag{5.2}$$

where $\Theta$ is the angle between the planes of the equator and the moon's orbit, and $m = P\Omega_a$. From spherical triangle $PB_0\Omega_a$, the law of cosines for side $m$ gives

$$\cos m = \cos\bar{u}\sin\psi_0 - \sin\bar{u}\cos\psi_0\cos a_S. \tag{5.3}$$

Formula (5.3) is applicable for type-I trajectories when $a_S = -a_0$ and $\bar{u} = u_0$, where $u_0$ is the latitude argument of the launch point. Therefore, the

relation $u(\Omega_a)$ is identical to the relation $u_0(\Omega_a)$ for type-I trajectories (Figure 2.4). It is also easy to verify that, when calculating the inclination $i_1 = s - \tau$ (Figure 2.9), the quantities $\tau$ and $s$ are found using the same formulas as for type-I trajectories, if $\bar{u} = u_0$ and $a_S = -a_0 + \pi$:

$$\sin\tau = \frac{\cos\Theta}{\sin m}, \quad \sin s = \frac{\sin a_S}{\sin m}\cos\psi_0. \tag{5.4}$$

Clearly, in order to obtain the value $\Omega_a^*$ corresponding to the end of the striking interval, we have to set $u_1 = 0$, so that $\bar{u} = \Phi_a$.

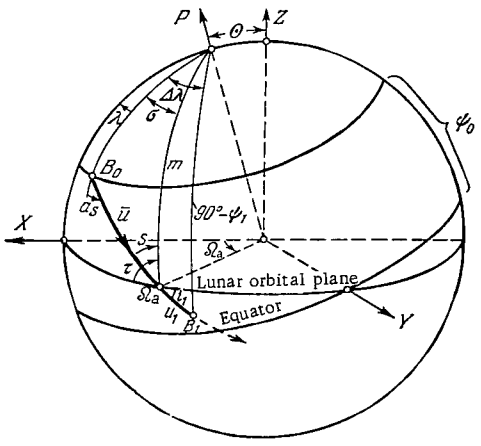


FIGURE 2.9. Route of active part of type-II trajectory through absolute space.

It should be noted that, contrary to flights along type-I trajectories, for flights along type-II trajectories with specified inclinations of the trajectory plane to the lunar orbital plane, the following will be true: lunar impacts at the end points of the striking interval will require minimum energy expenditures, whereas impacts at the midpoint of the interval will require maximum expenditures. Actually, due to the constancy of the azimuth and the slight variability of the length $\Phi_a(\theta_1, \beta_1)$ of the active part, as the advance point moves from the end of the striking interval to its midpoint, the latitude argument $u_1$ increases monotonically. Accordingly, the passive range $\Phi_1 = \pi - u_1$ decreases monotonically (Figure 2.9), which according to Figures 1.10 and 2.1 must lead to an increase in the energy expenditures. The energy requirements for different values of $\Omega_a$ for type-II trajectories are calculated in just the same way as for type-I trajectories, except that in this case $\bar{u}$ replaces $u_0$. For type-II trajectories it is convenient to take the values $\theta_1 = 0$ and $\beta_1 = \beta_{1\,min}$ as a zero approximation.

It is interesting to ascertain how the probability of a lunar impact is increased for larger active ranges $\Phi_a$. The maximum value of the velocity increment due to the earth's rotation is reached for an azimuth of 90° (Figure 2.6). Therefore, with an increase in $\Phi_a$, for $\Omega_a = 0$ and $\Phi_1 = 180°$, the gain in velocity increases and reaches a maximum at the value of $\Phi_a$ for which the maximum azimuth $(a_S)_{max} = 90°$. Here the flight direction will be directly eastward. For a further increase in $\Phi_a$, the azimuth $a_S$ becomes less than 90° and the gain in velocity diminishes. Therefore, the inclination $i_e$ for which the trajectory azimuth is directly to the east is the energetically optimum one for type-II trajectories.

The calculation of the velocity increment $\Delta V_\Omega$ for various $\Phi_a$, using the formulas of § 2.4, is quite simple in this case. First we assume that $\Omega_a = 0$ and that the latitude of the end of the active part $\psi_1 = \Theta$ is constant. Then we can plot $\Delta V_\Omega(\Phi_a)$ and $\Delta\lambda(\Phi_a)$, where $\Delta\lambda$ is the angle between the meridians of the beginning and end points of the active part. Figure 2.10 shows these

curves for an initial height $H_1 = 300$ km and an angle of elevation of the initial-velocity vector above the local horizon $\theta_1 \approx 0°$.

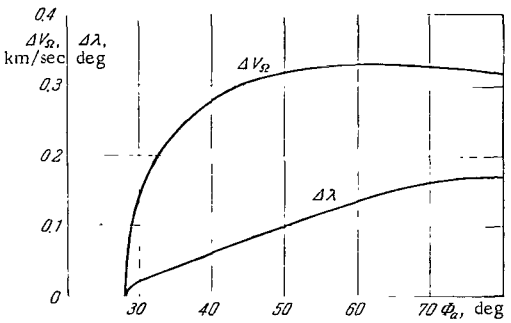


FIGURE 2.10. Velocity increment $\Delta V_\Omega$ due to earth's rotation and duration $\Delta\lambda$ (longitude) of active part of type-II trajectory, as functions of angular range $\Phi_a$ of active part.

The curve for $\Delta\lambda$ was obtained using the following formula, which follows directly from a study of Figure 2.9:

$$\sin\Delta\lambda = \frac{\sin a_S}{\cos\psi_1}\sin\Phi_a. \tag{5.5}$$

Now let us find the value of $\Phi_a$ corresponding to the maximum possible velocity increment and determined by the condition that the arc $u = \Phi_a$ be tangent to the parallel $\psi_0$ of the launch point, ending at the point with $\Omega_a = 0$. From the right triangle with the hypotenuse $m = 90° - \Theta$ and legs $\Phi_a$ and $90° - \psi_0$, we obtain

$$\cos\Phi_a = \frac{\sin\Theta}{\sin\psi_0}. \tag{5.6}$$

In the present case $\Theta = 18°20'$, $\psi_0 = 47°$, and $\Phi_a \approx 65°$. Then, for $a_0 = 90°$ and $\psi_1 = \Theta$ formula (5.5) becomes

$$\sin\Delta\lambda = \frac{\sin\Phi_a}{\cos\Theta}, \tag{5.7}$$

from which we obtain $\Delta\lambda \approx 70°$.

The energy requirements corresponding to optimum type-II trajectories will be considerably less than those for trajectories of type I. However, to execute a type-II trajectory, the initial velocity and the initial height must have certain much more precise values than in the case of type-I trajectories. This is explained by the fact that minimum or close to minimum flight velocities are required for type-II trajectories. As the initial velocity rises above minimum, the required accuracy of the parameters is rapidly reduced. It should also be mentioned in passing that, for a constant azimuth of a type-II trajectory, a lower accuracy of the initial data is required for lunar impact at the midpoint of the striking interval than for impact at the end of the interval. In the subsequent study only trajectories of type I will be considered.

*Chapter III*

# *NOMINAL IMPACT TRAJECTORIES AND EFFECT OF INITIAL-DATA SCATTER, TAKING INTO ACCOUNT LUNAR ATTRACTION*

## 3.1. NOMINAL LUNAR-IMPACT TRAJECTORIES

In order to determine, even roughly, the effect of the scatter of initial data, it is not enough just to consider the influence of the earth. The moon's influence, at any rate within its sphere of action, must also be taken into account. In the following, we calculate the nominal trajectories using an approximate method in which the earth's attraction is taken into account outside the moon's sphere of action and the moon's attraction is taken into account inside this sphere. Many of the three-dimensional approach trajectories* involve six parameters. However, in the three-dimensional case nominal trajectories directed toward the moon's center will involve only four parameters. Therefore, it is always possible to specify arbitrarily any four of the quantities determining the initial data, and to find the other two quantities from the condition of impact at the lunar center. Then, by assuming various deviations of the initial parameters and calculating the corresponding trajectories, it is easy to determine the effect of the scatter of initial data.

The nominal trajectory can be determined using the iteration technique for two variables. However, it is possible to select the four arbitrary parameters in such a way that iteration need not be used for one of the correspondingly chosen variables.

Actually, let us take the following quantities as the arbitrary parameters: the height $H_1$ of the beginning $B_1$ of the passive part of the trajectory; the amount $\Delta V_1$ by which the initial geocentric velocity exceeds local parabolic; the angle $\alpha_1$ between the initial-velocity vector and the initial radius; and the angle $i_1$ of inclination of the trajectory plane to the base plane (plane of lunar orbit). These four quantities determine the plane and the shape of the trajectory and they enable the complete determination of a lunar-approach trajectory, provided the point of entry into the moon's sphere of action is specified. If the corresponding trajectory is not directed toward the moon's center $m_2$, the selenocentric entry velocity $V_2'$ for this trajectory will not be directed toward $m_2$ either. The direction of velocity $V_2'$ varies slightly with the position of the entry point $B_2$ on the moon's sphere of action (see § 2.1). Thus, we can select a new point $B_2$ in such a way that the direction $\overrightarrow{B_2 m_2}$ will be parallel to the vector $V_2'$ corresponding to the previous point $B_2$, and each time we obtain trajectories which are closer to the moon's center.

* [Approach trajectories (see definition on p. 7) include impact trajectories, circumlunar trajectories, and flyby trajectories.]

The above idea can be carried out as follows (Figure 3.1). We designate the coordinates of the entry point $B_2$ in the selenocentric coordinate system as $\xi_2$, $\eta_2$, and $\zeta_2$. The $\xi$ axis is assumed to point toward the earth's center $m_1$ at all times, the $\eta$ axis lies in the base plane, and the $\zeta$ axis completes the system as a right-handed coordinate system. The geocentric radius $r_2$, the geocentric velocity $V_2$, and the angle $\alpha_2$ between the vectors of the geocentric entry velocity and the geocentric entry radius can now be found using the formulas:

$$\left.\begin{aligned} r_2 &= \sqrt{(a-\xi_2)^2+\eta_2^2+\zeta_2^2}, \\ r_1 &= r_0 + H_1, \quad \nu = \frac{r_1}{r_2}, \\ V_1 &= V_p + \Delta V_1, \quad V_p = \sqrt{\frac{2\mu_1}{r_1}}, \\ \Delta\beta_1 &= \frac{\Delta V_1}{V_p}\left(2+\frac{\Delta V_1}{V_p}\right), \\ \beta_2 &= \Delta\beta_1 + \nu, \quad V_2 = V_p\sqrt{\beta_2}, \\ \sin\alpha_2 &= \nu\frac{V_1}{V_2}\cos\theta_1, \quad \theta_1 = 90^\circ - \alpha_1. \end{aligned}\right\} \tag{1.1}$$

Here $a = 384{,}400$ km is the distance between the centers of the earth and the moon, $r_0 = 6371$ km is the radius of the earth, $V_p$ is the parabolic velocity for a height $H_1$, $\mu_1 = 397{,}529\ \text{km}^3/\text{sec}^2$ is the gravitational potential of the earth, and $\Delta\beta_1 = \beta_1 - 1$, where $\beta_1 = \left(\frac{V_1}{V_p}\right)^2$. The formulas $\beta_2$ and $\alpha_2$ obviously characterize the geocentric integrals of the energy and the areas, respectively, for points $B_1$ and $B_2$.

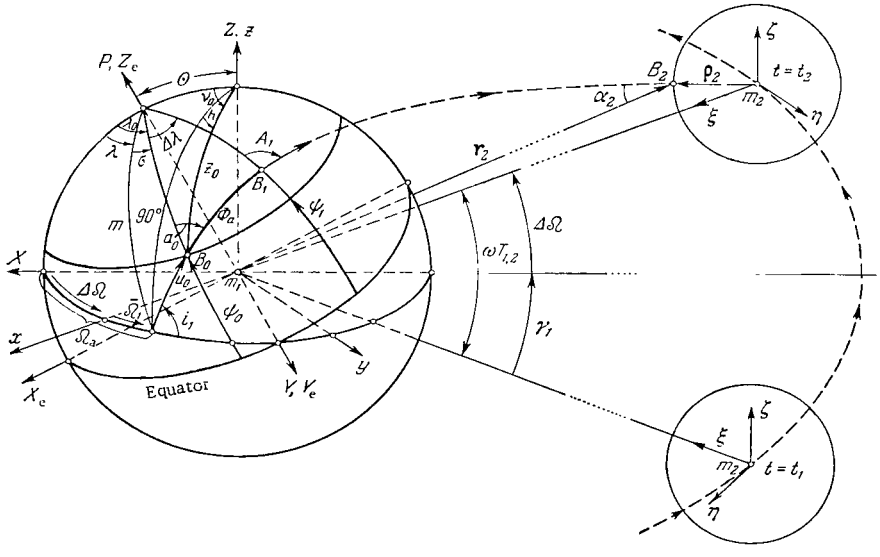


FIGURE 3.1. Geometrical parameters characterizing a three-dimensional lunar-approach trajectory outside moon's sphere of action.

Let us now determine the components $\dot{x}_2$, $\dot{y}_2$, and $\dot{z}_2$ of the velocity $V_2$ in the geocentric $xyz$ system. The axes of this system will be parallel to the $\xi$, $\eta$, and $\zeta$ axes, respectively, at the moment $t_2$ when the spacecraft enters the moon's sphere of action. These components are found as follows:

$$\left.\begin{aligned}
&\sin u_2 = \frac{\zeta_2}{r_2 \sin i_1},\\
&x_2' = r_2 \cos u_2, \quad y_2' = r_2 \sin u_2 \cos i_1,\\
&x_2 = \xi_2 - a, \quad y_2 = \eta_2, \quad z_2 = \zeta_2,\\
&\cos \overline{\Omega}_1 = \frac{x_2 x_2' + y_2 y_2'}{x_2'^2 + y_2'^2}, \quad \sin \overline{\Omega}_1 = \frac{y_2 x_2' - x_2 y_2'}{x_2'^2 + y_2'^2},\\
&\mathfrak{M}_2 = u_2 + \alpha_2,\\
&\dot{x}_2 = V_2 (\cos \mathfrak{M}_2 \cos \overline{\Omega}_1 - \sin \mathfrak{M}_2 \sin \overline{\Omega}_1 \cos i_1),\\
&\dot{y}_2 = V_2 (\cos \mathfrak{M}_2 \sin \overline{\Omega}_1 + \sin \mathfrak{M}_2 \cos \overline{\Omega}_1 \cos i_1),\\
&\dot{z}_2 = V_2 \sin \mathfrak{M}_2 \sin i_1.
\end{aligned}\right\} \qquad (1.2)$$

Here $u_2$ is the latitude argument of point $B_2$; $x_2$, $y_2$, and $z_2$ are the coordinates of point $B_2$ in the geocentric coordinate system; $\overline{\Omega}_1$ is the node longitude of the trajectory of motion toward the moon's sphere of action, measured in the base plane; and $\mathfrak{M}_2$ is the analog of the latitude argument for determining the components of the geocentric entry velocity $V_2$ using formulas similar to those used to determine the coordinates from the Keplerian elements.

The components of the selenocentric entry velocity $V_2'$, its absolute value $U$, and the angle $\alpha_2'$ between it and the selenocentric entry radius $\rho_2$ at the point of entry into the moon's sphere of action are determined using the following formulas (Figure 3.2):

$$\left.\begin{aligned}
&\dot{\xi}_2 = \dot{x}_2, \quad \dot{\eta}_2 = \dot{y}_2 - V_1, \quad \dot{\zeta}_2 = \dot{z}_2, \quad U = \sqrt{\dot{\xi}_2^2 + \dot{\eta}_2^2 + \dot{\zeta}_2^2},\\
&\sin \alpha_2' = \frac{1}{\rho_* U} [(\eta_2 \dot{\zeta}_2 - \zeta_2 \dot{\eta}_2)^2 + (\zeta_2 \dot{\xi}_2 - \xi_2 \dot{\zeta}_2)^2 +\\
&\qquad + (\xi_2 \dot{\eta}_2 - \eta_2 \dot{\xi}_2)^2]^{\frac{1}{2}},
\end{aligned}\right\} \qquad (1.3)$$

where $\rho_* = 66{,}000$ km is the radius of the moon's sphere of action, and $V_1 = 1.023$ km/sec is the velocity of the moon. The deviation of the trajectory from the moon's center will obviously be characterized by the quantity $\sin \alpha_2'$. If it turns out that $|\sin \alpha_2'| < \varepsilon$, where $\varepsilon$ is the specified accuracy, then the nominal values $\xi_2$, $\eta_2$, and $\zeta_2$ are found. However, if $|\sin \alpha_2'| > \varepsilon$, then more accurate values of $\xi_2$, $\eta_2$, and $\zeta_2$ will obviously be given by the formulas:

$$\xi_2 = -\frac{\rho_*}{U} \dot{\xi}_2, \quad \eta_2 = -\frac{\rho_*}{U} \dot{\eta}_2, \quad \zeta_2 = -\frac{\rho_*}{U} \dot{\zeta}_2, \qquad (1.4)$$

after which the calculation can be repeated from the beginning.

The values $\xi_{2_0}$, $\eta_{2_0}$, and $\zeta_{2_0}$ at the point on the sphere of action where the direction of the selenocentric radius is opposite to that of the selenocentric velocity at the distance of the lunar orbit, without taking into account the moon's attraction, can be taken as a zero approximation for

$\xi_2$, $\eta_2$, and $\zeta_2$. These values can be calculated using formulas (1.4) of this chapter, for the values $\dot{\xi}_2$, $\dot{\eta}_2$, and $\dot{\zeta}_2$ given by the formulas:

$$\left.\begin{aligned} \dot{\xi}_2 &= -V_2 \cos \alpha_2, \\ \dot{\eta}_2 &= V_L - V_2 \sin \alpha_2 \cos i_1, \\ \dot{\zeta}_2 &= -V_2 \sin \alpha_2 \sin i_1, \end{aligned}\right\} \qquad (1.5)$$

where $V_2$ and $\alpha_2$ are found from formulas (1.1) of this chapter, for $\xi_2 = \eta_2 = \zeta_2 = 0$.

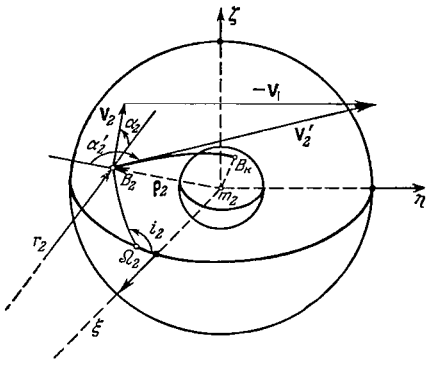


FIGURE 3.2. Geometrical parameters characterizing a three-dimensional lunar-approach trajectory inside the moon's sphere of action.

When formulas (1.1) through (1.4) are used to calculate a trajectory passing about 1 km from the center of the moon, no more than 6 iterations are required, so that the convergence of the described process will be rapid enough.

When the iterations using formulas (1.1) through (1.4) converge with the required accuracy, all the parameters of the nominal trajectory are easily calculated. The familiar formulas of celestial mechanics are used to determine the missing geocentric Keplerian elements $p_1$, $e_1$, and $\omega_1$ of the trajectory of motion toward the moon's sphere of action, in terms of coordinates $x_2$, $y_2$, and $z_2$ and velocities $\dot{x}_2$, $\dot{y}_2$, and $\dot{z}_2$. In addition, the selenocentric Keplerian elements $p_2$, $e_2$, $i_2$, $\Omega_2$, and $\omega_2$ of the trajectory of motion in the sphere of action are found in terms of coordinates $\xi_2$, $\eta_2$, and $\zeta_2$ and velocities $\dot{\xi}_2$, $\dot{\eta}_2$, and $\dot{\zeta}_2$.

The true anomalies $v_1$ and $v_2$ and the flight time $T_{1,2}$ outside the sphere of action are determined in terms of elements $p_1$ and $e_1$ and radii $r_1$ and $r_2$. Similarly, the flight time $T_{2,i}$ from the limit of the sphere of action to impact on the moon, and also the total flight time $T = T_{1,2} + T_{2,i}$, are found in terms of elements $p_2$ and $e_2$ and the selenocentric radii $\rho$ and $\rho_L = 1736.7$ km (the radii of the sphere of action and the lunar surface, respectively).

The position of the $xyz$ coordinate system (Figure 3.1) depends on the values selected for $H_1$, $\Delta V_1$, $\theta_1$, and $i_1$. Thus it is of interest to determine the motion according to some stationary coordinate system, for example, system $XYZ$, whose $Y$ axis is directed toward the descending node (relative to the equator) of the lunar orbit, whose $Z$ axis is orthogonal to the lunar orbital plane on the side of the north pole $P$ of the earth, and whose $X$ axis is in the lunar orbital plane, forming a right-handed coordinate system with the $Y$ and $Z$ axes (Figure 3.1). The trajectory characteristics can be determined in this system only in terms of the earlier found parameters, provided the latitude $\psi_0$ of the launch point and the angular range $\Phi_a$ of the active part of the trajectory are given. For instance, the node longitude $\Omega_a$

is determined using the following formulas:

$$\left.\begin{aligned} u_1 &= v_1 + \omega_1, \quad u_0 = u_1 - \Phi_a, \\ \cos z_0 &= \sin u_0 \sin i_1, \quad \cos h = \frac{\cos u_0}{\sin z_0}, \\ \cos v_0 &= \frac{\sin \psi_0 - \cos \Theta \cos z_0}{\sin \Theta \sin z_0}, \\ \Omega_a &= v_0 - h \quad \text{or} \quad \Omega_a = -v_0 - h \end{aligned}\right\} \tag{1.6}$$

(depending on whether we wish to locate point $B_0$ to the right or to the left of the meridian of the $X$ axis). Obviously, for specified values of $i_1$ and $u_0$, there will be two positions of point $B_0$ corresponding to each value of angle $v_0$ (Figure 3.1). In formulas (1.6): $u_0$ is the latitude argument of the launch point $B_0$; $z_0$ is the angular distance of point $B_0$ from the $z$ axis; $h$ is the angle between the arcs of great circles drawn from the $z$ axis to points $B_0$ and $\Omega_a$ (Figure 3.1); and $\Theta = 18°20'$ is the angle between the planes of the equator and the lunar orbit.

Once elements $r_1$, $i_1$, $u_1$, and $\Omega_a$ are known, the familiar formulas of celestial mechanics can be used to find the initial coordinates and velocities in the $XYZ$ system:

$$\left.\begin{aligned} X_1 &= r_1 (\cos u_1 \cos \Omega_a - \sin u_1 \sin \Omega_a \cos i_1), \\ Y_1 &= r_1 (\cos u_1 \sin \Omega_a + \sin u_1 \cos \Omega_a \cos i_1), \\ Z_1 &= r_1 \sin u_1 \sin i_1, \end{aligned}\right\} \tag{1.7'}$$

$$\left.\begin{aligned} \mathfrak{M}_1 &= u_1 + (90° - \theta_1), \\ \dot{X}_1 &= V_1 (\cos \mathfrak{M}_1 \cos \Omega_a - \sin \mathfrak{M}_1 \sin \Omega_a \cos i_1), \\ \dot{Y}_1 &= V_1 (\cos \mathfrak{M}_1 \sin \Omega_a + \sin \mathfrak{M}_1 \sin \Omega_a \cos i_1), \\ \dot{Z}_1 &= V_1 \sin \mathfrak{M}_1 \sin i_1. \end{aligned}\right\} \tag{1.7''}$$

Azimuths $a_0$ and $a_1$ of the launch point $B_0$ and the beginning $B_1$ of the passive part, the latitude $\psi_1$ of point $B_1$, and angles $\lambda_0$ and $\Delta\lambda$ respectively, the angle between the meridians of the $X$ axis and the launch point $B_0$ and the angle between the meridians of points $B_0$ and $B_1$) can be found using the following formulas of spherical trigonometry:

$$\left.\begin{aligned} \cos m &= \sin \Theta \cos \Omega_a, \quad \cos a_0 = \frac{\cos u_0 \sin \psi_0 - \cos m}{\sin u_0 \cos \psi_0}, \\ \sin \psi_1 &= \sin \psi_0 \cos \Phi_a + \cos \psi_0 \sin \Phi_a \cos a_0, \\ \cos a_1 &= \frac{\sin \psi_1 \cos \Phi_a - \sin \psi_0}{\cos \psi_1 \sin \Phi_a}, \\ \sin \Delta\lambda &= \sin \Phi_a \frac{\sin a_0}{\cos \psi_1}, \quad \sin \lambda = \frac{\sin \Omega_a}{\sin m}, \\ \cos \sigma &= \frac{\cos u_0 - \cos m \sin \psi_0}{\sin m \cos \psi_0}, \quad \lambda_0 = \lambda + \sigma, \end{aligned}\right\} \tag{1.8}$$

where $m$ is the angular distance $\Omega_a$ of the node from pole $P$, $\lambda$ is the angle between the meridians of the node and the $X$ axis, and $\sigma$ is the angle between the meridians of the node and the launch point $B_0$.

When we know the difference between the node longitudes in the $XYZ$ and $xyz$ coordinate systems:

$$\Delta\Omega = \Omega_a - \bar{\Omega}_1, \tag{1.9}$$

we can find the angle $\gamma_1$ between the geocentric radius of the moon at the moment $t_1$ of engine cutoff and the negative $X$ axis, as well as the initial coordinates and velocities of the moon:

$$\left.\begin{aligned} &\gamma_1 = \omega T_{1,2} - \Delta\Omega, \\ &X_L = -a\cos\gamma_1, \quad Y_L = a\sin\gamma_1, \quad Z_1 = 0, \\ &\dot{X}_L = -V_L\sin\gamma_1, \quad \dot{Y}_1 = -V_L\cos\gamma_1, \quad \dot{Z}_1 = 0, \end{aligned}\right\} \tag{1.10}$$

where $\omega$ is the moon's angular velocity of rotation.

Finally, let us find the coordinates $\xi_1$, $\eta_1$, and $\zeta_1$ of the point of impact on the lunar surface, the impact velocity $U_1$, and the angle $\theta_1$ between this velocity and the lunar surface at the impact point:

$$\left.\begin{aligned} &\cos v_1 = \frac{1}{e_2}\left(\frac{p_2}{\rho_1} - 1\right), \quad u_1 = v_1 + \omega_2, \quad \Omega_{\zeta 2} = \bar{\Omega}_{\zeta 2} - \omega T_{2,1}, \\ &\xi_1 = \rho_1(\cos u_1\cos\Omega_{\zeta 2} - \sin u_1\sin\Omega_{\zeta 1}\cos i_2), \\ &\eta_1 = \rho_1(\cos u_1\sin\Omega_{\zeta 2} + \sin u_1\cos\Omega_{\zeta 2}\cos i_2), \\ &\xi_1 = \rho_1\sin u_1\sin i_2, \\ &U_1^2 = 2\mu_2\left(\frac{1}{\rho_1} - \frac{1}{\rho_*}\right) + U_2^2, \\ &\cos\theta_1 = \frac{\rho_*}{\rho_1}\frac{U_2}{U_1}\sin\alpha_2'. \end{aligned}\right\} \tag{1.11}$$

Here $v_1$ and $u_1$ are the true anomaly and latitude argument of the impact point, $\bar{\Omega}_{\zeta 2}$ and $\Omega_{\zeta 2}$ are the node longitudes in the $\xi\eta\zeta$ coordinate system at the moment of entry into the moon's sphere of action and the moment of impact, respectively, $\mu_2$ is the gravitational potential of the moon, $U$ is the absolute value of the selenocentric entry velocity, and $\alpha_2'$ is the angle between this velocity and the selenocentric radius $\rho_2$ at the limit of the sphere of action.

It should be noted that, when the trajectory comes close enough to the moon's center, $v_1$ is close to 180°, the coordinates of the impact point are proportional to the impact-velocity components, and the angle $\theta_1$ is close to 90°.

The formulas given in this section were used to calculate the nominal impact trajectories, and the results were compared with the results of a more exact calculation (taking into account perturbations by the earth and the moon). The differences between the values obtained for the coordinates at the limit of the sphere of action and at the lunar surface only amounted to some tens of kilometers. This indicates that the approximate method is, after all, of sufficient accuracy (see § 4 of this chapter).

## 3.2. CALCULATION OF MODIFIED TRAJECTORIES

When the nominal trajectory has been found, the corresponding effect of initial-data scatter can be determined accurately enough by calculating the deviations of impact points on the lunar surface corresponding to trajectories with different known deviations of the initial data from nominal. Therefore, in contrast to the boundary problem of the preceding section, the determination of the deviated trajectories involves a simpler problem, the Cauchy problem. However, in spite of the fact that the initial

data for the spacecraft and the moon's sphere of action are known, this problem is still an impact-point problem. The simplest way to solve it is by successive approximations, by one-dimensional iterations according to time at the given distance $\rho_*$ of the spacecraft from the moon's center $m_2$. A method for determining the initial data for the deviated trajectories, together with an iteration method for calculating the latter, will be given below.

It is convenient to give the deviations of the initial data from nominal in terms of an *hls* coordinate system, rather than in terms of the *XYZ* system. This system is related to the beginning of the passive part of the trajectory, and its base plane is the trajectory plane *lh*. The *h* axis is directed along radius $r_1$, and the *l* axis is parallel to the transversal in the direction of flight. The deviations of initial data fall into three classes:

I. A deviation of the initial radius vector of the spacecraft from nominal.

II. A deviation of the initial-velocity vector of the spacecraft from nominal.

III. A deviation of the time of beginning of motion from nominal.

For terrestrial missions the latter deviation has no effect on the impact, but for moon flights it is very important, since the relative positions of the initial point and the target are affected.

In this section only the simplest case will be considered, that is, a deviation of only one of the components of $r_1$ or $V_1$ in the *hls* coordinate system, or a deviation of only one time.

I. Variation of initial coordinates.

1) $\delta H_1 \neq 0$ (height deviation given). In this case $r_1$, $V_\rho$, and $\Delta V_1$ are replaced by the quantities:

$$\left.\begin{aligned} r_1^\vee &= r_1 + \delta H_1, \quad V_\rho^\vee = \sqrt{\frac{2\mu_1}{r_1^\vee}}, \\ \Delta V_1^\vee &= \Delta V_1 + \frac{2\mu_1}{V_\rho + V_\rho^\vee} \cdot \frac{\delta H_1}{r_1 r_1^\vee} \end{aligned}\right\} \tag{2.1}$$

Since the latitude argument $u_1$, the node position $\Omega_a$, and the inclination $i_1$ of the trajectory remain the same, formulas (1.7') can be used to find the varied values $X_1^\vee$, $Y_1^\vee$, and $Z_1^\vee$.

2) $\delta l \neq 0$ (shift in flight direction given). Obviously, in this case a vector with components

$$L_1 = c_2 Z_1 - c_3 Y_1, \quad L_2 = c_3 X_1 - c_1 Z_1, \quad L_3 = c_1 Y_1 - c_2 X_1,$$

where $c_1$, $c_2$, and $c_3$ are the components of the areal velocity, will be directed along the *l* axis. Once we have found the absolute value of this vector

$$L = \sqrt{L_1^2 + L_2^2 + L_3^2},$$

we obtain the modified values of the coordinates

$$X_1^\vee = X_1 + \frac{L_1}{L}\delta l, \quad Y_1^\vee = Y_1 + \frac{L_2}{L}\delta l, \quad Z_1^\vee = Z_1 + \frac{L_3}{L}\delta l. \tag{2.2}$$

the initial radius $r_1^v$, the parabolic velocity $V_p^v$, and the amount $\Delta V_1^v$ by which the initial velocity exceeds local parabolic:

$$\left.\begin{aligned} r_1^v &= \sqrt{r_1^2 + \delta l^2}, \quad V_p^v = \sqrt{\frac{2\mu_1}{r_1^v}}, \\ \Delta V_1^v &= \Delta V_1 + \frac{2\mu_1}{V_p + V_p^v} \cdot \frac{\delta l}{r_1 r_1^v} \cdot \frac{\delta l}{r_1 + r_1^v}. \end{aligned}\right\} \tag{2.3}$$

Here, the angle $\theta_1$ will also vary by a small amount of first order:

$$\sin \theta_1^v = \frac{\dot{X}_1 X_1^v + \dot{Y}_1 Y_1^v + \dot{Z}_1 Z_1^v}{r_1^v V_1}.$$

3) $\delta s \neq 0$ (lateral deviation given). Obviously, in this case:

$$\left.\begin{aligned} X_1^v &= X_1 + \frac{c_1}{c}\delta s, \quad Y_1^v = Y_1 + \frac{c_2}{c}\delta s, \quad Z_1^v = Z_1 + \frac{c_3}{c}\delta s, \\ r_1^v &= \sqrt{r_1^2 + \delta s^2}, \quad V_p^v = \sqrt{\frac{2\mu_1}{r_1^v}}, \\ \Delta V_1^v &= \Delta V_1 + \frac{2\mu_1}{V_p + V_p^v} \cdot \frac{\delta s^2}{(r_1 + r_1^v) r_1 r_1^v}. \end{aligned}\right\} \tag{2.4}$$

Although the angle $\theta_1$ also varies by a small amount of second order, the effect of this variation will be less than the effect of $\Delta V_1^v$.

II. Variation of initial-velocity vector. Let us consider variations of the magnitude $\delta V_1$ and direction $\delta\theta_1$ of the velocity in the trajectory plane, and also variations of the lateral component $\delta\dot{s} = \dot{s}$ of the velocity (since for the nominal trajectory $\dot{s} = 0$).

1) $\delta V_1 \neq 0$. In this case $\Delta V_1^v = \Delta V_1 + \delta V_1$, $V_1^v = V_p + \Delta V_1^v$, and from formulas (1.7'') it is easy to find components $\dot{X}_1^v$, $\dot{Y}_1^v$, and $\dot{Z}_1^v$ of the initial velocity.

2) $\delta\theta_1 \neq 0$. In this case $\theta_1^v = \theta_1 + \delta\theta_1$, $\mathfrak{M}_1^v = \mathfrak{M}_1 - \delta\theta_1$. The velocity components are once again found using formulas (1.7'').

3) $\delta\dot{s} \neq 0$. In this case

$$\left.\begin{aligned} \dot{X}_1^v &= \dot{X}_1 + \frac{c_1}{c}\delta\dot{s}, \quad \dot{Y}_1^v = \dot{Y}_1 + \frac{c_2}{c}\delta\dot{s}, \quad \dot{Z}_1^v = \dot{Z}_1 + \frac{c_3}{c}\delta\dot{s}, \\ V_1^v &= \sqrt{V_1 + \delta\dot{s}^2}. \end{aligned}\right\} \tag{2.5}$$

and $\Delta V_1^v$ is the smaller root of the quadratic equation

$$(2V_p + \Delta V_1^v)\Delta V_1^v = (2V_p + \Delta V_1)\Delta V_1 + \delta\dot{s}^2. \tag{2.6}$$

III. Variation only of moment $t_1$ of entry into passive part ($\delta t_1 \neq 0$). In this case the coordinates and velocity components are found using the similar formulas:

$$\left.\begin{aligned} X_c &= X_1 \cos\Theta - Z_1 \sin\Theta, \\ Y_c &= Y_1, \\ Z_c &= X_1 \sin\Theta + Z_1 \cos\Theta, \end{aligned}\right| \quad \left.\begin{aligned} \dot{X}_c &= \dot{X}_1 \cos\Theta - \dot{Z}_1 \sin\Theta, \\ \dot{Y}_c &= \dot{Y}_1, \\ \dot{Z}_c &= \dot{X}_1 \sin\Theta + \dot{Z}_1 \cos\Theta; \end{aligned}\right\} \tag{2.7}$$

$$\delta\lambda = \Omega\,\delta t_1; \tag{2.8}$$

$$\left.\begin{aligned} X_e^v &= X_e\cos\delta\lambda - Y_e\sin\delta\lambda, \\ Y_e^v &= X_e\sin\delta\lambda + Y_e\cos\delta\lambda, \\ Z_e^v &= Z_e, \end{aligned}\right| \left.\begin{aligned} \dot X_e^v &= \dot X_e\cos\delta\lambda - \dot Y_e\sin\delta\lambda, \\ \dot Y_e^v &= \dot X_e\sin\delta\lambda + \dot Y_e\cos\delta\lambda, \\ \dot Z_e^v &= \dot Z_e; \end{aligned}\right\} \tag{2.9}$$

$$\left.\begin{aligned} X_1^v &= X_e^v\cos\Theta + Z_e^v\sin\Theta, \\ Y_1^v &= Y_e^v, \\ Z_1^v &= -X_e^v\sin\Theta + Z_e^v\cos\Theta. \end{aligned}\right| \left.\begin{aligned} \dot X_1^v &= \dot X_e^v\cos\Theta + \dot Z_e^v\sin\Theta, \\ \dot Y_1^v &= Y_e^v, \\ \dot Z_1^v &= -X_e^v\sin\Theta + \dot Z_e^v\cos\Theta. \end{aligned}\right\} \tag{2.10}$$

In addition, the angular variation of the moon's position during the time $\delta t_1$ is determined using the fomula $\gamma_1^v = \gamma_1 - \omega\delta t_1$.

Consequently, we have initial coordinates and velocities for all the deviated trajectories. The familiar formulas of celestial mechanics can thus be used to find from them the Keplerian elements $p_1^v$, $e_1^v$, $i_1^v$, $\Omega_a^v$, and $\omega_1^v$ of the part of the flight up to the moon's sphere of action and the latitude $u_1^v$ for point $B_1$.

Now let us consider the iteration process for determining the point of entry into the moon's sphere of action for a deviated trajectory. It is numerically easier to determine the flight time $T_{1,2}$ from the point $(v_2, r_2)$ (where $v_2$ is the true anomaly corresponding to the radius $r_2$), than to determine point $(v_2, r_2)$ from a given value of $T_{1,2}$. Therefore, to obtain $\rho_2 \to \rho_*$ it will be more convenient to carry out the iterations for the radius $r_2$ than for the time $T_{1,2}$.

We assume that some value $r_2^{(n)}$ is given, for instance, the value of $r_2$ for the nominal trajectory. Then, from $p_1^v$, $e_1^v$, and $r_2^{(n)}$, we find the true anomaly $v_2^{(n)}$ using the conic-section equation and determine the flight time $T_{1,2}^{(n)}$. Now we find the coordinates of the moon at the moment $t_2^{(n)} = t_1^v + T_{1,2}^{(n)}$:

$$X_1^{(n)} = -a\cos\varphi^{(n)}, \quad Y_1^{(n)} = -a\sin\varphi^{(n)}, \quad Z_1^{(n)} = 0, \tag{2.11}$$

where $\varphi^{(n)} = -\gamma_1^v + \omega T_{1,2}^{(n)}$ is the angle between the geocentric radius of the moon at the moment $t_2^{(n)}$ and the negative $X$ axis. The distance $\rho_2^{(n)}$ at the moment $t_2^{(n)}$ is given by the formula

$$\rho_2^{(n)} = \sqrt{\left[X_2^{(n)} - X_1^{(n)}\right]^2 + \left[Y_2^{(n)} - Y_1^{(n)}\right]^2 + \left[Z_2^{(n)}\right]^2}, \tag{2.12}$$

in which $X_2^{(n)}$, $Y_2^{(n)}$, and $Z_2^{(n)}$ are given by formulas (1.7') in terms of $r_2^{(n)}$, $\Omega_1^v$, $i_1^v$, and $u_2^{(n)} = v_2^{(n)} + \omega_2^v$.

If it turns out that $|\rho_2^{(n)} - \rho_*| > \varepsilon$, where $\varepsilon$ is the required accuracy, then the method of chords can be used: first $r_2^{(n)}$ is increased slightly, by an amount $\Delta r_2$ (in the calculations $\Delta r_2$ was taken to be 5000 km), and the calculation is made for $r_2^{(n+1)} = r_2^{(n)} + \Delta r_2$. Once we have obtained the value $\rho_2^{(n+1)}$ corresponding to $r_2^{(n+1)} = r_2^{(n)} + \Delta r_2$, we can make the following approximation:

$$\left.\begin{aligned} r_2^{(n+2)} &= r_2^{(n)} + \frac{\left[\rho_* - \rho^{(n)}\right]\left[r_2^{(n+1)} - r_2^{(n)}\right]}{\rho^{(n+1)} - \rho^{(n)}}, \\ \rho_2^{(n+2)} &= \rho_2\left[r_2^{(n+2)}\right]. \end{aligned}\right\} \tag{2.13}$$

The iterations are repeated until they converge to the limiting values, with the required accuracy. Let us designate these limiting values as

$$r_2^v,\ T_{1,2}^v,\ t_2^v = t_1^v + T_{1,2}^v,\ \rho_2^v = \rho_*,\ X_2^v,\ Y_2^v,\ Z_2^v,$$
$$X_1^v,\ Y_1^v,\ Z_1^v,\ v_2^v,\ u_2^v,\ \varphi^v.$$

Once the iterations converge, it is very simple to calculate the deviated trajectory. The energy integral gives the geocentric entry velocity $V_2^\nu = V_2(r_2^\nu)$, and the integral of the areas gives the angle $\alpha_2^\nu$ between the vector of this velocity and the geocentric entry radius. This is possible because, prior to the iterations, the initial data $r_1^\nu$, $V_1^\nu$, and $\theta_1^\nu$, as well as the elements of the deviated conic section, were found.

In addition, let us find the analog of the latitude argument $\mathfrak{M}_2^\nu = u_2^\nu + \alpha_2^\nu$ and, using formulas (1.7''), the velocity components $\dot{X}_2^\nu$, $\dot{Y}_2^\nu$, and $\dot{Z}_2^\nu$ at the point of entry into the moon's sphere of action. Then, we can determine the coordinates and velocities in the $\xi\eta\zeta$ coordinate system for $t = t_2^\nu$:

$$\left.\begin{aligned} \xi_2^\nu &= (X_2^\nu - X_1^\nu)\cos\varphi^\nu + (Y_2^\nu - Y_1^\nu)\sin\varphi^\nu, \\ \eta_2^\nu &= -(X_2^\nu - X_1^\nu)\sin\varphi^\nu + (Y_2^\nu - Y_1^\nu)\cos\varphi^\nu, \\ \zeta_2^\nu &= Z_2^\nu; \end{aligned}\right\} \tag{2.14}$$

$$\left.\begin{aligned} \dot{\xi}_2^\nu &= (\dot{X}_2^\nu - \dot{X}_1^\nu)\cos\varphi^\nu + (\dot{Y}_2^\nu - \dot{Y}_1^\nu)\sin\varphi^\nu, \\ \dot{\eta}_2^\nu &= -(\dot{X}_2^\nu - \dot{X}_1^\nu)\sin\varphi^\nu + (\dot{Y}_2^\nu - \dot{Y}_1^\nu)\cos\varphi^\nu, \\ \dot{\zeta}_2^\nu &= \dot{Z}_2^\nu. \end{aligned}\right\} \tag{2.15}$$

Using these quantities for the moment $t_2^\nu$, we can find the Keplerian elements $p_2^\nu$, $e_2^\nu$, $i_2^\nu$, $\overline{\Omega}_2^\nu$, and $\omega_2^\nu$ of the selenocentric conic section in the coordinate system; then from these we find the flight time $T_{2,1}^\nu$ from the boundary of the sphere of action to the lunar surface.

Finally, in order to calculate the coordinates $\xi_1^\nu$, $\eta_1^\nu$, and $\zeta_1^\nu$ of the point of impact on the lunar surface, we use formulas (1.11) to find the node longitude at the moment of impact in the $\xi\eta\zeta$ coordinate system, the latitude argument, the impact velocity, and the angle between this velocity and the lunar surface at the impact point.

## 3.3. EFFECT OF INITIAL-DATA SCATTER ON LOCATION OF POINT OF ENTRY INTO MOON'S SPHERE OF ACTION

In order to get an idea of the effect of the initial-data scatter, let us first consider the locations of the points of entry of deviated trajectories into the sphere of action. Then we can look at the corresponding points of impact on the lunar surface. In the $\xi\eta\zeta$ coordinate system these points will be projected onto the $\eta\zeta$ plane in a very graphic manner, since (for initial velocities not close to minimum) impact trajectories in the vicinity of the moon do not deviate very much from the earth-moon line.

Let us take a nominal impact trajectory with the following parameters as an example: amount which initial velocity exceeds local parabolic, $\Delta V_1 = 0.170$ km/sec; radius of beginning of passive part, $r_1 = 7000$ km; and inclination of trajectory plane to lunar orbital plane, $i_1 = 70°$.

For such a trajectory the coordinates of the nominal point of entry into the moon's sphere of action can be found using the formulas of §3.1. The values obtained are: $\xi = 62{,}663$ km, $\eta = -20{,}218$ km, and $\zeta = 4539$ km (Figure 3.3). The smallness of $\zeta$ in comparison with $\xi$ and $\eta$ is explained by the fact that the target lies in the $\zeta = 0$ plane, while the component $\dot{\zeta}$ is small in comparison with the selenocentric entry velocity (according to the geocentric integral of the areas, $|\dot{\zeta}|$ does not exceed 0.2 km/sec).

Radial lines drawn from the point of entry of the nominal trajectory into the moon's sphere of action will be the geometric loci of the entry points for deviated trajectories obtained by varying one of the initial parameters with respect to its nominal value. The amount of the deviation is shown in Figure 3.3 by a number next to the radial line. The units are as follows: $\delta H_1$, $\delta l$, and $\delta s$ in km; $\delta V_1$ and $\delta \dot{s}$ in m/sec; $\delta\theta_1$ in angular minutes; and $\delta t_1$ in seconds. The arrows indicate the directions of entry-point shifts resulting from positive errors. The direction of shifts due to errors $\delta l$ are seen to be close to the direction of shifts due to errors $\delta\theta_1$. The slopes of these two lines with respect to the $\eta$ axis are about 70° (that is, they are close to $i_1$). This is because the errors $\delta l$ and $\delta\theta_1$ do not modify the plane of a trajectory directed toward the moon's sphere of action and have practically no effect on the flight time (which depends basically on the initial velocity).

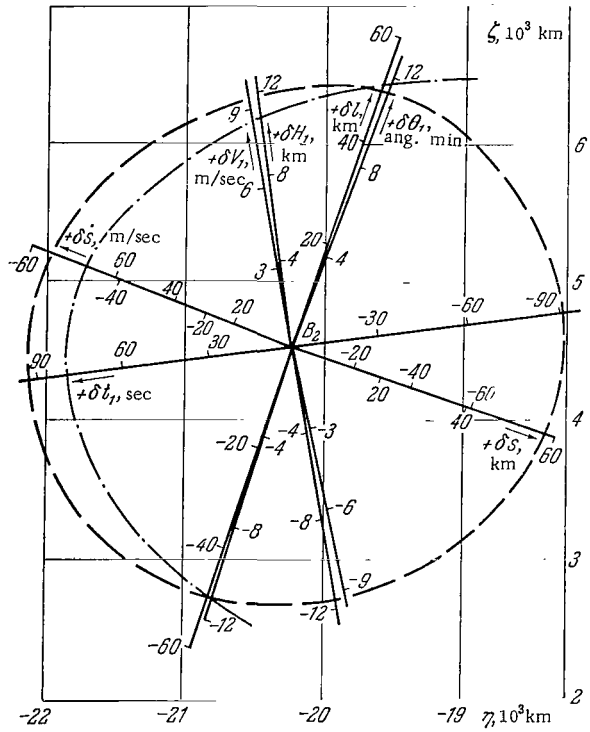


FIGURE 3.3. Shift of point of entry of trajectory into moon's sphere of action, for deviation of one of six initial parameters and initial time from nominal values. Nominal value of $\Delta V_1 = +0.170$ km/sec. Points on dashed curve correspond to trajectories tangent to lunar surface; points on dot-dash curve correspond to trajectories reaching lunar surface at points dividing earth-turned part of surface from averted part.

It should be noted that a positive value of $\delta l$ results in an upward shift (that is, a shift in the same direction as for $\delta\theta_1 > 0$), although one would

think that in general an error $\delta l$ should increase the initial latitude argument, thus turning the orbit and shifting the entry point downward, in the opposite direction. The upward shift of the entry point for $\delta l > 0$ can be explained as follows: an error of $\delta l > 0$ is accompanied by a linear (with respect to the error) variation of the inclination of the initial-velocity vector to the local horizon $\overline{\delta\theta}_1 = \frac{\delta l}{r_1} > 0$ (see formulas (2.3)). This exerts a determining effect on the shift of the entry point. Actually, Figure 3.3 shows that errors of $\delta l = 50$ m [sic] and $\delta\theta_1 \approx 12' \approx 0.0035$ rad cause approximately equal shifts in the entry point. The quantities $\delta u_1$ and $\overline{\delta\theta}_1$ associated with $\delta l$, however, are both equal to the value $\frac{\delta l}{r_1} \approx 0.007$ rad (with an accuracy up to second-order terms). Now it is known that, for initial velocities close to parabolic, a variation $\overline{\delta\theta}_1$ of the angle $\theta_1$ turns the trajectory through an angular distance which is about twice as great as this (that is, $2\overline{\delta\theta}_1$). Thus, the effect of $\delta u_1$ only compensates for half the effect of $\overline{\delta\theta}_1$, and the other half, $\frac{\overline{\delta\theta}_1}{2} = 0.0035$ rad, causes a shift exactly equivalent to an error $\delta\theta_1 = 12'$.

The shifts in the entry point caused by lateral errors $\delta s$ and $\delta\dot{s}$ in position and velocity (Figure 3.3) turn out to be perpendicular to the trajectory plane, since these errors have practically no effect on the flight time.

However, for positive errors the signs of the shifts will be opposite. This is because, for $\delta\dot{s} > 0$, the trajectory plane is turned to the left with respect to the initial radius vector, as viewed from its end, while for $\delta s > 0$ it is turned to the right, but with respect to a geocentric line parallel to the initial-velocity vector (as viewed from its end). The error $\delta V_1$ does not cause a rotation of the trajectory plane, but it changes the flight time up to the moon's sphere of action considerably. For $\delta V_1 > 0$ the trajectory lies above the nominal one and reaches the moon's sphere of action at a point to the left of nominal, since, due to the reduction of the flight time, the nominal point does not manage to reach the trajectory plane.

Errors in the initial radius $\delta r_1 = \delta H_1$ do not turn the trajectory plane either. The direction of the entry-point shifts due to these errors is close to that of the shifts caused by the errors $\delta V_1$. This is because the errors $\delta H_1$ have their effect mainly by varying the amount $\Delta V_1$ by which the initial velocity exceeds local parabolic. Obviously, the variation $\Delta V_1$ for a fixed value of $V_1$ will be opposite (in sign) to the variation of the local parabolic velocity as a function of the radius. Actually, the change in the parabolic velocity is given by the formula $\delta V_p = -\frac{1}{2} V_p \frac{\delta r_1}{r_1}$, according to which, for example for $\delta r_1 = 12$ km and $r_1 = 7000$ km, we obtain $\delta(\Delta V_1) = -\delta V_p = \frac{1}{2} \cdot 10.4 \times$ $\times \frac{12}{7000} \approx +0.009$ km/sec. On the other hand, it is obvious from Figure 3.3 that an error $\delta V_1 = 9$ m/sec results in about the same shift as an error $\delta H_1 = \delta r_1 = 12$ km. Thus it follows that a change in the initial height, without a variation in the amount the initial velocity exceeds local parabolic, will have only a very slight effect. This conclusion is in accordance with the results obtained for two-dimensional trajectories in /21/.

Finally, an error $\delta t_1$ does not change the shape of the trajectory, but only turns it, like a rigid body, from west to east about the earth's axis. The angular velocity $\Omega$ of the earth's diurnal rotation is about thirty times greater than the angular velocity $\omega$ of the moon's orbital motion. Therefore,

in an analysis of the effect of an error $\delta t_1 \neq 0$, it is possible to consider the moon's sphere of action as stationary. Accordingly, for $\delta t_1 > 0$ the end of the trajectory will be shifted to the left and downward on a sphere with a radius equal to that of the lunar orbit for $\Omega_a > 0$, and it will be shifted to the left and upward for $\Omega_a < 0$ (for $|\Omega_a| < 90°$). On the moon's sphere of action these shifts will be turned counterclockwise somewhat, due to the fact that the tangent plane to the sphere of action is not orthogonal to the geocentric radius of the nominal entry point $B_2$ at this point (Figure 3.3 corresponds to $\Omega_a > 0$).

Now let us consider how the radial lines [center at $B_2$] drawn on the sphere of action (Figure 3.3) shift with a variation of the node longitude $\Omega_a$ of the trajectory, for a specified bearing azimuth $a_0$. Figure 2.4 shows that, for constant $a_0$ and for $|\Omega_a| < 90°$, the inclination $i_1(\Omega_a)$ of the trajectory is a monotonically increasing function. Consequently, as $\Omega_a$ increases, the pairs of lines $\delta l$, $\delta\theta_1$ and $\delta s$, $\delta\dot{s}$, which remain orthogonal, will rotate counterclockwise. The pair of lines $\delta V_1$, $\delta H_1$ also rotates counterclockwise, remaining at about the same distances (relative to the $\eta$ axis) from the new position of the pair of lines $\delta l$, $\delta\theta_1$. Finally, line $\delta t_1$ will turn in the same sense, as we know from the previous considerations. If $\Omega_a$ decreases, then all the rotations will be in the opposite sense (that is, clockwise).

If the azimuth $a_0$ varies (for instance, if it increases), then Figure 2.4 shows that for all values of $\Omega_a$ the inclination $i_1$ will increase, by approximately the same amount. Consequently, all the lines except $\delta t_1$ will rotate counterclockwise. The sense of rotation of the $\delta t_1$ line will depend mainly on $\Omega_a$ (if the initial velocity exceeds local parabolic by some fixed amount $\Delta V_1$), and so it will not vary much.

Finally, let us see how the shifts of the points of entry into the moon's sphere of action vary with the amount $\Delta V_1$ that the initial velocity exceeds parabolic. The variations of $a_0$ and $\Omega_a$ considered above caused, in general, rotations of the lines about the nominal entry point, whereas the lengths of the lines were almost unaffected. However, a variation in the nominal value of $\Delta V_1$ has a very considerable effect on the lengths of the lines corresponding to specified deviations of the initial data from the nominal values. For example, the lengths of the $\delta V_1$ and $\delta H_1$ lines increase rapidly as $\Delta V_1$ approaches its minimum value. For a trajectory with $\Delta V_1 = -0.084$ km/sec, $r_1 = 7000$ km, and $i_1 \approx 70°$ (Figure 3.4), the lengths of the lines will be about four times greater than for a trajectory with $\Delta V_1 = +0.170$ km/sec (see Figures 3.3 and 3.4). This is explained by the substantial increase which takes place in the trajectory curvature and the flight time.

The length of the $\delta\dot{s}$ line varies less as $\Delta V_1$ decreases, but the line becomes bent. The reason for this is that, for low values of $\Delta V_1$, the lateral velocity increment $\delta\dot{s}$ changes the flight time considerably.

The lengths and shapes of the $\delta s$, $\delta l$, $\delta\theta_1$, and $\delta t_1$ lines are found to vary less, because of the geometricity of the effects which deviations $\delta s$, $\delta l$, $\delta\theta_1$, and $\delta t_1$ have on the shift of the entry point into the moon's sphere of action.

The directions of the pairs of lines $\delta s$, $\delta\dot{s}$ and $\delta l$, $\delta\theta_1$ obviously will not depend on $\Delta V_1$. The deviations of the directions of the $\delta V_1$ and $\delta H_1$ lines from those of the $\delta l$ and $\delta\theta_1$ lines will increase in accordance with the increased effect of the flight-time variations due to the errors $\delta V_1$ and $\delta H_1$.

The directions of the $\delta t_1$ lines are turned counterclockwise somewhat, because of a movement of the nominal entry point toward lower values of $\eta$

and because of a reduction of the angle between the tangent to the geocentric trajectory and the surface of the sphere of action at the entry point.

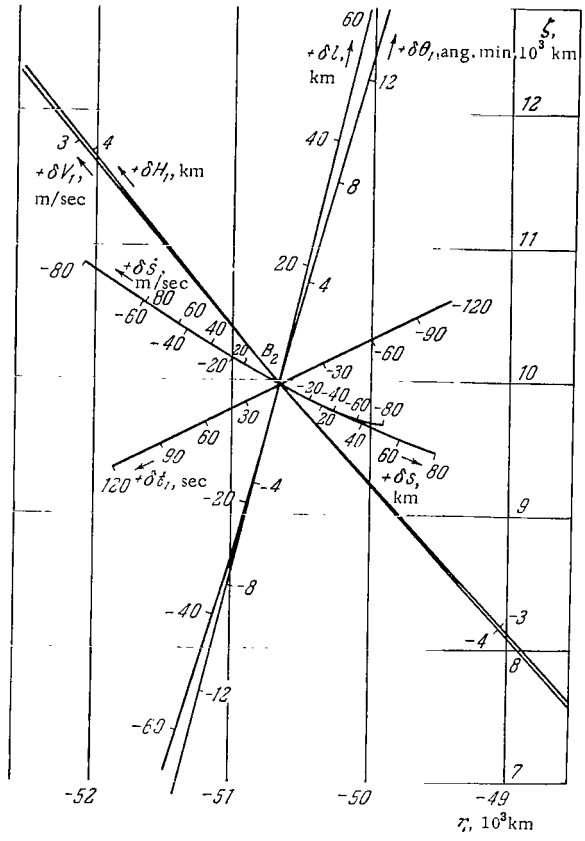


FIGURE 3.4. Shift of point of entry of trajectory into moon's sphere of action, for deviation of one of six initial parameters and initial time from nominal values. Nominal value of $\Delta V_1 = -0.084$ km/sec.

The effects of changes in the nominal values of parameters $H_1$ and $\theta_1$ need not be considerd separately, since (according to Chapter II) these quantities do not vary independently. They are both completely determined by the values of the azimuth $a_0$, the node longitude $\Omega_a$ of the trajectory, and the amount $\Delta V_1$ the initial velocity exceeds local parabolic, from the condition of impact with minimum weight losses.

For initial velocities which are not close to minimum, the linearity of the dependence of the entry-point shift $d$ on the initial-data deviations is shown by two things: the lines are more rectilinear, and the shifts are proportional to the deviations. For example, in Figure 3.3 the deviations from rectilinearity and proportionality are much smaller than those which could be observed in such a graph.

When secondary factors are taken into account (Chapter V), the pattern of lines drawn on the sphere of action will differ only slightly from the one considered here: the nominal entry point will be shifted by several tens of kilometers, causing the entire pattern of lines to be turned through an angular distance of about a thousandth of a radian. The angular distortions of the lines will be about the same as this. For example, taking into account perturbations in the version of the calculation presented in Figure 3.3, the point of entry into the moon's sphere of action will have the following coordinates:

$$\xi = 62{,}675\,\text{km}, \quad \eta = -20{,}183\,\text{km}, \quad \zeta = 4533\,\text{km},$$

instead of those given at the beginning of § 3.3 (a shift of only about 40 km).

## 3.4. EFFECT OF INITIAL-DATA SCATTER ON LOCATION OF IMPACT POINT

Let us consider the pattern of impact points on the lunar surface (Figure 3.5) corresponding to the points of entry into the sphere of action considered above (Figure 3.3).

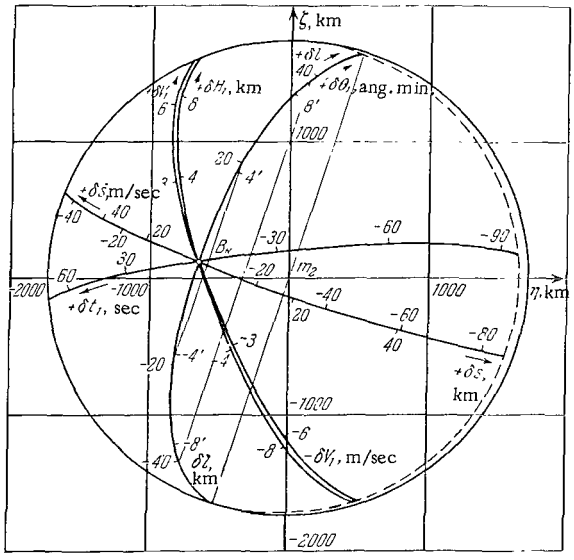


FIGURE 3.5. Shift of impact point over lunar surface, for deviation of one of six initial parameters and initial time from nominal values.

Let us draw a number of lines through the nominal impact point on the lunar surface, each line corresponding to a deviation $x$ of only one of the initial data from nominal. If we take the nominal impact point $B_к$ as the pole of the lunar sphere, then (with sufficient accuracy) these lines will lie along the meridians of this sphere. This means that the direction

of the selenocentric velocity of entry into the moon's sphere of action deviates very little from the selenocentric plane of the corresponding line on the sphere of action.

The shift $y$ of the impact point from nominal along the line is not everywhere quite proportional to the deviation of the corresponding initial parameter. This will only be the case on some circle with a radius of about 500 km. Beyond this circle the shift increases, changing more and more rapidly further away from the circle. Finally, at the end points, where the trajectories are only tangent to the lunar surface, the derivative $\frac{dy}{dx}$ becomes unbounded. However, the symmetry of the impact points corresponding to values of $x$ and $-x$ remains, right up to the end points of the line. This means that the deviations of the selenocentric entry velocity from nominal, if they exist, will also be symmetrical.

Let us assume that such deviations actually exist and are directed away from the moon's center. Then, according to § 1.1, for velocities not close to minimum the deviations (from nominal) of the geocentric entry velocity $V_2$ and the angle $\alpha_2$ between it and the geocentric radius will be comparatively small, for variations of the geocentric radius of the entry point over the wide range $a-\rho_* < r < a+\rho_*$. For example, for the trajectory considered in Figure 3.3, these deviations will be: $|\delta V_2| < 0.09$ km/sec and $|\delta\alpha_2| < 0.9°$ (Figure 1.1). The size of the area on the moon's sphere of action corresponding to the limit trajectories (the trajectories of tangency) is small in comparison with the range of $2\rho_*$ indicated above. This area can be found approximately, according to Chapter I, by assuming that the vector $V_2'$ of the selenocentric entry velocity does not depend on the position of the entry point in the area. Then, the area in question turns out to be a circle of radius $d(U)$, where $U=|V_2'|$ (Figure 1.4). For instance, for the trajectory in Figure 3.3, $U \approx 2.6$ km/sec (Figure 1.1) and $d(U) = 2340$ km. Now $\frac{d(U)}{2\rho_*}$ is less than 0.02, while the variations of $V_2$ and $\alpha_2$ within the area must be analogous fractions of the values of $\delta V_2$ and $\delta\alpha_2$ obtained above. Therefore, for the lunar-impact trajectories being considered here, these variations can be neglected. Accordingly, variations in the direction of vector $V_2'$ must in general be related to a deviation of the directions of the geocentric radii $r_2$ (of different entry points in the area) from nominal. It is easy to see that this deviation will in turn cause a deviation of the direction of $V_2'$ from the lunar center by a maximum amount when the trajectory is located in the lunar orbital plane. An approximate calculation of the deviation $\Delta\theta_2$ of vector $V_2'$ from nominal (Figure 3.6) for this case can be made using the formulas:

$$\sin\psi_2 \approx \frac{V_2}{U_*}\cos\alpha_2$$

(where $V_2$, $\alpha_2$, and $U_*$ are found from the curves in Figure 1.1),

$$\left.\begin{aligned} \sin\varphi_2 &= \frac{\rho_*}{r_2}\cos\psi_2, \quad r_2^2 = a^2+\rho_*^2-2a\rho_*\sin\psi_2, \\ \Delta\varphi_2 &= \frac{d(U)}{r_2}\sin\psi_2, \quad \cos\theta_2 = \frac{V_L - V_2\sin(\alpha_2+\varphi_2)}{U}, \end{aligned}\right\} \tag{4.1}$$

$$\Delta\theta_2 = \frac{V_2}{U}\left[\frac{V_2}{U} - \frac{V_L}{U}\sin(\alpha_2+\varphi_2)\right]\Delta\varphi_2. \tag{4.2}$$

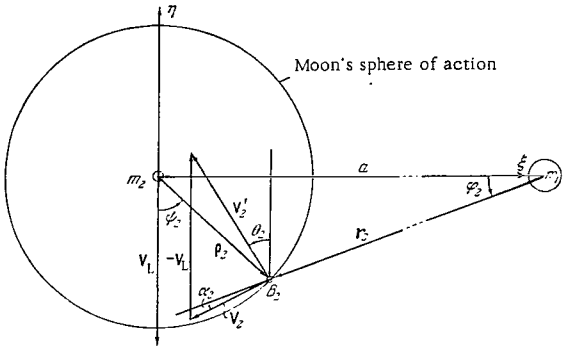


FIGURE 3.6. Conversion of geocentric parameters of motion (in lunar orbital plane) to selenocentric parameters at limit of moon's sphere of action.

The meaning of the notation is clear from Figure 3.6. The results of calculations of the limits of the deviation range ($\Delta\theta_2^+$, $\Delta\theta_2^-$) have been plotted in Figure 3.7. Here, these limits are shown as functions of the amount $\Delta V_1$ by which the initial velocity exceeds local parabolic, for a zero angle of elevation $\theta_1$ of the initial-velocity vector above the local horizon (and thus for inclinations of $i_1 = 0$ and $i_1 = \pi$). This same figure shows the reduction $\Delta d^{\pm} = \rho_* \Delta\theta_2^{\pm}$ of the diameter of the area as a function of the quantity $\Delta V_1$. This reduction of the diameter of the area on the moon's sphere of action may reach hundreds of kilometers.

Actually determined contours of the area on the moon's sphere of action (shown by dashed curve in Figure 3.3) agree with the curves in Figure 3.7. The quantity $\rho_{eff} = d - \Delta d$, it should be noted, is essentially the effective radius of the moon for an impact from the earth.

Now let us determine the length of a line drawn on the lunar surface (Figure 3.5), that is, the angular distance along the line from the nominal impact point to the point of contact of the deviated trajectory with the lunar surface. If there were no deviations $\Delta\theta_2$ (from nominal) of the selenocentric entry velocity corresponding to the point of contact, then it is easy to show that the desired angular distance would be given by the formula $\Phi_к = 90° + \frac{\alpha}{2}$, where $\alpha$ is the angle between the selenocentric exit and entry velocities for a tangent trajectory (Figure 1.4). Obviously, when the deviation $\Delta\theta_2$ is taken into account, the minimum length of the line on the sphere is given approximately by the formula

$$\Phi_к = 90° + \frac{\alpha}{2} - \Delta\theta_2. \qquad (4.3)$$

For the case represented in Figure 3.3, we obtain the values of $\alpha$ and $\Delta\theta_2$ from Figures 1.4 and 3.7, for $U \approx 2.6$ km/sec. Then formula (4.3) gives a value somewhat greater than 100° for $\Phi_к$.

The shifts of the impact point along the lines on the lunar surface cannot cover the entire moon, no matter what the initial velocity is. Even for minimum initial velocities the angle $\alpha < 120°$ (Figure 1.4), and thus $\Phi_к < 150°$. This means that for any specified initial velocity there is a region of the

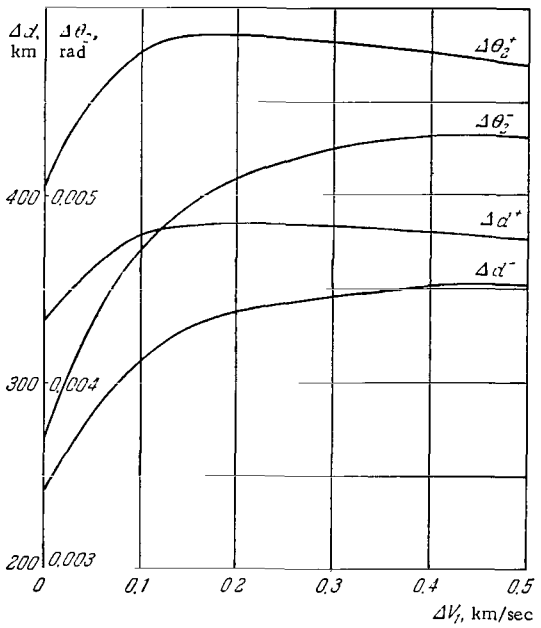


FIGURE 3.7. Limits of variations $\Delta\theta_2$ and $\Delta d$: of direction of selenocentric velocity of entry into moon's sphere of action, and of size of area on sphere of action corresponding to deviation of entry point from nominal.

moon which is unreachable. This region is nearly circular, with its center at the point opposite to the nominal impact point. For the case shown in Figure 3.3, the radius of this circle is about 900 km.

By drawing lines on the moon's sphere of action (Figure 3.3), it is possible to determine the optimum initial data for impacts on the visible side of the moon (optimum in the sense that the extreme values of initial-data deviations are the same on both sides of the mean). Obviously, this can be done by using an interpolation method to determine the points on the lines (on the sphere of action) for which $\xi_p = 0$, provided the coordinate $\xi_p$ passes through zero somewhere along the corresponding lines on the surface. When these points are joined by a curve (the dot-dash line in Figure 3.3), the region containing impact points on the opposite side of the moon is separated from the rest of the impact area. Now, the middle of this remaining region will obviously correspond to the nominal trajectory for an impact on the visible side of the moon. This midpoint always lies to the right and below point $B_2$.

Inspection of Figure 3.3 shows that the maximum permissible errors for impacts on the visible side of the moon are about the same as the permissible errors for impacts over the entire lunar surface. The latter errors can be determined for any one of the initial parameters, for zero values of the errors of the other parameters, using Figure 3.3. This is done by carrying out interpolations along the corresponding line, up to the point of its intersection with the dashed circle. The results of such calculations for various parameters are listed in Table 3.1.

TABLE 3.1

| Error | Limit value | Measurement units |
|---|---|---|
| $\delta H_1$ | 11.6 | km |
| $\delta l$ | 50.6 | km |
| $\delta s$ | 56.4 | km |
| $\delta V_1$ | 9.14 | m/sec |
| $\delta\theta_1$ | 11.4 | ang. min. |
| $\delta\dot{s}$ | 98.4 | m/sec |
| $\delta t_1$ | 93.9 | sec |

Now let us consider deviations of the impact point from nominal as a result of errors in the initial data. To do this, we first draw an arbitrary line along the surface of the moon. The angular shift of the impact point along this line is designated as $y$, and the corresponding linear combination of errors in the initial data is designated as $x$. It can be shown by an approximate method that, in the vicinity of $x = 0$, the function $y(x)$ goes through an inflection point. To show this, the functions $y(x)$ on the surfaces of an attracting and a nonattracting moon are compared, the deviation from nominal of the direction $\Delta\theta_2$ of the selenocentric entry velocity being neglected.

At the limit of the moon's sphere of action, the vector $V_2'$ of the selenocentric entry velocity, for a trajectory deviating from nominal by a distance $d$, forms an angle $\alpha$ with the selenocentric entry radius. The value of this angle is such that

$$\sin\alpha(x) = \frac{d(x)}{\rho_*}. \tag{4.4}$$

For a nonattracting moon, the distance $d$ between trajectories remains unchanged right up to the lunar surface, so that we have:

$$\sin\bar{y} = \frac{d(x)}{\rho_L}, \quad \text{that is, } \sin\bar{y} = \frac{\rho_*}{\rho_L}\sin\alpha(x). \tag{4.5}$$

For small distances $d$, that is, for small values of $x$, we have:

$$\bar{y} = \frac{\rho_*}{\rho_L}\alpha(x). \tag{4.6}$$

In the case of an attracting moon, $y$ will be less than $\bar{y}$. In order to determine this difference, let us find the angle $\Phi_{2,1}$ between the selenocentric radii of the entry point and the impact point. For motion along a hyperbola in the moon's sphere of action, the following relation is easy to obtain using formulas of the theory of conic sections for small values of $x$:

$$\Phi_{2,1} = \left[\sqrt{\left(\frac{\rho_*}{\rho_1} + \beta' - 1\right)\beta'} + \beta'\right] 2\alpha(x).$$

Here $\beta' = \left(\frac{U}{V_p'}\right)^2$, where $U = |V_2'|$ and $V_p' = 0.383$ km/sec is the selenocentric

parabolic velocity at a distance $\rho_*$. Now we can write

$$y = \alpha + \Phi_{2,1} = \left\{ 1 + \frac{1}{4} \frac{\left(\frac{\rho_L}{\rho_*} - 1\right)\beta'}{\left[\sqrt{\left(\frac{\rho_*}{\rho_L} + \beta' - 1\right)\beta'} + \beta'\right]^2} \right\} \alpha(x). \tag{4.7}$$

The quantity inside the braces does not exceed 1.13 for lunar-impact trajectories. Consequently, close to the nominal trajectory (that is, for small values of $x$), the attraction of the moon reduces $\bar{y}$ to less than 1/30 (that is, $1.13\ \frac{\rho_L}{\rho_*} \approx 30$). However, far away from the nominal trajectory, that is, for large $x$, this reduction of $\bar{y}$ disappears.

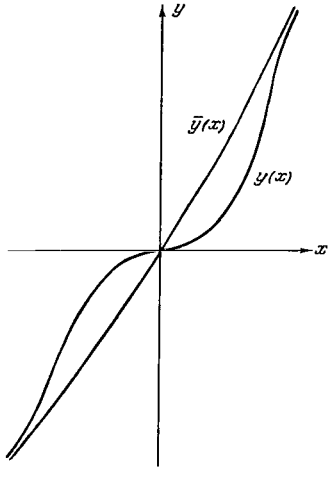


FIGURE 3.8. Angular deviation $y(x)$ of impact point from nominal (where $x$ is deviation of one of initial parameters from nominal value).

In general the function $y(x)$ has a finite derivative in some region around the point $x = 0$ (Figure 3.8). However, in the vicinity of $x = 0$ the function $y(x)$ has a derivative which is only 1/30 of that of function $\bar{y}(x)$. The zero values are the same, though, since $y(0) = \bar{y}(0) = 0$, and as $x$ increases, the $y(x)$ curve approaches the $\bar{y}(x)$ curve asymptotically. Consequently, in the vicinity of $x = 0$ the $y(x)$ curve must go through an inflection point. The second derivatives $y''(x)$ must be very close to zero in this vicinity, since (according to § 3.3) the function $d(x)$ is practically linear there.

Since the direction of the line on the sphere was selected arbitrarily, the linearity of function $d(x)$ and the fact that its transformations into function $y(x)$ for different lines $l_1$ and $l_2$ will be the same mean that the following is true: if $x$ is measured in fractions of the (maximum) permissible deviation $x_p$, then for arbitrary directions of $l_1$ and $l_2$ the ratio of the shifts $y_1\left(\frac{x_1}{x_{1p}}\right) : y_2\left(\frac{x_2}{x_{2p}}\right)$ will be the same for all $\frac{x_1}{x_{1p}} = \frac{x_2}{x_{2p}}$ and will be very close to unity. Here the situation is such that, for known combinations of initial-data errors, it is not necessary to know the higher derivatives of the shift $y(x)$ in order to determine whether impact occurs or not. It is enough just to know the first derivative $y'(0)$. Actually, the shift $d(x)$ is linear and has a derivative which differs from the derivative $y'(0)$ by a constant factor. This factor may be found from equations (4.4) and (4.7). Then, once the linear combination of errors $x$ and the value of $y'(0)$ are known, it is possible to find $d(x)$. Clearly, for $d(x) < \rho_{\text{eff}}$ impact occurs, whereas $d(x) > \rho_{\text{eff}}$ corresponds to a miss.

The relative narrowness of the pencil of impact trajectories, together with the linearity of the shift of the entry point (into the moon's sphere of action) along the corresponding line in the area, makes it possible to use the following approximate method to plot the predicted impact point on the lunar surface (provided the deviations $\delta x_i$ of the initial data from

nominal are known with sufficient accuracy). Since we know the shifts $\boldsymbol{d}_i$ along the $i$th line on the moon's sphere of action, which are caused by individual deviations of the parameters $x_i$, we can use the linearity of the relation $d(x)$ to find the total shift of the entry point on the sphere of action in the form of the vector sum $\boldsymbol{d} = \sum_{i=1}^{i=7} \boldsymbol{d}_i \delta x_i$. Then, since there is practically a one-to-one correspondence between the points of entry and the points on the lunar surface, we can find the impact point on the corresponding curved line on the surface. Obviously, the accuracy of the impact-point calculation will depend on the accuracy of the measurements of the initial-data deviations from nominal.

It should be noted that Cartesian variables, which are suitable as dependent variables for terrestrial problems, do not provide an adequate description of lunar flight problems. As an example of this, we note that for $x \to x_p$ the functions $\eta(x)$ and $\zeta(x)$ have a vertical tangent (because of the tangency of the limit trajectories to the lunar surface), and it is difficult to evaluate the closeness of $x$ to $x_p$ from the closeness of $\xi$ to $\xi_p$.

The functions $y = \sqrt{\rho_{min}} \cos i$ and $z = \sqrt{\rho_{min}} \sin i$ are examples of dependent variables which are more suitable for lunar problems. Here, $\rho_{min}$ is the minimum distance of the trajectory from the moon's center, and $i$ is the slope of the plane of the selenocentric trajectory to some specified line drawn on the lunar surface. In particular, to find the maximum allowable errors in the initial data, it is advisable to make the interpolations for the errors using the function $y = \sqrt{\rho_{min}}$ for the value $\sqrt{\rho_l}$ rather than the function $y = \rho_{min}(x)$ for the value $\rho_L$, where $\rho_l = 1736$ km is the radius of the moon. This follows from the fact that the moon is an attractive center.

Finally, it should be noted that the pencil of trajectories corresponding to small deviations of the initial data from nominal diverges monotonically out to about the limit of the moon's sphere of action, after which (with the approach to the moon) it converges monotonically. This was also confirmed by calculations carried out using the method of numerical integration, for trajectories deviating from nominal and passing sufficiently close to the lunar surface.

*Chapter IV*

# *DETERMINATION OF POINT OF LUNAR IMPACT AND CALCULATION OF PARAMETERS OF MOTION RELATIVE TO EARTH'S SURFACE*

## 4.1. DETERMINATION OF POINT OF LUNAR IMPACT FOR SPECIFIED INCLINATION OF TRAJECTORY PLANE TO PLANE OF EQUATOR

It is quite simple to determine the impact point if the amount $\Delta V_1$ by which the initial velocity exceeds local parabolic is known. As pointed out in Chapter I, the flight time $T$ varies only slightly with the angle $\theta_1$ between the initial velocity and the transversal. Thus, as an approximation, it can be assumed that the advance point moves along ahead of the moon at a constant angular distance $\omega T$. Obviously, at the moment $t_1$ when the trajectory plane, which rotates along with the earth in its diurnal motion, passes through the point

$$\Omega_a = \Omega_L(t) + \omega T, \tag{1.1}$$

a launch toward the moon will be possible. The corresponding optimum value of $\theta_1$ is defined uniquely as a function of $\Omega_a$ in terms of the quantity $\Delta V_1$ and the passive angular range $\Phi_1$; iterations similar to those used in § 2.3 are used for these calculations.

We assume that the longitude of the launch point and the position $\Omega_L(t)$ of the moon (given by an astronomical almanac) are known. For any $\Delta V_1 > \Delta V_{1\min}$, the relations $\lambda(\Omega_a)$ (Figure 2.5), $\Omega_a(\Omega_L)$ (equation (1.1)), and $\Omega_L(t)$ can be used to precalculate for each day the moment $t_1$ of entry into the trajectory, the angle $\theta_1$ between the initial velocity and the transversal, the height $H_1$, and the angular range $\Phi_a$ of the active part of the flight. In these calculations different values of $t$ are specified and interpolations are made. Then it is possible to find the impact point quite accurately, by taking into account the dependence of the flight time on the angle $\theta_1$ and the height $H_1$.

During one day the moon moves an average distance of 13.2° along its orbit, in approximately the same direction as that of the earth's rotation. Thus the intervals between two successive moments $t_1$ will be, on the average, 0.9 hour longer than a day (the launch point turns at a rate of 15°/hr).

The following problem concerning the impact point is a more interesting one: without specifying the quantity $\Delta V_1$ arbitrarily, let us so define it that for any given day the entry into the trajectory at the corresponding moment

$t_1$ will involve minimum energy expenditures. Since the moment $t_1$ is not known in advance, the problem should be solved in the following order. First, some arbitrary value of $\Omega_a$ is selected and the latitude argument $u_0(\Omega_a)$ (Figure 2.4) is found. Then, using the method of iterations, we find the following quantities from the condition that the characteristic velocity $U_x$ be a minimum: the amount $\Delta V_1$ by which the initial velocity exceeds local parabolic, the angle $\theta_1$ between the initial velocity and the transversal, the initial height $H_1$, and the active angular range $\Phi_a$. Now we can determine the time $T(\Delta V_1, \theta_1, H_1) = T(\Omega_a)$ and the quantity

$$\Omega_L(\Omega_a) = \Omega_a - \omega T(\Omega_a). \tag{1.2}$$

Whenever the flight time $T(\Omega_a)$ is determined in terms of the values of $r_1$, $\theta_1$, and $\Delta\beta_1$ found by iterations for a specified value of $\Omega_a$, we use formulas (2.2) of Chapter I to calculate the parameter $p$ of the conic section, its semimajor axis $a$, its eccentricity $e$, and, finally, the true anomalies $v_1$ and $v_2$ of the points corresponding to the beginning and end of the passive part of the flight path:

$$v_1 = \arccos\left[\frac{1}{e}\left(\frac{p}{r_1} - 1\right)\right], \quad v_2 = \arccos\left[\frac{1}{e}\left(\frac{p}{r_2} - 1\right)\right]. \tag{1.3}$$

For $\Delta V_1 < 0$ the flight time is given by the formulas

$$E_1 = 2\arctan\left(\sqrt{\frac{1-e}{1+e}}\tan\frac{v_1}{2}\right), \tag{1.4}$$

$$E_2 = 2\arctan\left(\sqrt{\frac{1-e}{1+e}}\tan\frac{v_2}{2}\right), \tag{1.5}$$

$$T(\Omega_a) = \sqrt{\frac{a^3}{\mu}}\,[E_2 - E_1 - e(\sin E_2 - \sin E_1)], \tag{1.6}$$

where $E_1$ and $E_2$ are the eccentric anomalies of the initial and final points of the passive part of the trajectory. For $\Delta V_1 > 0$ the following formulas are used:

$$\bar{f}_1 = \operatorname{arc\,cosh}\left[\frac{1}{e}\left(1 - \frac{r_1}{a}\right)\right], \quad \bar{f}_2 = \operatorname{arc\,cosh}\left[\frac{1}{e}\left(1 - \frac{r_2}{a}\right)\right], \tag{1.7}$$

$$T(\Omega_a) = \sqrt{-\frac{a^3}{\mu}}\,[\bar{f}_1 - \bar{f}_2 + e(\sinh\bar{f}_2 - \sinh\bar{f}_1)]. \tag{1.8}$$

Since the functions $\lambda(\Omega_a)$, $\Omega_L(\Omega_a)$, and $\Omega_L(t)$ are known, we can determine, as in the preceding case, the moment $t_1$ and the corresponding initial data for any given day.

If $\theta_1$ is constant, the amount the initial velocity exceeds parabolic will obviously vary considerably for different values of $\Omega_a$ (that is, for different days of the month). Thus, the flight time $T$ and the amount of lead will vary substantially with a change in the position $\Omega_a$ of the advance point.

In the problem being considered, the maximum possible value $\theta_{1\max}$ of $\theta_1$ is completely determined. It obviously corresponds to the maximum $\Phi_{1\max}$ of the passive angular range and the minimum value $\Delta V_{1\min}$, that is,

to a minimum value $\Delta\beta_{1\,\min}$ of the quantity $\Delta\beta_1 = \frac{\Delta V_1}{V_p} \times \left(2 + \frac{\Delta V_1}{V_p}\right)$. The maximum value $\theta_{1\,\max}$ can be determined by successive approximations. First we select some values $\theta_1 < \theta_{1\,\max}$ and $\Delta\beta_1 > \Delta\beta_{1\,\min}$ and find $r_1(\theta_1, \Delta\beta_1)$ and $\Phi_a(\theta_1, \Delta\beta_1)$ from Figure 2.2. Then we find

$$\nu = \frac{r_1}{r_2} \text{ and } \Phi_1 = 180° - [(u_0)_{\min} + \Phi_a], \tag{1.9}$$

where $r_2 = 384{,}400$ km is the distance between the centers of the earth and the moon, and $(u_0)_{\min} = u_0|_{\Omega_a = 0}$.

Finally, we find new values of $\theta_1$ and $\Delta\beta_1$ using the formulas

$$\left.\begin{aligned} \cos^2\theta_1 &= \frac{\sin^2\frac{\Phi_1}{2}}{(1-\nu^2) + \nu(2-\nu)\sin^2\frac{\Phi_1}{2}}, \\ \Delta\beta_1 &= -\nu(1 - \nu\cos^2\theta_1). \end{aligned}\right\} \tag{1.10}$$

obtained with the aid of expression (3.3) of Chapter II, and we repeat the iterations until the values of $\theta_1$ and $\Delta\beta_1$ are established to the required accuracy. By specifying different values of $\theta_1 = \text{const} < \theta_{1\,\max}$ and $\Omega_{La}$ and carrying out iterations to determine $\beta_1$, $r_1$, $\Phi_a$, and $T$, we can find the latter as functions of $\Omega_{La}$.

Some typical curves of $T(\Omega_{La})$ for constant values of $\theta_1$ are shown in Figure 4.1. A family of $\Omega_L(\Omega_{La})$ curves are given in Figure 4.2. In addition, just as in the previous problems, for each value of $\theta_1$ we have the functions $\lambda(\Omega_{La})$ and $\Omega_L(t)$. The only task remaining now is to determine for each day the moments $t_1$ when the spacecraft enters the trajectory of the passive part of the flight, by selecting different values of $t$ and interpolating.

An astronomical almanac for the given year should be used to determine these moments, with a view toward reaching the moon when it is near the optimum point on its orbit, during the specified month of the specified year. Since the optimum point $\Omega_L = 0$ corresponds to the minimum declination of the moon (relative to the plane of the equator), we can find the sidereal time $h_0$ when the moon passes through this point from the almanac. Let us designate the right ascension of the moon at the moment $h_0$ as $\alpha^0$. In angular coordinates, the sidereal time is the angle of rotation of the Greenwich meridian away from the vernal equinox $\gamma$. Correspondingly, the right ascension $\alpha^0$ of the moon is the angle of rotation of the latter away from $\gamma$. Therefore, from the definition of the $X$ axis (see §2.2 and Figure 2.3), we have:

$$\alpha_X^0 = \alpha^0 - 180°, \quad \lambda_G = h - \alpha_X^0, \tag{1.11}$$

where $\alpha_X^0$ is the angle of rotation of the meridian of this axis away from point $\gamma$, and $\lambda_G$ is the angle of rotation of the Greenwich meridian away from the meridian of the $X$ axis (the zero superscript indicates that the quantity corresponds to the time $h_0$). Consequently, the angle of rotation of the launch-point meridian away from the $X$-axis meridian at a time $h$ is

$$\lambda_h = \lambda_G^0 + \lambda_{go}, \tag{1.12}$$

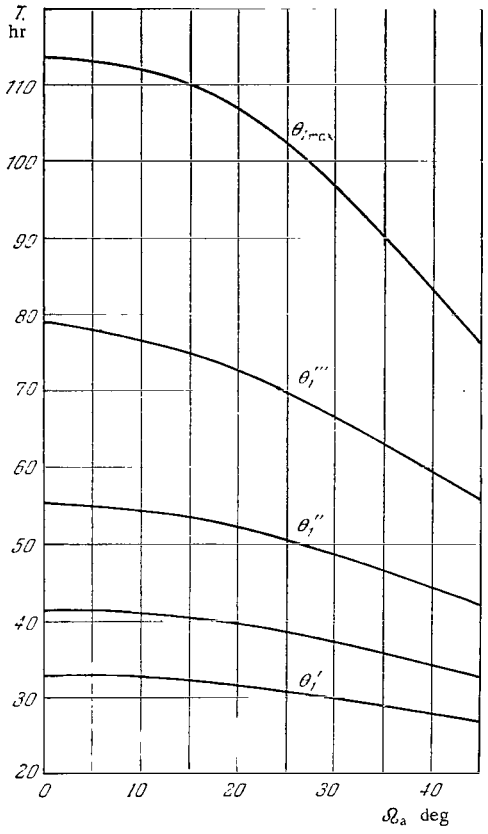


FIGURE 4.1. Typical curves for flight time $T$ in passive part of trajectory as function of position $\Omega_a$ of advance point, for selected angles $\theta_1$ between initial velocity and transversal. $\theta_1 < \theta_1'' < \theta_1''' < \ldots < \theta_{1\,max}$.

where $\lambda_{go}$ is the geographic longitude of the launch point $B_0$. Formula (1.12) and the second formula of (1.11) are valid for any $h$, while the first formula of (1.11) is valid only for $h = h_0$ (that is, for the case when the moon is at the optimum point on its orbit $\Omega_L = 0$). We designate the value $\lambda(h_0)$ corresponding to this lunar position as $\lambda^0$. Now, if we specify $\theta_1$, the inclination of the vector of the initial geocentric velocity to the local horizon, we can find the value $\Omega_a(\Omega_L)$ corresponding to $\Omega_L = \omega(h - h_0)$ for the time $h$, using the curves in Figure 4.2 (here $\omega$ is the angular velocity of revolution of the moon). Then, from this we can use Figure 2.5 to find the required value $\lambda(\Omega_a) = \lambda_a$ On the other hand, the attainable angle of rotation of the launch-point meridian away from the $X$-axis meridian at the moment $h$ is

$$\lambda_h = \lambda^0 + \Omega(h - h_0), \tag{1.13}$$

where $\Omega$ is the angular velocity of the earth's diurnal motion.

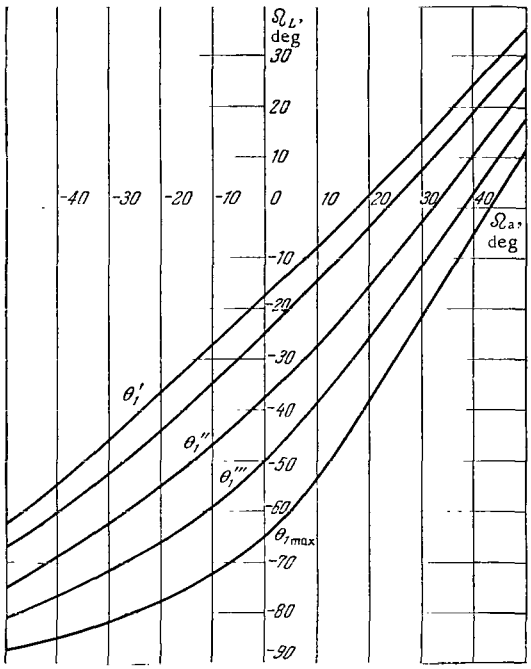


FIGURE 4.2. Relation between advance position ($\Omega_a$) and instantaneous position ($\Omega_L$) of moon, for various angles $\theta_1$ between initial velocity and transversal ($\theta_1' < \theta_1'' < \theta_1''' < \ldots < \theta_{1\,\max}$).

Next, we can find the values of $\Lambda = \lambda_h - \lambda_a$ for two values of $h$ and interpolate these according to $h$ at the value $\Lambda = 0$. Then, in the limit we obtain (for each day) the moment $t_1$ of entry into the passive part of the trajectory and the corresponding values of $\Omega_a$,

$$\Omega_L(\Omega_a),\ \lambda(\Omega_a),\ T(\Omega_a).$$

Some typical curves for the flight time $T$ as a function of the position ($\Omega_a$) of the point where the spacecraft meets the moon are shown in Figure 4.3, for four values of $\theta_1$. Let us consider the distribution of points on the $T = T(\Omega_a)|_{\theta_1 = \text{const}}$ curves, corresponding to lunar impacts for definite launch dates. These points form slightly curved oblique lines (Figure 4.1). The slanting of the lines is explained by the fact that for a fixed launch day higher values of $\theta_1$ will correspond to lower values of $\Delta V_1$ and thus to longer flight times, larger leads, and higher values of $\Omega_a$.

The size of the striking interval on the moon's orbit, as noted previously, is determined by the energy capabilities of the spacecraft. The extreme values of $|\Omega_a|$ are completely determined by the energetically optimum values of $\theta_1$ and the amount $\Delta V_1$ by which the initial velocity exceeds local parabolic. However, the energetically optimum values of $\Delta V_1$ may correspond to flight times which are too long, so that it will be inconvenient to observe the lunar impact from a given point on the earth.

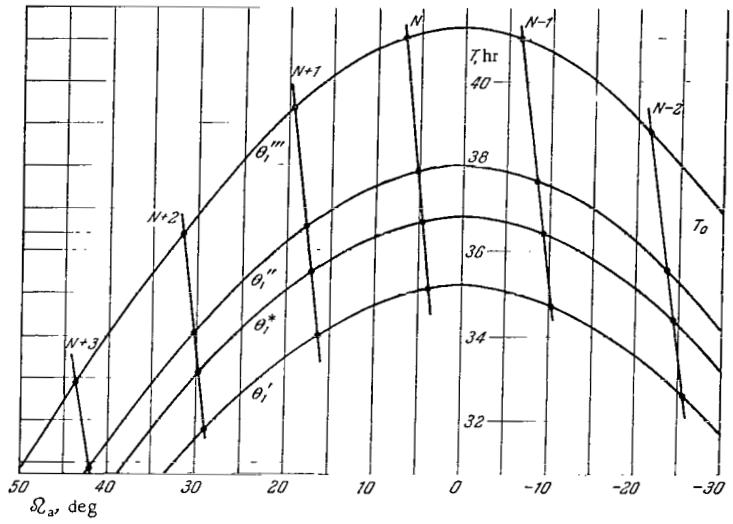


FIGURE 4.3. Flight time $T$ in passive part of trajectory, as function of advance positions $\delta\Omega_a$ of moon for energetically optimum launch date $N$ and dates in same month close to it.

Ways of carrying out the complex selection of $\theta_1$ will be described in the following sections, in connection with problems related to the observation of a spacecraft in flight.

## 4.2. SELECTION OF UNPERTURBED LUNAR TRAJECTORY, ALLOWING FOR DIRECT VIEWING OF IMPACT FROM SPECIFIED POINT

In the preceding section the amount $\Delta V_1$ by which the initial velocity exceeds local parabolic and the flight time $T$ were found as functions of the angular distance $\Omega_a$ between the moon and the energetically optimum advance point on the lunar orbit. In this case the angle of elevation $\theta_1$ of the vector of the initial geocentric velocity above the local horizon was taken as constant. The lunar trajectories are expressed as points on the above curves, and the task of this section will be to select a nominal point, for which the visibility of the spacecraft (from some given point H) prior to lunar impact is optimum.

Let us assume that this point, which has a geographical longitude $\lambda_H$, is located in the northern hemisphere (in particular, it may be the initial point of the flight path). Optimum visibility will be assumed to mean that the angle of elevation of the direction of the point-spacecraft above the horizon of point H during a certain period of time $\tau$ prior to lunar impact is a maximum. Obviously, at the moment of encounter with the moon this angle will be a maximum if for this moment the longitude of the spacecraft equals the longitude of point H. This condition can be expressed in the following form (see Figure 2.3):

$$180^\circ + [(\lambda_{B_0} - \lambda_H) - \sigma(a_0,\ \Omega_a)] = \Omega(t_a + T_0) - 2\pi n, \qquad (2.1)$$

where $(\lambda_{B_0} - \lambda_H) =$ constant is the difference between the geographical longitudes of the launch point $B_0$ and the point H, $\sigma$ is the difference between the longitudes of the launch point and the node $\Omega_a$ at the moment of launch, as determined by formulas (3.1) through (3.3) of Chapter I (Figure 2.5), $\Omega$ is the angular velocity of the earth's diurnal rotation, $t_a$ is the time of flight in the active part of the trajectory, $T_0$ is the optimum flight time in the passive part, and $n > 0$ is the whole number of sidereal days contained in the time $T_0$.

Actually, the difference (reckoned from the meridian of the $X$ axis) between the longitudes of the impact point and the node will be 180°, for the approximate case being considered. This quantity added to the difference $(\lambda_{B_0} - \lambda_H) - (\sigma + \Omega t_a)$ is, with an accuracy up to integral multiples of $2\pi$, the angle through which the observation point must rotate during the flight time $T_0$, in order for the impact point to be at the meridian of the observation point (Figure 2.3). If the angle of elevation of the object is to be a maximum not at the moment of impact but rather at a time $\frac{\tau}{2}$ prior to this, then obviously the flight time $T_0$, determined from expression (2.1), should be increased by $\frac{\tau}{2}$. Then, we obtain the following formula for the time $T_0$:

$$T_0 = \frac{1}{\Omega}[\pi(2n+1) + (\lambda_{B_0} - \lambda_H) - \sigma(a_0, \Omega_a)] + \left(\frac{\tau}{2} - t_a\right). \qquad (2.2)$$

The quantity $\sigma$ in (2.2) varies considerably with the azimuth $a_0$. For example, when $a_0$ increases from 35° to 60°, it increases by about 20° for the launch point selected in Chapter I. The time $T_0$, however, will obviously only decrease by about an hour (a relatively small decrease). For small variations in the azimuth the changes in $T_0$ will also be small.

However, if the azimuth is constant (as will be assumed in the following), the quantity $\sigma$ will change very little as $\Omega_a$ varies in the range $|\Omega_a| < 30°$ (Figure 2.5). Thus, to calculate an example with an accuracy of the order of 1° (around 4 min), it can be assumed that $\sigma$ is constant and equal to 20°. The left side of (2.1) will therefore be about 190°, so that, if we take Moscow ($\lambda = 37.6°$) as the observation point, the flight time in hours is

$$T_0 = 23.93 \cdot n + 12.45 + \left(\frac{\tau}{2} - t_a\right). \qquad (2.3)$$

It now only remains to determine $n$, which may be equal to 0, 1, 2, 3, or 4, since the flight time to the lunar orbit may be as much as 4.5 days. Let us determine this quantity for the simplified case in which $\frac{\tau}{2} = t_a$ and the energetically optimum initial velocities are close to the local parabolic velocity. A flight time of around two days corresponds to such velocities. Consequently, the values which are most suitable energetically are $n = 1$ and $n = 2$. The latter value, $n = 2$, corresponds to considerably lower values of $\Delta V_1$, the amount the initial velocity exceeds local parabolic. Moreover, according to Chapter III, for $n = 2$ the initial data must be specified more accurately. Therefore, we take $n = 1$, so that $T_0 = 36.38$ hours. The flight time in the passive part, it should be noted, depends only slightly on the initial height $H_1$ and the angle of inclination $\theta_1$ of the

initial-velocity vector to the local horizon (see Chapter I), and it is determined mainly by the amount $\Delta V_1$ by which the initial velocity exceeds parabolic. Therefore, when determining $T(\vartheta_a)$ (Figure 4.1) and $\Delta V_1(\vartheta_a)$, we obtain for different values of $\vartheta_a$ and $\theta_1$ a number of points $(T, \Delta V_1)$, which will lie essentially along a single $T(\Delta V_1)$ curve (the solid curve for $a = 384{,}400$ km in Figure 4.4).

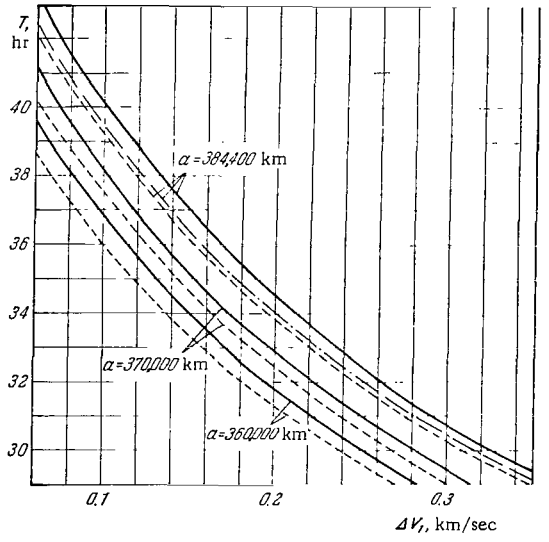


FIGURE 4.4. Flight time $T$ in passive part of trajectory, as function of amount $\Delta V_1$ by which initial velocity exceeds local parabolic, for different distances $a$ from center of earth to point of lunar impact.

From the solid curve in Figure 4.4, we find that an optimum flight time $T_0 \approx 36.4$ hours corresponds to $\Delta V_1 \approx 0.158$ km/sec.

Now let us determine the range of permissible values of the flight time $T$. To do this, we plot the angle of elevation $\varepsilon$ of the direction of the point-spacecraft above the horizon of the observation point as a function of the time $\Delta t$ elapsing from the moment $t_м$ of culmination of the spacecraft. In these calculations the declination $\delta$ of the spacecraft will be assumed to go through a minimum ($\delta \geqslant -\Theta$, where $\Theta$ is, as previously, the angle between the planes of the earth's equator and the moon's orbit). The movement of the spacecraft relative to the stars can be neglected in this calculation, since it is quite small (the angular velocity of a spacecraft at the distance of the moon is about one fifth of the angular velocity of revolution of the moon about the earth).

Let us define the angle $S$ as the angle through which the observed object moves from its culmination point during the time $\Delta t$ (this movement being caused by the diurnal rotation of the earth). Then, from Figure 4.5, which shows the celestial sphere above the observation point, we obtain the

following formula (assuming that the object is quite far from the earth):

$$\sin \varepsilon = \cos S \cos \delta \cos \psi_H + \sin \delta \sin \psi_H, \tag{2.4}$$

where $\psi_H$ is the latitude of the observation point.

In the region $\varepsilon > 0$, for latitudes $\psi_H > |\delta|$ ($\delta < 0$), the function $\varepsilon(S)$ increases monotonically from zero, reaches a maximum $\varepsilon_{max}$, and then decreases monotonically to zero in a symmetrical manner.

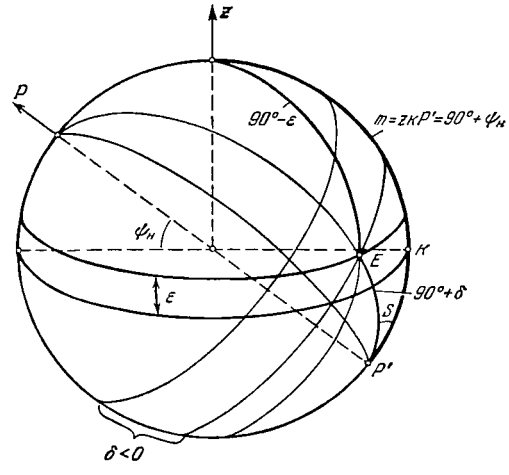


FIGURE 4.5. Celestial sphere above horizon of observation point.

If we measure angle $S$ in hours and construct the family of $\varepsilon(S)|_{\delta=\text{const}}$ curves, we can use the $\delta = \delta_{min}$ curve and the critical value $\varepsilon = \varepsilon_{min} = 0$ to find the range of nominal flight times $(T_1^e, T_2^e)$, which is symmetrical relative to the abscissa of the culmination point. However, the permissible range of $T$ will be even narrower, as a result of possible deviations of the velocity from nominal, due to injection errors. For example, if the spread of velocity values is $\delta V_1 \approx \pm 8$ m/sec, with a maximum derivative $\frac{\partial T}{\partial V_1} \approx -300$ sec$^2$/m (for the minimum values of $\Delta V_1$ considered in this example), then the range of nominal flight times decreases by an amount $\delta t \approx 0.7$ hour on each side. Consequently, the limits of the region of guaranteed impact visibility will be

$$T_1^e + \delta t \leqslant T \leqslant T_2^e - \delta t.$$

For $T \geqslant T'' = T_2^e + \delta t$ the impact will not be visible, since it occurs too late. For $T \leqslant T' = T_1^e - \delta t$ the impact will not be visible because it occurs too early. Thus, outside the interval $(T'', T')$ an impact will definitely not be visible, while for $T' < T < T_1^e + \delta t$ and $T_2^e - \delta t < T < T''$ there is a possibility that the impact will not be visible.

Let us plot the obtained range of flight times in Figure 4.1 and consider the $T(\Omega_a)|_{\theta_l=\text{const}}$ curves corresponding to it. Then it is possible to determine the maximum $\theta_{l\,max}$ and minimum $\theta_{l\,min}$ values of $\theta_l$ for which, in the vicinity of the point $\Omega_a = 0$, a lunar impact controllable from the observation point is still feasible.

Therefore, for the curves of constant $\theta_l$ there is a region $(\theta_{l\,min}, \theta_{l\,max})$. Obviously, for the maximum value $\theta_l = \theta_{l\,max}$ there will be a certain maximum number of days of the month on which a moon launch is possible. Consequently, even if there were no energy limitations, the number of days in the month on which spacecraft could be launched into trajectories with a fixed angle of elevation of the initial-velocity vector above the local horizon would be limited. The energy limitations, of course, can only reduce this number of days even further.

If the energy limitations are narrow (that is, for $|\Omega_a| < |\Omega_a|_{max}$), there is in general a whole range of $\theta_l$ values for which the $T(\Omega_a)|_{\theta_l=\text{const}}$ curves will everywhere lie in the region where impact is visible from the observation point. Therefore, the optimum value of $\theta_l$ should be sought taking into account the position on the $T(\Omega_a)|_{\theta_l=\text{const}}$ curves of the points corresponding to lunar impact in a specific month, while the previous consideration pertained to any month. For example, once the $T(\Omega_a)$ curves (Figure 4.3) have been calculated for a specific month, interpolation can be used to find the parameters $\theta_l^0$ and $\theta_l^*$ of the curves passing through the intersection point of the $T = T_0$ line and, respectively, the line $N$ of the energetically optimum date or the line $N-1$ of the preceding date. The characteristics of trajectories with $\theta_l = \theta_l^*$ for other dates can easily be found by interpolating all the parameters along the lines of these dates for the value $\theta_l = \theta_l^*$.

## 4.3. CHARACTERISTICS OF MOTION RELATIVE TO EARTH AND MOON

In this section we will consider how to obtain information concerning the following subjects: the azimuths and angles of elevation of a spacecraft as observed from the earth; the trace of its motion on the earth's surface; the distances to a spacecraft; its angular and radial velocities at different points on the earth; the region on the earth from which the spacecraft is visible; the region on the moon visible from the spacecraft; and the trace of its motion on the lunar surface. It is assumed that the observations are carried out using radio techniques, independently of the illumination conditions, and that the observation points are specified.

Let us select some right-handed coordinate system, such as the system with the $Z$ axis normal to the lunar orbital plane, and the $Y$ axis directed along the line of intersection between the lunar orbital plane and the equatorial plane at the descending node. If we know the numerical values of coordinates $X$, $Y$, and $Z$ and velocities $\dot{X}$, $\dot{Y}$, and $\dot{Z}$ of the spacecraft (Figure 4.6) at some arbitrary time, as well as the geographical coordinates $(\lambda_i, \psi_i)$ $(i = 1, 2, \ldots, n)$ of the observation points and the angle $\lambda = \lambda_0$ (Figure 2.3) between the meridians of the $X$ axis and the launch point $B_0$ at the nominal moment $t_1$ of the beginning of the passive part of the flight, then it is possible to calculate all the quantities mentioned above.

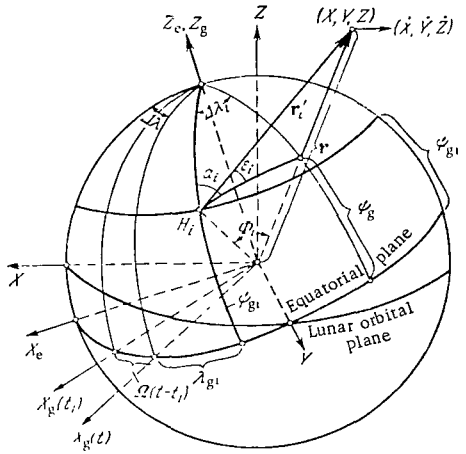


FIGURE 4.6. Determination of parameters of visibility of object along trajectory from observation point $H_i$.

First let us calculate the geographical coordinates $\lambda_g$ and $\psi_g$ of the point at which the geocentric radius vector of the object intersects the earth (the geometric locus of such points is the trace of the object's motion on the earth's surface). For this calculation we use the equatorial system $X_e Y_e Z_e$ instead of the $XYZ$ system. The $Y_e$ axis coincides with the $Y$ axis and the $Z_e$ axis is directed along the earth's rotation axis. The $X_g Y_g Z_g$ system will also be used, in which the $Z_g$ axis coincides with $Z_e$ axis and the $X_g$ axis is directed toward the point of intersection between the Greenwich meridian and the equator. The following formulas are used to convert between the first two systems:

$$X_e = X\cos\Theta - Z\sin\Theta,\ Y_e = Y,\ Z_e = X\sin\Theta + Z\cos\Theta, \tag{3.1}$$

where $\Theta$ is the angle between the planes of the equator and the lunar orbit. The following formulas are used for the second conversion:

$$\left.\begin{aligned} \Delta\lambda &= \lambda_0 - \lambda_g + \Omega(t - t_1),\\ X_g &= X_e\cos\Delta\lambda + Y_e\sin\Delta\lambda,\\ Y_g &= -X_e\sin\Delta\lambda + Y_e\cos\Delta\lambda,\\ Z_g &= Z_e, \end{aligned}\right\} \tag{3.2}$$

where $\lambda_g$ is the geographical longitude of the launch point, $\Omega$ is the angular velocity of the earth's diurnal rotation, and $\Delta\lambda$ is the angle between the Greenwich meridian and the meridian of the $X$ axis (Figure 4.6).

Now the geographical coordinates $\lambda_g$ and $\psi_g$ of the point in question will obviously be given by the formulas

$$\left.\begin{aligned} \sin\psi_g &= \frac{Z_g}{r},\quad \sin\lambda_g = \frac{Y_g}{r\cos\psi_g},\\ \cos\lambda_g &= \frac{X_g}{r\cos\psi_g},\quad r = \sqrt{X_g^2 + Y_g^2 + Z_g^2}. \end{aligned}\right\} \tag{3.3}$$

The region on the earth from the boundaries of which the spacecraft will be visible at the horizon will be a circle with its center at ($\lambda_g$, $\psi_g$) and an angular radius of

$$\gamma_0 = \arccos \frac{r_0}{r}, \tag{3.3'}$$

where $r_0$ is the radius of the earth and $r$ is the geocentric distance.

Next let us determine the visibility of the spacecraft from the specified observation points with coordinates ($\lambda_i$, $\psi_i$). The angle $\Phi_i$ between the geocentric radii of the observation point and the spacecraft can be found using the formula

$$\cos \Phi_i = \frac{1}{r} (X_g c_{Xi} + Y_g c_{Yi} + Z_g c_{Zi}), \tag{3.4}$$

where $c_{Xi} = \cos \psi_i \cos \lambda_i$, $c_{Yi} = \cos \psi_i \sin \lambda_i$ and $c_{Zi} = \sin \psi_i$ are the direction cosines of the geocentric radius vector of the given point.

The angle of elevation of the point-spacecraft above the horizon of the observation point is expressed in terms of $\Phi_i$ by the formula

$$\tan \varepsilon_i = \frac{r \cos \Phi_i - r_0}{r \sin \Phi_i}. \tag{3.5}$$

After determining the difference between the longitudes of the spacecraft and the observation point

$$\Delta\lambda_i = \lambda_g - \lambda_i, \tag{3.6}$$

we find the azimuth and range of the spacecraft for the $i$ th point:

$$\left.\begin{aligned} \sin a_i = \frac{\sin \Delta\lambda_i}{\sin \Phi_i} \cos \psi_g, \quad \cos a_i = \frac{\sin \psi_g - \cos \Phi_i \sin \psi_i}{\sin \Phi_i \cos \psi_i}, \\ r_i' = \sqrt{r^2 + r_0^2 - 2rr_0 \cos \Phi_i}. \end{aligned}\right\} \tag{3.7}$$

It is a little more complicated to find the apparent angular and radial velocities of motion of the spacecraft. To obtain these, we first calculate the vector of the relative spacecraft velocity in the $V_i N_i H_i$ coordinate system. Here the $H_i$ axis is parallel to the geocentric radius of the observation point, the $N_i$ axis is directed northward, and the $V_i$ axis is directed eastward, while the origin is at the $i$ th point. The velocities can be calculated most easily by a step-by-step method, as in the case of the coordinates. The components of the relative velocity along the $X_e$, $Y_e$ and $Z_e$ axes are:

$$\left.\begin{aligned} \dot{X}_e &= \dot{X} \cos \Theta - \dot{Z} \sin \Theta + \Omega Y_e, \\ \dot{Y}_e &= \dot{Y} - \Omega X_e, \\ \dot{Z}_e &= \dot{X} \sin \Theta + \dot{Z} \cos \Theta. \end{aligned}\right\} \tag{3.8}$$

The components of this velocity along the $X_g$, $Y_g$, and $Z_g$ axes are given by formulas analogous to formulas (3.2):

$$\left.\begin{aligned} \dot{X}_g &= \dot{X}_e \cos \Delta\lambda + \dot{Y}_e \sin \Delta\lambda, \\ \dot{Y}_g &= -\dot{X}_e \sin \Delta\lambda + \dot{Y}_e \cos \Delta\lambda, \\ \dot{Z}_g &= \dot{Z}_e. \end{aligned}\right\} \tag{3.9}$$

Finally, as a result of the rotation of the $X_g Y_g Z_g$ coordinate system through an angle $\lambda_i$ relative to the $Z_g$ axis and the rotation of the resulting system by an angle $\psi_i$ about the new $V_i$ axis directed eastward, we obtain:

$$\left.\begin{aligned} \dot{V}_i &= -\dot{X}_g \sin\lambda_i + \dot{Y}_g \cos\lambda_i, \\ \dot{N}_i &= -(\dot{X}_g \cos\lambda_i + \dot{Y}_g \sin\lambda_i)\sin\psi_i + \dot{Z}_g \cos\psi_i, \\ \dot{H}_i &= (\dot{X}_g \cos\lambda_i + \dot{Y}_g \sin\lambda_i)\cos\psi_i + \dot{Z}_g \sin\psi_i. \end{aligned}\right\} \tag{3.10}$$

Using the above relations, together with the formulas for rotation of the $V_i N_i H_i$ coordinate system through the azimuthal angle $a_i$ and through the angle of elevation $\varepsilon_i$, it is easy to obtain the angular and radial velocities:

$$\left.\begin{aligned} \dot{a}_i &= \frac{1}{r_i \cos\varepsilon_i}(\dot{V}_i \cos a_i - \dot{N}_i \sin a_i), \\ \dot{\varepsilon}_i &= \frac{1}{r_i}[-(\dot{W}_i \sin a_i + \dot{N}_i \cos a_i)\sin\varepsilon_i + \dot{H}_i \cos\varepsilon_i], \\ \dot{r}_i &= (\dot{W}_i \sin a_i + \dot{N}_i \cos a_i)\cos\varepsilon_i + \dot{H}_i \sin\varepsilon_i. \end{aligned}\right\} \tag{3.11}$$

Now it only remains to determine the point on the moon above which the spacecraft is located and the angular radius of the portion of the lunar sphere visible from the spacecraft. This gives an idea of the visibility of the moon during the period of flight; a knowledge of the latter is necessary, for example, to ensure the earthward transmission of pictures of the lunar surface.

Let us designate $X_L$ and $Y_L$ as the coordinates of the moon's center (recalling that the $XYZ$ system was so selected that $Z_L = 0$ and $\dot{Z}_L = 0$). Then the angle of deviation $\varphi$ of the radius vector of the moon's center from the $X$ axis, and the magnitude of the radius vector, will be given by the formulas

$$\sin\varphi = \frac{Y_L}{r_L}, \quad \cos\varphi = \frac{X_L}{r_L}, \quad r_L = \sqrt{X_L^2 + Y_L^2}. \tag{3.12}$$

Conversion from the $XYZ$ coordinate system to the $\xi\eta\zeta$ system shown in Figure 3.1 can be carried out using the formulas

$$\left.\begin{aligned} \xi &= (X_L - X)\cos\varphi + (Y_L - Y)\sin\varphi, \\ \eta &= -(X_L - X)\sin\varphi + (Y_L - Y)\cos\varphi, \\ \zeta &= Z. \end{aligned}\right\} \tag{3.13}$$

The polar coordinates $\lambda'$ and $\psi'$ of an arbitrary point on the trace of the spacecraft's motion on the lunar surface are found using the formulas

$$\sin\psi' = \frac{\zeta}{\rho}, \quad \sin\lambda' = \frac{\eta}{\rho\cos\psi'}, \quad \cos\lambda' = \frac{\xi}{\rho\cos\psi'}, \tag{3.14}$$

where $\rho = \sqrt{(X - X_L)^2 + (Y - Y_L)^2 + (\dot{Z} - \dot{Z}_L)^2}$ is the distance from the spacecraft to the center $(X_L, Y_L, 0)$ of the moon, which moves with a velocity $(\dot{X}_L, \dot{Y}_L, 0)$. The angle $\psi'$ is reckoned from the $\xi\eta$ plane on the side where $\zeta > 0$, and $\lambda'$ is reckoned in the $\xi\eta$ plane from the $\xi$ axis on the side where $\eta > 0$. The angular radius of the part of the lunar surface visible from the spacecraft will obviously be given by a formula similar to formula (3.3'), but with $\frac{r_0}{r}$ replaced by $\frac{\rho_L}{\rho}$.

To get a more complete idea of the motion of the spacecraft and its approach to the moon, it is necessary to calculate the absolute geocentric velocity of the spacecraft

$$V = \sqrt{\dot{X}^2 + \dot{Y}^2 + \dot{Z}^2},$$

the radial and transversal components of this velocity

$$V_r = \frac{X\dot{X} + Y\dot{Y} + Z\dot{Z}}{r}, \quad V_\tau = \sqrt{V^2 - V_r^2}, \tag{3.15}$$

the angular geocentric velocity of the spacecraft $\omega_g = \frac{V_\tau}{r}$, and also the corresponding selenocentric velocities of the spacecraft

$$\left.\begin{aligned} U_\pi &= \sqrt{(\dot{X} - \dot{X}_L)^2 + (\dot{Y} - \dot{Y}_L)^2 + (\dot{Z} - \dot{Z}_L)^2}, \\ U_\rho &= \frac{(X - X_L)(\dot{X} - \dot{X}_L) + (Y - Y_L)(\dot{Y} - \dot{Y}_L) + Z\dot{Z}}{\rho}, \\ U_\tau &= \sqrt{U_\pi^2 - U_\rho^2}, \quad \omega_\pi = \frac{U_\tau}{\rho}, \end{aligned}\right\} \tag{3.16}$$

where $U_\pi$ is the magnitude of the selenocentric velocity, $U_\rho$ is the magnitude of the selenocentric-velocity component along the selenocentric radius, $U_\tau$ is the magnitude of the selenocentric-velocity component in the plane normal to the selenocentric radius, and $\omega_\pi$ is the angular velocity of revolution of the spacecraft around the moon. Finally, the angle $\beta$ between the geocentric radii of the spacecraft and the moon is found using the formula

$$\cos\beta = \frac{XX_L + YY_L}{rr_L}, \text{ where } r_L = \sqrt{X_L^2 + Y_L^2}.$$

The formulas given above do not involve any assumptions concerning the forces acting on the spacecraft and they are suitable for either an approximate or an exact description of these forces, for any launch date. However, for the sake of generality, it is convenient to use the system of equations of motion given in Chapter I to calculate the parameters of motion of the spacecraft relative to the earth's surface.

## 4.4. RESULTS OF A SAMPLE CALCULATION

Figures 4.7 and 4.8 show some results of a sample calculation using the formulas of § 4.3. The trajectory in this case is characterized by an initial velocity which is 170 m/sec above local parabolic ($\Delta V_1 = 170$ m/sec). The trajectory calculations were carried out by means of numerical integration of the equations of the three-dimensional restricted circular three-body problem (that is, the moon's influence was taken into account). These calculations indicated that the determination of the optimum flight time (with direct visibility of the impact from a given point) made using the approximate method of §§4.1 and 4.2 is of sufficient accuracy. Actually, if the initial velocity exceeds local parabolic by the above amount $\Delta V_1$,

the flight time obtained is $T_0 = 35.4$ hours (see dot-dash curve in Figure 4.4 for $a = 384{,}400$ km, plotted taking into account lunar attraction and also taking into account that the spacecraft impacts the lunar surface rather than the center of the moon). The actual flight time is $T_0 = 35.35$ hours.

Due to the deviation of the flight time from the nominal value ($T_0 \approx 36.4$ hours), the curve showing the angle of elevation $\varepsilon$ of the direction of the point-spacecraft above the Moscow horizon as a function of the flight time $t$ ends at some value $\varepsilon < \varepsilon_{max}$. The shape of this curve is shown in Figure 4.7 (for the initial point selected in Chapter I).

Now let us consider how the various parameters of motion change with a variation in the flight time $t$. Figure 4.8 shows some typical curves for the following instantaneous parameters as functions of $t$: the geocentric distance $r$ of the spacecraft; the selenocentric distance $\rho$, the geocentric velocity $V$, the geocentric angular distance $\beta$ between lines drawn from the earth's center to the spacecraft and to the moon's center, and the angular radius $\gamma_0$ of the region on the earth's surface from points of which the spacecraft is visible on the horizon. The $r(t)$ and $\rho(t)$ plots are curved only near the beginning of motion, after which they straighten out to become almost linear. For $t \approx 15$ hours these curves intersect, that is, $r(t) = \rho(t)$.

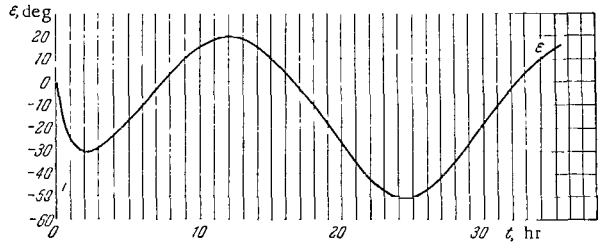


FIGURE 4.7. Typical time variation of $\varepsilon$, angle of elevation of point-spacecraft above Moscow horizon.

The curve showing $V(t)$ drops sharply at the beginning of the motion: from a starting value above 10 km/sec, this velocity drops to about 3 km/sec during ten hours of flight. Then, it decreases gradually and reaches a stable value in the vicinity of the point of entry into the moon's sphere of action. Finally, just before the moment of impact, it increases again (back up to about 3 km/sec) under the influence of the moon's attraction.

Functions $\beta(t)$ and $\gamma_0(t)$ undergo their main change at the beginning of flight: $\beta(t)$ drops rapidly because the angular velocity of the spacecraft is high at the beginning of flight, while $\gamma_0(t)$ increases rapidly because the spacecraft moves away from the earth quickly. After about five hours of flight $\beta(t)$ becomes almost linear, since the areal velocity of the spacecraft is less than one fifth of that of the moon. For high values of $r$ the angular velocity of the spacecraft becomes several times lower than the angular velocity of the moon, so that the latter "overtakes" the spacecraft at a nearly uniform rate. The $\gamma_0(t)$ curve begins to approach its asymptote $\gamma_0 = 90°$ even earlier, which agrees with the geometrical meaning of this quantity.

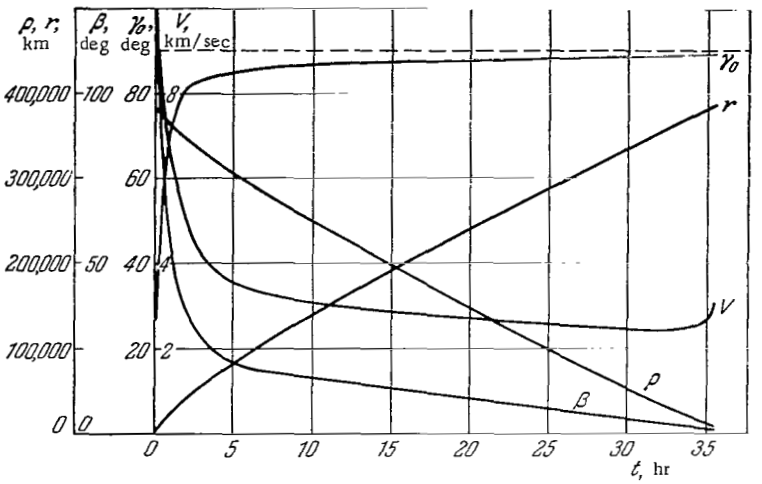


FIGURE 4.8. Time changes of: geocentric distance $r$, selenocentric distance $\rho$, geocentric velocity $V$, geocentric angular radius $\gamma_0$ of region on earth from which spacecraft is visible at horizon, and geocentric angular distance $\beta$ between lines from earth's center to spacecraft and to moon's center.

The trajectory plane is inclined by an angle $i_1 = 60°$ to $80°$ with respect to the lunar orbital plane. Thus, on an immobile celestial sphere the spacecraft will gradually approach the impact point from the right and from above (as seen from the northern hemisphere of the earth), while the moon comes in from the right five times as fast.

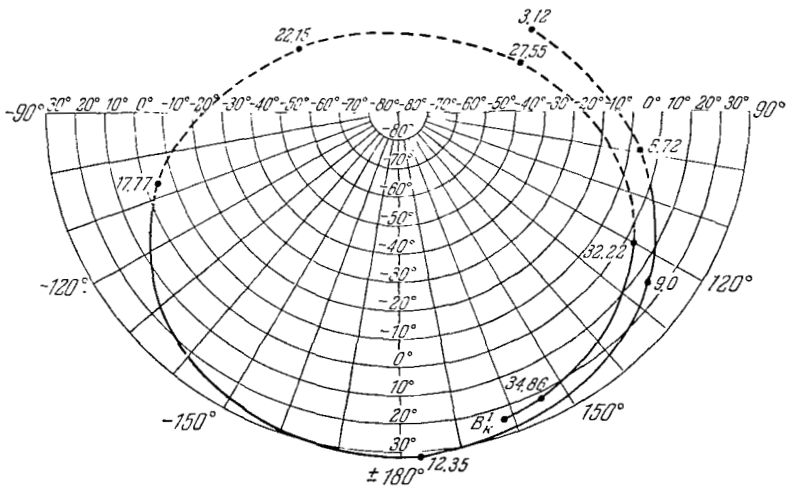


FIGURE 4.9. Typical variation of azimuth and angle of elevation of object along passive part of flight path.

Now let us consider how the azimuth and angle of elevation vary with time. It will be more graphic to designate the azimuth of the spacecraft as the azimuth of the direction of some polar radius, and to define the angle of elevation $\varepsilon$ as the shift of a point along this radius (Figure 4.9). This shift will be measured from some circle, toward the circle's center for $\varepsilon < 0$ and away from its center for $\varepsilon > 0$. The circle itself then corresponds to an angle of elevation $\varepsilon = 0$, that is, to the earth's surface. The resulting diagram is shown in Figure 4.9 (in which the flight time in hours is indicated along the curves). If the spacecraft happens to pass through the zenith of the observation point (which may occur only for points located on the trace), the azimuth will vary suddenly by 180°.

*Chapter V*

## *EFFECTS OF SECONDARY FACTORS*

In Chapter IV a method was given for determining the nominal initial data and the moment of beginning of the passive part of the trajectory, without taking into account the effects of secondary factors. In practice, however, it is more useful to take into account, however roughly, all the factors which have a substantial influence on the passive part of a lunar trajectory. This chapter will present a method for taking into account approximately the effects of the moon's attraction, the ellipticity of the lunar orbit, and the earth's oblateness. In addition, the sun's influence will be evaluated, in relation to selecting the nominal lunar trajectory and the nominal moment of entry into this trajectory. The secondary factors have only a slight effect on the variation of the energy of motion and the shape of the trajectory. Therefore, in this chapter the determination of the nominal initial data using the methods of Chapter IV will be taken as a natural starting point for the analysis, and the effects of perturbing factors will be allowed for by introducing corrections. Thus, it will be possible to carry out a simultaneous evaluation of which perturbing factors affect the nominal initial parameters most. The technique described provides a good approximation for moon-flight calculations using more exact methods.

### 5.1. EFFECT OF THE MOON AS A MATERIAL BODY

The method presented in Chapter IV for determining the optimum initial data and the beginning moment of the passive part of the nominal lunar trajectory was an approximate one, primarily because the perturbing effects of the moon were neglected. Let us see how the nominal initial data vary when the moon's effect is taken into account.

First of all, it should be noted that the energy expenditures will vary only slightly as a result of taking into account the lunar effect. According to /21/, even for flight in the lunar orbital plane (where the effect of the moon is greatest) the minimum flight speeds required to get to the moon are changed by less than 0.2 m/sec when the lunar effect is allowed for.

The other initial parameters also vary only slightly. Let us assume that all the initial parameters of a lunar trajectory are determined without taking into account the moon's effect, after which the trajectory taking into account this effect is calculated according to these initial parameters. The latter trajectory will still pass through the moon, but it will be shifted along the lunar surface by about 100 km for flight velocities close

to the minimum. For flight velocities close to parabolic, the trajectory will be shifted by only a few kilometers.

Consequently, the Keplerian elements of the initial part of a nominal lunar trajectory, calculated without taking into account the moon's effect, will not differ much from the Keplerian elements of a trajectory directed toward the moon's center and calculated taking into account the lunar effect. However, the latter effect, which alters the shape of the trajectory very slightly, reduces the flight time appreciably. Thus lunar impact will take place at some earlier point on the spacecraft orbit (that is, for lower values of $\Omega_a$).

The reduction in flight time is due to two things: the accelerating effect of the moon, which is felt primarily in the lunar sphere of action, and the fact that impact occurs on the moon's surface rather than at its center (that is, it occurs sooner). The former flight-time reduction $\Delta T_{acc}$ can be determined by numerical integration of the equations for perturbed motion. This quantity decreases monotonically (Figure 5.1) with an increase in the amount $\Delta V_1$ by which the initial velocity exceeds local parabolic, in accordance with the rise in the selenocentric velocity of entry into the moon's sphere of action. The latter flight-time reduction $\Delta T_{sur}$ also decreases monotonically with a rise in $\Delta V_1$ (Figure 5.1), since the velocity $U_1$ of impact of the spacecraft on the moon increases with a rise in the selenocentric entry velocity.

The total reduction

$$\Delta T = \Delta T_{acc} + \Delta T_{sur} \tag{1.1}$$

for the range

$$0.1 < \Delta V_1 < 0\ 2 \text{ km/sec}$$

amounts to from 1800 to 2000 seconds (that is, about 30 minutes). The dot-dash curve for $T(\Delta V_1)$ in Figure 4.4 was plotted taking into account this correction.

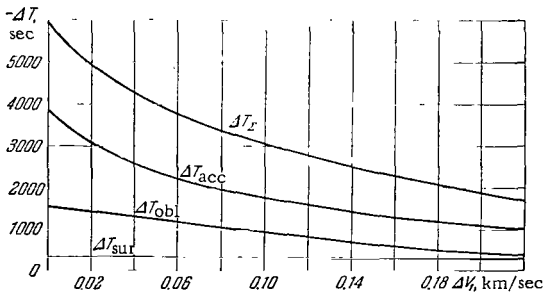


FIGURE 5.1. Reductions $\Delta T_i$ of flight time in passive part due to various factors, and total reduction $\Delta T_\Sigma$ ($\Delta V_1$ is amount by which initial geocentric velocity exceeds local parabolic).

Now let us consider how the time of engine cutoff and the corresponding initial data vary when the flight-time reduction $\Delta T$ and the decrease in the

longitude $\Omega_a$ of the moon's center at the moment of encounter, both due to the perturbing effect of the moon, are taken into account. First of all, it should be noted that the angle $\Omega_a$ will not be the same as the original node longitude, which we now designate as $\Omega_1$. Evidently, $\Omega_a < \Omega_1$ and

$$\Omega_1 - \Omega_a = \Delta\Omega_a = \omega\Delta T. \tag{1.2}$$

The angular velocity of revolution of the moon is $\omega = 13.2°/\text{day}$. Thus, if $\Delta T$ is of the order of 30 minutes, we obtain a value of 0.2° to 0.3° for $\Delta\Omega_a$, and this can be neglected in calculations with an accuracy of the order of a degree.

The optimum flight time $T_0$ for the passive part of the trajectory will now be given by the equation

$$180° + \lambda_{B_0} - \lambda_H - \sigma - \Delta\Omega_a = \Omega T_0 - 2\pi n + \Omega t_a. \tag{1.3}$$

instead of by equation (2.1) of Chapter IV. This time is smaller by an amount $\frac{\Delta\Omega_a}{\Omega}$ (where $\Omega$ is the angular velocity of rotation of the earth), that is, it is about a minute less.

Since the optimum flight time $T_0$ is practically unchanged (see § 4.2), while all the values of function $T(\Delta V_1)$ are reduced by a considerable amount $\Delta T(\Delta V_1)$, the optimum amount $\Delta V_1$ by which the initial velocity exceeds local parabolic is reduced: from the dot-dash curve in Figure 4.4 we find that $\Delta V_1 = 0.152$ km/sec.

Let us now take another look at Figures 2.5 and 4.2. Clearly, if the moon's influence is allowed for, the dependence of the angle $\lambda$ (between the meridians of the $X$ axis and the launch point) on the node longitude $\Omega_a$ will not vary, since it is a purely geometric function. Thus, since $\Delta\Omega_a$ is small, the curve for $\lambda(\Omega_a)$ is the same as the previous one (Figure 2.5). The relation $\Omega_L = \Omega_a - \omega T[\Delta V_1(\Omega_a)]$ only varies as a result of the change in the flight time $T$ by an amount $\Delta T$, since the values of $\Delta V_1(\Omega_a)$ remain the same as previously. However, the product $\omega\Delta T$ is small, so that the change in $\Omega_L$ can be neglected. Finally, relation (1.13) of Chapter IV:

$$\lambda_h = \lambda^0 + \Omega(h - h_0)$$

obviously will be the same as previously.

Thus the relations specifying the moments of entry into the passive part of the trajectory, as well as the corresponding initial data, are essentially unchanged. This is because the flight-time variations $\Delta T$ result in only small changes in $\Omega_a$ ($\Delta\Omega_a = \omega\Delta T$), and these may be compensated by very small variations in the moment of entry into the passive part of the trajectory, since $\Omega \gg \omega$. The iteration method of determining the nominal initial data is once again used, so that there is no qualitative change in the curves of Figure 4.3 due to taking the moon's effect into account. Hence, the nominal initial data are altered only as a result of the drop, by the comparatively small amount $\Delta T$, in the $T(\Omega_a)$ curves relative to the stationary line $T = T_0$ (Figure 4.3).

It should be noted that the limits of the range of values of $\Delta V_1$ corresponding to the condition of spacecraft visibility from the specified point will also change, although the corresponding range $T_{min} < T < T_{max}$ will not. Just as in

§ 4.2, from the value of $T_0$ it is easy to find $\theta_1^*$, $\Omega_a$, the time of beginning of the passive part, and the corresponding values of $t_1$, $\Phi_a$, $r_1$, and $H_1$ for various launch dates giving a possibility of guaranteed visibility of the impact from a specified point.

## 5.2. EFFECT OF ELLIPTICITY OF MOON'S ORBIT

The lunar orbit has an eccentricity $e \approx 0.0549$, a semimajor axis $a \approx 384{,}400$ km, and a parameter $p \approx 383{,}240$ km. Consequently, the minimum earth-moon distance is about 363,300 km and the maximum distance is about 405,500 km. The minimum and maximum angular velocities of revolution $\omega$ of the moon are given approximately by the area integral

$$r_2^2\omega(r_2) = \sqrt{(\mu_1 + \mu_2)\, p}, \tag{2.1}$$

where $\mu_1$ and $\mu_2$ are the gravitational potentials of the earth and moon. These velocities are: $\omega_{min} = 2.27 \cdot 10^{-6}$ rad/sec and $\omega_{max} = 2.96 \cdot 10^{-6}$ rad/sec.

Actually, because of the disturbing effect of the sun and other perturbations, the extreme value of the geocentric distance $r_2$ from the earth's center to the point of lunar impact and the extreme value of the moon's angular velocity of revolution will be somewhat different. For example, the minimum distance may be less than 360,000 km and the maximum angular velocity may exceed $3 \cdot 10^{-6}$ rad/sec.

The deviations of the earth-moon distance and the shifts of the moon from the point with lowest declination from their average values (corresponding to circular motion) are given by the formulas

$$\Delta r_2 = 384{,}400 - r_2, \quad \Delta\Omega = \Omega_L - \omega(h - h_0), \tag{2.2}$$

where $h$ is the given moment of universal time and $h_0$ is the moment when the moon passes through the point of minimum declination.

As far as the nominal initial data are concerned, the decrease $\Delta r_2$ in the distance to the moon (the direction of vector $r_2$ remaining unchanged) reduces both the flight time and the required initial velocity. The increase in the moon's angular velocity of revolution increases the angular distances between the advance points corresponding to lunar impacts on different days of the month. The reduction in flight time $\Delta T_e$ due to the ellipticity of the lunar orbit gives a correction of the order of a few hours, for a geocentric flight speed of about 2 km/sec near the lunar orbit. This correction turns out to be quite stable for a given value of $\Delta V_1$, the amount by which the initial velocity exceeds local parabolic. Obviously, however, the correction $\Delta T_e$ will vary considerably if there is any change in the nominal value of $\Delta V_1$. For different months and for different days $r_2$ may vary by thousands of kilometers. Consequently, each day will have its own value of correction $\Delta T_e$ and, accordingly, each day of the month will have its own nominal values of the velocity and the region of impact visibility from a specified point.

The middle and lower solid curves in Figure 4.4 give an idea of the decrease in flight time as a function of the distance to the moon. The middle curve corresponds to $r_2 = 370{,}000$ km and the lower curve to

$r_2 = 360{,}000$ km. It should be noted that the decrease in $\Delta V_1$ (the amount by which the initial velocity $V_1$ exceeds the local parabolic velocity $V_p$) caused only by a reduction of the distance is very slight. Actually, the ratio $\beta_1 = \left(\frac{V_1}{V_p}\right)^2$ depends only on the small ratio $\nu$ between the initial geocentric radius $r_1$ of the trajectory and the final radius $r_2$ (see formula (3.3) of Chapter II). It is easy to show that for a decrease in $r_2$ of around 20,000 km the nominal value of $\Delta V_1$ is reduced by about 5 m/sec.

We should also note that the ellipticity of the lunar orbit causes a shift in the position of $\Omega_a^*$, the energetically optimum point of encounter on this orbit, away from the position $\Omega_a = 0$ corresponding to minimum lunar declination. This shift will be toward lower radii $r_2$ (thus, for 1959—1960 it was toward $\Omega_L < 0$). However, due to the above-mentioned smallness of the effect which small variations in $\nu$ have on the required energy expenditures, it is to be expected that this shift will be only slight. Let us calculate the shift.

The condition that $\frac{d\beta_1}{d\Omega_a} = 0$ defines the optimum point for specified values of the trajectory azimuth $a_0$ at the launch point and the angle of elevation $\theta_1$ of the initial-velocity vector above the local horizon. Here $\beta_1 = 1 + \Delta\beta_1$, and $\Delta\beta_1$ is given by formula (3.3) of Chapter II. In this formula

$$\Phi_1 = 180^\circ - [\Phi_a(\Omega_a) + u_0(\Omega_a)],$$
$$\nu = \frac{r_1}{r_2(\Omega_a)}, \tag{2.3}$$

since the variation of $r_1$ with $\Omega_a$ can be neglected. The active angular range $\Phi_a$ varies only very slightly with $\Omega_a$, but it is easy enough to take this variation into account. The derivative $\frac{du_0}{d\Omega_a}$ of the latitude argument of the launch point can be found without difficulty by differentiating the equation

$$\sin\Theta\cos\Omega_a = \cos u_0 \sin\psi_0 - \sin u_0 \cos\psi_0 \cos a_0, \tag{2.4}$$

where $\Theta$ is the angle between the lunar orbital plane and the plane of the equator, and $\psi_0$ is the latitude of the launch point (Figure 2.3). Equation (2.4) was obtained by equating two expressions for the angle $m$ between the line of nodes $\Omega_a$ and the pole $P$. These expressions followed from a consideration of spherical triangles $P\Omega_a X$ and $P\Omega_a B_0$, where $B_0$ is the launch point (Figure 2.3). Differentiation of (2.4) gives:

$$\frac{du_0}{d\Omega_a} = \frac{\sin\Theta\sin\Omega_a}{-\sin\psi_0\sin u_0 + \cos\psi_0\cos u_0\cos a_0}. \tag{2.5}$$

Now let us find the derivative of the radius

$$r_2 = \frac{p}{1 + e\cos(v_0 + \Omega_a)}, \tag{2.6}$$

where $v_0$ is the true anomaly of the point on the lunar orbit with a minimum declination. This derivative is

$$\frac{dr_2}{d\Omega_a} = \frac{r_2^2}{p} e\sin(v_0 + \Omega_a). \tag{2.7}$$

When the above values of the derivatives are substituted into the relation $\frac{d\beta_1}{d\delta\Omega_a} = 0$, then after some simple transformations we obtain the equation

$$[\sin\Phi_1 [v\cos\theta_1 - \cos(\Phi_1 + \theta_1)] - (1 - \cos\Phi_1)\sin(\Phi_1 + \theta_1)] \times$$

$$\times \left( \frac{du}{d\delta\Omega_a} + \frac{d\Phi_a}{d\delta\Omega_a} \right) = (1 - \cos\Phi_1)\cos\theta_1 \cdot \frac{r_2^2}{p} e \sin(v_0 + \Omega_a), \qquad (2.8)$$

the root of which is the desired shift in $\Omega_a$. For $e = 0$ the right side becomes zero and the equation simplifies to $\frac{du}{d\delta\Omega_a} + \frac{d\Phi_a}{d\delta\Omega_a} = 0$, giving the root $\Omega_a = 0$. For $e \neq 0$ the root $\Omega_a^*$ is different from zero. As the nominal initial velocity is reduced, $|\Omega_a^*|$ increases, until at the minimum velocity it reaches $|\Omega_a^*| \approx +1.5°$. Since the maximum shift $|\Omega_a^*|$ is small in comparison with the diurnal lunar shift (which amounts to more than 13°), the correction $\Omega_a^*$ can be neglected when selecting the optimum launch date.

## 5.3. EFFECT OF THE EARTH'S OBLATENESS

Due to the oblateness of the earth the force of gravity is greater near the equator and smaller near the poles. However, the effect of the oblateness diminishes in inverse proportion to the fourth power of the geocentric distance $r$.

Let us find the perturbing acceleration caused by the earth's oblateness. This acceleration will have the following components in the directions of the radius $r$, the transversal $\tau$, and their normal $w$ /20/:

$$\left.\begin{aligned} R &= \frac{\varepsilon_1}{r_4}(3\sin^2\psi - 1),\ T = -\frac{\varepsilon_1}{r^4} 2\sin\psi\sin i_e\cos u_e, \\ W &= -\frac{\varepsilon_1}{r^4} 2\cos i_e\sin\psi, \end{aligned}\right\} \qquad (3.1)$$

where $\varepsilon_1 = \mu_1 a_e^2\left(\alpha - \frac{m}{2}\right)$; $\mu_1$ is the gravitational potential of the earth; $a_e$ is the equatorial radius; $\alpha = \frac{a_e - b}{a}$ is the oblateness [apparently $b$ is here the polar radius (Translator)]; $m = \frac{\Omega^2}{g_e}$; $\Omega$ is the angular velocity of the earth's diurnal rotation; $g_e$ is the acceleration of gravity at the equator; $i_e$ is the inclination of the trajectory plane to the equatorial plane; $u_e$ is the latitude argument of the spacecraft relative to the equatorial plane; and $\psi$ is the geocentric latitude of the spacecraft.

Let us consider as an example trajectories whose planes are inclined about 65° to the equator. During flight along such a trajectory a spacecraft will first reach a north latitude of the order of 65°, and then a south latitude of around 18°. The oblateness effect at the beginning of the trajectory is partially compensated by the corresponding effect in the rest of the trajectory.

Somewhere along such a trajectory each of components (3.1) goes through zero. Since the oblateness effect diminishes very rapidly with increased distance from the earth's center, the compensation will be greatest for movements along the radius and the transversal (when components $R$ and $T$ pass through zero for relatively low values of $r$).

For the component $W$ along the normal to the plane of the unperturbed trajectory, the compensation will be less, since this component goes through zero later (at $\psi = 0$).

In order to get an idea of the overall effect of the oblateness, it is advisable to evaluate the quantity

$$I = \int_0^T \left( \int_0^t \frac{\varepsilon_1}{r^4} dt \right) dt. \tag{3.2}$$

Here we assume that the spacecraft motion, taking into account the earth's oblateness, is not very different from the unperturbed motion (that is, the motion when the oblateness is neglected). Thus it is permissible to use the expression for $r(t)$ which describes unperturbed motion:

$$r = \frac{p}{1 + e \cos v}, \qquad dt = \frac{r^2}{\sqrt{\mu_1 p}} dv. \tag{3.3}$$

Using formula (3.3), we can rewrite expression (3.2) with $v$ as the variable instead of $t$ (where $v$ is the true anomaly of the given trajectory point). Then we have

$$I = \frac{\varepsilon_1}{\mu_1 p} \int_{v_1}^{v_2} \left( \int_{v_1}^{v} \frac{dv}{r^2} \right) r^2 dv. \tag{3.4}$$

After integrating the expression in brackets, we obtain

$$I = \frac{\varepsilon_1}{\mu_1 p} \int_{v_1}^{v_2} \left[ (v - v_1) \left( 1 + \frac{e^2}{2} \right) + 2e (\sin v - \sin v_1) + \right.$$
$$\left. + \frac{e^2}{4} (\sin 2v - \sin 2v_1) \right] \frac{dv}{(1 + e \cos v)^2}. \tag{3.5}$$

In order to simplify the subsequent transformations, let us set $e = 1$ (that is, we consider the unperturbed trajectory to be a parabola). This makes the quantity $I$ somewhat high, since the effect of the oblateness is enhanced when $\Delta V_1$ is reduced. For $e = 1$ we obtain

$$I = \frac{\varepsilon_1}{\mu_1 p} \int_{v_1}^{v_2} \left( \frac{3}{2} v + 2 \sin v + \frac{1}{4} \sin 2v - C \right) \frac{dv}{1 + \cos^4 \frac{v}{2}}, \tag{3.6}$$

where

$$C = \frac{3}{2} v_1 + 2 \sin v_1 + \frac{1}{4} \sin 2v_1. \tag{3.7}$$

Next we convert to the variable $\alpha = \tan \frac{v}{2}$ and integrate the first term in brackets by parts. After some simple transformations we obtain

$$I = \frac{\varepsilon_1}{2\mu_1 p} \left[ \left\{ \left( \frac{3}{2} v - C \right) \left( 1 + \frac{1}{3} \tan \frac{v}{2} \right) + \tan \frac{v}{2} \right\} \tan \frac{v}{2} \right]_{v_1}^{v_2}. \tag{3.8}$$

For a parabolic trajectory with a slope to the equator of $i_e \approx 65°$ and an initial height $H_1 \approx 1000$ km, formula (3.8) gives $l \approx 940$ km. Since $W < \frac{\varepsilon_1}{r^4}$, $T < \frac{\varepsilon_1}{r^4}$, and $R < \frac{3}{2}\frac{\varepsilon_1}{r^4}$, the change in the shape of the trajectory due to the earth's oblateness will be relatively small. The attendant shift of the impact point amounts to some fraction of a degree, and when the compensation is taken into account it may become an order of magnitude less.

It should be noted that we took $e = 0$ above just to simplify the transformations and that the equation is also solved in quadratures for $e \neq 1$. In addition, the quantity $W$ is expressed in quadratures, in terms of elementary functions.

Now let us consider the variation in flight time caused by the earth's oblateness. The flight time is

$$T(r_2) = \int_0^{s(r_2)} \frac{ds}{V}, \tag{3.9}$$

where $r_2$ is the geocentric radius of the impact point, $s$ is the distance traversed by the spacecraft, and the flight velocity $V$ is determined by the energy integral

$$V^2 = \left(\frac{2\mu_1}{r} - \frac{\mu_1}{a_1}\right) + 2\varepsilon_1\left(\frac{\sin^2\psi_1 - \frac{1}{3}}{r_1^3} - \frac{\sin^2\psi - \frac{1}{3}}{r^3}\right), \tag{3.10}$$

in which $r_1$, $\psi_1$, and $a_1$ are the initial radius, latitude, and osculating semimajor axis.

The change in the flight time to the moon is due primarily to a variation in the velocity of motion at large distances from the earth, where the spacecraft spends a major portion of the flight time, moving at an asymptotically diminishing velocity. Keeping in mind that the trajectory shape does not vary much, let us evaluate the flight-time variation $\Delta T$. The spacecraft will be assumed to reach the distance $r_2$ in perturbed motion and to traverse the same distance $s(r_2)$ as in the case of unperturbed motion. In other words, we assume that

$$\Delta s(r_2) = \int_0^{T(r_2)} \Delta V\, dt + V(r_2)\,\Delta T(r_2) = 0,$$

from which

$$\Delta T = \frac{-\int_0^{T(r_2)} \Delta V\, dt}{V(r_2)}.$$

The velocity variation $\Delta V$ resulting from the earth's oblateness is associated only with the variation $\delta h$ of the constant in energy integral (3.10) at a specified distance $r$ from the earth:

$$V\,\Delta V = \frac{\delta h}{2} = \varepsilon_1\left(\frac{\sin^2\psi_1 - \frac{1}{3}}{r_1^3} - \frac{\sin^2\psi - \frac{1}{3}}{r^3}\right).$$

From this it follows that, as time passes, the quantity $|\Delta V|$ increases monotonically from zero to its maximum value

$$|\Delta V(r_2)|_{\max} \approx \frac{\varepsilon_1}{V(r_2)} \frac{\left|\sin^2 \psi_1 - \frac{1}{3}\right|}{r_1^3},$$

so that we have the limiting condition

$$|\Delta T| < \tau_{\max}, \text{where} \tau_{\max} = \frac{|\Delta V(r_2)|}{V(r_2)} T. \tag{3.11}$$

For example, if we set $T \approx 1.5$ days, $r_1 = a_e + 1000$ km, $r_2 = 384{,}400$ km, and $\psi_1 = 65°$, we obtain $\tau_{\max} \approx 1000$ seconds.

Now let us calculate the flight-time variation, once again assuming that for both perturbed and unperturbed motion along a trajectory one and the same distance $s$ must be traversed in order to reach some specified distance $r$.

If $d\varphi$ is the angular displacement of the geocentric radius vector corresponding to an element $ds$ on the perturbed trajectory, then we have $ds = \sqrt{dr^2 + r^2 d\varphi^2}$. However, in the present case we can take $ds$ to be an element of the unperturbed trajectory. Therefore

$$ds = \sqrt{1 + \frac{r^2}{p^2} e^2 \sin^2 v}\, r dv,$$

where $v$ is the true anomaly corresponding to the radius $r$. Let us substitute (3.10) into (3.9) and expand the denominator in a Taylor series (powers of $\varepsilon_1$). Then, with an accuracy up to second-order terms, we obtain

$$T = \int_{v_1}^{v_2} \frac{1}{\Gamma} \sqrt{1 + \frac{r^2}{p^2} e^2 \sin^2 v} \left\{ 1 - \frac{1}{\Gamma^2} \frac{\varepsilon_1}{p^3} \times \right.$$
$$\left. \times \left[ A - \left( \sin^2 \psi - \frac{1}{3} \right) \frac{p^3}{r^3} \right] \right\} r\, dv, \tag{3.12}$$

where

$$\Gamma = \sqrt{\frac{2\mu_1}{r} - \frac{\mu_1}{a_1}} = \sqrt{\frac{2\mu_1}{p}} \left( \frac{p}{r} - \frac{p}{2a_1} \right)^{\frac{1}{2}} =$$
$$= \frac{V_p(p)}{\sqrt{2}} \sqrt{1 + 2e \cos v + e^2}, \tag{3.13}$$

$$A = \left( \sin^2 \psi_1 - \frac{1}{3} \right) \left( \frac{p}{r_1} \right)^3. \tag{3.14}$$

After integration the first term in brackets in (3.12) gives the flight time $T_0$ for unperturbed motion, while the second term gives the change in flight time $\Delta T_{ob} = T - T_0$ due to the oblateness. It can be shown that

$$\sqrt{1 + \frac{r^2}{p^2} e^2 \sin^2 v} = \frac{\Gamma \sqrt{2}}{V_p(p)(1 + e \cos v)}, \tag{3.15}$$

so that in (3.12) the factor before the braces becomes

$$\frac{\sqrt{2}}{V_p(p)(1+e\cos v)} = \frac{r\sqrt{2}}{V_p(p)\,p}.$$

Consequently, the integrand in the formula

$$\Delta T_{ob} = -\frac{2\sqrt{2}\varepsilon_1}{V_p^3(p)\,p^2}\int_{v_1}^{v_2}\frac{\left[A-\left(\sin^2\psi-\frac{1}{3}\right)(1+e\cos v)^3\right]dv}{(1+2e\cos v+e^2)(1+e\cos v)^2} \tag{3.16}$$

does not contain a radical. Here

$$\sin\psi = \sin u_e \sin i_e = \sin(v+\omega_e)\sin i_e = \alpha\cos v + \beta\sin v,$$

where $i_e$ is the inclination of the trajectory plane to the plane of the equator, $\omega_e$ is the longitude of the trajectory perigee relative to the equatorial plane,

$$\alpha = \sin i_e \sin\omega_e, \quad \beta = \sin i_e\cos\omega_e. \tag{3.17}$$

Thus we can write

$$\Delta T_{ob} = -\frac{2\sqrt{2}\varepsilon_1}{p^2V_p^3(p)}(I_1+I_2),$$

where

$$I_1 = \int_{v_1}^{v_2}\frac{A\,dv}{(1+2e\cos v+e^2)\sqrt{1+e\cos v}}, \tag{3.18}$$

$$I_2 = \int_{v_1}^{v_2}\frac{\left[(\alpha^2\cos^2 v+\beta^2\sin^2 v+2\alpha\beta\sin v\cos v)-\frac{1}{3}\right]}{1+2e\cos v+e^2}(1+e\cos v)\,dv. \tag{3.19}$$

Integrals $I_1$ and $I_2$ become integrals of rational functions when we make the substitution $x=\tan\frac{v}{2}$, facilitating the integration; the absolute values of these integrals will decrease as $e$ increases from unity.

In the case where $e=1$ (parabolic initial velocity), the integration of (3.19) is a simple matter, and it leads to the following formula:

$$\Delta T_{ob} = \frac{\varepsilon_1}{2\sqrt{2}\,p^2V_p^3}\left[2\left(\alpha^2+\beta^2-\frac{2}{3}\right)+(\alpha^2-\beta^2)\sin 2v - \right.$$
$$\left. -2\alpha\beta\cos 2v - A\tan\frac{v}{2}\left(1+\frac{2}{3}\tan^2\frac{v}{2}+\frac{1}{5}\tan^5\frac{v}{2}\right)\right]_{v_1}^{v_2}. \tag{3.20}$$

For the parabolic trajectory assumed above, this formula gives $\Delta T_{ob} = -1630$ seconds. Here the integral $I_2$ produces the sum of the first three terms in (3.20), which amounts to less than 0.001 of $I_1$ (that is, of the last term). Consequently, $I_2$ can be neglected in the correction $\Delta T_{ob}$.

For a hyperbolic velocity $\Delta T_{ob}$ will be lower than for the parabolic case. For example, for a trajectory with $\Delta V_1 = 0.130$ km/sec and an initial height of 1000 km, the correction $\Delta T_{ob}$ is about 750 seconds (Figure 5.1). The variation of the correction along a parabolic trajectory is plotted in Figure 5.2, where the abscissa is the latitude argument $u$.

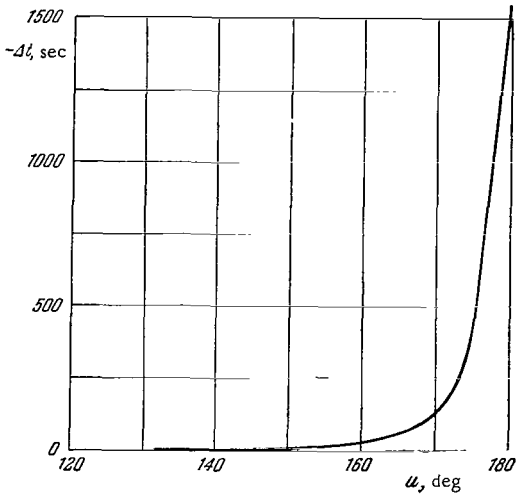


FIGURE 5.2. Oblateness-caused reduction $\Delta t$ in flight time, as function of latitude argument $u$ along trajectory.

A negative value of $\Delta T_{ob}$ signifies that the lower velocity decrease (in comparison with the unperturbed case) at the beginning of flight, due to the earth's oblateness, is only partially compensated by the enhanced velocity decrease at the end of flight, when the spacecraft impacts at a low latitude. In this case the trajectory is straightened somewhat as a result of the oblateness.

## 5.4. EFFECT OF THE SUN

The sun disturbs the motion of a spacecraft relative to the earth, since it imparts different accelerations to the spacecraft and to the earth. The components of this perturbing acceleration may be represented in the following form ($\mu$ being the mass of the earth):

$$2(1-\mu)\xi, \quad -(1-\mu)\eta, \quad (1-\mu)\zeta, \tag{4.1}$$

provided we take the sun's mass as unit mass, the distance between the centers of the earth and sun as unit length, and the quantity $\frac{P}{2\pi}$ as unit time, where $P$ is the sidereal year. It is assumed that the $\xi$ axis is always directed toward the sun, and that the $\eta$ and $\zeta$ axes pass through the center of the earth, orthogonally to the $\xi$ axis. Terms of the order of $\xi^2$, $\eta^2$, and $\zeta^2$ or above may be neglected.

From (4.1) we obtain the radial and transversal components of the perturbing acceleration (for example, in the $\xi\eta$ plane):

$$\left.\begin{aligned} F_r &= \frac{2(1-\mu)\xi^2 - (1-\mu)\eta^2}{r}, \\ F_\tau &= -\frac{3\xi\eta}{r}, \end{aligned}\right\} \tag{4.2}$$

where $r = \sqrt{\xi^2 + \eta^2}$. These expressions can be used to evaluate the sun's effect upon the lunar trajectory.

It follows from formulas (4.2) that the radial component is a maximum for motion along the earth-sun line, while the transversal component is a maximum for motion along lines lying at angles of 45° or 135° to the earth-sun line.

Obviously, the effect of the sun on the lateral movement $x$ of the spacecraft will be greatest when the maximum perturbing acceleration acts orthogonal to the trajectory during the entire flight time. Therefore, the lateral movement $x$ corresponding to purely radial motion at an angle of 45° to the earth-sun line may be used to evaluate the lateral movement in other cases. In order to determine the absolute value of the maximum lateral shift, we write $\xi = \eta = \frac{r\sqrt{2}}{2}$. Then, the second formula of (4.2) gives

$$\ddot{x} = \frac{3}{2} r(t). \tag{4.3}$$

The variation $r(t)$ for unperturbed motion can be used to integrate this equation. Let us assume that the unperturbed motion takes place at the parabolic velocity

$$\frac{dr}{dt} = \sqrt{\frac{2\mu}{r}},$$

so that

$$dt = \frac{\sqrt{r}}{\sqrt{2\mu}} dr. \tag{4.4}$$

Then, taking into account the zero-point initial data, we obtain

$$\dot{x} = \frac{3}{5} \frac{r^{5/2}}{\sqrt{2\mu}}, \quad x = \frac{3}{20} \frac{r^4}{2\mu}. \tag{4.5}$$

If we now substitute in the values $r = \frac{384{,}400}{150 \cdot 10^6} = 2.56 \cdot 10^{-3}$ and $\mu^{-1} = 332{,}000$, and if we take the earth-moon distance as unity, we obtain $x \approx 160$ km. This means that the lateral movement caused by the perturbing effect of the sun can be neglected in the problem under consideration.

Next let us consider the radial shift. First of all, we know that the radial shift must be of the same order as the lateral shift. Secondly, for a moon flight the variation in flight time $\Delta T'$ caused by this shift is in general substantial. The quantity $\Delta T'$ can be evaluated by integrating the equation of motion along a radial trajectory, assuming a maximum purely radial solar perturbation:

$$\ddot{r} = -\frac{2\mu}{r^2} - 2(1-\mu) r. \tag{4.6}$$

This gives the energy integral

$$\dot{r}^2 = \left(\frac{2\mu}{r} - \frac{1}{a}\right) 2(1-\mu)(r^2 - r_1^2). \tag{4.7}$$

where $a$ is the semimajor axis of the spacecraft orbit. When we substitute $\dot{r}$ into the expression

$$T = \int_{r_1}^{r_2} \frac{dr}{\dot{r}},$$

then, similarly to the case of the oblateness effect, we obtain

$$T = \int_{r_1}^{r_2} \frac{dr}{\sqrt{\frac{2\mu}{r} - \frac{1}{a} \cdot \left[1 - 2\frac{1-\mu}{\left(\frac{2\mu}{r} - \frac{1}{a}\right)}(r^2 - r_1^2)\right]^{1/2}}},$$

and from this it is possible to find the flight-time variation $\Delta T'$ caused by the sun's action:

$$\Delta T' = \int_{r_1}^{r_2} \frac{(1-\mu)(r^2 - r_1^2)\, dr}{\left(\frac{2\mu}{r} - \frac{1}{a}\right)^{3/2}}. \tag{4.8}$$

Assuming a parabolic initial velocity, we finally obtain

$$\Delta T' = \frac{1-\mu}{(2\mu)^{3/2}} \int_{r_1}^{r_2} (r^2 - r_1^2)\, r \sqrt{r}\, dr \approx \frac{r_2^{9/2}}{9\sqrt{2\mu^3}}.$$

Since unit time was taken to be $e_t = 365 \cdot 86{,}400$ seconds, the flight-time variation is $\Delta T' \approx 170$ seconds.

## CONCLUDING REMARKS

As we have seen, the effect of the sun only changes the flight time by less than three minutes. If this effect is ignored, the approximate method considered previously turns out to be quite simple and gives an accuracy of the order of a degree. However, if an attempt is made to take this variation into account, the accuracy of the approximate method will not be raised much, since it is governed by other factors as well.

Consequently, to obtain approximate results accurate to about a degree, only the effects of the ellipticity of the lunar orbit and the earth's oblateness need be taken into account. However, these factors have only a slight effect on the trajectory shape and on the energy requirements. Thus, taking these factors into account merely means that (just as in § 5.1) the variation in (reduction of) the flight time in the passive part of the trajectory is taken into account. The total flight-time reduction $\Delta T_{\Sigma}(\Delta V_1)$ due to the effects of lunar attraction, the finite dimensions of the moon, and the earth's oblateness was plotted in Figure 5.1. The flight-time variation taking into account this reduction is shown in Figure 4.4 by dashed curves (for the corresponding solid lines).

The calculation of the nominal initial data taking into account all the secondary factors is carried out in a way similar to that described in Chapter IV. Now, however, the distances and angular positions of the moon are corrected for the ellipticity of the lunar orbit. The total flight-time variation resulting from this ellipticity and from the other secondary factors is also allowed for. The latter calculation is made as accurately as in § 5.1.

Figure 5.3 shows some typical curves for the nominal flight time $T(\Omega_a)$, taking into account the effects of secondary factors, The launch dates to $(N+3)$ are the same as in Figure 4.3. The conditions for impact visibility can obviously be optimized if, for each day, we specify the angle of elevation $\theta_1$ corresponding to the optimum flight time $T_0$.

The approximate method always provides an indirect check of whether, for each date in a specified interval of dates, the impact visibility for any given set of $T = T(\Omega_a)|_{\theta_1 = \text{const}}$ curves (Figure 5.3) is satisfactory.

One possible way of selecting the nominal initial data using the approximate method was outlined above. However, this method also makes possible a consideration and evaluation of other means of data selection. For instance, it is somewhat simpler to determine the nominal initial data for a number of days according to the condition $\beta_1 =$ constant rather than the condition $\theta_1 =$ constant. The calculation then reduces to determining by the method of iterations the value of $\Omega_a$ corresponding to the specified value of $\beta_1$ and any value of $\theta_1$. First the zero approximation $\Omega_a^0$ is selected. Then the function $r_2(\Omega_a)$, obtained using the first formula (2.2) of Chapter V and an astronomical almanac, is used to find the distance $r_2(\Omega_a^0)$ to the moon

at the moment of impact and the ratio $\nu = r_1(\theta_1, \beta_1)/r_2(\Omega_a^0)$ of the initial radius to the final radius. Formulas (3.2) and (3.3) of Chapter II give the passive angular range $\Phi_1$ and the latitude argument of the launch point $u_0 = 180° - \Phi_a(\theta_1, \beta_1) - \Phi_1$, where $\Phi_a(\theta_1, \beta_1)$ is the angular range of the active part of the trajectory. Finally, we can find a more precise value of $\Omega_a$ using formula (2.4).

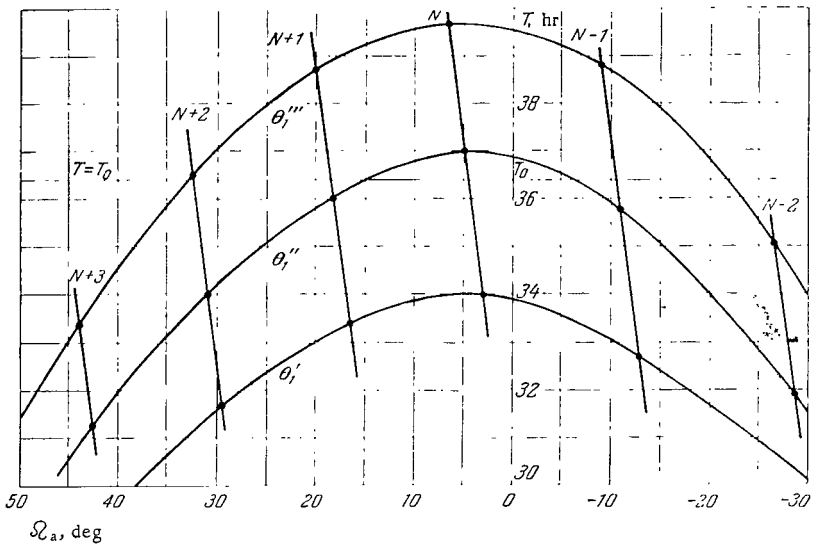


FIGURE 5.3. Typical dependence of flight time $T$ in passive part of trajectory on advance position $\Omega_a$ of moon, for energetically optimum set of launch dates in a single month; effects of secondary factors are taken into account (compare with Figure 4.3).

To determine the angle $\Phi_1$, it is convenient to replace formula (3.3) of Chapter II by the following set of formulas:

$$\alpha = 2\beta_1 \cos\theta_1, \quad \gamma = \sqrt{1 + \alpha^2 - 2\alpha\cos\theta_1},$$
$$\sin x = \frac{1 - \alpha\cos\theta_1}{\gamma}, \quad \cos x = \frac{\alpha\sin\theta_1}{\gamma},$$
$$\sin y = \frac{1 - \alpha\nu\cos\theta_1}{\gamma}, \quad \Phi_1 = y + x.$$

The flight time and the other nominal parameters are determined just as in the case $\theta_1$ = constant.

We assume Keplerian motion of the moon relative to the earth. Then, since the mass ratio of the earth and moon as material points is known, Kepler's third law (for the semimajor axis of the orbit $a$ = 384,400 km and the sidereal month) gives the earth's gravitational potential as $\mu_1$ = 397,529 km$^3$/sec$^2$. This potential differs from the actual one by an amount proportional to the effect of the perturbations on the geocentric motion of the moon. When converting from Keplerian motion to real motion, the effect of the potential variation on the flight time should be taken into account. However, checks have shown that, using the approximate

method with its accuracy of about 1°, this variation (which amounts to around 1/400 part of $\mu_1$ and about 1/800 part of the quantity $\sqrt{\mu_1}$ entering into the expression for the parabolic velocity) can be neglected.

It should also be noted that the ephemeris can be calculated without taking into account the secondary factors, on condition that the total flight time is selected in the same way as for an accurate calculation. Sample calculations show that for sesquidiurnal trajectories the ephemeris error in determining the direction of the spacecraft's radius vector does not exceed 0.5° and that it is usually in the orbital plane. In particular, for a flight time of the order of 1.5 days, we compared the latitude argument of a trajectory calculated taking into account all the factors acting with that of a trajectory calculated ignoring secondary factors. The difference between the latitude arguments at the beginning and end of flight was zero, while the maximum value of this difference was attained between 15,000 and 25,000 seconds of flight and did not exceed 0.5°. The possible deviation of a lunar trajectory in a direction orthogonal to its plane turns out to be even less.

In closing, we should mention that the accuracy of the above approximate method was checked by carrying out numerical integrations for three trajectories. In these calculations all the perturbations affecting the initial data obtained using the approximate method for different days and months were taken into account. The minimum distances of these trajectories from the moon's center turned out to be 2582, 1498 and 1533 km. These sample calculations proved that the approximate method actually provides an accuracy of angular approach to the moon of the order of 1°. Moreover, the initial velocity obtained was accurate to about 1 m/sec and the angle of elevation of the initial-velocity vector above the local horizon was accurate to about 0.1°.

*Supplement*

## *A GENERAL ANALYSIS OF LUNAR TRAJECTORIES WITH APPLICATION TO THE TWO-DIMENSIONAL CASE*

The restricted circular three-body problem, even for the two-dimensional case, has not been solved in a general form. For certain particular cases involving the motion of bodies in the solar system, some methods for finding solutions have been worked out. However, the trajectories of single-shot flights from the earth to the moon bear little resemblance to the usual orbits of bodies in the solar system, so that the above methods for finding solutions are no longer applicable.

In this supplement approximate methods will be used to find possible types of lunar trajectories and to carry out rough calculations for them. The parameters of motion can be found more accurately and the effect of initial-data scatter determined by a numerical integration of the equations of motion.

An energy approach similar to that used by Hill /23/ provides a theoretical solution of problems related to the minimum velocities required to reach the moon and the possibility of lunar capture of a spacecraft from the earth.

### D. 1. THEORETICAL DETERMINATION OF MINIMUM INITIAL VELOCITIES

Let us consider the restricted circular three-body problem, with $m_0$ as the spacecraft, $m_1$ as the earth, and $m_2$ as the moon. The equations are:

$$\left.\begin{aligned} \ddot{x} &= 2\dot{y} + \frac{\partial J}{\partial x}, \\ \ddot{y} &= -2\dot{x} + \frac{\partial J}{\partial y}, \\ \ddot{z} &= \frac{\partial J}{\partial z}. \end{aligned}\right\} \tag{1.1}$$

where

$$J = \frac{1}{2}(x^2 + y^2) + \frac{fm_1}{r} + \frac{fm_2}{\rho}, \tag{1.2}$$

$f$ is the gravitational constant, $r$ is the distance of the spacecraft from the earth, and $\rho$ is the distance of the spacecraft from the moon. The $x$ axis always joins the centers of the earth and moon, while the $y$ axis lies in the lunar orbital plane and passes through the center of gravity of the system of bodies $m_1 m_2$.

The units of measurement used are as follows: unit length is the distance $a$ between the centers of the earth and moon, and unit time is the quantity $T/2\pi$, where $T$ is the sidereal month (the period of revolution of bodies $m_1$ and $m_2$ in absolute space). According to Kepler's third law, we can write the following relation (in the measurement units taken):

$$f(m_1+m_2)=a^3\left(\frac{T}{2\pi}\right)^{-2}=1.$$

Equations (1.1) have the following Jacobi integral /25/:

$$\frac{1}{2}V^2=J+h, \tag{1.3}$$

where $V$ is the spacecraft velocity in the $xyz$ coordinate system, and $h$ is a constant. Obviously, for a given value of $h$, the motion will be limited by the zero-velocity surfaces introduced by Hill:

$$J=-h. \tag{1.4}$$

A study of equation (1.4) shows /25/ that for high negative values of $h$ motion is possible only within certain nonosculating surfaces $s'$ and $s''$, which are close to spheres with centers $m_1$ and $m_2$ and are, moreover, outside the envelopes $s'$ and $s''$ of some surface $s$. The sections of each of the surfaces $s$, $s'$, and $s''$ in the $xy$ plane are nearly circular. For an initial velocity $V_0 = 0$, the surface $s'$ passes through the initial point of the passive part of the trajectory, and with an increase in $V_0$ this surface becomes larger and further away from body $m_1$.

The passive part of the trajectory begins at distances which are much smaller than the distance to the moon. Thus, for low initial velocities $V_0$ motion can take place only inside the surface $s'$ and an approach to the moon is not possible.

With an increase in $V_0$ the constant $h$ has higher values. In addition, surfaces $s'$ and $s''$ become larger and converge, while surface $s$ contracts. For some velocity $V_0=V_0^{(1)}$ the quantity $h$ has a value $h=h_1$, for which surfaces $s'$ and $s''$ have one common point $L_1$ (Figure D. 1). When the difference $(h-h_1)$ is small, these surfaces will be joined by a corridor near point $L_1$. This means that a trajectory originating near body $m_1$ can reach a region in the vicinity of body $m_2$ (that is, approach of the spacecraft to the moon is possible). Half of the cross sections of surfaces $s, s'$ and $s''$ in the $xy$ plane, for $h=h_1$ are shown in Figure D. 1 (curves $s_1$, $s_1'$, and $s_1''$).

With a further increase in $h(V_0)$, the critical value $h_2 > h_1[V_0=V_0^{(2)}]$, is reached, which corresponds to contact between surfaces $s$ and $s''$ at point $L_2$ (curve $s_2$ in Figure D. 1). Then, the escape of a spacecraft from earth into infinity becomes possible, through a corridor near point $L_2$. Consequently, the minimum velocity required to reach the moon is $V_0^{(1)}$, and the minimum velocity for which the spacecraft will go off into infinity is $V_0^{(2)}$.

In addition to the critical values $h_1$ and $h_2$, there are also two other critical values $h_3 > h_2$ and $h_4 > h_3$. For $h_3$ the spacecraft can escape into infinity through a corridor near point $L_3$ (see curve $s_3$ in Figure D. 1). The value $h_4$ is negative and corresponds to a disappearance of the zero-

velocity curves in the $xy$ plane, at two points $L_4$ and $L_5$ which are symmetrical with respect to the $x$ axis.* For this value the spacecraft can escape into infinity along any direction in the $xy$ plane. For $h = 0$ the surfaces limiting three-dimensional motion will disappear.

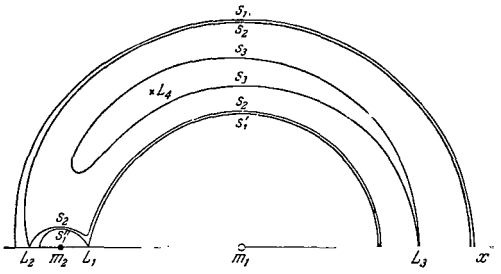


FIGURE D.1. Sections of critical zero-velocity surfaces for earth-moon system in lunar orbital plane. For velocities somewhat higher than minimum, a spacecraft can get through to the moon only via a corridor near point $L_1$.

Points $L_i$ (the so-called **libration points**) lie in the lunar orbital plane and may be found as singularities of surfaces (1.4). The values of $h$ are found from the Jacobi integral (1.3) for $V = 0$, using the coordinates of points $L_i$; the corresponding initial velocities $V_0^{(i)}$ are found from the same integral for $h = h_i$, using the coordinates of the specified initial point.

The magnitude of the critical initial velocity $V_0^{(i)}$ obtained will be the same, irregardless of its direction, although naturally this magnitude will vary from point to point. However, it follows from expressions (1.2) and (1.3) that the velocities $V_0^{(i)}$ vary only slightly from point to point on a sphere of small radius $r$. For example, on a sphere corresponding to a height of 200 km, the variation in $V_0^{(i)}$ will be of the order of $5 \cdot 10^{-7}$ $\frac{2\pi a}{T}$, where $a = 384{,}400$ km. Therefore, in practice the velocities $V_0^{(i)}$ will not depend on the position of the initial point on the sphere (here, as in the calculation of the curves in Figure D.1, it was assumed that $m_1 : m_2 = 81.45$).

Table D.1 lists the computed values of: the distances $r_i$ and $\rho_i$ of the libration points from the earth and moon, respectively; the critical values $h_i$; and the critical velocities $V_0^{(i)}$.

TABLE D.1.

| | $r_i$ | $\rho_i$ | $h_i$ | $V_0^{(i)}$, units of $\frac{2\pi a}{T}$ | $V_0^{(i)}$, $\frac{\text{km}}{\text{sec}}$ |
|---|---|---|---|---|---|
| $L_1$ | 0.8491539 | 0.1508461 | −1.594067 | 10.60335 | 10.84890 |
| $L_2$ | 1.1677237 | 0.1677237 | −1.585991 | 10.60411 | 10.84968 |
| $L_3$ | 0.9929263 | 1.9929263 | −1.506062 | 10.61165 | 10.85738 |
| $L_4$ | 1 | 1 | −1.494001 | 10.61278 | 10.85854 |

* These points are designated by x's in Figures D.1 and D.3.

The height of the initial point on the trajectory is taken as 200 km. This initial height was selected because the trajectories calculated for it are also valid for greater initial heights. Lower initial heights are not suitable, however, due to the increased effect of atmospheric resistance.

The table shows that the difference between the first and fourth critical velocities amounts to less than 10 m/sec, whereas the difference between the first and second, or the third and fourth, velocities is only around 1 m/sec. The distances of points $L_1$ and $L_2$ from the moon are, respectively, 58,000 km and 65,000 km, that is, both of these points are situated within the moon's sphere of action, quite close to its boundary.

## D. 2. NUMERICAL DETERMINATION OF TWO-DIMENSIONAL TRAJECTORIES

It is of interest to ascertain, even just for the two-dimensional case, what the minimum-velocity trajectories will be. Also, we would like to know whether a spacecraft can be so launched from the earth, with an initial velocity slightly higher than minimum, that it will ascend along an upward trajectory to the libration point $L_1$, traverse the corridor at a low velocity, and then reach the moon. We can find this out by calculating the trajectories using one of the methods of numerical integration.

The right sides of equations of motion (1.1) increase rapidly as the spacecraft nears the moon, and they become indefinitely large for accurate impacts at the lunar center. This state of affairs can be avoided if a regularizing transformation of variables is carried out.

For the two-dimensional problem, the familiar Thiele transformation /26/ is the most suitable. First, the origin of the coordinate system is transferred to the middle of segment $m_1m_2$ (Figure D. 2), and the quantity $c=\frac{a}{2}$ is taken as the unit of length instead of $a$. Now we can write

$$\xi = c_1 + 2x, \quad \eta = 2y, \quad \text{where} \quad c_1 = \frac{m_1 - m_2}{m_1 + m_2} = 0.9757478. \tag{2.1}$$

The equations of motion are then

$$\ddot{\xi} = 2\frac{d\eta}{d\xi} = \frac{\partial J'}{\partial \xi}, \quad \ddot{\eta} = -2\frac{d\xi}{dt} = \frac{\partial J'}{\partial \eta}, \tag{2.2}$$

and the Jacobi integral becomes

$$V^2 = 2J' + H, \tag{2.3}$$

where

$$J' = \frac{1}{2}(\xi^2 + \eta^2) - c_1\xi + \frac{8m_1}{r} + \frac{8m_2}{\rho}, \quad H = \text{const.}$$

The Thiele transformation consists in converting to the new variables $\tau$, $u(\tau)$ and $v(\tau)$, using the formulas $dt = r\rho\, d\tau$ and $\zeta = \cos w$, where

$$\zeta = \xi + i\eta \quad \text{and} \quad w = u + iv. \tag{2.4}$$

It is easy to show that this transformation actually leads to equations with right sides which are regular throughout the entire finite $w$ plane.

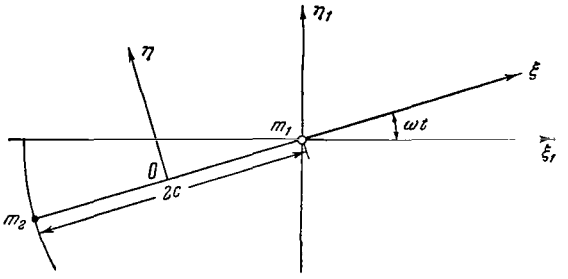


FIGURE D. 2. Relation between geocentric coordinates $\xi_1$ and $\eta_1$ and rotating coordinates $\xi$ and $\eta$. Initial direction of $\xi_1$ axis from $m_2$ to $m_1$.

In Thiele variables all the trajectories are calculated to 5 or 7 significant places. Jacobi integral (2.3) serves as an adequate means of checking the accuracy.

The results of a flight-path calculation for a spacecraft with a minimum velocity will now be presented. The first critical velocity $V_0 = V_0^{(1)}$ was taken to be perpendicular to the initial geocentric radius $r_1$, in the direction of the moon's rotation. Thus the initial geocentric velocity of the spacecraft was, as can be deduced from Figure D. 2, a maximum (in comparison with velocities in the other direction having the same critical value). The trajectory began at a height of 200 km for $\rho = a$. This trajectory returned earthward, without reaching the critical $s_1'$ curve at about 30,000 km. Five more circuits for the given trajectory were distinguished in an interval a little longer than a month, but the apogee distance remained almost unchanged.

Figure D. 3 shows the calculated trajectory in rotating coordinates (the trajectory of the sixth circuit is not shown, since it intersects that of the first circuit). Here and below the flight time in days is shown alongside the curves. In the nonrotating geocentric $m_1\xi_1\eta_1$ coordinate system (the $\xi_1$ axis lies along the $\xi$ axis at the moment $t = 0$; see Figure D. 2), the "figure eights" (Figure D. 3) are shown as curves circumventing the earth in the same sense as the moon does. These curves lie in almost exactly the same ellipse with one focus at the earth's center (Figure D. 4). The increase in the apogee radius, though perceptible, is small.

Sooner or later, according to § D. 1, some flight path of a spacecraft with an initial velocity $V_0 = V_0^{(1)}$ may reach surface $s_1'$. However, the foregoing calculation shows that this can take place only after quite a large number of circuits around the earth's center $m_1$.

Some trajectories deviating from the considered initial-velocity direction were also calculated (Figure D. 5). It was found that, for the apogee distance of the first circuit, the choice of the initial-velocity direction is significant. A comparison of the trajectories in Figure D. 5 (for example, trajectories I and IV) indicates that the apogee distance increases with an increase in the magnitude of the initial geocentric velocity.*

* This magnitude will be greater when the angle between the vectors of the transfer velocity and the relative initial velocity is less.

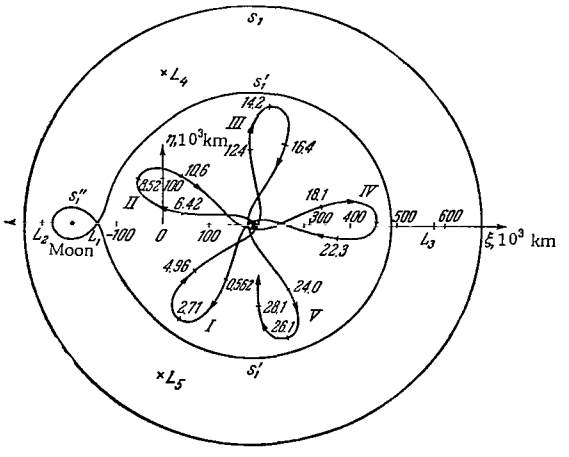


FIGURE D.3. Flight paths of spacecraft with minimum critical initial velocity, calculated in rotating coordinates. Critical curve $s_1'$ not reached during the course of a month.

Curves of type IV (Figure D.5), which go around the earth in a clockwise sense, are very close to ellipses with one focus at the earth's center, in the geocentric system of coordinates. Thus they are similar to the curves in Figure D.4, except that the ellipses described by the spacecraft are clockwise.

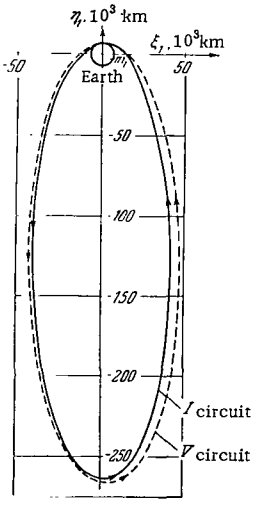


FIGURE D.4. Previous trajectory in geocentric coordinates. Enlargement of orbit under influence of lunar perturbations is perceptible.

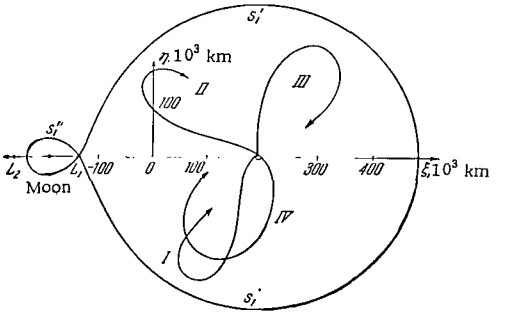


FIGURE D.5. Effect on trajectory of variation in direction of initial velocity (in rotating coordinates 0, $\xi, \eta$).

The descriptions of trajectories with $V_0 = V_0^{(i)}$ $(i = 2, 3, 4)$ are analogous to those for trajectories with initial velocities $V_0 = V_0^{(1)}$. It turns out that on the first circuit these trajectories do not even reach the corresponding $s_i$ curves, much less the $s_1'$ curves (Figure D. 1).

Consequently, the minimum velocities obtained in §D. 1 using the Jacobi integral are definitely unsatisfactory, if we wish to reach the moon on the first circuit around the earth (the case of greatest interest).

## D. 3. TRAJECTORIES OF MINIMUM ABSOLUTE INITIAL VELOCITY

It has been shown that, in geocentric coordinates, the motion along a minimum-velocity trajectory during the first circuit is very close to being motion along an ellipse with a focus at the earth's center. Consequently, for such a trajectory the effect of the moon during the first circuit will be practically nil. Thus it would be reasonable to try to find the approximate values of the minimum velocities required to reach the moon on the first circuit, completely neglecting the moon's effect.

In this case the initial velocity $\mathbf{V}_1$ in the nonrotating geocentric coordinate system $m_1\xi_1\eta_1$ will be considerable, but not the velocity $\mathbf{V}_0$ in the $O\xi\eta$ system (Figure D. 2). It is clear that the minimum initial geocentric velocity must correspond to the attainment of an apogee radius $r_a$ equal to the distance out to the moon.

Let us now determine the magnitude $V_1$ of this minimum velocity, assuming that the angle $\alpha_1$ between this velocity and the initial geocentric radius $r_1$ is known. Using the condition $r_a = a$, we obtain an expression for the major axis of the ellipse along which the moon can be reached at the minimum initial velocity:

$$2a_e = \frac{a^2 - r_1^2 \sin^2 \alpha_1}{a - r_1 \sin^2 \alpha_1}. \tag{3.1}$$

With the aid of the geocentric energy integral, we can now find the minimum initial velocity $V_1(r_1, \alpha_1)$:

$$V_1^2 = r_1 V_p^2(r_1)\left(\frac{1}{r_1} - \frac{1}{2a_e}\right), \tag{3.2}$$

where $V_p^2(r_1) = \frac{2fm_1}{r_1}$ (here, $V_p$ is the local parabolic velocity). If the height is 200 km and the initial velocity is vertical $(\alpha_1 = 0)$, we obtain

$$V_p = 10.99967 \text{ km/sec},$$

and a minimum initial velocity $V_1 = 10.90525$ km/sec. This velocity is about 60 or 50 m/sec higher than the geocentric velocities corresponding, respectively, to the first and fourth critical velocities for $\alpha_1 = 0$.

It follows from (3.1) and (3.2) that, as the direction of the initial velocity varies from vertical to horizontal (that is, as $\alpha_1$ varies from 0 to $\frac{\pi}{2}$), the magnitude of the initial velocity will increase monotonically. Consequently, the value of the initial velocity given above for the vertical direction will be less than the actual minimum velocity. However, the deviation of this

value from that for $|\alpha_1| = \frac{\pi}{2}$ (horizontal direction) is small. For example, if the initial height is 200 km, this deviation only amounts to 1.6 m/sec.

The position of the initial point of the passive part of a lunar trajectory is quite easy to calculate. From the magnitude $V_1$ and direction $\alpha_1$ of the initial velocity, we find the ellipse parameters, the angular distance $\Phi_1$, and the flight time between the initial and final points of the passive part. The condition that the spacecraft encounter the moon at the advance point on the lunar orbit determines the initial position corresponding to arrival at the moon.

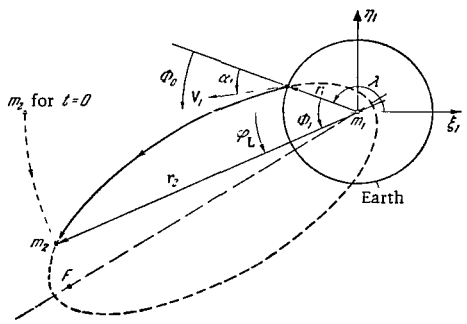


FIGURE D. 6. Calculation of lunar impact for $\alpha_1 > 0$ (without taking into account perturbing effect of moon).

For flight in the lunar orbital plane, the initial position is determined only by the angle $\lambda$ between the initial radius and the $\xi$ axis ($|\lambda| < \pi$). If we stipulate that, at the initial moment, the $\xi$ axis coincides with the $\xi_1$ axis, then (Figure D. 6):

$$\lambda = \pi \operatorname{sgn} \alpha_1 - \Phi_0, \quad \Phi_0 = \Phi_1 - \varphi_1, \quad \varphi_1 = \omega T_{1,2}, * \tag{3.3}$$

where $\omega$ is the moon's angular velocity of revolution, and $T_{1,2}$ is the flight time to the advance point, determined using the formulas of conic-section theory. Here and in the following, counterclockwise motion will be considered to be positive for all angles.

Numerical integration was used to find the trajectories determined by equations (2.2) and by the initial data obtained from formulas (3.1) through (3.3). The values of $\alpha_1$ were $-\frac{\pi}{2}$, 0; $+\frac{\pi}{2}$, and a number of close values. One of these trajectories is shown in Figure D. 7. The condition $r_a = a$ gives a quite accurate value of the minimum velocity required to reach the lunar center (accurate to about 0.02 m/sec), so that the corresponding initial data can actually be calculated completely neglecting the moon's effect.

The above result signifies that, in order to hit the moon, it is not enough just to reach a point where the attractions of the earth and moon are equal. This is borne out by calculations of the corresponding trajectories taking into account the moon's attraction, for $\alpha_1 = -\frac{\pi}{2}$; 0; $+\frac{\pi}{2}$ (see, for example, the trajectory in Figure D. 8 for $\alpha_1 = +\frac{\pi}{2}$).

* [Note that sgn $\alpha_1$ refers to a "sign," and not a "sine" (cf. p. 130 below).]

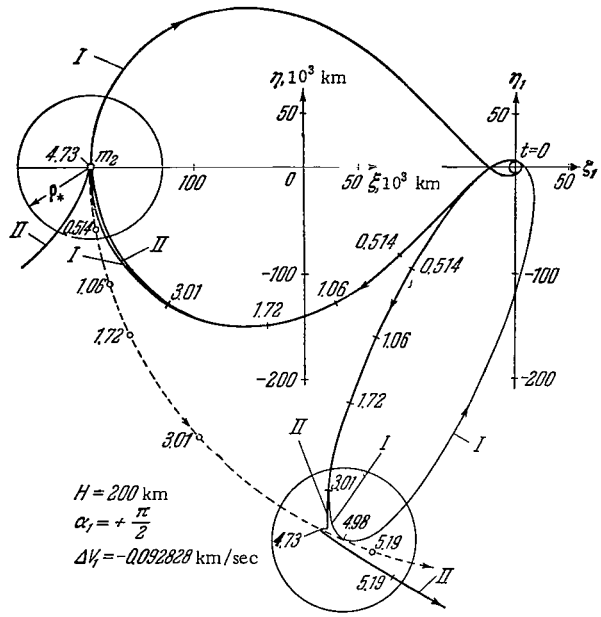


FIGURE D.7. Deviation of lunar trajectory *II* from corresponding ellipse *I* for minimum initial velocity. Obviously, the initial data for lunar impact can be calculated without taking into account the moon's effect.

In the cases portrayed in Figures D.7 and D.8, when the spacecraft and the moon go around the earth in the same direction prior to impact and when the moon's effect is especially marked, the trajectories taking into account the moon's effect (thick curves) still practically coincide with the trajectories (thin curves) for which the moon's effect prior to entry into the lunar sphere of action (circle of radius $\rho = \rho_*$) was not taken into account. For velocities higher than minimum, the effect of the lunar perturbations will be even less.

Now it is easy to explain why, in the $O\xi\eta$ system, a spacecraft with an initial velocity slightly higher than the first critical velocity $V_0^{(1)}$ (see §D.1) cannot, on its first circuit, ascend to libration point $L_1$, pass through the corridor at a very low velocity, and then reach the moon. Actually, the geocentric area constant $\sigma_к(L_1)$ corresponding to relative rest at point $L_1$ is at least 3.9 times greater than the initial area constant $\sigma_к(A_1)$,* so that the lunar perturbations cannot reduce this difference to zero during the course of a single circuit.

Let us determine the number of circuits required to get out to critical surface $s_1'$ (Figure D.1) for the first critical initial velocity. For the trajectory shown in Figure D.3, if the initial value of the area constant is $\sigma_к(A_1) = 71{,}300$ km$^2$/sec, then after six circuits the variation of the areal

* $\sigma_к(L_1) = \omega r_{L_1}^2 \approx 282{,}000$ km$^2$/sec; $|\sigma_к(A_1)| \approx r_1 V_0^{(1)} < 72{,}400$ km$^2$/sec.

velocity will amount to $\Delta\sigma_1 = 6810$ km$^2$/sec. Thus the following number of circuits should be necessary in order to reach the $s_1'$ curve:

$$\frac{\sigma_K(L_1) - \sigma_K(A_1)}{\Delta\sigma_1} \cdot 6 = \frac{282{,}000 - 71{,}300}{6810} \cdot 6 \approx 186,$$

that is, about 200 circuits.

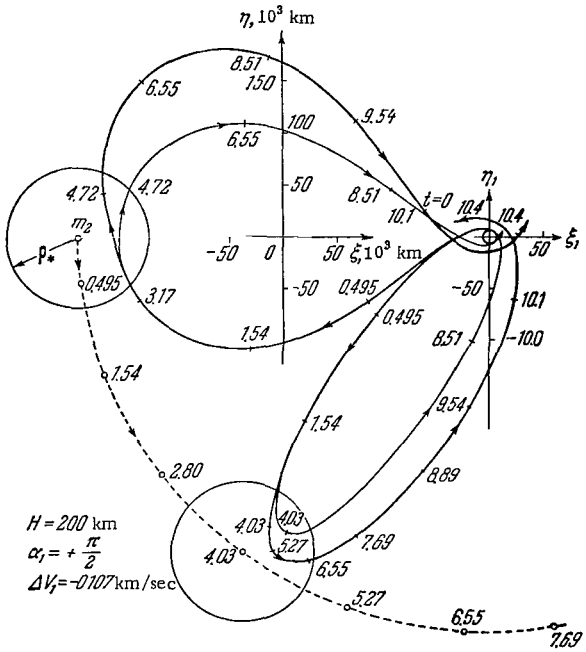


FIGURE D. 8. Lunar perturbation of ellipse reaching point where attractions of earth and moon are equal.

It should be noted that the difference between the geocentric energy of a spacecraft at relative rest at point $L_1$ and the geocentric energy of a spacecraft having a critical initial velocity $V_0^{(1)}$ will be negligible in comparison with its initial kinetic energy, which is equal to $\frac{1}{2}[V_0^{(1)}]^2$. Therefore, for initial spacecraft velocities close to $V_0^{(1)}$, the perturbing effect of the moon mainly shows up as a variation of the geocentric areal velocity $\sigma_1$.

## D. 4. IMPOSSIBILITY OF LUNAR CAPTURE OF SPACECRAFT LAUNCHED FROM EARTH

In the calculations of trajectories for minimum initial velocities, no trajectories were found which corresponded to capture of the spacecraft by the moon. The results of Hopf /27/ can be used to show that all the

spacecraft trajectories in phase space, for which it is impossible to say that capture cannot take place, have Lebesgue measures equal to zero. In order to solve moon-flight problems it is important to know whether there is even one trajectory which corresponds to capture. Really good initial data for such a trajectory, provided one exists, are impossible to obtain with any accuracy. However, by obtaining fairly close data, it should be possible to find trajectories which execute as many circuits around the moon as could be desired before leaving it. This will obviously be of interest in connection with designing artificial lunar satellites which do not need engines.

It is clear, however, that capture by the moon of a spacecraft arriving from the earth is impossible on the first circuit of the trajectory, no matter what the initial data. That this is the case can be confirmed using a technique of Fesenkov /24/, in which Jacobi integral (1.3) is expressed in geocentric elements $a_1$, $p_1$, and $i_1$ before capture of the spacecraft by the moon and in selenocentric elements $a_2$, $p_2$, and $i_2$ after capture; in this calculation the constant $h$ is excluded and the inconsistency of the result is established.

This inconsistency follows directly from the characteristics of the initial data for trajectories originating near the earth and coming close to the moon on the first circuit /24/. Here, we assume, as did Fesenkov, that capture takes place if, beginning at a certain moment, the trajectory does not leave the sphere within which the attraction of the moon is stronger than that of the earth. The radius of this sphere is $\rho_0 \approx \left(\frac{m_2}{m_1}\right)^{1/2} a \approx 42{,}700$ km. If the moon's sphere of action ($\rho = \rho_* = \left(\frac{m_2}{m_1}\right)^{2/5} a = 66{,}000$ km) is used instead of this sphere, the result is the same. The same conclusion can also be drawn for smaller ratios $m_2 : m_1$ of the attracting masses, provided the initial distance of body $m_0$ from body $m_1$ is small enough in comparison with the distance $m_1 m_2$.

Therefore, a spacecraft launched from the earth to enter the moon's sphere of action on the first circuit must then leave this sphere. This means that it is impossible to produce a permanent lunar satellite on the first circuit without using the spacecraft engines. If the spacecraft approaches the moon along an **arbitrary** trajectory, however, the impossibility of lunar capture cannot be proven. The impossibility of capture for arbitrary trajectories in the restricted circular three-body problem can be proven only when the ratio of the attracting masses is quite small (much smaller than the ratio of the moon's mass to the earth's mass) /22/.

Regardless of whether capture is possible or not, a temporary lunar satellite can in principle be put into orbit without using the spacecraft engines. Actually, if the initial flight speed is greater than the first critical velocity but is less than the second critical velocity (that is, if $h_1 < h < h_2$), then according to §D.1 the spacecraft may go to the moon through the corridor near libration point $L_1$ (Figure D.1) rather than go off into infinity. Finally, according to §D.2, it must first make a sufficient number of circuits around the earth. The corridor can be made as narrow as desired if the initial velocity is reduced sufficiently. Therefore, the spacecraft can apparently be made to move around the moon as long as desired before it returns through the corridor.

The actual creation of such an artificial lunar satellite, however, would hardly be possible, for the following reasons. First, the difference between the first and second critical velocities is less than 1 m/sec, so that it is difficult to achieve a flight speed between them. Second, the spacecraft may fall back to earth before it reaches the corridor. Third, solar perturbations (which were neglected) can easily cause $h$ to have a value which is not in the range $h_1 < h < h_2$, so that the corridor becomes closed or the spacecraft escapes into infinity.

## D.5. AN APPROXIMATE METHOD FOR STUDYING TRAJECTORIES

Let us define approach trajectories as trajectories beginning near the earth (body $m_1$) and entering into the sphere of action of the moon (body $m_2$) on the first circuit around the earth [cf. definition on p. 7].

An approach trajectory entering the moon's sphere of action must leave this sphere. Consequently, the motion along an approach trajectory can be divided into three parts: motion up to the sphere of action, motion within the sphere of action, and motion away from the sphere of action.

As noted in §§ D.2 and D.3, the lunar perturbation of the geocentric motion up to the moon's sphere of action is practically negligible. The same will be true of the motion away from the sphere of action. Moreover, the earth will perturb the selenocentric motion inside the moon's sphere of action just as little (this follows from the definition of the sphere of action). Therefore, in all cases these perturbations can be neglected in comparison with the attraction of the central body.

Consequently, neglecting perturbations, we find that the parts of the trajectory outside the sphere of action (referred to the geocentric system $m_1\xi_1\eta_1\zeta_1$) are conic sections with foci at $m_1$. Analogously, the part of the trajectory inside the moon's sphere of action (referred to the selenocentric system $m_2\xi_2\eta_2\zeta_2$) is a conic section with a focus at $m_2$ (see Figure D.9, which portrays motion in the lunar orbital plane).

The portion of the trajectory from the initial point of the passive part to the point of entry into the moon's sphere of action may be an ellipse, a hyperbola, or a parabola, depending on the initial geocentric velocity. Obviously, for an elliptic velocity greater than the minimum, the spacecraft can enter the sphere of action either on the ascending branch of the geocentric trajectory or on the descending branch. For hyperbolic or parabolic velocities, on the other hand, entry is possible only on the ascending branch.

The motion up to the sphere of action is calculated in terms of the geocentric initial data: $r_1$, $\lambda_1$, $V_1$, and $\alpha_1$. At the point of entry the geocentric coordinates and velocity $V_2$ (the geocentric entry data) are converted into selenocentric entry data (Figure D.9, selenocentric system $m_2\xi_2\eta_2\zeta_2$).

The part of the approach trajectory located inside the moon's sphere of action will always be a hyperbola, when expressed in selenocentric coordinates. At the boundary of the sphere of action the selenocentric velocity $V_2'$ is more than twice the parabolic velocity $V_p' = \sqrt{2\frac{fm_2}{\rho_*}} \approx 0.383$ km/sec at this boundary.

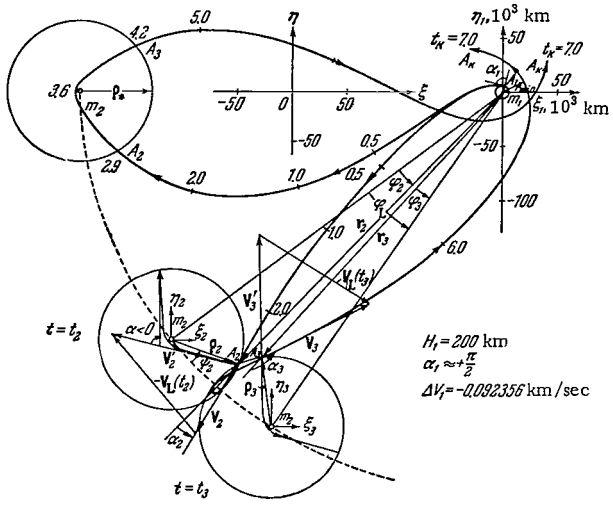


FIGURE D.9. Rough calculation of trajectory for motion: outside moon's sphere of action, neglecting lunar perturbations; inside sphere of action, neglecting earth's perturbations. Inside sphere of action selenocentric motion is along hyperbola.

The above fact is explained by the impossibility of lunar capture of a spacecraft traveling on an approach trajectory. In addition, the following should be noted: since the selenocentric velocity is always hyperbolic, the spacecraft will traverse the region around the boundary of the moon's sphere of action very rapidly. Thus, even though the perturbations amount to about 0.7 of the attraction of the central body, still they cannot exert any appreciable effect on the approach trajectory.

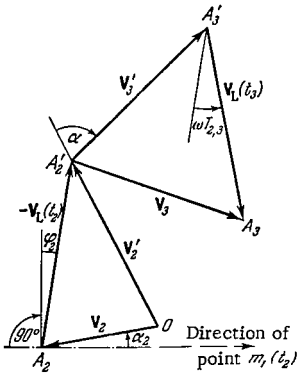


FIGURE D.10. Vector diagram of velocities at points where trajectory intersects moon's sphere of action.

The motion inside the moon's sphere of action is determined from the selenocentric integrals of the energy and areas. At the point of exit from the sphere of action, the selenocentric coordinates and the exit velocity $V_3'$ (the selenocentric exit data) are converted (Figure D.9) into geocentric exit data.

After the spacecraft leaves the moon's sphere of action, the motion is calculated from the geocentric integrals of the energy and the areas, but with new values of the constants. This motion may be either ascending or descending, relative to the earth.

Using the trajectory in Figure D.9 as an example, let us construct the vector diagram of the entry and exit velocities. The direction of the geocentric radius at the moment $t_2$ of exit from the sphere of action is taken as the horizontal direction (Figure D.10). From some point $O$ we draw the vector $V_2$ of the geocentric entry velocity, which forms an angle $\alpha_2$ with the geocentric entry radius. Next, from the end of

$\mathbf{V}_2$, we draw the vector $-\mathbf{V}_{L}(t_2)$, which forms an angle $\varphi_2$ with the vertical (equal to the angle between the entry radius and the earth-moon line). The vector sum $\mathbf{V}_2 = \mathbf{V}_2 - \mathbf{V}_{L}(t_2)$ is then the vector of the selenocentric entry velocity.

Since the selenocentric motion takes place along a conic section, we know that $|\mathbf{V}_3'| = |\mathbf{V}_2'|$. Let us define $\alpha$ as the angle by which the direction of selenocentric motion changes due to the moon's influence, during the time the spacecraft stays in the lunar sphere of action. From the end of vector $\mathbf{V}_2'$, we draw the vector $\mathbf{V}_3'$, which forms the angle $\alpha$ with $\mathbf{V}_2'$. Finally, from the end of $\mathbf{V}_3'$ we draw the vector $+\mathbf{V}_{L}(t_3)$, which forms an angle $\omega(t_3 - t_2) = \omega T_{2,3}$ with vector $\mathbf{V}_{L}(t_2)$. The vector sum $\mathbf{V}_3 = \mathbf{V}_3' + \mathbf{V}_{L}(t_3)$ is the vector of the geocentric exit velocity.

## D.6. ANALYSIS OF APPROACH TRAJECTORIES

Using the technique outlined in §D.5, any approach trajectory can be calculated and plotted. It will be of interest here to analyze, even if only roughly, all the various motions which are possible along an approach trajectory. In this analysis the characteristics of the set of possible approach trajectories, at the beginning and end of each successive phase of the motion, will be considered. At the same time, the corresponding velocities will be drawn in on the vector diagram.

The part of the motion up to the moon's sphere of action is determined by the initial data. In the calculations the initial height will be assumed to be 200 km. However, the results will also be valid for initial heights twice, or even several times, as great as this (for example, for the height of an orbiting space station), since the changes in initial height are small in comparison with the initial geocentric radius. The angle $\alpha_1$ between the initial velocity and this radius will vary over a range from $-90$ to $+90°$, and the amount $\Delta V_1$ by which the initial velocity $V_1$ exceeds the local parabolic velocity $V_p(r_1)$ will be the basic variable parameter.

The various possible values of the geocentric entry data $r_2$, $V_2$, and $\alpha_2$ [at the boundary of the moon's sphere of action] were considered above (see Chapter I). For initial velocities not close to minimum, the change in the magnitude and direction of the geocentric entry velocity within the range

$$|r_2 - a| < \rho, \tag{6.1}$$

turns out to be small. For such initial velocities it can be assumed, as a good approximation, that for specified $V_1$ and $\alpha_1$ the magnitude and direction of the geocentric entry velocity do not depend on the position of the point of entry into the moon's sphere of action, that is, on the trajectory. They will have certain average values:

$$V_2(r_2) \equiv V_2(a) \text{ and } \alpha_2(r_2) \equiv \alpha_2(a). \tag{6.2}$$

Here and in the following, only approach trajectories in the lunar orbital plane will be considered. The initial velocity $V_1$ and the angle $\alpha_1$ between it and the initial geocentric radius are assumed to be given. Moreover, the approach trajectory is assumed to vary only because of

the change in the angle $\lambda$ between the initial radius and the earth-moon line. Then, for initial velocities not close to minimum, vector $\mathbf{V}_2$ on the diagrams in Figures D.10 and D.11 will (according to (6.2)) be one and the same for all the trajectories considered.

The flight times $T_{1,2}(V_1)$ up to the moon's orbit are very close for vertical and horizontal directions of the initial velocity (Figure 1.6). This fact, together with the sharpness of the variations in Figures 1.1 and 1.6 (curves for velocities close to minimum), accounts for the elongation of the conic sections corresponding to motion up to the moon's sphere of action along the approach trajectories (the eccentricity of these sections is close to unity).

When the rise in initial velocity is great enough, the curves for

$$V_2(V_1),\ \alpha_2(V_1) \text{ and } T_{1,2}(V_1)$$

approach, respectively, the asymptotes of

$$V_2 = V_1,\quad \alpha_2 = \arcsin\frac{r_1 \sin\alpha_1}{r_2},\quad T_{1,2} = 0, \tag{6.3}$$

where $r_1$ and $r_2$ are the initial and entry radii. The asymptotic nature of these curves is already evident for initial velocities only 0.5 km/sec above parabolic (Figures 1.1 and 1.6).

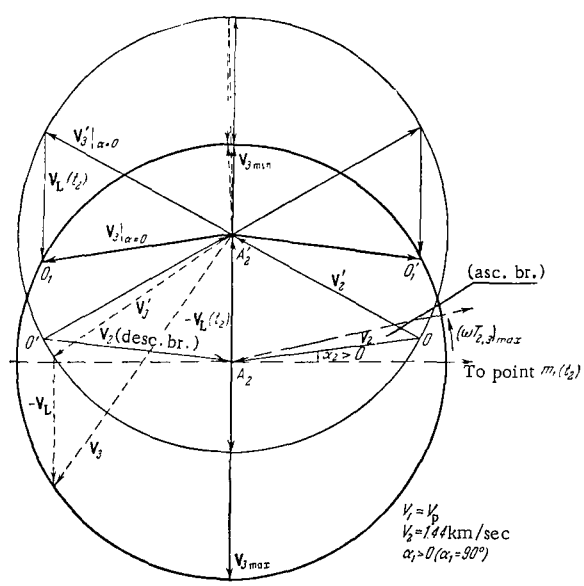


FIGURE D.11. Vector diagram of exit velocities. Upper circle shows selenocentric velocities, lower circle geocentric velocities. Motion after lunar approach (moon considered to be material point) possible in all directions. Velocities $V_3'|_{\alpha=0}$ and $V_3|_{\alpha=0}$ correspond to trivial solution.

As pointed out in Chapter I, the selenocentric entry data are determined by the geocentric data. Thus the small angle $\varphi_2$ between the geocentric radii of the moon and the entry point (Figures D. 9 and D. 10) need not be taken into account in the following calculations. When this angle is neglected, the vector of the moon's velocity at the moment $t_2$ of entry into the lunar sphere of action will be orthogonal to the entry radius. The magnitude and direction of the selenocentric entry velocity $\mathbf{V}_2'$ on the vector diagram turn out to be the same for all the trajectories considered (Figure D. 11), so that the first parts of the selenocentric trajectories in the sphere of action are parallel (Figure 1.2).

Let us characterize the entry point in terms of the angle $\psi_2$ between its selenocentric radius vector and the direction of the moon's velocity (Figure D. 9). Then, as the angle $\lambda$ varies, entry will be possible over a range of $\psi_2$ close to 180°. The curves for half of this range go clockwise around the lunar center (Figure 1.2b), while the curves for the other half go counterclockwise (Figure 1.2a).

For two-dimensional approach trajectories the region around $|\psi_2| = 180°$ will be a forbidden zone on the moon's sphere of action. Entry into the sphere will be impossible in this zone, no matter what the initial data are. This means that a spacecraft cannot enter the sphere of action by overtaking the moon in its orbital motion.

Let us recall that the selenocentric entry and exit velocities are equal in magnitude. This magnitude $U$ is a monotonically increasing function of the initial velocity (Figure 1.1). For arbitrary values of the initial velocities, it should be noted, the selenocentric velocity at the boundary of the moon's sphere of action is greater than the geocentric entry velocity (that is, $U(V_1) > V_2(V_1)$ (Figure 1.1)).

Since the trajectories considered all have the same entry velocity, the angle $\alpha$ between the selenocentric entry and exit velocities is determined only by the distance $d$ from the moon's center to the line of action of the selenocentric entry velocity. Let us give this distance the sign of the angle $\alpha$, that is, the same sign as the motion around the moon.

It will be of interest to find the variation in the velocities and trajectories in the moon's sphere of action as $\lambda$ (the angle between the initial geocentric radius and the earth-moon line) varies, that is, as the part of the motion up to the sphere of action turns as a whole around the earth's center. Let us assume that the ascending trajectory first is tangent to the sphere of action, and goes around it in a counterclockwise direction (Figure 1.2a). Then,

$$d = \rho_*, \quad \alpha = 0 \text{ and } \mathbf{V}_3'|_{\alpha=0} = \mathbf{V}_2'$$

(Figure D. 11). As $\lambda$ increases, the trajectory will approach the moon more and more, the distance $d$ will be reduced, and the angle $\alpha$ will increase, that is, the vector $\mathbf{V}_3'$ will rotate counterclockwise. When $d$ becomes equal to zero, $\alpha$ will reach 180° and the impact will be at the lunar center (Figure 1.2a). As $\lambda$ increases further, $d$ becomes less than zero and the angle $\alpha$ jumps to $-180°$, since the direction of motion around the lunar center changes (Figure 1.2b). However, the point of exit from the sphere of action and the end of the exit-velocity vector $\mathbf{V}_3'$ will move continuously around the corresponding circle, everywhere in a counterclockwise direction. When the vector $\mathbf{V}_3'$ completes an entire circle, it will happen again that $\alpha = 0$ and $\mathbf{V}_{3\,\alpha=0} = \mathbf{V}_2'$ (Figure D. 11), so that approach is impossible. The solutions with $\mathbf{V}_3|_{\alpha=0} = \mathbf{V}_2'$ may be considered trivial.

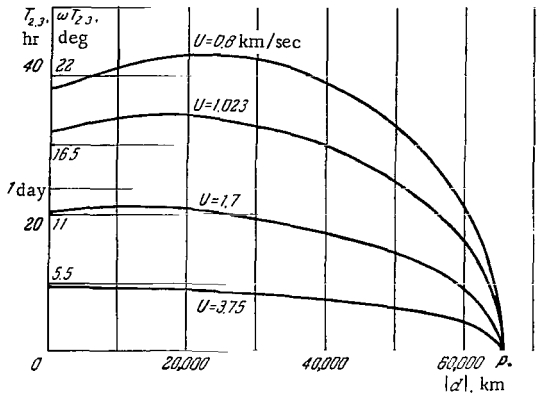


FIGURE D. 12. Flight time in moon's sphere of action. Considerably rapid reduction of flight time with increase in selenocentric velocity $U$.

For low values of $d$, it is easy to show that the distance $\rho_{min}$ of the trajectories from the moon's center is a small quantity of the order of $d^2$, for any selenocentric velocities at the boundary of the sphere of action. This is an important factor, with respect to ensuring impact on the moon (see §D. 7). Moreover, for low $d$ the trajectories in the sphere of action bend so sharply that they have an appearance similar to the angle formed by the corresponding velocities $\mathbf{V}_2'$ and $\mathbf{V}_3'$ on the vector diagram (Figure D. 11).

The flight time $T_{2,3} = t_3 - t_2$ inside the sphere of action is shown in Figure D. 12, as a function of the distance $|d|$ for several values of the selenocentric velocity $U$ at the limit of the sphere of action. The longest flight times correspond to $d = \frac{\rho_* V_p'}{U\sqrt{2}}$, where $V_p'$ is the selenocentric parabolic velocity at the boundary of the sphere of action. However, the maxima on the flight-time curves are very gradual, so that for distances $|d|$ which are not close to the radius of the moon's sphere of action $T_{2,3}$ can be taken as constant and a function of $U$ only.

Finally, let us consider the geocentric exit data. Without analyzing these data in detail, let us just plot the geocentric exit velocities $\mathbf{V}_3(d)$ on the vector diagram. These velocities are obtained from the corresponding selenocentric velocities $\mathbf{V}_3'(d)$ by adding on the lunar-velocity vector $\mathbf{V}_L(t_3)$, which turns relative to the vector $\mathbf{V}_L(t_2)$ through the small angle $\omega(t_3 - t_2) < (\omega T_{2,3})_{max}$ between the directions of the earth-moon line at the moments of entry and exit (Figure D. 11). It can be shown that this angle need not be taken into account in the present analysis, so it will be neglected. Then the geometric locus of the ends of the vectors of the geocentric exit velocities $\mathbf{V}_3(d)$, which are drawn from point $A_2'$, will be a circle of radius $U$, but with its center at $A_2$ (lower circle in Figure D. 11). Consequently, the vector diagram of the exit velocities is extremely simple.

Now let us consider approach along the descending branches for the same initial data $r_1$, $V_1$, and $\alpha_1$, assuming that the initial velocities $V_1$ are elliptic. Making the same assumptions as for the ascending branches, we obtain the vectors $\overline{O'A_2} = \mathbf{V}_2$ and $\overline{O'A_2'} = \mathbf{V}_2'$ (Figure D. 11), which are, as in the previous case, symmetrical with respect to line $A_2A_2'$. A vector $\mathbf{V}_3'$

for the ascending branches (having an angle $-\alpha$) which is symmetrical with respect to line $A_2A_2'$ will correspond to any vector $\mathbf{V}_3'$ having an angle $\alpha$. Therefore, the vector diagram for the velocities will be simply symmetrical to the diagram for the ascending branches, and the circles described by the ends of the $\mathbf{V}_3$ vectors will coincide. As a result, the two vector diagrams can be studied simultaneously.

In both cases Figure D.11 shows that the maximum geocentric exit velocity is $V_{3\,max} = U + V_L$ (where $U$ is the magnitude of the selenocentric velocity and $V_L$ is the moon's velocity), while the minimum velocity is $V_{3\,min} = U - V_L$. For $U > V_L$ the geocentric exit velocities $\mathbf{V}_3$ can be in any direction, regardless of the magnitude and direction of the initial velocity. The quantity $U$ decreases monotonically with an increase in the angle $\alpha_1$ between the initial velocity and the initial geocentric radius. Consequently, a vector diagram constructed for $\alpha_1 = 90°$ will be somewhat smaller than a diagram for $\alpha_1 = -90°$, whereas for intermediate angles all the characteristics of the vector diagram will be intermediate.

Let us follow the evolution of the velocity diagram as the initial velocity $V_1$ varies, beginning at high values of $\Delta V_1$, the amount by which the initial velocity exceeds local parabolic. For hyperbolic velocities approach will clearly be possible only along the ascending branch. For $\Delta V_1 = 0.5$ km/sec, we have (Figure 1.1): $|\alpha_2^{\pm}| = 3°$, $V_2 = 3.64$ km/sec, $U^+ = 3.73$ km/sec, and $U^- = 3.83$ km/sec, where the plus sign refers to $\alpha_1 = +90°$ and the minus sign to $\alpha_1 = -90°$. Since $U^+$ and $U^-$ do not differ much, the velocity diagrams for different values of $\alpha_1$ will be practically identical, All the geocentric exit velocities are definitely hyperbolic.

With a reduction in initial velocity all the velocities on the vector diagram in Figure D.11 will decrease, and the minimum geocentric exit velocities rapidly become elliptic, although the entry velocities remain hyperbolic. This first occurs for $\Delta V_1 = 0.149$ km/sec when $\alpha_1 = +90°$. With a further decrease in initial velocity, elliptic exit velocities also appear for negative values of $\alpha_1$. When $\alpha_1 = -90°$ they only appear for $\Delta V_1 = 0.114$ km/sec.

As the initial velocity $V_1$ passes through the parabolic value, approach becomes possible on the descending branch. For $V_1 = V_p$ we have (Figure D.11):

$$V_2 = 1.44 \text{ km/sec}, \quad |\alpha_2^{\pm}| = 7.5°$$
$$U^+ = 1.65 \text{ km/sec}, \quad U^- = 1.87 \text{ km/sec}.$$

On the velocity diagram the region of elliptic geocentric exit velocities takes up about one third of the corresponding circle (Figure D.11). For $\alpha_1 = \pm 90°$ the maximum velocities are

$$V_{3\,max}^+ = 2.67 \text{ km/sec}, \quad V_{3\,max}^- = 2.9 \text{ km/sec}$$

and the minimum velocities are

$$V_{3\,min}^+ = 0.63 \text{ km/sec}, \quad V_{3\,min}^- = 0.85 \text{ km/sec}.$$

Finally, as the initial velocity for $\alpha_1 = +90°$ is decreased, the selenocentric entry velocity is reduced until it equals the moon's velocity (1.023 km/sec); then the geocentric exit velocity will be zero (Figure D.13). Thus we have:

$$V_{3\min} = 0, \quad V_{3\max} = 2V_L \approx 2.05 \text{ km/sec},$$
$$V_2 \approx 0.6 \text{ km/sec}, \quad \alpha_2^+ \approx 18.4^\circ$$

In Figure D.13 the sector of practically realizable selenocentric exit velocities (between the dashed lines) is greater than 180°. The corresponding value of $\Delta V_1$ is $\Delta V_{1*} \approx -0.077$ km/sec.

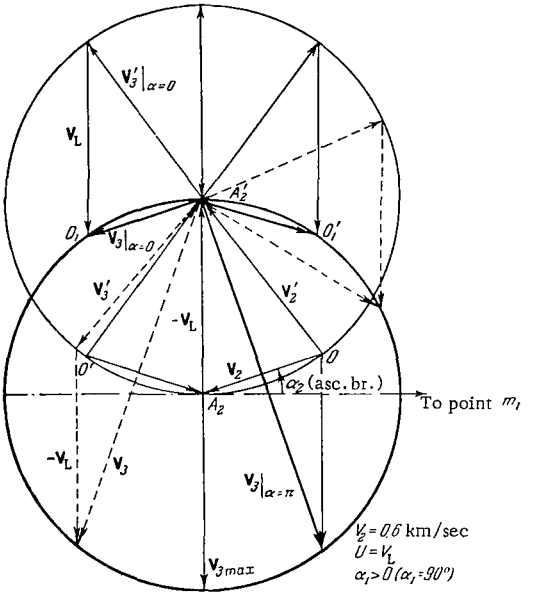


FIGURE D.13. Vector diagram of exit velocities for case when selenocentric entry velocity $V_2'$ equals lunar velocity $V_L$. Motion outside lunar sphere of action (moon considered to be material point) possible only on one side of direction of geocentric exit radius $m_1 A_2$.

As is evident from Figure 1.1, the corresponding vector $V_2$ of the geocentric entry velocity can no longer be considered constant for a variation of the entry point. However, for $\Delta V_1 > \Delta V_{1*}$ the variation of this velocity, as well as the variation of the selenocentric entry velocity $V_2'$, need not be taken into account. For $\Delta V_1 < \Delta V_{1*}$, it is not difficult to show that trajectories with $\alpha_1 = \pm 90°$ cannot reach distances $d$ close to $-\rho_*$, and so the angles $\alpha < 0$ will not be small enough. A special forbidden zone exists on the vector diagram of the exit velocities. Consequently, a special analysis is required, but it will not be carried out here.

As $V_1$ is reduced, this forbidden zone spreads, until it covers the entire diagram, except for the vector $V_3|_{\alpha=0}$, corresponding to a trivial solution $V_3|_{\alpha=0} = \overline{A_2'O_1'}$ for the descending branches; (cf. Figures D.11 and D.13). For $U < V_L$ motion is possible only on one side of the geocentric exit radius $r_3$, and not on both sides, as previously (Figure D.13).

For initial velocities close to minimum, the geocentric entry velocities $V_2$ are low, so that motion takes place almost as if the moon's sphere of action were "flying toward" a spacecraft at rest in space.

The analysis of the motion following exit from the moon's sphere of action is similar to that for the motion preceding lunar approach, so it need not be carried out here.

## D.7. TWO-DIMENSIONAL PROBLEM OF LUNAR IMPACT

For the two-dimensional lunar-impact problem, it is not necessary to know the nature of the trajectory after lunar approach, so that the trajectory classification is very simple. The following initial data are assumed to be known: geocentric radius $r_1$, spacecraft velocity $V_1$, and angle $\alpha_1$ between initial velocity and initial geocentric radius. The angle $\lambda$ between the latter radius and the $\xi$ axis (Figure D.6) is selected from the condition of lunar impact.

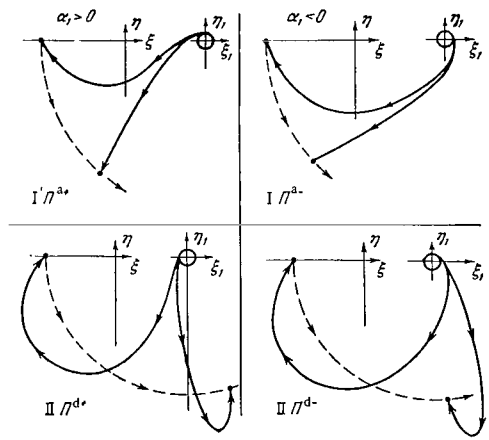


FIGURE D.14. Types of impact trajectories: *I* corresponds to impact on ascending branch of trajectory; *II* corresponds to impact on descending branch.

For elliptic initial velocities, approach of the spacecraft to the moon will be possible on both the ascending (a) and descending (d) branches of the trajectory. Accordingly, there are two types of lunar impact: type $\Pi^a$ and type $\Pi^d$. The extreme trajectories of each of these types (that is, the trajectories corresponding to angles $\alpha_1 = +\frac{\pi}{2}$ and $\alpha_1 = -\frac{\pi}{2}$) are shown schematically in Figure D.14. According to the direction the spacecraft flies around the earth (that is, according to the sign of $\alpha_1$), each type can be divided into two subtypes:

type $\Pi^a$ into subtypes $\Pi^{a+}$ and $\Pi^{a-}$,
type $\Pi^d$ into subtypes $\Pi^{d+}$ and $\Pi^{d-}$.

The trajectory separating the two types is purely radial relative to the earth. As $\alpha_1$ varies monotonically from $-\frac{\pi}{2}$ to $+\frac{\pi}{2}$, the trajectory varies monotonically within one type, from one trajectory extreme to the other.

Let us consider how the trajectories change as the initial velocity is reduced. For hyperbolic initial velocities, all the trajectories will obviously be of type $\Pi^a$. When the initial velocity is reduced to parabolic, descending branches also appear and there are trajectories of type $\Pi^d$ for all values of angle $\alpha_1$. With a decrease in initial velocity, trajectories of the two types which correspond to the same value of $\alpha_1$ will approach one another. Finally, as the initial velocity goes through a minimum $V_{1\min}(\alpha_1)$, the corresponding trajectories of each type merge and disappear. The trajectories corresponding to $\alpha_1 = \frac{\pi}{2}$ disappear first, so that for $\alpha_1 = \frac{\pi}{2}$ impact at the lunar center becomes impossible, although there are some angles $\alpha_1 < \frac{\pi}{2}$ for which it can still occur.

The value of $\lambda$ corresponding to impact can be found approximately from formula (3.3), without taking the moon's effect into account (see §D.3). First the formulas of conic-section theory are used to find the angle $\Phi$ between the geocentric radii of the initial point and the impact point, and also the flight time $T_{1,2}$ between these points. Functions $\Phi(V_1)$, $\lambda^+(V_1)$, $\lambda^0(V_1)$, and $\lambda^-(V_1)$ are plotted in Figure D.15, and the function $T_{1,2}(V_1)$ is plotted in Figure 1.6. All these curves were calculated for type $\Pi^a$ trajectories and for an initial height of 200 km. The function $\Phi(V_1)$ corresponds to $\alpha_1 = +\frac{\pi}{2}$, and the functions $\lambda^+(V_1)$, $\lambda^0(V_1)$ and $\lambda^-(V_1)$ correspond, respectively, to $\alpha_1 = +\frac{\pi}{2}$, 0, and $-\frac{\pi}{2}$. When the amount by which the initial velocity exceeds local parabolic is $\Delta V_1 = 0.5$ km/sec, the curves are already quite close to the asymptotes.

Trajectories of type $\Pi^a$ corresponding to an initial height of 200 km, an angle $\alpha_1 = +\frac{\pi}{2}$, and the previously calculated (Figure D.15) approximate values of $\lambda^+(V_1)$ were computed taking into account the lunar attraction. For this, numerical integration of equations (2.2) was carried out. The deviation $\rho_{\min}$ of the trajectory from the lunar center, as a result of not taking the lunar attraction into account when determining $\lambda$, was found to diminish very rapidly as the initial velocity was increased above the minimum. If the miss $\rho_{\min}$ for the minimum initial velocities is some tens of kilometers, then for initial velocities close to parabolic the quantity $\rho_{\min}$ will be less than a kilometer.

An accuracy of some tens of kilometers would be sufficient to give an idea of the impact trajectories themselves. However, in order to assess the effect of the initial-data scatter, the accuracy of an impact at the moon's center should be of the order of a kilometer.

Trajectories hitting the center of the moon can be calculated as accurately as desired, using the iteration method for $\rho_{\min} = 0$ with $\lambda$ as the variable. In this case the convergence will be of a higher order if we take as a function not $\rho_{\min}$ with the sign of the direction of flight around the moon, but rather the quantity $\sqrt{\rho_{\min}}$ with this same sign. Figure D.16 shows

the results for trajectories of type $\Pi^a$, with $\alpha_1 = +\frac{\pi}{2}$ and taking the moon's effect into account. An $O\xi\eta$ coordinate system is used, which rotates along with the moonward direction (numbers along curves indicate flight time $T_{1,2}$ in days). The curves showing $T_{1,2}$, $\Phi$, and $\lambda$ as functions of the initial velocity for these trajectories turn out to be practically the same as the curves in Figures 1.6 and D.15, in which the lunar mass was taken as zero.

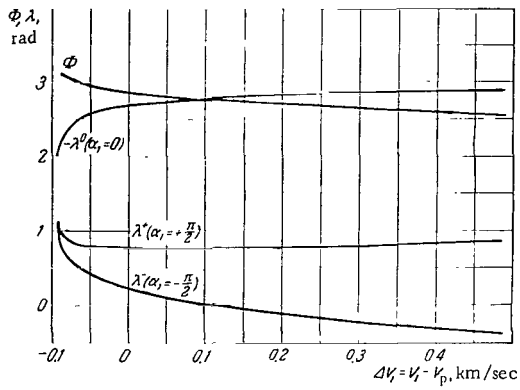


FIGURE D.15. Angle $\lambda$ between initial geocentric radius and earth-moon line (guaranteed lunar impact), as function of amount initial velocity exceeds local parabolic, for both vertical ($\alpha_1 = 0$) and horizontal ($|\alpha_1| = \frac{\pi}{2}$) launches. $\Phi$ is total angular range.

Now let us decide what accuracy is required for the initial data. If we neglect the lunar effect while determining the effect of small errors in the initial data, the miss-distance $\rho_{min}$ will be a linear function of the errors. However, if we take the moon's effect within its sphere of action into account, then the quantity $d$ (the distance from the lunar center to the line of action of the selenocentric entry velocity) will be a linear function of the errors. Moreover, according to §D.6, for small values of $d$ the quantity $\rho_{min}$ is proportional to $d^2$. Therefore, when the lunar effect is taken into account, the miss-distance turns out to be a quadratic function of the errors. This means that it is much easier to achieve a lunar impact of sufficient accuracy than to hit some nonattractive point moving in the same manner as the moon.

It is rather tedious to determine the miss-distances $\rho_{min} = \rho_{V_1}, \rho_{\alpha_1}, \ldots$, corresponding to errors $\delta V_1, \delta\alpha_1, \ldots$, using an approximate method (that is, taking the moon's effect into account only within its sphere of action). It is easier and more accurate to determine the deviations $\rho_{min}$ by calculating directly the trajectories close to the trajectory giving a sufficiently accurate impact at the lunar center (nominal trajectory).

By varying one of the nominal initial data $x_i$ by a small amount $\delta_{x_i}$ and computing the corresponding trajectory, we can find its distance from the lunar center $\rho_i \approx k_i(\delta x_i)^2$. The curves for $k_{\alpha_1}(\Delta V_1)$ and $k_{V_1}(\Delta V_1)$ are shown in Figure D.17. The function $k_{\alpha_1}(\Delta V_1)$ increases monotonically, while $k_{V_1}(\Delta V_1)$ decreases monotonically, passing through zero. Accordingly, the maximum

allowable error $|\delta\alpha_1|_{\rho_L}$ in the direction (that is, the error corresponding to a miss-distance $\rho_{min}$ equal to the lunar radius $\rho_L$, all the other initial data being assumed accurate) is a monotonically decreasing function of the initial velocity $V_1$. The maximum allowable error $|\delta V_1|_{\rho_L}$ in the initial velocity, however, goes through a definite maximum for $V_1$ (Figure D. 18). The curve for $k_{V_1}(\Delta V_1)$ passes through zero because, for the corresponding initial velocity at $\alpha_1 = +\frac{\pi}{2}$, the shift of the impact point due to the change in trajectory curvature is compensated by the shift of the moon due to the change in flight time up to the impact point.

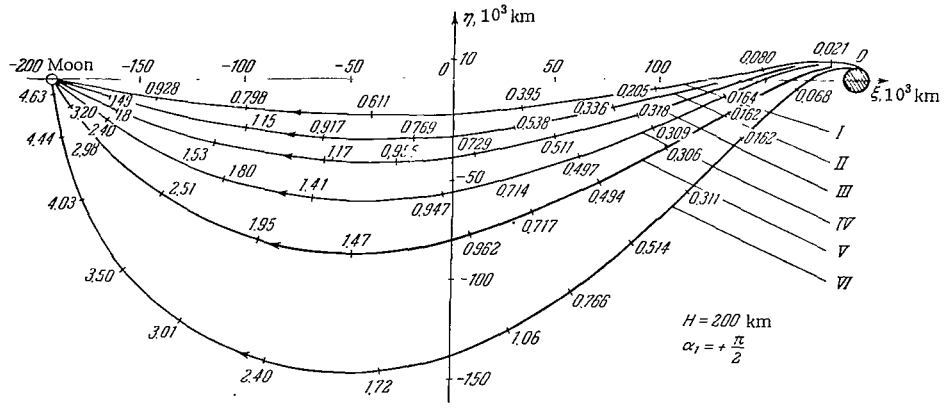


| | $\Delta V_1, \frac{km}{sec}$ | $T_{1,2}$, days | | $\Delta V_1, \frac{km}{sec}$ | $T_{1,2}$, days |
|---|---|---|---|---|---|
| I | +0.48251 | 1.08386 | IV | −0.057828 | 2.64816 |
| II | +0.106094 | 1.62688 | V | −0.082828 | 3.33284 |
| III | 0 | 2.06981 | VI | −0.092828 | 4.73092 |

FIGURE D. 16. Ascending impact trajectories in rotating coordinates.

The maximum value of function $|\delta V_1|_{\rho_L}$ (Figure D. 18) can be found approximately using the formula $|\delta V_1|_{\rho_L} = \sqrt[4]{\frac{\rho_L}{k_4}}$, which follows from the relation $\rho_{min} = k_{V_1}(\delta V_1)^2 + k_4(\delta V_1)^4 + \ldots$ for $k_{V_1} = 0$ (the value of this maximum is shown roughly in Figure D. 18).

From Figure D. 18 we see that, for example for velocities close to parabolic, $|\delta\alpha_1|_{\rho_L} \approx 0.3°$, while $|\delta V_1|_{\rho_L} \approx 50$ m/sec. The optimum initial velocity obviously depends on the ratio of obtainable accuracies. It is also evident that the effect of the scatter $\delta V_1$ is especially marked for velocities close to minimum. Figure D. 19 shows how much an error $\delta V_1 = \pm 2$ m/sec can vary the spacecraft trajectory for initial velocities close to minimum.

For $\alpha_1 = -\frac{\pi}{2}$ the shifts of the trajectory and moon for errors in initial velocity are additive, instead of compensating one another. Thus the maximum allowable errors $|\delta V_1|_{\rho_L}$ for $\alpha_1 = -\frac{\pi}{2}$ will be considerably lower than those for $\alpha_1 = +\frac{\pi}{2}$.

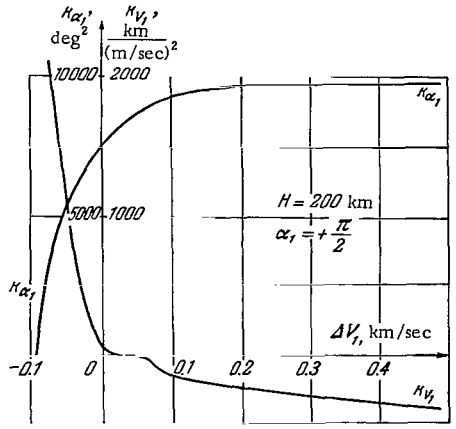


FIGURE D.17. Coefficients determining deviation of trajectory from lunar center.

The effect of the errors $\delta r_1$ turned out to be practically negligible. For example, for $\delta r_1 = 50$ km, when the initial velocity exceeded parabolic by the following amounts: $\Delta V_1 = V_1 - V_p = -0.092828$ km/sec, 0, and +0.106094 km/sec, the miss-distances were, respectively, $\rho_r = 56$ km, 43 km, and 140 km.

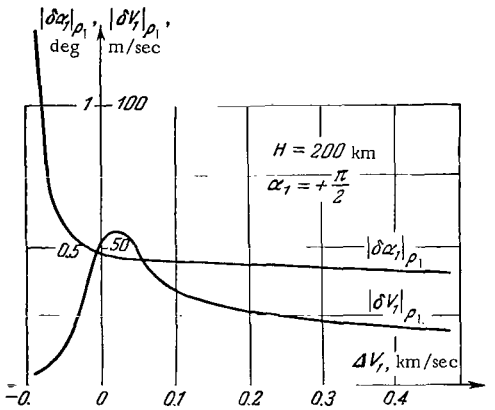


FIGURE D.18. Error corresponding to deviation of trajectory out to lunar limb. Optimum initial velocity depends on attainable accuracies.

Errors $\delta\lambda$ are mainly related to errors in the launch time. The maximum allowable errors in $\lambda$ are of the order of one degree, so that the launch time must be specified to within about a minute.

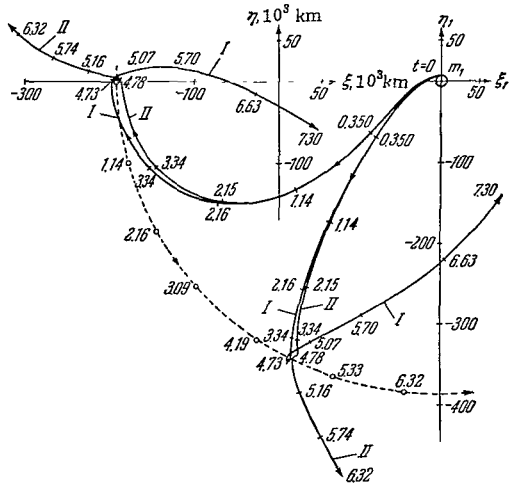


FIGURE D. 19. Change in nature of impact trajectory, for errors in initial velocity close to minimum value. For $H_1 = 200$ km, $\alpha_1 = 75°$, and $\Delta V_1 = -0.0919$ km/sec, impact takes place. For errors $\delta V_1 = \pm 2$ m/sec there is no impact; plus sign corresponds to trajectory *I*, and minus sign to trajectory *II*.

Now let us evaluate the errors $\delta\zeta$ in the coordinate and $\delta\dot{\zeta}$ in the velocity along the normal $\zeta$ to the lunar orbital plane. It can be shown that these errors lead, respectively, to deviations characterized by impact ranges $|d| \approx \frac{a|\zeta|}{r_1}$ and $|d| < \frac{a\dot{\zeta}}{4V_1}$, where $a$ is the mean distance between the centers of the earth and moon. For $V_1 \approx V_p$, we have $U^+ \approx 1.65$ km/sec, and from Figure 1.4 we obtain the allowable values $|d| < 3000$ km. From these calculations it is clear that, in any event, impact will still take place for $\delta\zeta < 50$ km or $\delta\dot{\zeta} < 50$ m/sec.

Consequently, the allowable errors for perturbation of only one of the initial data will be: about 50 m/sec for the velocity; about 0.5° for the direction; about 50 km for the position of the initial point; and about a minute for the launch time. It can be shown that the order of the simultaneously allowable errors is approximately the same.

The range of allowable errors remains the same even when solar perturbations and other factors not taken into account in equations (2.2) are considered. Actually, these perturbing factors are minor and their terms have small parameters (in equations (2.2) they were taken as zero) in the accurate equations of motion. It is easy to show that the derivatives of the solutions for the initial data, in terms of which the required accuracies are determined in the given case, will depend continuously on the small parameters. Thus these derivatives and the required accuracies will be about the same as when the small parameters are assumed to be zero.

The effect of initial-data scatter for lunar approach along the descending branch of a trajectory is from 2 to 5 times greater than for approach along the ascending branch.

To sum up, the above results indicate that the effect of initial-data scatter on actual lunar-impact trajectories is comparatively small, so that impact is possible without carrying out midcourse corrections during the passive part of the flight.

## D.8. TWO-DIMENSIONAL PROBLEM OF CIRCUMLUNAR FLIGHT

As early as Hohmann /28/ the possibility of a quite distant circumlunar flight was discussed. More recently, circumlunar flight along symmetrical trajectories was considered in /29, 30/. However, it is of interest to analyze all the possible two-dimensional trajectories for close circumlunar flight (that is, all the circumlunar approach trajectories), and also to ascertain the initial-data accuracies required in order to execute these trajectories. In order to obtain the circumlunar approach trajectories, let us solve a somewhat more general problem, namely to find the approach trajectories which return to some specified region on the earth (such as a sphere with a radius $r_k \ll a$, where $a$ is the mean distance between the centers of the earth and the moon). Let us call this problem the **problem of lunar approach with return.**

The set of two-dimensional solutions of the problem in question involves four parameters. The set of return trajectories tangent to a geocentric region of given radius $r_k \ll a$ involves three parameters. The set of symmetrical return trajectories involves two parameters. Using the principle of reversibility of motion /31/, it is easy to show that the symmetrical trajectories must intersect the earth-moon line (the symmetry axis) at right angles. Therefore, these trajectories are defined explicitly by the distance of this intersection point from the center of the moon and by the spacecraft velocity at this point. This fact was made use of in /7, 8/ for a numerical determination of the symmetrical trajectories.

Now let us analyze the problem as formulated above. Analogously to the case of lunar-impact missions, where trajectories passing through the moon's center were considered nominal, for lunar approach with return, trajectories passing through the earth's center are taken as nominal. The nominal trajectories will have zero geocentric area constants $\sigma_k$ in the region after exit from the moon's sphere of action.

The small angle $\varphi_3$ between the geocentric exit radius and the earth-moon line may be neglected (Figure D.9), since it turns out that taking this angle into account does not change the results significantly. Thus there are only two geocentric-exit-velocity vectors $V_3$, parallel to the line $A_2 m_1$ (Figures D.20 and D.22), which can correspond to the desired trajectories on the vector diagram in Figure D.11. One of these, $V_{3a}$, describes an ascending motion after lunar approach, and the other, $V_{3d}$, describes a descending motion (this irregardless of the motion prior to approach). Motion along an ascending trajectory, as opposed to descending motion, can be a solution of the problem only if $V_3 < V_p(a)$, where $V_p(a) = 1.44$ km/sec is the geocentric parabolic velocity of the spacecraft at a distance $a$ from the earth's center.

Assuming that the latter condition is true, let us first consider approach along the ascending branch, corresponding to a positive value of $\alpha_1$, the angle between the initial velocity and the initial geocentric radius. As Figure D.20 shows, the selenocentric exit velocities $V'_{3a}$ and $V'_{3d}$ form

angles $\alpha_a < 0$ and $\alpha_d < 0$ with the selenocentric entry velocity $V_2'$. Accordingly, the corresponding trajectories pass clockwise around the moon's center, and circumlunar flight takes place. Let us designate these trajectories as $C_a^{a+}$ and $C_d^{a+}$, respectively. Here the sign at the superscript indicates $\operatorname{sgn}\alpha_1$ (the sign of the initial areal velocity $\sigma_1$). The superscript itself indicates the type of trajectory branch before approach, and the subscript indicates the type after approach. The $C_d^{a+}$ trajectories pass much closer to the moon's center than the $C_a^{a+}$ trajectories, since $|\alpha_d| \gg |\alpha_a|$. The flight times prior to approach for both trajectory types will obviously be about the same as for lunar-impact trajectories corresponding to the same initial velocities. At the time of approach the geocentric areal velocity must vary from $\sigma_1$ to zero. The geocentric motion after approach will be purely radial. These trajectories are shown schematically in Figure D.21.

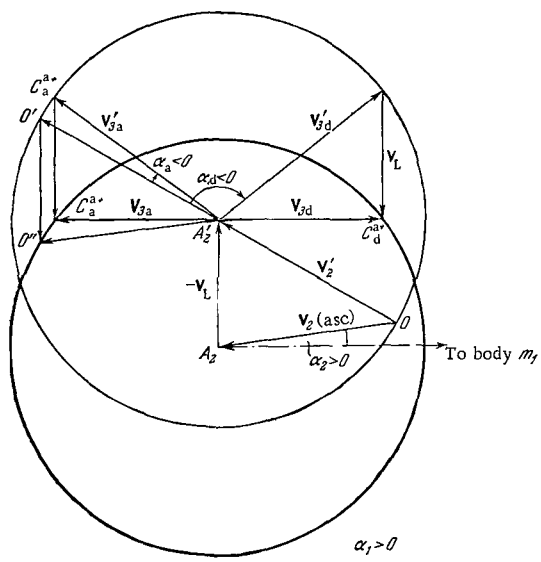


FIGURE D.20. Velocity-vector diagram for return of approach trajectory to earth's center (positive initial areal velocity).

When $\alpha_1 < 0$ (Figure D.22), the angle $\alpha_d$ is once again negative and corresponds to a type $C_d^{a-}$ flight (Figure D.21). However, in this case $\alpha_a > 0$, so that the trajectory goes around the moon's center in a counterclockwise sense, and circumlunar flight does not take place. Let us call such approach trajectories **flyby trajectories** and denote them by the letter $D$. The latter trajectory will thus be a $D_a^{a-}$ trajectory (Figure D.23).

Finally, let us consider approach along the descending branch of a trajectory. The corresponding vector diagrams for the velocities are, according to §D.6, symmetrical with respect to line $A_2A_2'$ for the diagrams shown in Figures D.20 and D.22. Just as in the preceding case, there are four solutions: trajectories $D_a^{d+}$ and $D_d^{d+}$ for $\alpha_1 > 0$ (Figure D.23), and

trajectories $D_a^{d-}$ (Figure D.23) and $C_d^{d-}$ (Figure D.21) for $\alpha_1 < 0$. An analysis of Figures D.20 through D.22 indicates that, in terms of what happens after approach, circumlunar trajectories (Figure D.21) can be divided into two types:

I. Close approach, for which the trajectory branch type changes to the opposite after approach (type $C_d^a$).

II. Weak approach, for which the trajectory branch type does not vary. This type, unlike type I, is divided into subtypes ($C_a^{a+}$ and $C_d^{d-}$), which do not change into one another for a continuous variation of $\alpha_1$ and for a given initial velocity.

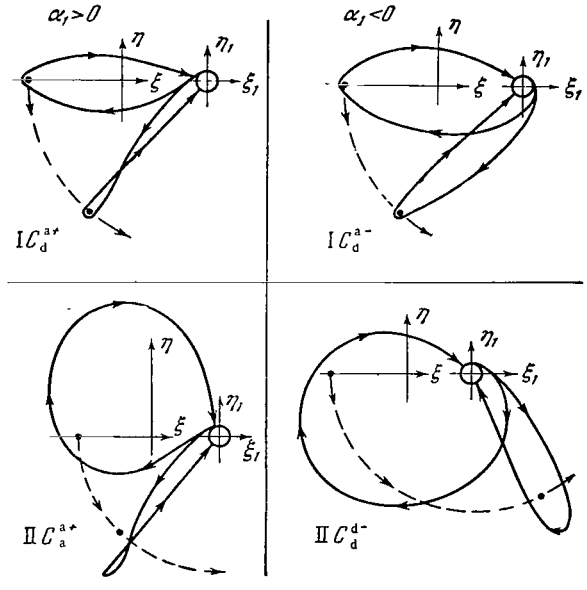


FIGURE D.21. Types of nominal circumlunar trajectories. Reduction of areal velocity to zero under influence of moon is evident.

Similarly, the flyby trajectories are also divided into two types: I. $D_a^d$; II. $D_a^{a-}$ and $D_d^{d+}$ (Figure D.23). As $\alpha_1 \to 0$, the nominal circumlunar and flyby trajectories of both types degenerate into trivial cases, that is, entry into the moon's sphere of action does not take place (lunar approach does not take place).

The above system of nominal circumlunar and flyby trajectories of approach is complete. This means that it comprises all the basic types of approach trajectories beginning near the earth's surface and returning toward the earth's center.

The nominal trajectories are found, just as in the case of lunar impact, using an iteration technique, with any one of the initial data serving as the variable for a value of the function $y = 0$. Here $y = \sqrt{r_{min}} \operatorname{sgn} \sigma_k$, where $r_{min}$ is the distance from the return branch of the trajectory to the earth's center. The circumlunar trajectories of all subtypes, and also some

of the flyby trajectories, were calculated using this method, with the aid of numerical integration; this provided a good check of the validity of the approximate method. The iterations were carried out with $\lambda$ as the variable for specified values of the initial data: $r_1 = 6571$ km, $\Delta V_1 = -0.07228$ km/sec, and $\alpha_1 = \pm \frac{\pi}{2}$, where $\Delta V_1$ is the amount by which the initial velocity exceeds local parabolic. The trajectory type $C_d^a$ corresponds to a flight time $T_{1,k} = 5$ to 10 days; type $D_a^d$ corresponds to $T_{1,k} = 15$ to 20 days; and the other types correspond to intermediate times.

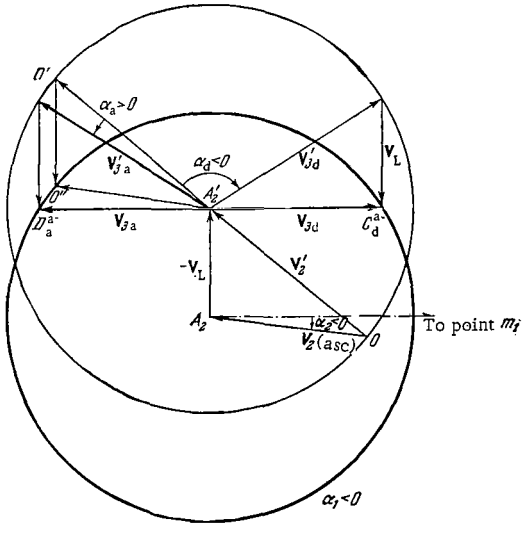


FIGURE D. 22. Velocity-vector diagram for trajectories of return to earth's center (negative initial areal velocity).

Now let us consider the evolution of the nominal trajectories as the initial velocity $V_1$ is reduced. For quite high initial velocities only trajectories of type $C_d^a$ are possible. For $\Delta V_1 = 0.017$ km/sec, $C_a^{a+}$ trajectories appear; for $\Delta V_1 < 0$ there are $D_d^{d+}$, $D_a^{d+}$, and $C_d^{d-}$ trajectories; and, finally, for $\Delta V_1 = -0.017$ km/sec, there are $D_a^{d-}$ and $D_a^{a-}$ trajectories. With a further reduction of the initial velocity, pairwise approach takes place, and then merging and disappearance of the trajectories: first the $C_d^{a+}$ and $C_a^{a+}$ trajectories disappear, then the $D_a^{d+}$ and $D_d^{d+}$ trajectories, and next the $C_d^{a-}$ and $C_d^{d-}$ trajectories. The last to disappear are the $D_a^{a-}$ and $D_a^{d-}$ trajectories. For lower initial velocities it is impossible to obtain a geocentric area constant $\sigma_k = 0$, although the trajectories can still reach the moon's sphere of action.

For all initial velocities, trajectories of the second types pass outside the lunar disk. For trajectories of the first types, this is only true for initial velocities close to minimum.

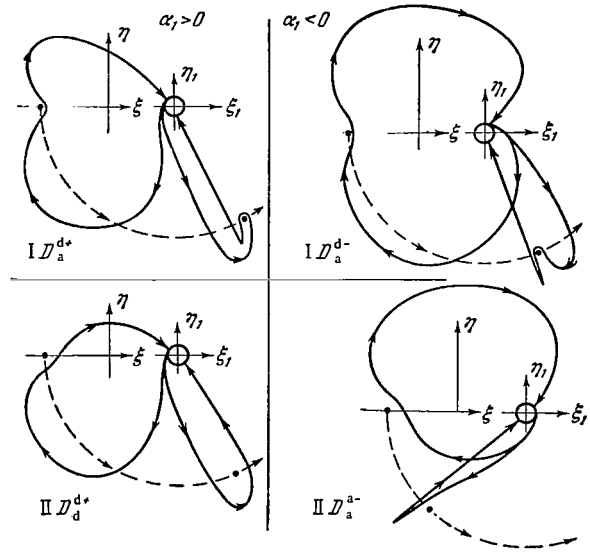


FIGURE D. 23. Types of nominal flyby trajectories. The similarity to types of circumlunar trajectories is evident (Figure D. 21).

Now let us consider the effect of initial-data scatter. For nominal trajectories, as opposed to others, the distance from the earth's center $r_{min}$ is a quadratic function of the small errors, rather than a linear function. Thus the nominal trajectories are more favorable than trajectories close to them, with respect to the required accuracy of the initial data.

Just as in the case of lunar impact, for a circumlunar flight the scatter of the following two quantitites has a determining effect: the initial velocity $V_1$ and the angle $\alpha_1$ between this velocity and the initial geocentric radius.

The effect of initial-data scatter in the given case depends on the distance $\rho_{min}$ of the trajectory from the moon's center, as well as on the nature of the trajectory transfer relative to the earth. As $\rho_{min}$ decreases, the effect of the errors increases rapidly. Therefore, for trajectories of type I it is more pronounced than for trajectories of type II, the errors in the direction of a reduction of $\rho_{min}$ having more effect than those in the direction of higher $\rho_{min}$. For example, for circumlunar flight along a $C_a^{a+}$ trajectory, for $\alpha_1 = +\frac{\pi}{2}$ and $\Delta V_1 = -0.07228$ km/sec we have $\rho_{min} = 12{,}900$ km. If the errors are $\delta V_1 = -1$ m/sec and $\delta\alpha_1 = -0.01$ rad, or else $\delta V_1 = +10$ m/sec and $\delta\alpha_1 = +0.1$ rad, the trajectories will still return to the earth. However, for errors of $\delta V_1 = -10$ m/sec and $\delta\alpha_1 = -0.1$ rad, the trajectories will either hit the moon or else go counterclockwise around it, so that circumlunar flight is impossible. Circumlunar flights much closer than this, with a return earthward, are hardly possible without making midcourse corrections during the passive part of the flight.

If the minimum distance of the trajectory from the moon is increased, the accuracy requirements will diminish rapidly. In the case of trivial trajectories corresponding to Hohmann-type circumlunar flights (when the spacecraft passes by the moon at a distance $\rho_{min} \approx \rho_*$, that is, at quite a large distance), the effect of initial-data scatter will be comparatively small. Thus, in order to return to the earth, the required accuracy of the initial data turns out to be no higher than that for a lunar impact with initial geocentric velocities which exceed local parabolic by the same amount.

## D.9. SPECIAL PROBLEM OF CIRCUMLUNAR FLIGHT

The special problem of circumlunar flight consists in finding trajectories along which the spacecraft returns to the earth's atmosphere on a gently sloping curve. Such flights are the most interesting, since they correspond to conditions of easiest atmospheric re-entry. For such circumlunar flights the minimum geocentric radius $r_{min}$ in the earth-return part of the trajectory will have to be equal to the radius $R$ of the upper layers of the atmosphere.

If the initial velocity $V_1 < V_p + 0.5$ km/sec, then for approach trajectories with $r_{min} = R$ at the point of exit from the moon's sphere of action it will be approximately true that $|V_{3\tau}| \approx \frac{R}{r_3} V_p$, where $V_{3\tau}$ is the component of the geocentric exit velocity $V_3$ normal to the exit radius $r_3$ (Figure D.9), and $V_p$ is the geocentric parabolic velocity for the height $R$. The above fact enables us, as in the preceding case, to find from the velocity-vector diagram all the trajectory types.

It turns out that to each pair of trajectory subtypes in the preceding problem there is an analogous pair of subtypes in the special problem. These trajectories go around the moon in the same sense as in the previous problem, but they go around the earth in the opposite sense. However, in the present case the trajectory types need not be divided into subtypes, since the trajectories vary continuously as the angle $\alpha_1$ (between the initial velocity and the initial geocentric radius) goes through zero. Consequently, these trajectories can be designated without any sign on the superscript: $C^a_{d+}$ and $C^a_{d-}$ for type-I circumlunar trajectories; $C^a_{a-}$ and $C^d_{d+}$ for type-II trajectories. Analogously, the flyby trajectories are designated as $D^d_{a+}$, $D^d_{a-}$, $D^a_{a+}$, and $D^d_{d-}$. The sign on the subscript indicates the sense of motion around the earth. When $\alpha_1 = \left|\frac{\pi}{2}\right|$, the second pair of trajectories may be considered trivial (they do not correspond to lunar approach). These trajectories are ellipses with foci at the earth's center; at perigee they are tangent to the upper layers of the atmosphere. For an average value of $\alpha_1 = 0$, the types of circumlunar trajectories are shown in Figure D.24. For simplicity, the geocentric areal velocity $\sigma_1$ at the beginning of flight is taken as zero, and the trajectories are assumed to begin radially. Then, the lunar perturbations will increase the areal velocity so much that the re-entry branch will be tangent to the upper layers of the atmosphere.

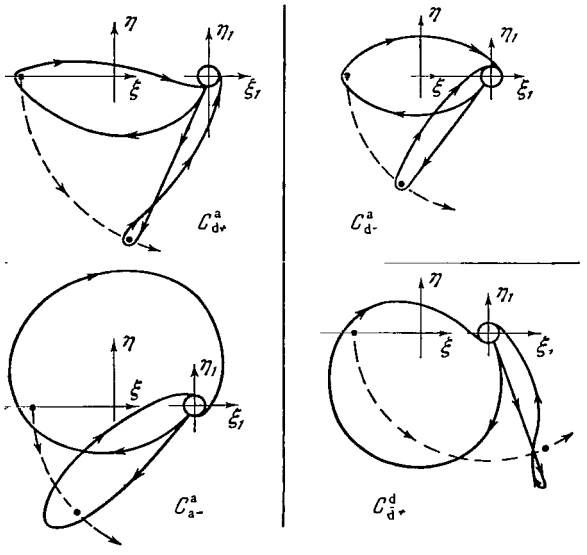


FIGURE D. 24. Types of trajectories ensuring gently sloping reentry into earth's atmosphere.

In this case the evolution of the trajectories with a variation in initial velocity is determined in the same way as for trajectories of the corresponding types in the preceding problem.

It should be noted that the shapes of all the approach trajectories which return earthward are intermediate between the shapes of the corresponding trajectories for the given problem having angles $\alpha_1 = +\frac{\pi}{2}$ and $\alpha_1 = -\frac{\pi}{2}$ and having the same initial radius and initial velocity. In addition, symmetrical trajectories of the problem of special return can only be trajectories of types $C^a_{d+}$, $D^d_{a+}$ (for $\alpha_1 = +\frac{\pi}{2}$) and $C^a_{d-}$, $D^d_{a-}$ (for $\alpha_1 = -\frac{\pi}{2}$), as is evident from Figure D. 24. By varying the initial radius and initial velocity independently, we obtain (according to §D. 8) the set of symmetrical approach trajectories (cf. /30/).

The method used to obtain the trajectories in the preceding problem is also applicable to this problem, provided the value $y = \pm\sqrt{R}$ is used for the iterations instead of the value $y = \sqrt{r_{min}} = 0$. However, the relative thinness of the atmosphere means that the accuracy of the initial data must be much higher than in the preceding problem.

For example, for symmetrical circumlunar flight, with $\Delta V_1 = -0.083773$ km/sec, $\alpha_1 = +\frac{\pi}{2}$, and a flight time of 823,600 sec, the distance from the moon to the closest point on the trajectory is $\rho_{min} = 27{,}000$ km. For a reentry trajectory, even such small errors in the initial data as $\delta V_1 = 0.2$ m/sec and $\delta\alpha_1 = 5 \cdot 10^{-3}$ rad will vary the perigee height by 160 and 190 km, respectively, that is, by an amount which is unacceptable (the variation in perigee cannot exceed some tens of kilometers).

The value of $\rho_{min}$ was relatively high in this example. When $\rho_{min}$ is reduced, then, just as in the preceding problem, there is a rapid increase in the effect of the errors. The initial data for circumlunar flights along approach trajectories ensuring a gently sloping re-entry into the earth's atmosphere must be extremely accurate. Consequently, the practical execution of such flights without making midcourse corrections during the passive part of the flight is not very feasible.

## D.10. TWO-DIMENSIONAL PROBLEM OF PERIODIC CIRCUMLUNAR FLIGHT

In this section we consider the possibility of launching a spacecraft into the lunar orbital plane in such a manner that it circles the moon periodically and then returns to the earth. While going around the moon, the spacecraft will transmit information regularly, for example, information concerning the other side of the moon. All periodic trajectories will not be of interest in this case, but only trajectories which pass near the moon. Obviously, the problem may be considered solved if we find all the two-dimensional periodic approach trajectories.

Let us agree to call a point close to the earth's center the initial and final point of the period. The desired trajectories will then be closed paths in an $O\xi\eta$ coordinate system rotating along with the earth-moon line (see Figure D.2), rather than in the geocentric $m_1\xi_1\eta_1$ system. Nevertheless, at the final point of the period, the final values of the geocentric parameters (velocity $V_f$, radius $r_f$, and angle $\alpha_f = \pm\frac{\pi}{2}$ between these) must be identical to the initial values $V_1$, $r_1$, and $\alpha_1$.

Taking this into account, and also applying the principle of reversibility of motion, it is clear that the desired trajectories have a symmetry axis in the $O\xi\eta$ and $m_1\xi_1\eta_1$ systems. Therefore, they are only comparable to the symmetrical trajectories of the preceding problem (that is, to trajectories of types $C^a_{d+}$ and $D^d_{a+}$ with $\alpha_1 = +\frac{\pi}{2}$ and types $C^a_{d-}$ and $D^d_{a-}$ with $\alpha_1 = -\frac{\pi}{2}$). Moreover, the periodic trajectories must belong to a single-parameter family (parameter $r_1$), and they begin at the $\xi$ axis (that is, they correspond to values of $\lambda = 0$ or $\lambda = \pi$, where $\lambda$ is the angle between the initial geocentric radius and the earth-moon line).

Let us define $\Phi_1$ as the angle between the geocentric radii of the initial point and the point closest to the moon. The condition that $\lambda$ for the initial point be identical to $\lambda$ for the final point in the $O\xi\eta$ system then reduces to the following condition, imposed upon the angular displacements of the spacecraft and the moon during the period $T_{1,k}$:

$$2\Phi_1 - \omega T_{1,k} = \pm 2k\pi \qquad (k = 0, 1, 2, \ldots). \tag{10.1}$$

Because of the smallness of the radius $\rho_*$ of the moon's sphere of action in comparison with the distance $a$, we can assume that $\Phi_1 \approx \Phi$, where $\Phi$ is the angle between the geocentric radii $r = r_1$ and $r = a$ of the conic section with which the passive part of the trajectory begins. Thus the previous equation becomes

$$2\Phi - \omega T_{1,k} = \pm 2k\pi \qquad (k = 0, 1, 2, \ldots). \tag{10.2}$$

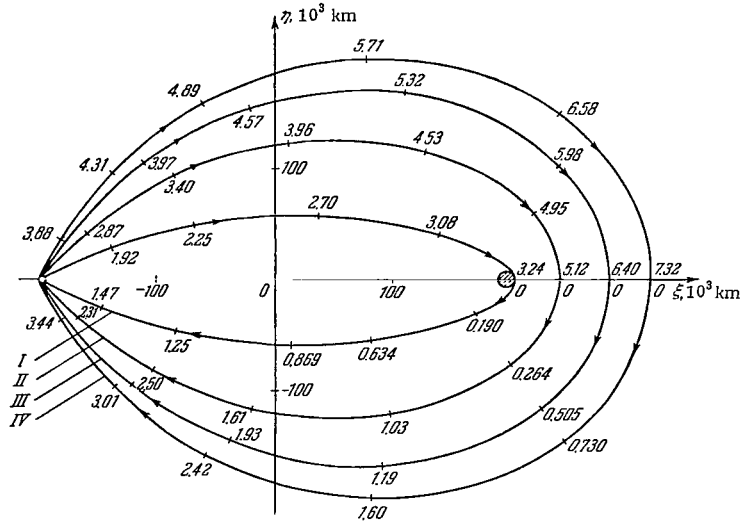


FIGURE D. 25. Trajectories for periodic flights around earth and moon. Trajectories passing over lunar surface are 94,800 km or more from earth.

| | $r_{min}$, km | $V_0$, $\frac{km}{sec}$ | $\rho_{min}$, km | | $r_{min}$, km | $V_0$, $\frac{km}{sec}$ | $\rho_{min}$, km | | $r_{min}$, km | $V_0$, $\frac{km}{sec}$ | $\rho_{min}$, km | | $r_{min}$, km | $V_0$, $\frac{km}{sec}$ | $\rho_{min}$, km |
|---|---|---|---|---|---|---|---|---|---|---|---|---|---|---|---|
| 1 | 6,571 | 11.1242 | 150 | II | 42,203 | 4.4008 | 825 | III | 82,824 | 3.1833 | 1,500 | IV | 116,371 | 2.7410 | 2,000 |

Condition (10.2) can be used to find all the periodic approach trajectories. It turns out that periodic circumlunar flight is not possible along a $C^a_{d+}$ trajectory, and also that there is only one family of periodic trajectories (corresponding to the condition $2\Phi - \omega T_{1,k} = -2\pi$) which is possible in the $C^a_{d-}$ group. The trajectories in this family go clockwise around the earth and moon (Figure D. 25), that is, they correspond to $\Phi < 0$; the numbers along the curves indicate the flight time in days.

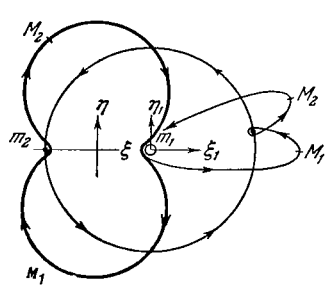


FIGURE D. 26. Simplest periodic flyby trajectory of subtype $D_+$ (sign indicates sense of motion around earth; $k = 0$, $\lambda = \pi$). Period somewhat longer than semimonthly.

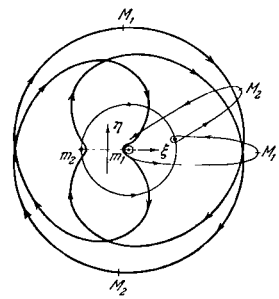


FIGURE D. 27. Periodic flyby trajectory of subtype $D_{1+}$ ($k = 1$, $\lambda = \pi$). Period somewhat longer than 1.5 months.

Periodic flyby trajectories of both types ($D^{d}_{a+}$ and $D^{d}_{a-}$) are possible. The $D^{d}_{a+}$ trajectories include two denumerable sets of families corresponding to the condition $2\Phi - \omega T_{1,k} = -2k\pi$ (one for $\lambda = \pi$ and $k \geqslant 0$ and one for $\lambda = 0$ and $k \geqslant 1$). The $D^{o}_{a-}$ trajectories, analogously, include two sets of families corresponding to $2\Phi - \omega T_{1,k} = -2l\pi$ (one for $\lambda = \pi$ and $l \geqslant 2$ and one for $\lambda = 0$ and $l \geqslant 3$).

The $D^{d}_{a+}$ trajectories go counterclockwise around the earth and moon and correspond to $\Phi > 0$. Accordingly, during a half period the moon executes somewhat more than 0.5, 1.5, ... $k + 0.5$, ... revolutions for the first denumerable set of families (with $\lambda = \pi$), and somewhat more than 1, 2, ... $k$, ... revolutions for the second denumerable set (with $\lambda = 0$). The trajectories of this type with $\lambda = \pi$ for $k = 0$ and 1 are shown schematically in Figures D.26 and D.27, and those with $\lambda = 0$ for $k = 1$ are shown in Figure D.28. The letters $M_1$ and $M_2$ denote the trajectory points furthest from the earth, in both the rotating and nonrotating coordinate systems.

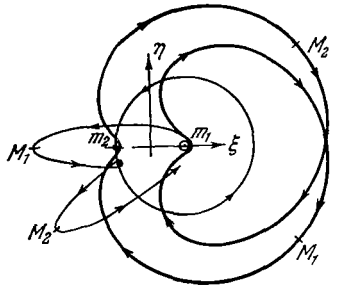


FIGURE D. 28. Periodic flyby trajectory of subtype $D'_{1+}$ ($k = 1$, $\lambda = 0$). Period somewhat longer than a month.

Type $D^{d}_{a-}$ trajectories go clockwise around the earth and counterclockwise around the moon, and they correspond to $\Phi < 0$. Accordingly, during a half period the moon executes somewhat less than 0.5, 1.5, ..., ..., $l - 2 + \frac{1}{2}$, ... revolutions for a denumerable set of families with $\lambda = \pi$, and somewhat less than 1, 2, ... $l - 2$, ... revolutions for a denumerable set with $\lambda = 0$. The trajectories with $\lambda = \pi$ for $l = 2$ and 3 are shown schematically in Figures D.29 and D.30; Figure D.31 shows the trajectories with $\lambda = 0$ for $l = 3$.

If we set $l = k + 2$, it is possible to establish a one-to-one correspondence between $D^{d}_{a+}$ and $D^{d}_{a-}$ trajectories having the same values of $\lambda$. Then it is easy to see that as parameter $r_1$ decreases to zero the corresponding trajectories will be identical. These limit trajectories for $\lambda = \pi$ and $k = 0$ and 1 ($l = 2$ and 3) are shown in Figures D.32. and D.33, while those for $\lambda = 0$ and $k = 1$ ($l = 3$) are shown in Figure D.34. The limit trajectories correspond to lunar angular displacements during a half period, with accuracies of 0.5, 1.5, ... $k + \frac{1}{2}$, ... and 1, 2, 3, ... $k$, ... revolutions, respectively.

Therefore, there are actually only two denumerable sets of families of periodic flyby trajectories (corresponding to $\lambda = 0$ and $\lambda = \pi$), rather than four. Let us denote the family corresponding to $k = 0$ and $\lambda = \pi$ by the letter $D$, and the families corresponding to $\lambda = \pi$ and $\lambda = 0$ (for $k > 0$) by the letters $D_k$ and $D_k$, respectively. These designations also apply to the legends of Figures D.26 through D.34.

It is of interest to compare the above results with those of Strömgren and the Copenhagen school /26/, obtained for equal masses of the attracting bodies ($m_1 = m_2$). Our circumlunar family of trajectories (type $C$) corresponds to Strömgren's type "$m$" trajectory, and our type $D$ and $D_k$ trajectories are denoted by Strömgren as type "$c$". The $D'_k$ families of trajectories have

no counterpart in Strömgren's study. Conversely, he discusses periodic orbits (type "$k$", found by Lowes /26/) which have no counterpart in our study, at any rate not as approach trajectories for $m_1 = m_2$. The system of families $C$, $D$, $D_k$, $D_k$ of periodic approach trajectories are, due to the way they were obtained, a complete system for the earth-moon mass ratio ($\frac{m_1}{m_2} = 81.45$). Consequently, for $m_1 = m_2$ there can exist periodic solutions which disappear when the mass ratio $m_1/m_2$ is increased to 81.45.

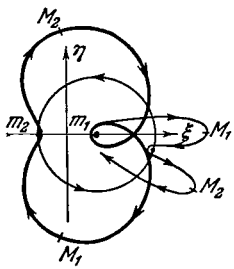


FIGURE D. 29. Simplest periodic flyby trajectory of subtype $D_-$ (goes around earth in negative sense, $l = 2$ and $\lambda = \pi$ ). Period somewhat less than a month.

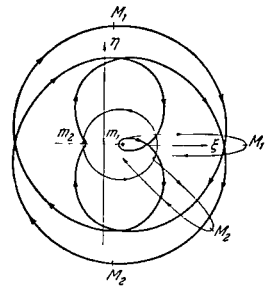


FIGURE D.30. Periodic flyby trajectory of subtype $D_{1-}$ ($l = 3$, $\lambda = \pi$). Period somewhat less than 1.5 months.

It should be noted that the $D_k$ and $D_k$ trajectories are not the simplest trajectories (that is, trajectories which complete not more than one revolution per period in the $O\xi\eta$ system). In the three-body problem involving the earth, the moon, and a spacecraft, only families $C$ and $D$ are families of the simplest periodic lunar-approach trajectories.

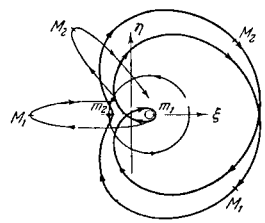


FIGURE D.31. Periodic flyby trajectory of subtype $D_{1-}$ ($l = 3$, $\lambda = 0$). Period somewhat less than a month.

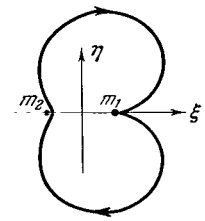


FIGURE D.32. Simplest periodic flyby trajectory (earth return) of type $D$, divided into subtypes $D_+$ and $D_-$ (Figures D.26 and D.29). Period of 0.5 month.

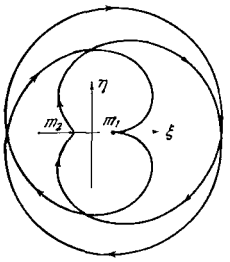


FIGURE D.33. Periodic flyby trajectory (earth return) of type $D_1$, divided into subtypes $D_{1+}$ and $D_{1-}$ (Figures D.27 and D.30). Period of 1.5 months.

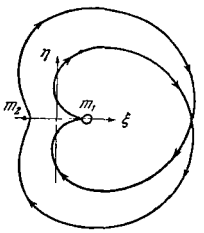


FIGURE D.34. Periodic flyby trajectory (earth return) of type $D_1'$, divided into subtypes $D_{1+}'$ and $D_{1-}'$ (Figures D.28 and D.31). Period of 1 month.

Let us consider family $C$ to be the only family of circumlunar trajectories. It turns out that the type-$C$ trajectories which are tangent to the atmosphere pass inside the moon (Figure D.25), while the trajectories passing over the lunar surface are more than 94,800 km from the earth's center. All the trajectories (Figure D.25) were found by a method similar to that used by Strömgren; the $O\xi\eta$ coordinate system was used, with $V_0$ as the spacecraft velocity at the initial point of the period in this system. These trajectories were found to be unstable. For example, a trajectory with a distance from the earth's center $r_{min} = 82{,}800$ km and a distance from the moon's center $\rho_{min} = 1500$ km will go off into infinity on the fourth revolution, for an error $\delta V_0 = 0.001$ m/sec (Figure D.35). Thus, a periodic circumlunar flight coming close to the moon is not practicable.

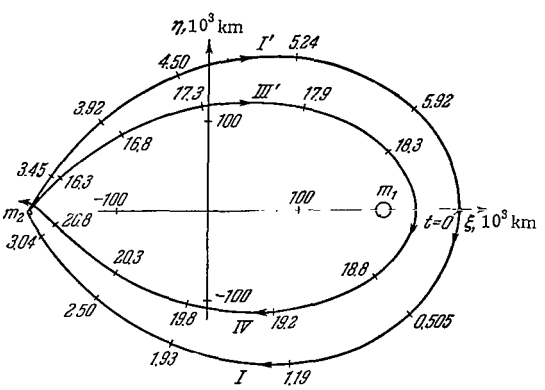


FIGURE D.35. Escape into infinity from nearly periodic orbit. Revolutions $II$ and $III$ situated between those shown. $H_1 = 76{,}253$ km, $\alpha_1 = -\frac{\pi}{2}$, $\Delta V_0 = 0.085058$ km/sec, $\delta V_0 < 0.001$ m/sec, $I - I'$ is first revolution, $III'$ is final part of revolution $III$, $IV$ is fourth revolution.

If $h < h_2$ in the Jacobi integral (1.3) for a periodic trajectory, then according to §D.1 the trajectory will not go off into infinity. However, in order for the trajectory to pass from the earth to the moon, we must have $h > h_1$. For approach trajectories, periodic ones included, §D.3 shows that $h > h_2$. Consequently, periodic trajectories satisfying the condition $h_1 < h < h_2$, if they exist, must pass quite far from the earth. Since the difference $h_2 - h_1$ is very small, such trajectories, even provided they do exist, cannot be important in practice. This is because the initial-data scatter inevitably makes it difficult to remain in the range $h_1 < h < h_2$, and also because the perturbations of the sun, etc., which were not taken into account, can easily cause $h$ to lie outside the range $h_1 < h < h_2$.

## D.11. TWO-DIMENSIONAL PROBLEM OF ACCELERATION OR BRAKING USING PERTURBING ACTION OF MOON

Let us consider the maximum acceleration which can be imparted to a spacecraft by the perturbing action of the moon, without using the engines /32/. It is clear from the velocity-vector diagram (see Figure D.11) that the maximum geocentric exit velocity after approach is $U_{3\max} = U + V_L$, where $U$ is the magnitude of the selenocentric exit velocity and $V_L$ is the moon's velocity. However, it can be shown that the corresponding approach trajectory will intersect the lunar surface, no matter what the initial data.

A practically feasible trajectory corresponding to the maximum acceleration $\Delta V_{2,3} = V_3 - V_2$ (where $V_2$ is the geocentric entry velocity) must pass near the surface of the moon. Such a trajectory will go around the moon clockwise if the approach is along the descending branch (type $\tilde{C}^d$) and counterclockwise if the approach is along the ascending branch (type $\tilde{D}^a$). Type-$\tilde{D}^a$ trjaectories correspond to the larger of the dashed $V_3$ vectors in Figures D.11 and D.13. To find the acceleration trajectories, iterations are carried out for the function $y = \pm\sqrt{\rho_{min}}$ (sign indicates sense of circumlunar motion). The value $+\sqrt{\rho_L}$ is used for the $\tilde{D}^a$ trajectories and the value $-\sqrt{\rho_L}$ for the $\tilde{C}^d$ trajectories. Here $\rho_{min}$ is the distance of the trajectory from the moon's center, and $\rho_L = 1736$ km is the radius of the moon. The limit trajectories of each type were found (that is, the trajectories with $\alpha_1 = +\frac{\pi}{2}$ and the trajectories with $\alpha_1 = -\frac{\pi}{2}$). These are shown schematically in Figure D.36, in both geocentric $(\xi_1, \eta_1)$ and rotating $(\xi, \eta)$ coordinates. Each type can be divided into two subtypes, according to the sign of $\alpha_1$ (that is, according to the sense of motion around the earth):

type $\tilde{D}^a$ is divided into $\tilde{D}^{a+}$ and $\tilde{D}^{a-}$,

type $\tilde{C}^d$ is divided into $\tilde{C}^{d+}$ and $\tilde{C}^{d-}$.

The acceleration trajectories go around the moon in such a way that exit from the moon's sphere of action is in a direction as close as possible to the direction of the lunar velocity.

The geocentric exit velocity $V_3$ after acceleration will always be hyperbolic, irregardless of the initial velocity $V_1$, so that the spacecraft will go off into infinity after approaching the moon. However, the amount of acceleration $\Delta V_{2,3}$ depends on $V_1$; it is a maximum (about 1.5 km/sec) for values of $V_1$ close to minimum, and it decreases monotonically as $V_1$ is

increased (down to zero as $V_1 \to \infty$). It is possible to obtain maximum velocities in the lunar orbital plane having any direction, thanks to the monthly rotation of the moon. Thus, since this plane makes small angles with the orbital planes of the planets, the acceleration without fuel expenditure can be utilized for interplanetary flight.

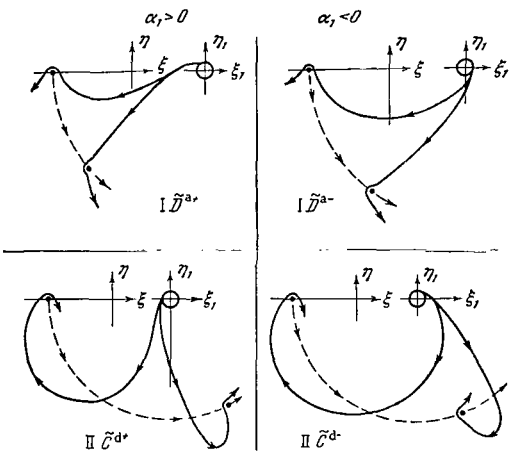


FIGURE D.36. Types of maximum-acceleration trajectories using perturbing action of moon. Similarity to types of impact trajectories (Figure D.14) is evident.

The effect which the initial-data scatter has on the acceleration trajectories turns out to be more pronounced than the effect on the impact trajectories, since the miss-distance $\delta\rho_{min}$ is a linear function of the errors rather than a quadratic function. For example, for acceleration along a $\tilde{D}^{a+}$ trajectory with an initial velocity which is 0.0723 km/sec less than parabolic and an angle $\alpha_1 = 90°$, errors of $\delta V_1 = 1$ m/sec and $\delta\alpha_1 = 1°$ will cause, respectively, changes $(\delta\rho_{min})_V = 120$ km and $(\delta\rho_{min})_\alpha = 100$ km.

Because there is a danger of collision with the moon due to errors in the initial data, the computed trajectory must lie somewhat above the lunar surface. However, such an elevated trajectory will be associated with a reduced gain in velocity. Thus it is hardly possible to obtain values of $\Delta V_{2,3}$ sufficiently close to the maximum without making trajectory corrections prior to lunar approach.

Trajectories with $\alpha_1 = +\frac{\pi}{2}$ are more suitable than other acceleration trajectories. This is because they make it possible to use the component of the earth's diurnal velocity in the lunar orbital plane during liftoff (just as did the trajectories in the previous problems corresponding to $\alpha_1 = +\frac{\pi}{2}$).

Because of the reversibility of motion, once the problem has been solved for any acceleration, $t$ can be replaced by $-t$ to give the solution for a like braking using the perturbing action of the moon, the motion in this case being along a trajectory which is the mirror image (relative to the $\xi$ axis) of the acceleration trajectory. The optimum braking trajectory will then be

obtained from the most suitable acceleration trajectory, since along such a trajectory the spacecraft utilizes the earth's diurnal rotation during re-entry to reduce the re-entry velocity relative to the earth's surface. Trajectories giving maximum braking may be used, for example, when a spacecraft returns from an interplanetary flight.

As the velocity-vector diagram in Figure D.11 shows, trajectories along which there is a greater or lesser retardation of the spacecraft motion (relative to the earth) may exist, in addition to impact and earth-return trajectories of lunar approach and trajectories for which the spacecraft is accelerated as a result of the approach. Consequently, the vector diagram makes possible a comprehensive classification of all the two-dimensional approach trajectories.

Certain geocentric exit velocities will correspond to the retardation trajectories in Figure D.11. These velocities form angles with the velocity $-\mathbf{v}_L$ which are smaller than the angles formed by the entry velocities corresponding to $C_d^a$ and $D_a^d$ trajectories. Maximum retardation is observed for a trajectory leaving the sphere of action in the direction opposite to that of the moon's velocity, regardless of the entry conditions.

Figure D.11 shows that the geocentric area constant $\sigma_k$ will be a maximum for the maximum-retardation trajectory, so that this trajectory passes the furthest from the earth's center, in comparison with close trajectories.

The velocity-vector diagram can be used to trace out the evolution of the trajectories with a variation of $\lambda$ or one of the other initial parameters in the range corresponding to lunar approach. Such an analysis will not be carried out here, however.

The following conclusions can be drawn concerning the problems considered above. Due to the very high accuracies required of the initial data, close circumlunar flights (and especially close circumlunar flights with slanting re-entry into the earth's atmosphere) are feasible only if midcourse corrections are made during the passive part of the flight. Lunar-impact trajectories and trajectories providing distant circumnavigation of the moon are not associated with such high accuracy requirements, so that flights along these trajectories are possible without midcourse corrections.

## REMARKS

1. Using the above results, the two-dimensional trajectories with the most appropriate shapes and properties can be selected for each specific moon mission. Once this selection has been made, the foregoing technique can be used to find the initial data and the required accuracies for these trajectories. Such initial data can serve as a first approximation for determining accurately the working initial data taking into account solar perturbations and other secondary factors.
2. It is advisable to integrate the corresponding accurate equations numerically, using high-speed computers. For the numerical determination of the working trajectory, iterations can be carried out, using the same functions and variables and the same methods as were used to find the nominal trajectories in the foregoing problems.
3. The solutions obtained by us for specific problems are of considerable practical interest even when midcourse corrections (using an auxiliary

engine) must be made during the passive part of the flight, in order to obtain the desired trajectory. This is because for such flights a minimum correction will be required, in comparison with the other solutions.

4. The approximate technique used is valid for $m_2 : m_1$ ratios which are as small as desired, as well as for the mass ratio of the earth and the moon ($m_2 : m_1 = 1:81.45$). Moreover, as the ratio $m_2 : m_1$ is reduced to zero, the accuracy of the method increases indefinitely. Consequently, the approximate method can be used to calculate the motion of a spacecraft in the attractive fields of the sun ($m_1$) and one of the superior planets ($m_2$). Trajectories passing through the spheres of action of the planets with respect to the sun will then be the approach trajectories.

Since the planetary orbits have small angles of inclination to the earth's orbit, the above method can be applied to study interplanetary trajectories. The greater part of such a trajectory will lie outside the earth's sphere of action relative to the sun. In this case the initial heliocentric radius or, alternatively, the radius of the earth's orbit, will be used as the initial radius $r_1$, while the radius of the planetary orbit will be used in place of the radius $a$ of the lunar orbit. The influence of other planets need not be taken into account, since it is not likely that approach trajectories for planet $m_2$ will enter the spheres of action of the other planets.

The following two-dimensional problems will be significant for interplanetary approach trajectories: impact on planet $m_2$, flight around the planet with return to the earth's orbit, special case of circumplanetary flight (with return tangential to earth's orbit), and acceleration due to perturbing effect of planet $m_2$ (for example, in order to fly out to the orbit of a more distant planet).

If the ratio $r_1 : a$ is small, as in the case of Neptune, for instance, then many of the foregoing results, as well the calculation method outlined, will be applicable to studies of approach trajectories for interplanetary flights. In particular, the theoretically possible types and shapes of trajectories for Neptune flights from the earth's orbit will obviously be the same as for trajectories from the earth or from a nearby artificial earth satellite to the moon.

*REFERENCES*


1. BUCHHEIM, R.W. Artificial Satellites of the Moon.—Proc. VII IAF Congress (Rome, 1956), Associatione Italiana Razzi (Rome, 1956).
2. EHRICKE, K.A. Cislunar Operations.— ARS Preprint. June 1957.
3. COLD [sic]. Earth-Moon Rocket Trajectories, I. — ARS Preprint. June 1958.
4. GOLDBAUM, G.C. and R.J.GUNKEL. Comparison of Two- and Three-Dimensional Analysis of Earth-Moon Flight. — Proc. Amer. Astronaut. Soc. Western Regional Meeting, Palo Alto, August 1958.
5. LIESKE, H.A. Circumlunar Trajectory Studies.— RAND Paper. June 1958.
6. WALTERS, L.G. Lunar Trajectory Mechanics.— Navigation, **6**, p.51-58. 1958.
7. MICKELWAIT, A.B. Lunar Trajectories.— ARS Journal, **29**, No.12. 1959.
8. MICKELWAIT, A.B. and R.C. BOOTEN. Analytical and Numerical Studies of Three-Dimensional Trajectories to the Moon. — Inst. Aerospace Sci. Paper No. 59-90. June 1959.
9. KOOY, J.M.J. and J. BERGHUIS. On the Numerical Computation of Free Trajectories of Lunar Space Vehicles.—Astronautica Acta, 6. No.2-3. 1960.
10. PASTERGELIS, M.M. — Report at Conference on Problems of Mathematical Theory of Motion of Artificial Celestial Bodies; cf. Astronomicheskii Zhurnal, 37, No.2. 1960 [In Russian].
11. TROSS, C. Opredelenie orbity dlya poleta k Lune (Determination of Lunar Orbits). — Raketnaya Tekhnika, Zhurnal Amerikanskogo Raketnogo Obshchestva (ARS Journal), Russian Translation, No.4. 1962.
12. SKIDMORE, L.J. and P.A. PENZO. Modelirovanie upravleniya na srednem uchastke traektorii poleta k Lune s pomoshch'yu metoda Monte-Karlo (Flight-Control Simulation for Middle Part of Lunar Trajectory, Using Monte Carlo Method). — Raketnaya Tekhnika i Kosmonavtika, Zhurnal Amerikanskogo Instituta Aeronavtiki i Kosmonavtiki (AIAA Journal), Russian Translation, No.4. 1963.
13. RIDDELL. Initial Azimuth and Times for Ballistic Lunar Impact Trajectories, ARS Journal, **30**, No.5. 1960.
14. ALMÁR, I. and B. BALÁZS. Approximate Method of Plotting the Orbit of a Space Rocket Passing near the Moon. — Magyar. tud. akad. Mat. Kutató int. közl., **4**, No.2. 1959; Békéssy, A. and K. Tóth. Remark on the Paper: "Approximate Method of Plotting the Orbit of a Space Rocket Passing near the Moon" by I. Almár and B. Balázs, ibid. See also journal of abstracts: Mekhanika, 1961. Abstracts 5A56 and 9A53.

15. NIRMAN, A. Astronautical Velocity and Timing Charts for Use in Space Travel. — J. Brit. Interpl. Soc., 19, No. 1. 1963.
16. ALEKSANDROV, S.G. and R.E. FEDOROV. Sovietskie sputniki i kosmicheskie korabli (Soviet Satellites and Spaceships), 2nd Edition. — Izdatel'stvo Akademii Nauk SSSR. 1961.
17. SEDOV, L.I. Orbity kosmicheskikh raket v storonu Luny (Lunar Orbits of Space Rockets). — In Sbornik: Iskusstvennye Sputniki Zemli, No. 5. 1960.
18. KIZNER, W.A. A Method of Describing Miss-Distances for Lunar and Interplanetary Trajectories. — Planetary and Space Sci., 7, 125-131. 1961.
19. TURSKII, V.S. K voprosu o traektoriyakh stolknoveniya i zakhvata v zadache trekh tochek (Impact and Capture Trajectories in the Three-Point Problem). — Soobshcheniya GAISh, No. 114. 1961.
20. TARATYNOVA, G.P. O dvizhenii iskusstvennogo sputnika Zemli v netsentral'nom pole tyagoteniya pri nalichii soprotivleniya atmosfery (The Motion of an Artificial Earth Satellite in a Non-central Gravitational Field in the Presence of Atmospheric Resistance). — Uspekhi Fizicheskikh Nauk, 63, No. 1a. 1957.
21. EGOROV, V.A. O nekotorykh zadachakh dinamiki poleta k Lune (Some Problems Related to the Dynamics of Moon Flight). — Uspekhi Fizicheskikh Nauk, 63, No. 1a. 1957.
22. EGOROV, V.A. K voprosu o zakhvate v ogranichennoi krugovoi probleme trekh tochek (Capture in the Restricted Circular Three-Point Problem). — In Sbornik: Iskusstvennye Sputniki Zemli, No. 3. 1959.
23. HILL, G.W. Lunar Theory. — Am. J. Math., Vol. I, Part 23. 1877.
24. FESENKOV, V.G. K voprosu o zakhvate pri blizkom prokhozhdenii (Capture during a Close Passage). — Astronomicheskii Zhurnal, 23, No. 1. 1946.
25. SUBBOTIN, M.F. Kurs nebesnoi mekhaniki (A Course in Celestial Mechanics). Vol. 2. — ONTI. 1937.
26. STRÖMGREN, E. — Publicationern fra Kobenhavns obs., No. 100. 1936.
27. HOPF, E. — Mathematische Annalen, No. 103. 1930.
28. HOHMANN, W. Die Erreichbarkeit des Himmelskörpers. — R. Oldenbourg-Verlag. München. 1925.
29. CHEBOTAREV, G.A. Simmetrichnaya traektoriya dlya poleta vokrug Luny (A Symmetrical Trajectory for Circumlunar Flight). — Byull. Instituta Teoretich. Astronomii, 6, No. 7(80). 1957.
30. LISOVSKAYA, M.S. O traektoriyakh poleta rakety vokrug Luny (Trajectories for Rocket Flights around the Moon). — Byull. Instituta Teoretich. Astronomii, 6, No. 8(81). 1957.
31. MIELE, A. Theorem of Image Trajectories in the Earth-Moon Space. — Astronautica Acta, 6, No. 5. 1960.
32. LAWDEN, D.F. — J. Brit. Interpl. Soc., 13, No. 6. 1954; 14, No. 4. 1955.
33. EHRICKE, K.A. Space Flight, Vol. II. — Van Nostrand. 1962.

*INDEX*


Active angular range. See Angular range, active
Advance point 15, 19—20, 37, 71, 76, 111
ALEKSANDROV 146
ALMÁR 145
Angular range 37
  active 28, 92, 102
  maximum 72
  passive 15—17, 23

BALÁZS 145
BERGHUIS 145
BOOTEN 145
Boundary problem 50—55
BUCHHEIM 145

Cauchy problem 55—58
Characteristic velocity 28, 34—36, 72
CHEBOTAREV 146
Circumlunar flight 129—141
  periodic 136—141
  special problem of 134—136
Coordinate system
  equatorial 81
  geocentric 6, 37, 52, 109—110, 115
  rotating 108—110, 126
  selenocentric 7, 51, 83, 115
Coriolis force 42
Culmination 78—79

Earth
  attraction of 50, 111
  flight around 108—110, 137, 141
  oblateness of iii, 3, 88, 93—98
  perturbations by 55, 115—116
Earth-return trajectories 129—136, 143
EGOROV 146
EHRICKE 145, 146
Energy limitations 80
Entry velocities 9—12, 51—64, 116—119
Envelopes, method of 34—36, 105
Escape corridor 105—107, 112, 114
Exit velocities 116—117, 121—123, 129, 134, 141—143

FEDOROV 146
FESENKOV 114, 146
Flight time 58—59, 77—80, 91, 95—100, 118—120
  nominal 79, 85
  optimum 78, 84, 90
  reduction of 89, 101

GOLDBAUM 145
GUNKEL 145

HILL 104, 105, 146
HOHMANN 129, 134, 146
HOPF 113, 146

Impact point
  determination of 71—87
  location of 64—70
Initial data
  deviations of 1, 50ff, 104, 125—129, 133, 142
  nominal 91, 101
Initial heights 107—108, 117
Initial velocities
  elliptic 12, 15, 115, 123
  hyperbolic 15, 97, 115, 124
  minimum 104ff, 132
  parabolic 34, 89, 97, 110, 115, 121, 124
  variation of 57, 109, 118, 124, 135
Interlaunch interval 23—25, 30
Interplanetary flights 144

Iterations 50, 53, 56, 72, 90, 101, 124, 131, 135, 141, 143

Jacobi integral 105—107, 114, 141

Kepler's laws 6, 105
KIZNER 146
KOOY 145
KULIKOVSKII 13

Launch interval 20
Launch point 20—22
Launch time 30, 75, 84, 91, 102, 127—128
LAWDEN 146
LEVANTOVSKII iii
Libration points 106—107, 114
LIESKE 145
Line of nodes 13
LISOVSKAYA 146
*Lunar approach, feasibility of* 105, 110, 119
Lunar capture 104, 113—117
Lunar impact 12 ff, 64—70, 85, 123—129
  area of 66—67, 128
  deviations of 88—89, 127
  feasibility of 25, 31—33, 37—39, 69, 128, 132
  observation of 75—80, 91, 101
Lunar orbit, ellipticity of 88, 91—93, 101
Lunar parameters 70
*Lunar satellites* 1—2, 114—115
Lunar sphere of action 7—10, 50, 59, 114—115
  entry into. See Entry velocities
  size of 52, 136
Lunar trajectories. See Trajectories

MICKELWAIT 145
Midcourse corrections 129, 133, 143—144
MIELE 146
Miss distances 124—127, 133—136
Moon
  attraction of 68, 85, 88—90, 111—112, 114, 124
  averted side of 136
  motion relative to 80—84
  perturbations by 84, 88—90, 110, 113, 115—116, 134, 141—143

NIRMAN 146
Node longitude 36

Passive angular range. See Angular *range, passive*
PASTERGELIS 145
PENZO 145

Re-entry 134—136, 143
RIDDELL 145

Secondary factors 64, 88 ff, 128
SEDOV 146
SKIDMORE 145
Spacecraft
  capture of. See Lunar capture
  control of 80
  escape of 105—106, 115, 140—141
  location of 87, 103
  velocities of 82—86, 111
Striking interval 15, 21, 37, 75
STRÖMGREN 138—140, 146
SUBBOTIN 146
Sun, influence of 88, 91, 97—101, 115, 128, 141, 143—144

TARATYNOVA 146
Thiele transformation 107—108
Three-body problem 6, 84, 104—107, 114, 139
Trajectories
  active part of 28—33
  approach 7—12, 50, 115—123, 131, 134
  ascending branch of 15, 115, 121—123, 126, 128—132, 141
  circumlunar 129—141
  curvature of 126
  descending branch of 121—123, 128—132, 141
  earth-return. See Earth-return trajectories
  flyby 130—141
  impact 12 ff, 50 ff
  modified 55—59
  nominal 13, 50 ff, 88, 131—133, 143
  optimum 34 ff

passive part of 1, 6, 14—17, 75, 90, 105
two-dimensional 1, 12, 61, 104 ff
types 33, 48—49, 123—125, 130—142
unperturbed 76—80
Trajectory plane, inclination of 26—27, 36 ff, 71 ff, 86, 93
TROSS 145
TURSKII 146

Visibility parameters 81—82

WALTERS 145

Zero-velocity surfaces 106

National Aeronautics and Space Administration
WASHINGTON, D. C. 20546

OFFICIAL BUSINESS

POSTAGE AND FEES PAID
NATIONAL AERONAUTICS AND
SPACE ADMINISTRATION

02U 001 55 51 3DS 70119 00903
AIR FORCE WEAPONS LABORATORY /WLOL/
KIRTLAND AFB, NEW MEXICO 87117

ATT E. LOU BOWMAN, CHIEF, TECH. LIBRARY

[5074]

Printed in Jerusalem, Israel

NASA TT F-504
TT 68-50306